National Library of Canada
Acquisitions and Bibliographic Services Branch
395 Wellington Street
Ottawa, Ontario
K1A 0N4

Bibliothèque nationale du Canada
Direction des acquisitions et des services bibliographiques
395, rue Wellington
Ottawa (Ontario)
K1A 0N4

Your file Votre référence

Our file Notre référence

NOTICE

The quality of this microform is heavily dependent upon the quality of the original thesis submitted for microfilming. Every effort has been made to ensure the highest quality of reproduction possible.

If pages are missing, contact the university which granted the degree.

Some pages may have indistinct print especially if the original pages were typed with a poor typewriter ribbon or if the university sent us an inferior photocopy.

AVIS

La qualité de cette microforme dépend grandement de la qualité de la thèse soumise au microfilmage. Nous avons tout fait pour assurer une qualité supérieure de reproduction.

S'il manque des pages, veuillez communiquer avec l'université qui a conféré le grade.

La qualité d'impression de certaines pages peut laisser à désirer, surtout si les pages originales ont été dactylographiées à l'aide d'un ruban usé ou si l'université nous a fait parvenir une photocopie de qualité inférieure.

Canada

Magmatic and Hydrothermal Processes in Rare-Element Granite-Pegmatite Systems: The Preissac-Lacorne Batholith, Quebec, Canada

by

Thomas Mulja

A thesis submitted to the Faculty of Graduate Studies and Research of McGill University (Québec, Canada) in partial fulfilment of the requirements for the degree of Doctor of Philosophy

ISBN 0-612-08137-0

Canada

To my wife Lee and family

ABSTRACT

Geological and mineralogical investigations of four moderately peraluminous monzogranitic plutons (Preissac, Moly Hill, Lamotte, Lacorne) in the Archean Preissac-Lacorne batholith (northwestern Quebec) indicate that each consists of biotite, two-mica and muscovite monzogranite facies, and that these facies are zonally distributed in this order from margin to core of the larger Lamotte and Lacorne plutons. Rare-element-enriched granitic pegmatites are associated with the Lamotte and Lacorne plutons and are also regionally zoned, in this case, with respect to their respective plutons, from beryl-bearing in the plutons to spodumene-bearing in the country rocks. Molybdenite mineralized albitites and stockworks occur beyond the spodumene pegmatites and in the Preissac and Moly Hill plutons. The monzogranites dispiay systematic mineralogical and major- and trace-element trends from biotite to muscovite monzogranite in the four plutons that are best explained by fractional crystallization of a biotite monzogranite-forming liquid. These petrochemical trends in the Lamotte and Lacorne plutons extend to the rare-element pegmatites, indicating that the latter are comagmatic with the monzogranite. A model is proposed in which the liquids of the Lamotte and Lacorne plutons underwent an initial side-wall crystallization to produce the observed zonation of the monzogranite types, followed by extreme differentiation inside the magma chamber, from where batches of pegmatite-forming liquid were sequentially injected into the overlying rocks. Pegmatites are rare and barren from the smaller Preissac and Moly Hill plutons due to early saturation of the residual liquid with aqueous fluid, from which quartz and molybdenite precipitate to form quartz vein stockworks adjacent to the muscovite-bearing monzogranite.

The fractionation of the pegmatite-forming liquid is recorded partly in the crystal-chemistry of columbite-tantalite solid-solutions, by progressively higher Ta/(Ta+Nb) and Mn/(Mn+Fe) values with evolution from beryl- to spodumene-bearing pegmatite. These trends correlate to the greater solubility of Mn- relative to Fe- and of Ta- relative to Nb-columbite-tantalite end-members in the magma. In the Lacorne

pegmatites, these trends were modified by contemporaneous crystallization of spessartine garnet, which buffered the Mn and Fe activities of the columbite-tantalite.

The pegmatite-forming liquid became saturated with an aqueous fluid at the onset of crystallization as shown by the entrapment of primary fluid inclusions in the paragenetically early beryl and spodumene. The orthomagmatic fluid was NaCl-dominated, had low salinity, contained appreciable dissolved CO_2, and evolved from Fe-bearing in beryl to Mn-, Li- and Cs-bearing in spodumene pegmatite in concert with the petrochemical evolution of the magma. Subsequent fluid evolution was marked by influx of externally derived Ca-brines of metamorphic origin and eventual unmixing of the orthomagmatic fluid into aqueous and carbonic phases.

The study represents the first comprehensive reconstruction of the petrological and fluid evolution in a comagmatic suite of monzogranites and rare-element granitic pegmatites.

RESUME

Dans le batholithe archéen de Preissac-Lacorne au nord-ouest du Québec, les études géologique et minéralogique de quatres plutons modérément peralumineux (Preissac, Moly Hill, Lamotte et Lacorne) indiquent que chacun d'entre eux est constitué de faciès monzogranitiques à biotite, à deux micas et à muscovite. Dans cet ordre, ces faciès sont distribués de façon concentrique de la bordure vers le centre dans les plus grands plutons, soit ceux de Lamotte et de Lacorne. Des pegmatites granitiques enrichies en terres rares sont associées avec les plutons de Lamotte et Lacorne et sont également zonées à une échelle régionale : elles contiennent du béryl dans les plutons et du spodumène dans les roches encaissantes. Des albitites minéralisées en molybdenite ainsi que des stockwerks sont présents au-delà de l'extension des pegmatites à spodumène, ainsi que dans les plutons de Preissac et de Moly Hill. Les monzogranites présentent des évolutions systématiques dans leur minéralogie ainsi que dans leur composition en éléments majeurs et en éléments traces. Ils passent d'un monzograntite à biotite à un monzogranite à muscovite dans les quatres plutons. Ces évolutions s'expliquent par la cristallisation fractionnée du liquide formant le monzogranite à biotite. L'évolution pétrochimique des plutons de Lamotte et de Lacorne se prolonge dans les pegmatites à terres rares, indiquant ainsi que ces pegmatites sont co-magmatiques avec le monzogranite. Un modèle est proposé, dans lequel les liquides des plutons de Lamotte et de Lacorne subirent d'abord une cristallisation à partir des parois afin de produire la zonation observée. Par la suite, une différenciation extrême eu lieu à l'intérieur de la chambre magmatique à partir de laquelle des paquets de liquide furent injectés de façon séquentielle dans la roche sus-jacente pour former les pegmatites. Les pegmatites sont rares et dépourvues de minéralisation dans les plus petits plutons de Preissac et de Moly Hill. Ceci s'explique par le fait que du liquide résiduel a rapidement été saturé par un fluide aqueux à partir duquel le quartz et la molybdenite ont précipité, formant ainsi les stockwerks à veine de quartz, adjacents au monzogranite à muscovite.

Le fractionnement du liquide responsable pour la formation des pegmatites est

partiellement enregistré dans la cristallochimie des minéraux de la solution solide columbite-tantalite. En effet, les rapports Ta/(Ta+Nb) et Mn/(Mn+Fe) augmentent avec l'évolution des pegmatites à béryl vers celles à spodumène. Ces évolutions correspondent à une plus grande solubilité de la columbotantalite riche en Mn et Ta par rapport à celle riche en Fe et Nb respectivement dans le magma. Dans les pegmatites de Lacorne, ces évolutions ont été modifiées par la cristallisation simultanée de grenat spessartin qui a tamponné l'activité du Mn et du Fe de la columbotantalite.

Le liquide responsable pour la formation des pegmatites a été saturé avec un fluide aqueux au début de la cristallisation, ce qui est démontré par la présence d'inclusions fluides primaires dans le béryl et le spodumène, tout deux étant des phases précoces dans la paragenèse. Le fluide orthomagmatique était dominé par du NaCl, avait une faible salinité et contenait une quantité appréciable de CO_2 dissous. De plus, il évolua d'un fluide à Fe dans les pegmatites à béryl, à un fluide à Mn, Li et Cs dans les pegmatites à spodumène, accompagnant ainsi l'évolution pétrochimique du magma. L'évolution ultérieure du fluide a été marquée par l'introduction d'une saumure externe, riche en Ca, d'origine métamorphique, et par la séparation du fluide orthomagmatique en une phase aqueuse et une phase carbonique.

L'étude est la première reconstitution globale de l'évolution pétrologique et de l'évolution du fluide dans une suite co-magmatique de monzogranites et de pegmatites granitiques à éléments rares.

ACKNOWLEDGEMENTS

No one walks alone.

(Sun Tse, 2530 before present)

This thesis would not have been completed without the tremendous efforts made by Professor Anthony E. "Willy" Williams-Jones, my principal supervisor, who put up with all my short comings and aberrations during the course of this study. I am very grateful for his liberty and guidance in the formulation of the objectives of the thesis, and, most of all, for his patience in reading, revising and rewriting many versions of the manuscripts, which eventually became readable and suitable for submission to recognized Journals. A special thank is directed to Colleen Williams-Jones, whose unselfishness facilicated her husband the precious time in order to complete the thesis on time.

I want to thank Professors Scott A. Wood and Robert F. Martin, co-supervisors of the thesis, for their advice on hydrothermal ore deposits and petrology of granites and pegmatites, respectively. Discussions with professors Don Baker and Jeremy Fein (McGill University) helped clarify some aspects of granitic magma and calcite solubility, respectively. The encouragements from earlier geology mentors, Professors Marcos Zentilli (Dalhousie University) and Roger H. Mitchell (Lakehead University), and from Mr. Stephen Holton and Dr. Rosemary Holton, who are both as teachers and friends, are sincerely appreciated.

I have the fortunate to befriend with the following individuals (in no particular order): Antoine Fournier, Anne Prefontaine, Pierre Hudon, Peta McLoughin, Wang Dong, Werner Halter and Willy Williams-Jones (as a friend here), who, among other things, shared much laughter--the most precious moment I could have during my study in an unusual environment. Similarly, Aphrodite "Aqin" Indares, Ralph Weberbauer, Corinne Santa, Sirinat, Sanya, Pam Scowen and Hojatollah Vali provided such a needed break.

I want to thank Antoine Fournier, Katrinka Gretchen, Shi Lang, Ardeshir Hazerkhani and Venetia Bodycomb, who helped draw some of the figures and type the tables. Moira MacKinnon and Glenn Poirier taught me how to operate the electron microprobe, and Jim Mungall the EDS-SEM. George Panagiotidis made many of the thin sections, frequently at a very short notice. Tariq Ahmedali analyzed some of the whole-rock major- and trace-element compositions. The French version of the abstract was kindly provided by Werner Halter.

I am grateful to John B. Felderhof, senior vice president of Bre-X Minerals Ltd., for giving me an extended "vacation" in order to complete this thesis.

Funding for this research was provided by various types of NSERC, FCAR and MERQ grants, and NATO travel grants, to A.E. Williams-Jones and S.A Wood, and by an NSERC operating grant to R.F. Martin.

PREFACE

This thesis contains four journal manuscripts: the first two are in press in the *Canadian Mineralogist*, the third is in review by the *American Mineralogist*, and the last one is to be submitted to *Geochimica et Cosmochimica Acta*. According to "Guidelines Concerning Thesis Preparation" of the Faculty of Graduate Studies and Research:

The candidate has the option, subject to the approval of his or her Department, of including as part of the thesis text, or duplicated published text, of an original paper or papers. Manuscript-style theses must still conform to all other requirements explained in the Guidelines Concerning Thesis Preparation. Additional material (procedural and design data as well as descriptions of equipment) must be provided in sufficient detail (e.g. in appendices) to allow clear and precise judgment to be made of the importance and originality of the research reported. The thesis should be more than a mere collections of manuscripts published or to be published. It must include a general abstract, a full introduction and literature review and final overall conclusions. Connecting texts which provide logical bridges between different manuscripts are usually desirable in the interest of cohesion. It is acceptable for the thesis to include, as chapters, authentic copies of papers already published, provided that they are duplicated clearly and bound as an integral part of the thesis. In such instances, connecting texts are mandatory and supplementary explanatory material is always necessary. Photographs or other materials which do not duplicate well must be included in their original form. While the inclusion of manuscripts co-authored by the candidate and others is acceptable, **the candidate is required to make an explicit statement in the thesis of who contributed to such work and to what extent, and supervisors must attest to the accuracy of the claims at the Ph.D Oral Defence.** Since the task of the examiners is made more difficult in these cases, it is in the candidate's interest to make the responsibilities of authors perfectly clear.

In the four manuscripts listed earlier, which form the major part of the thesis,

the candidate mapped the studied area, collected almost all the rocks used (additional samples were collected by M. Boily), analyzed the composition of the minerals with an electron microprobe, prepared most of the rock powders for whole-rock geochemical analyses (some were prepared by an assistant of M. Boily), and conducted the microthermometric analyses of fluid inclusions (a small number of fluid inclusion data were collected by Anne Prefontaine, see below). The candidate interpreted the data, conceived genetic models and wrote the manuscripts. Professor A.E. Williams-Jones, the principal supervisor of the thesis, participated in field work, proposed the topics and, together with the co-supervisor, Professor S.A. Wood, helped with the interpretation, recommended hypotheses for testing and edited the manuscripts. Dr. M. Boily was the third co-supervisor of the candidate from 1989-1991, and was a member of the McGill group who investigated the metallogeny of the candidate's study area. Professor R.F. Martin, who is a member of the supervisory committee, analyzed the unit-cell dimensions of feldspars (Appendix 2) and of columbite-tantalite in manuscript number 3 (Chapter 4), helped interpret the results, and edited the manuscript. Anne Prèfontaine, the fourth co-author of manuscript number 4 (Chapter 5), was an M.Sc student of Prof. Williams-Jones, whose thesis project (the genesis of spodumene-bearing pegmatite, one of the three types of pegmatite discussed in Chapter 5) was located in the same area as the candidate. She left the program for personal reasons after collecting a small amount of data. Her study was then continued by the candidate and was incorporated into this thesis.

Table of Contents

Chapter 3: Petrogenesis of Zoned Monzogranitic Plutons and Associated Rare-element Granitic Pegmatites and Quartz Veins: the Preissac-Lacorne Batholith, Quebec.

Chapter 4: Compositional Variation and Structural State of Columbite-tantalite in Rare-element Granitic Pegmatites of the Preissac-Lacorne batholith, Quebec, Canada.

Chapter 5: Physical and Chemical Evolution of Fluids in Rare-element Granitic Pegmatites associated with the Lacorne Pluton, Quebec, Canada.

Chapter 6: Epilogue

Appendices

List of Figures

List of Tables

CHAPTER 1

INTRODUCTION

Rationale

Granite-pegmatite intrusion: the dilemma

Rare-element-enriched (Be, Li, Nb, Ta, Mo) granitic pegmatites are arguably the most poorly understood type of granite-related mineral deposit, mainly because interpretation of their origin requires knowledge of the evolution of the related felsic magmas and understanding of the complex phase changes that alter the crystallization history of pegmatite. An exhaustive review of all proposed models for pegmatite genesis led Černý (1982) to conclude that differentiation of felsic liquid and partial melting of pre-existing rocks are the two most viable processes by which pegmatite-forming liquids can be generated. In the case of rare-element-enriched pegmatites, Černý (1982) and Černý and Meintzer (1988) suggested that extreme fractionation of felsic melt is the most plausible process by which the pegmatite-forming liquid is enriched in rare-elements. This enrichment is made possible through drastic changes in the partition coefficients of rare-elements in the volatile-rich felsic liquid (e.g., Mahood and Hildreth, 1983; Miller and Mittlefehdt, 1984; London, 1987), thus enabling the residual liquid to attain the high concentrations of these elements observed in pegmatites (Černý, 1992). Similarly, O'Connor et al. (1991), for the lithium pegmatites of the Leinster granite (Ireland), proposed that Li enrichment in the residual liquid was achieved by the crystallization of muscovite instead of biotite in the parental granite, thus promoting Li accumulation in the highly mobile, low viscosity pegmatite-forming liquid.

In the above model, the resulting intrusions are zoned and the pegmatites vary from least fractionated, beryl-bearing (Be-type) in the intrusion to most evolved, spodumene-bearing (Li-type) in the country rocks, i.e., farthest from the parental granite (Fig. 1). However, a complete exposure of all rock facies shown in this conceptual model rarely occurs in a single intrusion (Černý and Meintzer, 1988). The Ghost Lake

Figure 1. A conceptual model for rare-element granite-pegmatite systems (after Trueman and Černý, 1982).

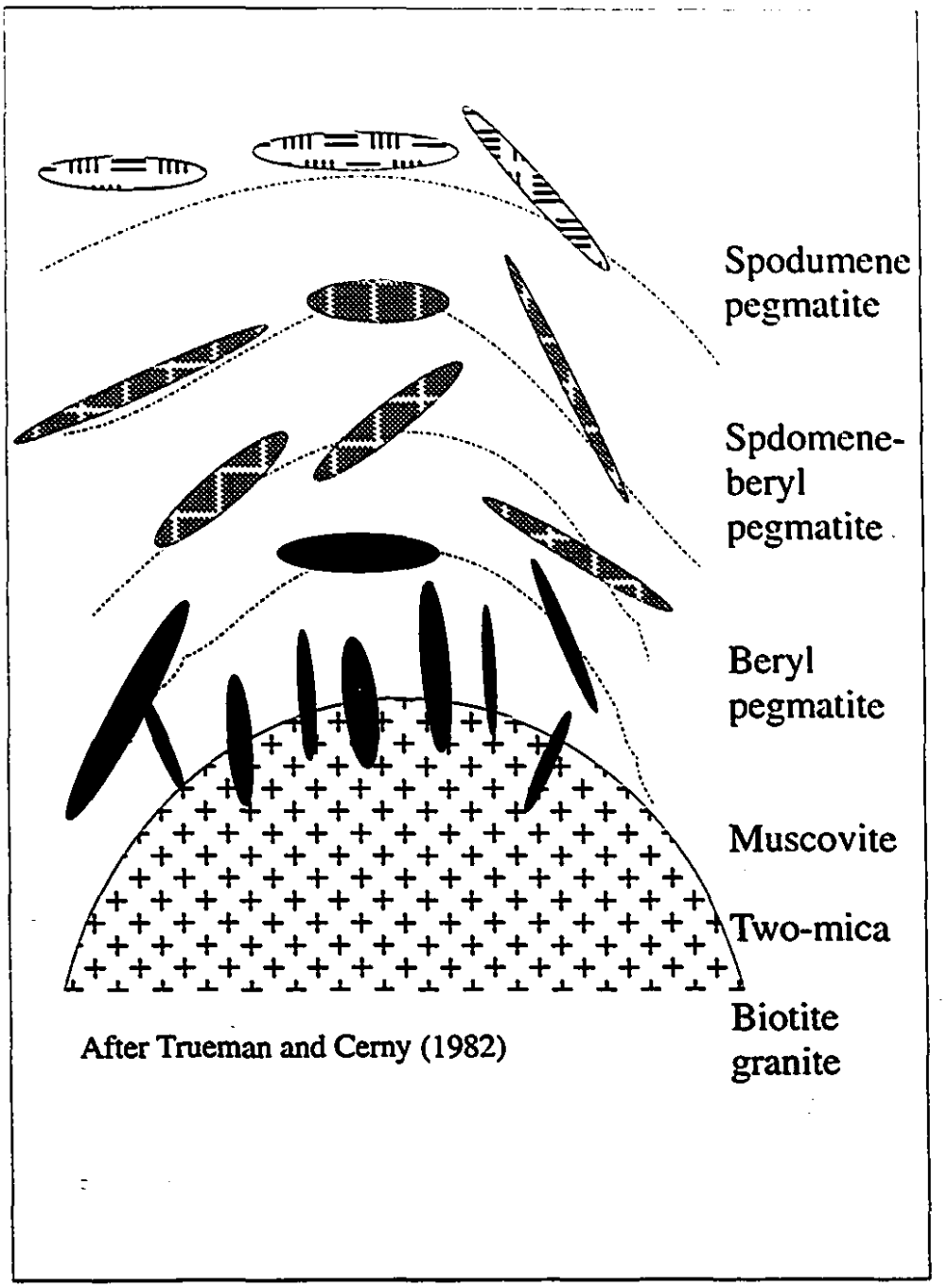
Spodumene pegmatite
Spdomene-beryl pegmatite
Beryl pegmatite
Muscovite
Two-mica
Biotite granite
After Trueman and Cerny (1982)

Figure 1

batholith in Ontario (Breaks and Moore, 1992) and the Harney Peak granite in South Dakota (Shearer et al., 1987) are, as far as the writer knows, the only two examples of rare-element granite-pegmatite systems that display zonation similar to that of the ideal model. Both groups of authors concluded that the various types of granite in their respective intrusions are related by fractional crystallization, and that the mineralized pegmatites crystallized from the residual liquids.

Those favoring a partial melting model (e.g., Steward, 1978) have argued for it on the grounds that fractional crystallization of felsic liquid does not explain how felsic liquid, with a typical content of 100 ppm Li in less evolved granite can produce enrichment of the levels, commonly found in Li-rich pegmatites ($\geq$ 1.5 wt.% Li_2O). Instead, they proposed that lithium pegmatites represent the first liquid from partial melting of Li-rich source rocks. In support of this alternative interpretation, Steward (1978) noted that lithium pegmatites are commonly intruded in isolation from potential parental granites.

The partial melting model for the petrogenesis of granite-pegmatite systems has recently been given additional credibility by Nabelek et al. (1992a, b), who interpreted their stable isotope and geochemical data for the Harney Peak granite as evidence that only the most evolved, tourmaline-bearing granite is comagmatic with the pegmatites, and that the other types of granite are the products of partial melting of different source rocks. On the other hand, Shearer et al. (1992) postulated that the Harney Peak granite and many pegmatites (unspecified, whether they are barren or mineralized) define a continuum of fractional crystallization, whereas the rare-element-enriched pegmatites represent fractionation of separate batches of chemically distinct magma. Černý (1982) believed that partial melting probably produces only barren and deep-seated types of pegmatite. The study of Damm et al. (1992) on the genesis of garnet-tourmaline pegmatites in the Eastern Pyrenes, Spain, corroborates this hypothesis.

The studies mentioned above dealt mainly with the petrogensis of the granites and granitic pegmatites, and much less with the evolution of the residual pegmatite-forming liquid. This liquid is believed to differentiate into batches of chemically distinct liquids, which are systematically emplaced into the overlying granite and

country rocks (Fig. 1). However, the mechanism by which the liquids are produced and sequentially intruded has not been addressed adequately. An explanation for the emplacement of distal pegmatite from the granite was given by Heinrich (1953), who suggested that because late, volatile-rich fluid is less viscous, it can therefore travel to great distances from the parental granite.

Another important aspect of pegmatite genesis that is still very poorly documented is the timing of exsolution of aqueous fluid from the felsic liquid and its role in the internal process of pegmatite crystallization. A landmark research paper on pegmatite genesis was that of Jahns and Burnham (1969), who proposed early saturation of the felsic magma with aqueous fluid. The exsolution of the fluid was considered by these authors to be the decisive event in the evolution of the pegmatite-forming liquid because it changes the dynamics of crystallization. The fluid-rich part of the liquid provides space for crystals to grow and accentuates movement of ions due to the lowered viscosity of the liquid. The transport of these ions, particularly the alkalis, is enhanced by the presence of Cl in the aqueous fluid (Burnham and Nekvasil, 1986); Cl is, by far, the most common anion in aqueous fluids associated with hydrothermal mineral deposits (Roedder, 1984). The fluid-poor fraction of the liquid tends to crystallize rapidly, resulting in a fine-grained rock, i.e., aplite. This process explains the segregation of aplite, normally found along the margins of the composite body of aplite-pegmatite, from pegmatite, which occurs at its center.

London (1986a), on the basis of a fluid inclusion study of the Tanco lithium pegmatite (Manitoba) and experiments in the system $LiAlSiO_4$-$NaAlSi_3O_8$-SiO_2-$Li_2B_4O_7$-H_2O, proposed that, in the case of boron-rich felsic magma, early saturation of aqueous fluid is not a prerequisite for pegmatite formation. Instead, London suggested that the role of the fluid envisaged by Jahns and Burnham was performed by dense, hydrous, alkali borosilicate fluids that he believed had been present during the crystallization of the Tanco pegmatite. In subsequent experiments, London et al. (1989) claimed that most of the textural characteristics of pegmatites could be produced by disequilibrium fractional crystallization of water-undersaturated, but volatile-rich liquid, in which early formed crystals fail to equilibrate with the residual liquid. Heterogenous side-wall

crystallization of this kind of liquid results in graphic and comb structures and in accumulation, in the center of the system, of volatiles P, B and F, which promote crystal growth. Furthermore, London et al. (1989) suggested that rare-element pegmatites may not become saturated in aqueous vapor until they approach solidus conditions.

By contrast, Thomas et al. (1988), who also conducted a fluid inclusion study on the Tanco pegmatite, showed that an aqueous fluid containing dissolved CO_2 and salts was present at the onset of pegmatite crystallization, and played an important role in the crystallization of pegmatite. According to these authors, the H_2O-CO_2 phase separation caused an increase in pH, which, in turn, promoted precipitation of beryl. The contrasting views of the genesis of the Tanco pegmatite are due to differences in the interpretation of the paragenesis of schorl, which contains fluid inclusions and occurs along the wall zone of the pegmatite: London considered the mineral to be late, whereas Thomas et al. regarded it as one of the earliest liquidus phases.

There have been several other modern, published studies of fluid inclusions in pegmatites (e.g., Ruggieri and Lattanzi, 1992; Chakuomakos and Lumpkin, 1990; Whitworth and Rankin, 1989; London, 1986b; Taylor et al., 1979), but none of these have addressed the question of timing of the saturation of an aqueous or other fluid in the liquid, or provided information about its subsequent compositional evolution. Ironically, the fluid problem is fundamental in our comprehension of how pegmatites are formed.

In summary, most current research on rare-element pegmatites is still centered on the genesis of the parental felsic liquid, and the processes by which the textural and mineralogical features of the pegmatite were formed. Aside from the papers on the Tanco pegmatite, few studies have elucidated the chemical evolution of the fluids separating from a pegmatite-forming liquid.

Objectives of the thesis

In light of our continued poor understanding of some of the important aspects

of the evolution of rare-element granitic pegmatites discussed above, this thesis was designed

1) to seek geological and petrochemical evidence for any petrogenetic relationships between zoned monzogranites and associated pegmatites.

2) to reconstruct the magmatic evolution of a pegmatite-forming liquid and establish the role that this evolution plays in the zonal distribution of the different types of rare-element pegmatite.

3) to determine the timing of fluid saturation in felsic magma and the physical and chemical evolution of the fluid with crystallization of the magma.

To meet the above objectives, the monzogranites and associated rare-element granitic pegmatites in the Preissac-Lacorne batholith (Quebec) were chosen for this study. As will be shown below, these intrusions represent one of the few examples of a complete granite-pegmatite system anywhere, and thus form an ideal setting in which to investigate the evolution of felsic liquid associated with rare-element pegmatite.

THE PREISSAC-LACORNE BATHOLITH

An ideal natural laboratory for studying rare-element granite-pegmatite evolution

For over twenty years (1950-1970s) the Preissac-Lacorne batholith in northwestern Quebec (long. 78°25'-77°45': lat. 48°30'-48°10') was a well-known mining locality, where several quartz-vein type molybdenum deposits and the largest lithium pegmatitic deposit in Eastern Canada were exploited (Fig. 2). In addition, sub-economic concentrations of beryllium, lithium and niobium-tantalum in granitic pegmatites occur extensively in the area. Both molybdenum deposits and rare-element-enriched pegmatites are spatially related to well-exposed zoned granitic intrusions, and in the case of the pegmatites, there is a zonal distribution from proximal beryl-bearing to distal spodumene-bearing types with respect to their associated intrusions (Fig. 2). In one of the intrusions (Lacorne), molybdenite-bearing albitite dikes and quartz veins occur beyond the spodumene pegmatites. Although this distribution has been inferred by Trueman and Černý (1982), based on observations at a large number of localities,

Figure 2. A geological map of the Preissac-Lacorne batholith showing major structural features, field relations among country rocks, early basic intrusions and late granitic rocks in the three massifs (Preissac, Lamotte, Lacorne), and the zonal distribution of rare-element-enriched pegmatites, albitite dikes and quartz veins (after Dawson, 1966 and Mulja et al., 1995). Each of the granitic rocks is zoned from biotite through two-mica to muscovite monzogranite. This zonation is depicted clearly in Figure 2 of Chapter 2. Abbreviations are Ab-d, albitite dikes; Brl, beryl; Mo, molybdenite; Qtz-v, quartz veins; Spd, spodumene. The lithologies are: grey, biotite schist and basic volcanic rock; black, gabbro-granodiorite series; cross hatching, undifferentiated monzogranite.

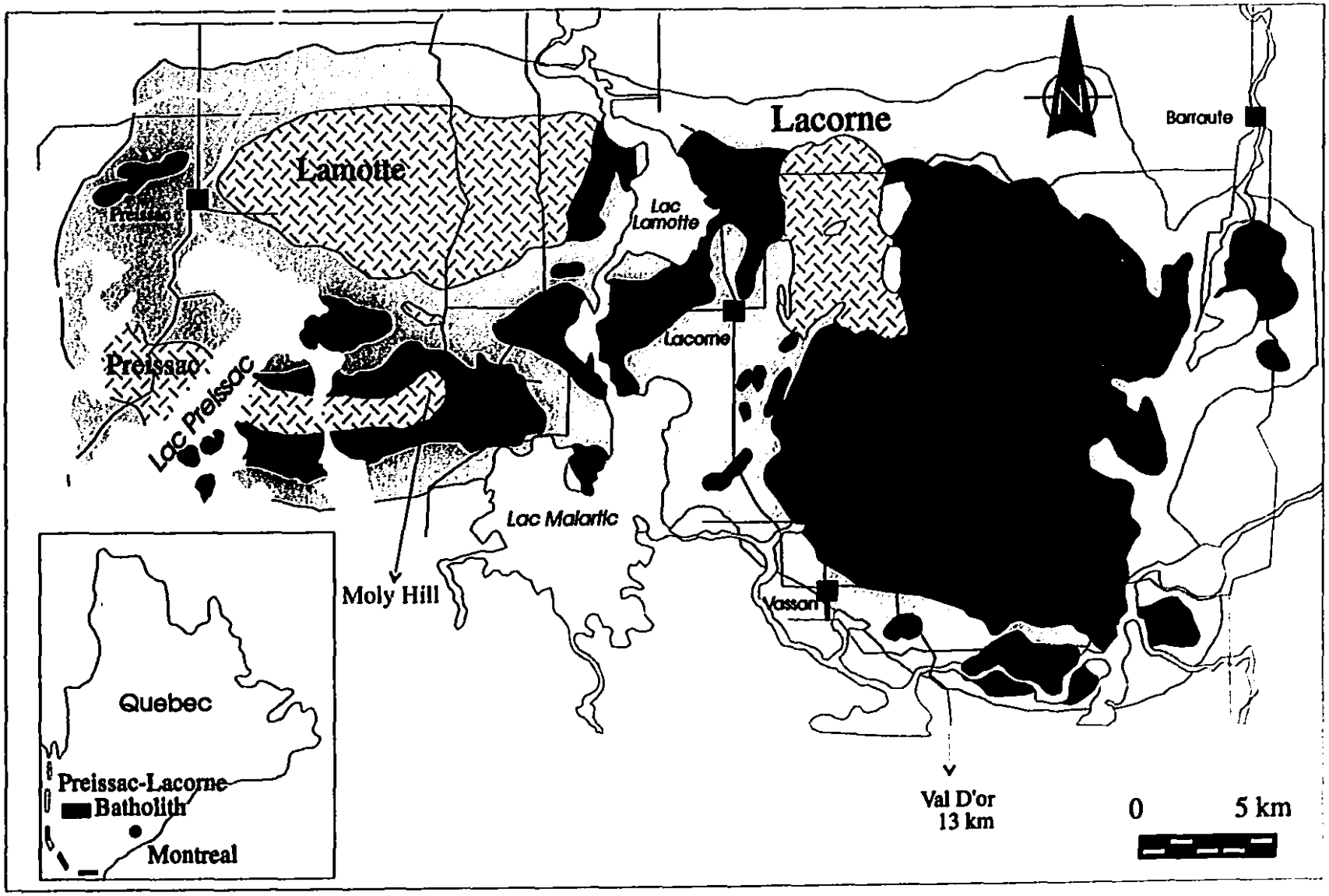
Lamotte
Lacorne
Barraute
Preissac
Lac Lamotte
Lacorne
Preissac
Lac Preissac
Lac Malartic
Moly Hill
Vassan
Quebec
Preissac-Lacorne
Batholith
Montreal
Val D'or
13 km
0
5 km

Figure 2

to our knowledge, there are only two other localities [the Ghost Lake batholith in Ontario (Breaks and Moore, 1992) and the Harney peak granite in South Dakota (Shearer et al., 1987)] where all the facies of monzogranite and associated rare-element pegmatites are exposed. However, the highly evolved spodumene-bearing pegmatite has not been reported for the Ghost Lake batholith, and the distribution of the rare-element pegmatites in the Harney Peak granite is very complex (Norton and Redden, 1990); these pegmatites tend to occur as clusters, each of which contains its own variety of pegmatites. The systematic zonation displayed by the monzogranites and mineralized pegmatites in the Preissac-Lacorne batholith, combined with the lack of evidence of post-intrusion metamorphism or deformation, therefore, make the Preissac-Lacorne batholith an ideal location in which to determine the link between the evolution of felsic magma and the formation of spatially-associated rare-element-enriched granitic pegmatites and related mineral deposits.

Regional setting

The Preissac-Lacorne batholith, which is composed of an older suite of pre- to syn-tectonic basic intrusions and a younger suite of post-tectonic monzogranites, is situated in the southeast corner of the southern volcanic zone (SVZ) of the Archean Abitibi greenstone belt (Fig. 3), a volcano-plutonic belt measuring 760 km long by 75-160 km wide (Goodwin and Ridler, 1970). To the east and west, the belt is bounded by the Grenville province and the Kapuskasing subprovince, respectively, and to the north and south by granitic forelands. The two prominent structural features of the belt are S-shaped regional folds with east-west axes, and faults, which generally trend NE-SW in the NVZ and E-W in the SVZ.

Ludden and Hubert (1986), on petrochemical grounds, divided the Abitibi belt into an older northern (> 2720 Ma) and younger southern volcanic (2710-2700 Ma) zone (NVZ and SVZ, respectively), a central granodiorite-gneiss zone and a southern granite-gneiss zone (Fig. 3). The NVZ consists of volcanic rock series that show a complete evolutionary spectrum from low magnesian (< 9 wt.%) basalt to rhyolite, whereas the SVZ comprises bimodal volcanic rocks (tholeiite and andesite-rhyolite) and

Figure 3. The location of the Preissac-Lacorne batholith within the Southern Volcanic Zone (SVZ) of the Abitibi greenstone belt (after Ludden and Hubert, 1986). 1: Northern Volcanic Zone, 2: Southern Volcanic Zone, 3: Central Granodiorite-gneiss Zone, 4: Southern Granite-gneiss Zone.

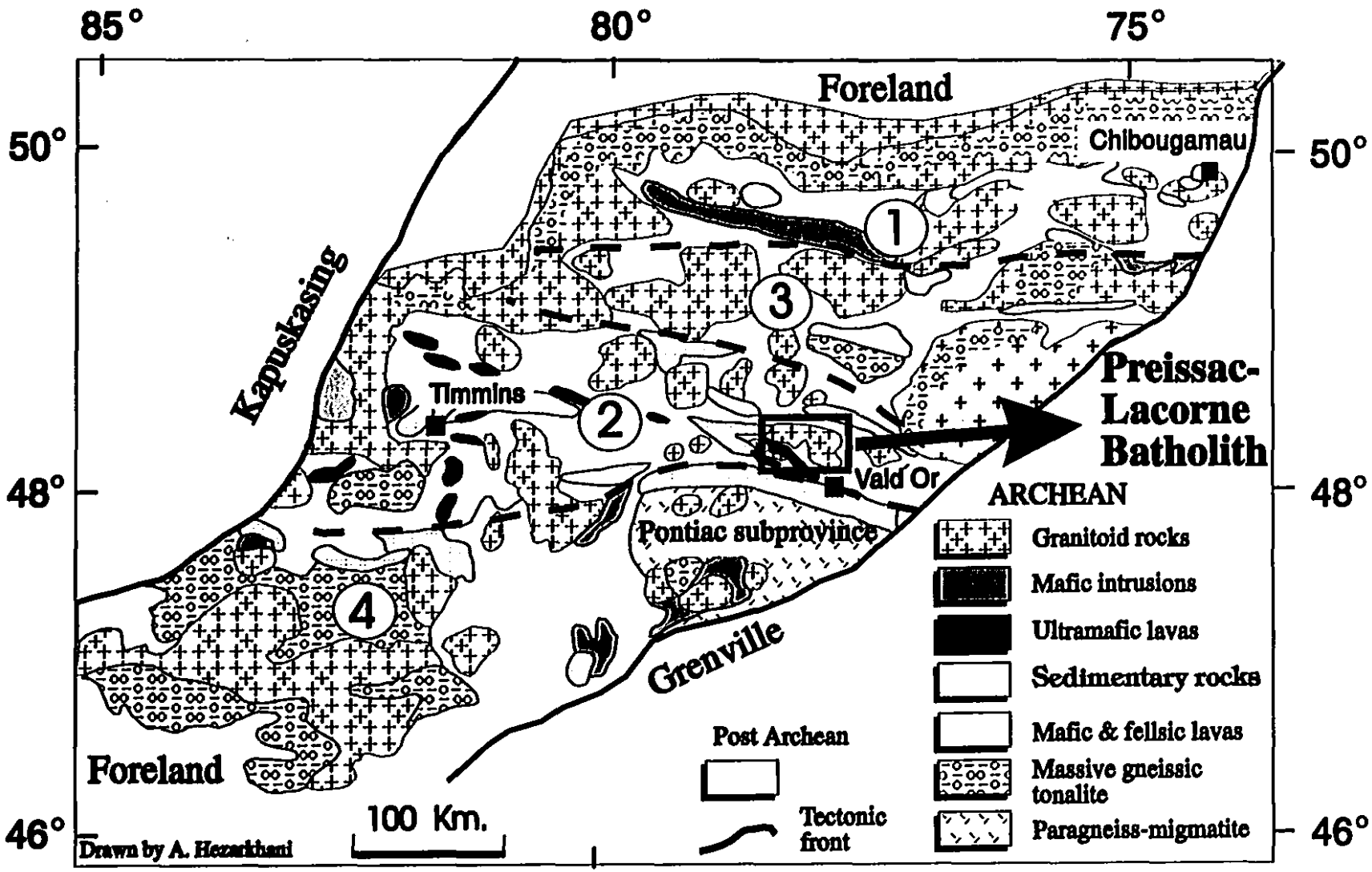
85°
80°
75°
50°
48°
46°
Foreland
Chibougamau
Kapuskasing
Timmins
Preissac-
Lacorne
Batholith
Val d'Or
Pontiac subprovince
Grenville
Foreland
100 Km.
Drawn by A. Hezarkhani
1
2
3
4
ARCHEAN
Granitoid rocks
Mafic intrusions
Ultramafic lavas
Sedimentary rocks
Mafic & fellsic lavas
Massive gneissic tonalite
Paragneiss-migmatite
Post Archean
Tectonic front

Figure 3

contains ultramafic rocks such as komatiite. Plutonic rocks in these two zones also differ; those of the NVZ are dominated by tonalite and granodiorite and have lesser volumes of layered gabbro-anorthosite intrusions. By contrast, the SVZ hosts intrusions of mainly tonalite to trondhjemite and subordinately monzonite to granite.

The central granodiorite-gneiss and granite-gneiss zones are poorly known, except that they are dominated by metasedimentary rocks, monzonitic plutons, orthogneiss and migmatite (Ludden and Hubert, 1986). The latter zone also includes the Pontiac subprovince, which has been recently investigated by, for example, Feng and Kerrich (1991) and Mortensen and Card (1994).

Although various models for the geologic evolution of the Abitibi greenstone belt have been proposed (see Desrochers et al., 1993 for details), most of the models invoke some kind of collision between oceanic arcs or between oceanic crust and continental crust. A three-stage model was proposed by Ludden et al. (1986). The first stage (~2720 Ma) involved subduction of oceanic crust underneath a continental crust (Andean-type) in which magmatism along the continental plate margin emplaced the volcanic and plutonic rocks of the NVZ. About 5-15 Ma later, stage 2 commenced with rifting and volcanism behind the NVZ in response to a rising thermal plume (ocean arc-type plutonism), creating a back-arc-like environment, part of which subsequently became the future SVZ. At about 2700 Ma, rifting and volcanism were succeeded by a Caledonian-type collision (Kenoran orogeny), which resulted in crustal thickening, deformation, uplift and anatexis. During this collision, the interval between the NVZ and SVZ was transformed into the present-day central granodiorite-gneiss zone, and the area between the SVZ and the Grenville front became the southern granite-gneiss zone.

Local geology and mineralization

Investigations of the Preissac-Lacorne batholith prior to 1965 have been described by Dawson (1966), and may be summarized as follows. Mapping activities in the area commenced in 1913 (41 years after the discovery of the granites) and geological reports were produced intermittently between 1931 and 1955. The most

important report during this period is that of Tremblay (1950), whose detailed map covers the entire Lacorne pluton and its eastern environs, and who also recognized the zonal distribution of metals in and around the pluton. The last major work was that of Dawson (1966), who described the regional geology, geophysics, geochemistry and geochronology of the batholith. The geological map which appeared in that report is still the most detailed available. However, as is the case with other, more recent maps (Boily et al. 1989; Imreh, 1982), it did not subdivide the monzogranite (adamellite) plutons, which as shown by mapping carried out during the course of the present study, is compositionally zoned from biotite to muscovite monzogranite.

The Preissac-Lacorne batholith has an elliptical shape in plan view and is bounded to the south by the Cadillac fault and the eastward extension of the Porcupine-Destor fault, and to the north by the Manneville fault (Fig. 2). These faults appear to have controlled the emplacement of the batholith along the northern limb of the LaPause anticline into mafic (mainly basalt plus smaller volumes of tuffs and komatiite) and metamorphic rocks of the Kinojevis and Malartic Groups and biotite schist of the Kewagama Group (Tremblay, 1950), which are the oldest rock formations exposed in the vicinity of the batholith.

Rocks distal to the Preissac-Lacorne batholith have been regionally metamorphosed to greenschist facies (Dawson, 1966) and, close to the batholith, display evidence of contact metamorphism. Powell (1994) has mapped biotite, actinolite, hornblende and garnet isograds around the intrusion, and using a garnet-hornblende-epidote-plagioclase-quartz assemblage, calculated the pressure-temperature conditions of contact metamorphism to be between 2.5 and 4 kbar, and range up to 450°C, respectively.

As mentioned earlier, the rock types comprising the Preissac-Lacorne batholith consist of an early suite of gabbro, monzonite, diorite, granodiorite and syenodiorite and a late suite of granite and granitic pegmatite (Fig. 2). Dawson (1966) grouped these intrusions into three massifs (Preissac, Lamotte, Lacorne), which are separated by the biotite schists and other older rocks. Recent mapping by Mulja et al. (1995) has shown that the monzogranitic intrusion in the Preissac massif is restricted mainly to the area

west of Lac Preissac, and that this rock type, in the eastern part of the massif, is different from that in the west. Therefore, throughout this thesis, the western monzogranite in the Preissac massif is designated the Preissac monzogranite, while the eastern equivalent is called the Moly Hill monzogranite after the name of the associated molybdenite deposit.

Cross-cutting relationships between the basic and felsic intrusions are rarely exposed: the pegmatites south of the Lacorne monzogranite cut granodiorite. In contrast, xenoliths of dioritic rocks are rather common at the margin of the Lacorne monzogranite. Radiometric ages of the various rock types of the Preissac-Lacorne batholith show that the monzogranites are 30 Ma younger than the basic intrusions, and that the monzogranite and the pegmatite are of the same age (Table 1).

The only modern petrological studies have been those of Bourne and Danis (1987) and Feng and Kerrich (1992). The former postulated that the Lacorne monzogranite and adjacent basic rocks are cogenetic and that the two rock types formed a reversely zoned pluton. However, the compositional (major- and trace-elements) and age (above) differences between the basic and felsic rocks rule out this genetic relationship. In addition, as will be shown later in this thesis, geochemical studies of the Lacorne monzogranite also do not support the reversed zonation. Feng and Kerrich (1992) postulated that the basic intrusions were products of partial melting of a mantle wedge above a subduction zone, and that the monzogranites originated from partial melting of mature sediments, induced by crustal thickening mentioned earlier. However, this study did not consider the geochemical evolution of the granites or associated pegmatites.

Despite the excellent exposure of the granites and associated deposits, reports and published research papers on economic geology are scanty and date back to the 1950s and 1960s. The molybdenite deposits were described by Rastall (1922), Vokes (1963), and Renault (1963), who suspected a genetic relationship between the granite and molybdenite deposits at Lacorne. Dawson (1974) described the occurrence of columbite-tantalite in pegmatites. Research papers by Norman (1945) and Siroonian et al. (1959) speculated that all the plutonic rocks, including the spodumene pegmatites,

Table 1. Radiometric age determinations of minerals and rocks from the Preissac-Lacorne batholith

Method	Material	Host rock	Ma	Reference
		PREISSAC PLUTON		
U/Pb	K-feldspar	Monzogranite	2697±40	Gariepy and Allegre (1985)
K/Ar	Muscovite	Pegmatite	2540±125	Dawson (1966)
Ar/Ar	Muscovite	Mo-bearing quartz vein	2564±14	Powell (1994)
		LAMOTTE PLUTON		
K/Ar	Biotite	Granodiorite	2450±125	Dawson (1966)
Pb/Pb	Zircon	Monzogranite	2631±20 & 2643±12	Feng and Kerrich (1991)
Ar/Ar	Muscovite	Pegmatite	2565±5	Powell (1994)
		LACORNE PLUTON		
K/Ar	Biotite	Granodiorite	2310±125	Dawson (1966)
K/Ar	Muscovite	Granodiorite	2630±125	Dawson (1966)
U/Pb	Zircon	Granodiorite	2695±65/25	Steiger and Wasserburg (1969)
Nd/Nd	Whole-rock	Granodiorite	2850± ?	DePaolo and Wasserburg (1976)
Pb/Pb	Zircon	Diorite-granodiorite	2675±24 & 2671±4	Feng and Kerrich (1991)
Pb/Pb	Zircon	Monzogranite	2643±4	Feng and Kerrich (1991)
K/Ar	Li-Mica	Pegmatite	2735±125	Dawson (1966)
K/Ar	Muscovite	Pegmatite	2735±125	Dawson (1966)
Ar/Ar	Muscovite	Pegmatite	2615±10 & 2594±7	Feng et al. (1992)

and molybdenite-bearing quartz veins were comagmatic, and were related by fractional crystallization. A subsequent review with some new information is that of Boily et al. (1990) on the metallogeny of the Preissac-Lacorne batholith. The most recent research on ore genesis was a 1989 M.Sc thesis by Havva Taner, who applied fluid inclusion microthermometry to determine the physical and chemical conditions of formation of the molybdenite stockwork deposits at Preissac.

In summary, previous studies have contributed mainly to understanding the general geological setting of the Preissac-Lacorne batholith and determining the chronology of events, but they largely have ignored the detailed geological and petrochemical characteristics of the monzogranites, which, together with their associated mineral deposits, are actually the most significant features of the batholith (Fig. 2). Only one modern study has addressed the origin of mineralization.

METHODS OF INVESTIGATION

To achieve the objectives of this thesis, the research methodology involved the following:

1) mapping and sampling of the monzogranites and pegmatites in order to establish field relations among the various types of monzogranite in the batholith.

2) mineralogical and geochemical (including oxygen isotopes) studies of the representative rocks for the purpose of elucidating petrogenetic relationships among the different types of monzogranite and pegmatite. The crystal-chemistry of columbite-tantalite in various types of pegmatite was used to infer the evolution of pegmatite-forming felsic liquid.

3) studies of fluid inclusions in minerals from the three types of pegmatite, in order to determine the timing and pressure-temperature conditions of fluid saturation in the pegmatites, and the subsequent P-T-x evolution of the fluid. The chemistry of the fluid was constrained by microthermometry, and analysis of trapped and daughter solids from decrepitated fluid inclusions.

ORGANIZATION OF THE THESIS

Following this introduction, chapters 2 and 3 collectively establish the geological framework and geochemical evolution of the Preissac-Lacorne monzogranites, culminating with a proposed model for the petrogenesis of zoned rare-element granitic plutons and of pegmatite-forming felsic liquid. The magmatic evolution of this pegmatite-forming liquid is deciphered through a study of the crystal-chemistry of columbite-tantalite [(Fe, Mn)(Nb, $Ta)_2O_6$] (chapter 4). The compositional evolution of fluids exsolved from the pegmatite-forming liquid, and the conditions during crystallization of the pegmatites are elucidated in the next chapter (5), using data obtained from fluid and solid inclusions in beryl, spodumene and quartz in various types of comagmatic pegmatite. The thesis ends with an epilogue summarizing the magmatic and hydrothermal processes that the felsic magmas underwent in order to produce rare-element-enriched granitic pegmatites.

The locations of samples used in this thesis, mineral and whole-rock compositions, and raw data on fluid inclusion microthermometry and decrepitates are given in the apppendices.

REFERENCES

Boily, M., Pilote, P. and Rallon, H (1989) *La metallogenie des metaux de haute technologie en Abitibi-Temiscamingue.* Publication of Gouvernement du Quebec 89-29.

Boily, M., Williams-Jones, A.E., Mulja, T. and Pilote, P. (1990) Rare-element pegmatites in the Abitibi greenstone belt: a case study of the Preissac- Lacorne batholith. *The Canadian Institute of Mining and Metallurgy Special Volume 43*, 299-311.

Bourne, J. and Danis, D. (1987) A proposed model for the formation of reversely zoned plutons based on a study of the Lacorne complex, Superior Province, Quebec. *Canadian Journal of Earth Sciences*, **24**, 2506-2520.

Breaks, F.W. and Moore, J.M. Jr (1992) The Ghost Lake batholith, Superior province of northwestern Ontario: a fertile, S-type, peraluminous granite-rare-element pegmatite system. *Canadian Mineralogist*, **30**, 835-875.

Burnham, C.W. and Nekvasil, H. (1986) Equilibrium properties of granite pegmatite magma. *American Mineralogist*, **71**, 239-263.

Černý, P. (1992) Rare-element granitic pegmatites. Part I: anatomy and internal evolution of pegmatite deposits. *Geoscience Canada*, **18**, 49-67.

Černý, P. (1982) Petrogenesis of granitic pegmatites. In P. Černý (ed) *Granitic pegmatites in Science and Industry. Mineralogical Association of Canada Short Course Hanbook* **8**, 405-461.

Černý, P. and Meintzer, M. (1988) Fertile granites in the Archean and Proterozoic fields of rare-element pegmatites: crustal environment, geochemistry and petrogenetic relationships. In R.P. Taylor and D.F. Strong (eds.) *Recent advances in the geology of granite-related mineral deposits. The Canadian Institute of Mining and Metallurgy Special Volume* **39**, 170-208.

Chakuomakos, B.C. and Lumpkin, G.R. (1990) Pressure-temperature constraints on the crystallization of the Harding pegmatite, Taos County, New Mexico. *Canadian Mineralogist*, **28**, 287-298.

Damm, K-W., Harmon, R.S., Heppner, P-M. and Dornsiepen, U. (1992) Stable isotope constraints on the origin of the Cabo de Creus garnet-tourmaline pegmatites, Massif des Alberes, Eastern Pyrenees, Spain. *Geological Journal*, **27**, 75-86.

Dawson, K.R. (1966) *A comprehensive study of the Preissac-Lacorne batholith, Abitibi County, Quebec*. Geological Survey of Canada Bulletin **142**.

Dawson, K.R. (1974) *Niobium (columbium) in Canada*. Geological Survey of Canada Economic Geology report **29**.

Desrochers, J-P., Hubert, C., Ludden, J. and Pilote, P. (1993) Accretion of Archean oceanic plateau fragments in the Abitibi greenstone belt, Canada. *Geology*, **21**, 451-454.

Feng, R. and Kerrich, K. (1991) Single zircon age constraints on the tectonic juxtaposition of the Archean Abitibi greenstone belt and Pontiac subprovince, Quebec, Canada. *Geochimica et Cosmochimica Acta*, **55**, 3437-3441.

Feng, R. and Kerrich, K. (1992) Geochemical evolution of granitoids from the Archean Abitibi Southern Volcanic Zone and the Pontiac Subprovince, Superior Province, Canada: implications for tectonic histories and source regions. *Chemical Geology*, **98**, 23-70.

Feng, R., Kerrich, R., McBride, S. and Farrar, E. (1992) $^{40}Ar/^{39}Ar$ age constraints on the thermal history of the Archean Abitibi greenstone belt and the Pontiac Subprovince: implications for terrane collision, differential uplift, and overprinting of gold deposits. *Canadian Journal of Earth Sciences*, **29**, 1389-1411.

Gariépy, C. and Allègre, C.J. (1985) The lead isotope geochemistry and geochronology of late-kinematic intrusives from the Abitibi greenstone belt, and the implications for late Archean crustal evolution. *Geochimica et Cosmochimica Acta*, **49**, 2371-2383.

Goodwin, A.M. and Ridler, R.H. (1970) The Abitibi orogenic belt. In A.J. Baer (ed): *Symposium of Basins and Geosynclines in the Canadian Shield*. Geological Survey of Canada, 1-24.

Heinrich, E.Wm. (1953) Zoning in pegmatite districts. *American Mineralogist*, **38**, 68-87.

Jahns, R. and Burnham, C.W. (1969) Experimental studies of pegmatite genesis: I. A model for the derivation and crystallization of granitic pegmatites. *Economic Geology*, **64**, 843-864.

Imreh, L. (1982) *Sillon de la Motte-Vassan et son avant-pays meridional: syntheses volcanologique, lithostraigraphique et gitologique.* Publication of Ministere de l'Energie et des Ressources 82-04.

London, D. (1987) Internal differentiation of rare-element pegmatites: effects of boron, phosphorous, and fluorine. *Geochimica et Cosmochimica Acta*, **51**, 403-420.

London, D. (1986a) Magmatic-hydrothermal transition in the Tanco rare-element pegmatite: evidence from fluid inclusions and phase-equilibrium experiments. *American Mineralogist*, **71**, 376-395.

London, D. (1986b) Formation of tourmaline-rich gem pockets in mioritic pegmatites. *American Mineralogist*, **71**, 396-405.

London, D., Morgan, G.B. VI. and Hervig, R.L. (1989) Vapor-undersaturated experiments with Macusani glass+H_2O at 200 MPa, and the internal differentiation of granitic pegmatites. *Contributions to Mineralogy and Petrology*, **102**, 1-17.

Ludden, J.N. and Hubert, C. (1986) Geologic evolution of the late Archean Abitibi greenstone belt of Canada. *Geology*, **14**, 707-711.

Ludden, J.N., Hubert, C. and Gariépy, C. (1986) The tectonic evolution of the Abitibi greenstone belt of Canada. *Geological Magazine*, **123**, 153-166.

Mahood, G. and Hildreth, W. (1983) Large partitioning coefficients for trace elements in high-silica rhyolite. *Geochimica et Cosmochimica Acta*, **47**, 11-30.

Miller, C. and Mittlefelhdt, D.W. (1984) Extreme fractionation in felsic magma chambers: a product of liquid-state diffusion or fractional crystallization ? *Earth and Planetary Science Letters*, **68**, 151-158.

Mortensen, J.K. and card, K.D. (1994) U-Pb age constraints for the magmatic and

tectonic evolution of the Pontiac Subprovince, Quebec. *Canadian Journal of Earth Sciences*, **30**, 1970-1980.

Mulja, M., Williams-Jones, A.E., Wood, S.A. and Boily, M. (1995) Geology and mineralogical evolution of rare-element monzogranites and pegmatites in the Preissac-Lacorne batholith, Quebec. *Canadian Mineralogist*, **33**, 000-000.

Nabelek, P.I., Russ-Nabelek, C. and Donison, J. (1992a) Petrologic and geochemical constraints on the petrogenesis of the Proterozoic Harney Peak leucogranite, Black Hills, South Dakota, U.S.A. *Contributions to Mineralogy and Petrology*, **110**, 173-191.

Nabelek, P.I., Russ-Nabelek, C. and Hausseler, T. (1992b) Stable isotope evidence for the petrogenesis an fluid evolution in the Proterozoic harney peak leucogranite, Black Hills, South Dakota. *Geochimica et Cosmochimica Acta*, **56**, 403-417.

Norman, G.W.H. (1945) Molybdenite deposits and pegmatites in the Preissac-Lacorne area, Abitibi County, Quebec. *Economic Geology*, **15**, 1-17.

Norton, J.J. and Redden, J.A. (1990) Relations of zoned pegmatites to other pegmatites, granite, and metamorphic rocks in the southern Black Hills, South Dakota. *American Mineralogist*, **75**, 631-655.

O'Connor, P.J., Gallagher, V. and Kennan, P.S. (1991) Genesis of lithium pegmatites from the Leinster granite margin, southeast Ireland: geochemical constraints. *Geological Journal*, **26**, 295-305.

Powell, W.G. (1994) *A petrological and geochronological study of the metamorphic history of the Rouyn-Noranda area, Quebec.* Unpublished Ph.D thesis, Queen's University, Kingston, Ontario, Canada.

Rastall, R.H. (1922) *Molybdenum ores*. Monographs on mineral resources with special reference to the British Empire, Imperial Institute, London.

Renault, J.R. (1963) Molybdenite paragenesis at the Lacorne mine, Quebec. *Economic Geology*, **58**, 1340-1344.

Roedder, E. (1984) *Fluid Inclusions*. Reviews in Mineralogy **12**, Mineralogical Association of America.

Rugieri, G. and Lattanzi, P. (1992) Fluid inclusion studies of Mt. Capanne

pegmatites, Isola d'Elba, Tuscany, Italy. *European Journal of Mineralogy*, **4**, 1085-1096.

Shearer, D.K., Papike, J.J. and Laul, J.C. (1987) Mineralogical and chemical evolution of a rare-element granite-pegmatite system: Harney Peak granite, Black Hills, South Dakota. *Geochimica et Cosmochimica Acta*, **51**, 473-486.

Shearer, D.K., Pipike, J.J. and Joliff, B.L. (1992) Petrogenetic links among granites and pegmatites in the Harney Peak rare-element granite-pegmatite system, Black Hills, South Dakota. *Canadian Mineralogist*, **30**, 785-809.

Siroonian, H.A., Shaw, D.M. and Jones, R.E. (1959) Lithium geochemistry and the source of the spodumene pegmatites of the Preissac-Lamotte-Lacorne region of western Quebec. *Canadian Mineralogist*, **6**, 320-338.

Steiger, R.H. and Wasserburg, G.J. (1969) Comparative U-Th-Pb systematics in 2.7 x 10^9 yr plutons of different geological histories. *Geochimica et Cosmochimica Acta*, **33**, 1213-1232.

Steward, D.B. (1978) Petrogenesis of lithium-rich pegmatites. *American Mineralogist*, **63**, 970-980.

Taner, H. (1989) *The nature, origin and physicochemical controls of hydrothermal Mo-Bi mineralization in the Cadillac and Preissac deposits, Quebec.* Unpublished M.S.c thesis, McGill university.

Taylor, B.E, Foord, E.E. and Friedrichsen, H. (1979) Stable isotope and fluid inclusion studies of GEM-bearing granite-pegmatite-aplite dikes, San Diego Co., California. *Contributions to Mineralogy and Petrology*, **68**, 187-205.

Thomas, A.V., Bray, C.J. and Spooner, E.T.C. (1988) A discussion of the Jahns-Burnham proposal for the formation of zoned granitic pegmatites using solid-liquid-vapour inclusions from the Tanco pegmatite, S.E. Manitoba, Canada. *Royal Society of Edinburg, Transactions, Earth Sciences*, **79**, 299-315.

Tremblay, L.P. (1950) *Fiedmont Map-area, Abitibi County, Quebec.* Geological Survey of Canada Memoir **253**.

Trueman, D.L. and Černý, P. (1982) Exploration for rare-element granitic pegmatites. In P. Černý (ed) *Granitic pegmatites in Science and Industry,*

Mineralogical Association of Canada Short Course Hand Book **8**. 463-493.

Vokes, F.M. (1963) *Molybdenum deposits of Canada*. Geological Survey of Canada Economic Geology Report **20**.

Withworth, M.P. and Rankin, A.H. (1989) Evolution of fluid phases associated with lithium pegmatites from SE Ireland. *Mineralogical Magazine*, **53**, 271-284.

CHAPTER 2

GEOLOGY AND MINERALOGICAL EVOLUTION OF RARE-ELEMENT MONZOGRANITES AND PEGMATITES IN THE PREISSAC-LACORNE BATHOLITH, QUEBEC

Thomas MULJA, Anthony E. WILLIAMS-JONES,
Scott A. WOOD[1], and Michel BOILY[2]
Department of Earth and Planetary Sciences, McGill University,
3450 University St., Montreal, Quebec, Canada H3A 2A7
[1]Department of Geology and Geological Engineering,
University of Idaho, Moscow, Idaho 83843, U.S.A.
[2]2121 de Romagne, Laval, Quebec, H7M 5P8

ABSTRACT

The monzogranitic plutons in the Preissac-Lacorne batholith (Québec) display geological and mineralogical features that resemble idealized zoned intrusions and associated rare-element quartz veins and pegmatites. The zoning comprises biotite, two-mica, and muscovite monzogranites, and the mineralization in pegmatite-poor plutons is dominated by molybdenite-bearing quartz veins, which are spatially related to the more evolved rocks (i.e. muscovite-bearing monzogranite). In contrast, pegmatite-rich plutons are surrounded by rare-element pegmatites, which vary systematically with distance from the plutons from beryl-bearing through spodumene-beryl-bearing to spodumene-bearing. In addition, Mo-bearing albitite dikes and quartz veins occur beyond the spodumene pegmatites. Mineralogical changes from biotite to muscovite monzogranite are characterized by a decrease in the abundance of oligoclase, biotite, magnetite, monazite, apatite, and zircon, and an increase in the abundance of albite, muscovite and garnet. The mineralogical trend continues into the pegmatites, which are composed of albite, K-feldspar, quartz, muscovite (biotite is absent), garnet, beryl, spodumene, molybdenite, and columbite-tantalite. The major element chemistry of the rock-forming minerals changes progressively from biotite through two-mica to muscovite monzogranite; plagioclase compositions vary from An_{13-17} to An_6, the Fe/(Fe + Mg) of biotite and muscovite increases from 0.7 to 0.85 and from 0.65 to 0.85, respectively. This mineral-chemical evolution extends into the pegmatites; the plagioclase in these rocks is almost pure albite (An_{1-5}), and muscovite is lower in Fe/(Fe + Mg) and richer in Al than that in the muscovite monzogranite. Concentrations of Cs, Ta, and Rb in muscovite increase, whereas Sc decreases, from the muscovite monzogranite to the rare-element pegmatites. The systematic mineralogical evolution and mineral-chemical trends, and the field relationships of the monzogranites are interpreted to indicate that the various subtypes of monzogranite were produced mainly by fractional crystallization of biotite monzogranitic magma. Further differentiation of the fractionated monzogranitic melts produced rare-element pegmatites.

Keywords: rare-element monzogranite, beryl and spodumene pegmatites, geology, mineralogy, mineral chemistry, Preissac-Lacorne batholith (Quebec).

INTRODUCTION

Petrologically zoned rare-metal (e.g. Be, Li, Nb, Ta, Sn)-enriched granitic intrusions have been described by a number of investigators, and a model has been developed in which fractional crystallization of biotite monzogranitic melt gives rise to successive residual melts of two-mica and muscovite monzogranite, and rare-metal pegmatites (e.g. Goad & Černý 1981, Černý et al. 1986, Shearer et al. 1987, 1992, Simmons et al. 1987, Breaks & Moore 1992). However, there are few examples where all the model facies are exposed. Consequently, details of the process of differentiation have been poorly documented, and the specific factors responsible for the concentration of the rare metals to economic levels remain largely unknown.

The Preissac-Lacorne batholith hosts well-exposed monzogranitic plutons, which vary systematically from a least evolved biotite monzogranite, through a two-mica, to a most evolved muscovite monzogranite, and are associated with rare-metal (Be, Li, Nb, Ta, Mo) pegmatites, albitites, and molybdenite-bearing quartz veins. These plutons thus afford an unusually fine opportunity to investigate the causes of zonation of rare-metal-bearing monzogranites, the petrogenetic relationships between the monzogranites and the later pegmatites, albitites and quartz veins, and the rare-metal enrichment processes. This paper, which is the first in a series of contributions dealing with the metallogeny of the batholith, discusses the geology and mineralogical and mineral-chemical evolution of the monzogranitic plutons and associated pegmatites, and the physical conditions of emplacement of the intrusion. A companion paper (Mulja et al. 1995) documents the geochemical evolution of the plutons and confirms the genetic relationship of the pegmatites to the monzogranites.

GEOLOGICAL SETTING

The Preissac-Lacorne batholith, located about 600 km northwest of Montréal (Fig. 1), is a syn- to post-tectonic intrusion that was emplaced in the Southern Volcanic Zone of the Archean Abitibi Greenstone Belt in the Superior Province of the Canadian

Fig. 1. A simplified geological map of the Preissac-Lacorne batholith (modified from Dawson 1966) showing the locations of monzogranitic plutons and regional structures. The Porcupine-Destor fault is located south of Lac Preissac and joins the east-west trending Cadillac fault further in the south. The boundaries of the plutons are based on the outermost occurrence of small and scattered monzogranite outcrops. The basic and intermediate plutonic rocks (gabbro, diorite, monzonite and granodiorite) are believed to extend as far as 10 km east and 15 km south of the Lacorne pluton.

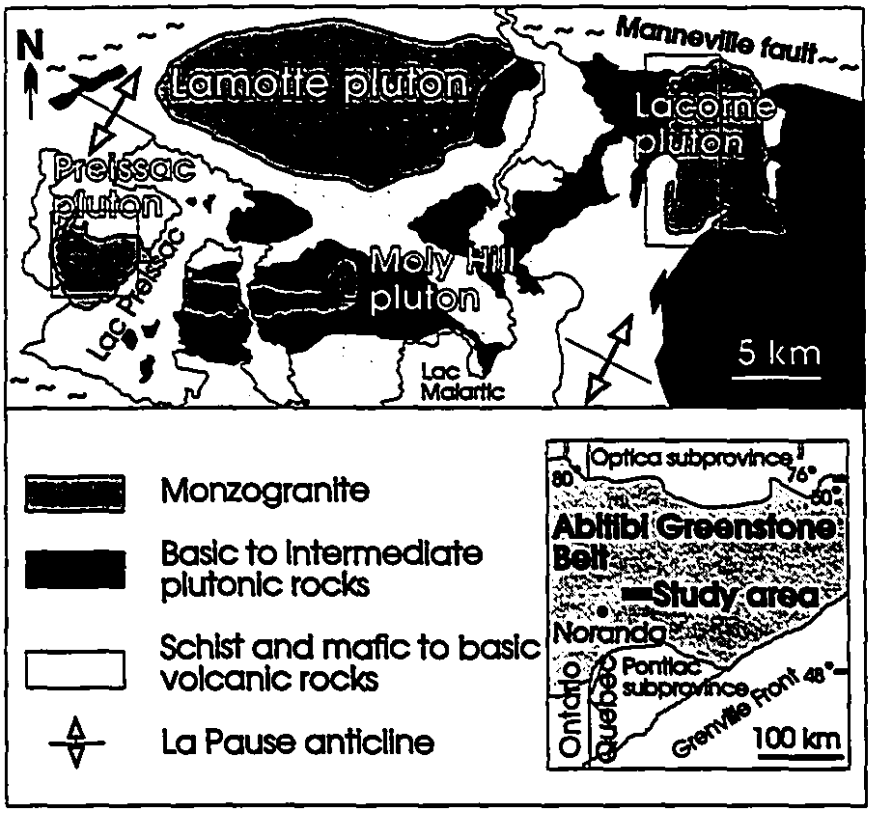
N
Lamotte pluton
Manneville fault
Lacorne pluton
Preissac pluton
Lac Preissac
Moly Hill pluton
Lac Malartic
5 km
Monzogranite
Basic to intermediate plutonic rocks
Schist and mafic to basic volcanic rocks
La Pause anticline
Opatica subprovince
80°
76°
60°
Abitibi Greenstone Belt
Study area
Noranda
Pontiac subprovince
48°
Ontario
Quebec
Grenville Front
100 km

Figure 1

shield. Previous work, especially that of Dawson (1966), has shown that the batholith intruded along the La Pause anticline into ultramafic to basic lavas of the Kinojevis (2718 Ma; Corfu 1993) and Malartic groups, and biotite schist of the Kewagama Group. To the north, the batholith is bounded by the Manneville fault, and to the south, by the Cadillac fault and the eastward extension of the Porcupine-Destor fault, which separates the batholith from the Pontiac Subprovince in the south. Gravity measurements indicate that the shape of the batholith resembles an outward-dipping, asymmetrical saddle with its highest points south of the center of the body, and suggest that the base of the batholith is probably at a depth of about 5 km (Dawson 1966).

The batholith is a composite body (Fig. 1), comprising early metaluminous gabbro, diorite, monzonite and granodiorite (ca. 2650 - 2760 Ma, Steiger & Wasserburg 1969; Feng & Kerrich 1991), and four late peraluminous monzogranitic plutons (Preissac, Moly Hill, Lamotte, and Lacorne) and associated pegmatites and quartz veins (ca. 2621-2655 Ma: Gariépy & Allègre 1985, Feng & Kerrich 1991). Intrusive activity in the region terminated with the emplacement of northeast-trending Proterozic diabase dikes. Contact metamorphism of the country rocks increased the grain size of both the volcanic rocks and biotite schist. The former is characterized by coarse-grained hornblende, magnetite and pyrite, and the latter by sillimanite, epidote, and cordierite.

The Preissac-Lacorne batholith is believed to have formed during the waning stages of the development of the Abitibi Greenstone Belt (Dimroth et al. 1983, Feng & Kerrich 1992, Sutcliffe et al. 1993), which involved the collision of continents in a convergent plate setting. The basic igneous rocks in the batholith are interpreted to be products of partial melting of a mantle wedge above a subduction zone, and the monzogranites to be products of partial melting of the Pontiac Subprovince sedimentary rocks (e.g. greywacke), induced by crustal thickening associated with the collision of the Pontiac Subprovince with the Southern Volcanic Zone of the Abitibi Greenstone Belt.

FIELD RELATIONSHIPS AND PETROGRAPHY OF THE MONZOGRANITE

Our detailed mapping and petrography indicate that the monzogranite is mineralogically and geologically divisible into biotite, two-mica, and muscovite subtypes (Figs. 2A-D). Biotite monzogranite is distinguished from the other monzogranites by the presence of up to 5 volume % biotite and by the lack of primary muscovite. The two-mica monzogranite has a preponderance of muscovite (2:1), and the muscovite monzogranite contains little or no biotite. In the case of the Preissac pluton, there is an additional monzogranite (muscovite-garnet), which occurs as fine-grained dikes, and differs from the other monzogranites by containing up to 3 volume % garnet, 5 volume % muscovite, and no biotite.

All the subtypes of monzogranite have similar proportions of interlocking anhedral quartz (25 - 35 %), euhedral to subhedral plagioclase (30 - 45 %), and perthitic to microperthitic K-feldspar (25 - 45 %). Plagioclase is the earliest major mineral to have crystallized; inclusions of this mineral are present in K-feldspar. A few plagioclase grains in biotite monzogranite have corroded cores with sericite flakes, and resemble restite plagioclase described by Chappel et al. (1987). However, this restite interpretation has been challenged by Wall et al. (1987), who argued that such corroded cores could represent formerly high temperature calcic-rich plagioclase which became unstable when the magma cooled. Moreover, geochemical evidence (Mulja et al. 1995) does not indicate that restite-unmixing could produce the petrological variations of the monzogranite. Quartz is anhedral, interstitial, and some grains contain inclusions of biotite and muscovite, suggesting its late crystallization.

Minor minerals include biotite, muscovite, epidote, and garnet. Magnetite, ilmenite, apatite, zircon, monazite, xenotime, and titanite are accessory minerals, which occur either as inclusions in the major or minor silicate phases, or are interstitial to them (Fig. 3). The distribution of both minor and accessory minerals changes systematically from biotite through two-mica to muscovite monzogranite (Fig. 4). The exceptions to this are xenotime and ilmenite, which have similar abundances in all subtypes of monzogranite. The contents of biotite, epidote, magnetite, ilmenite, apatite,

Figs. 2A, B & C. Geological maps of the Preissac (A), Moly Hill (B) and Lamotte (C) plutons showing the field relationships of the various subtypes of monzogranite and the mineral deposits. In the Preissac pluton, the biotite monzogranite (BG) rims a small part of the muscovite monzogranite in the north, and the muscovite-garnet monzogranite (MGG) occurs as dikes in the northeast corner of the muscovite monzogranite (details in text). Two former molybdenite mines (Mo) are the Preissac in the north and the Cadillac in the southeast. The biotite monzogranite in the Moly Hill pluton occurs as a small hill, the two-mica monzogranite as a flat-lying outcrop, and the muscovite monzogranite as a crest-like mass. The small transitional monzogranite has a mineralogy between two-mica and muscovite monzogranites. The Lamotte pluton has an asymmetrical normal zonation. A large part of this pluton consists of small granitic outcrops, which define the intrusive boundary. Be and Spd are beryl- and spodumene-bearing pegmatites, respectively.

2D. A geological map and an aerial (mosaic) photograph of the Lacorne pluton covering the western part of the intrusion where the main outcrops are exposed. Like the Lamotte pluton, small undifferentiated granitic rocks were taken as the boundary of the pluton (Fig. 1). The northern boundary of the biotite monzogranite is approximately a few hundred meters north of the gravel road. The Québec lithium (QL) mine is about 10 km east of the margin of this photograph. Other spodumene-bearing pegmatites and molybdenite-bearing quartz veins are located about 2.5 km south of the pluton. The northeast trending diabase dike is shown by dashed lines. Abbreviations are similar to those of Fig. 2A; the others shown here are: V, Valor (prospect name); GD, granodiorite; MG2, muscovite monzogranite dike (details in text); MBP, mass beryl pegmatite; P, pegmatite; AB, albitite dike; SV: biotite schist and mafic volcanic rocks (abitibi "greenstone" rocks). Mineral abbreviations: Brl, beryl; Spd, spodumene; Mo, molybdenite.

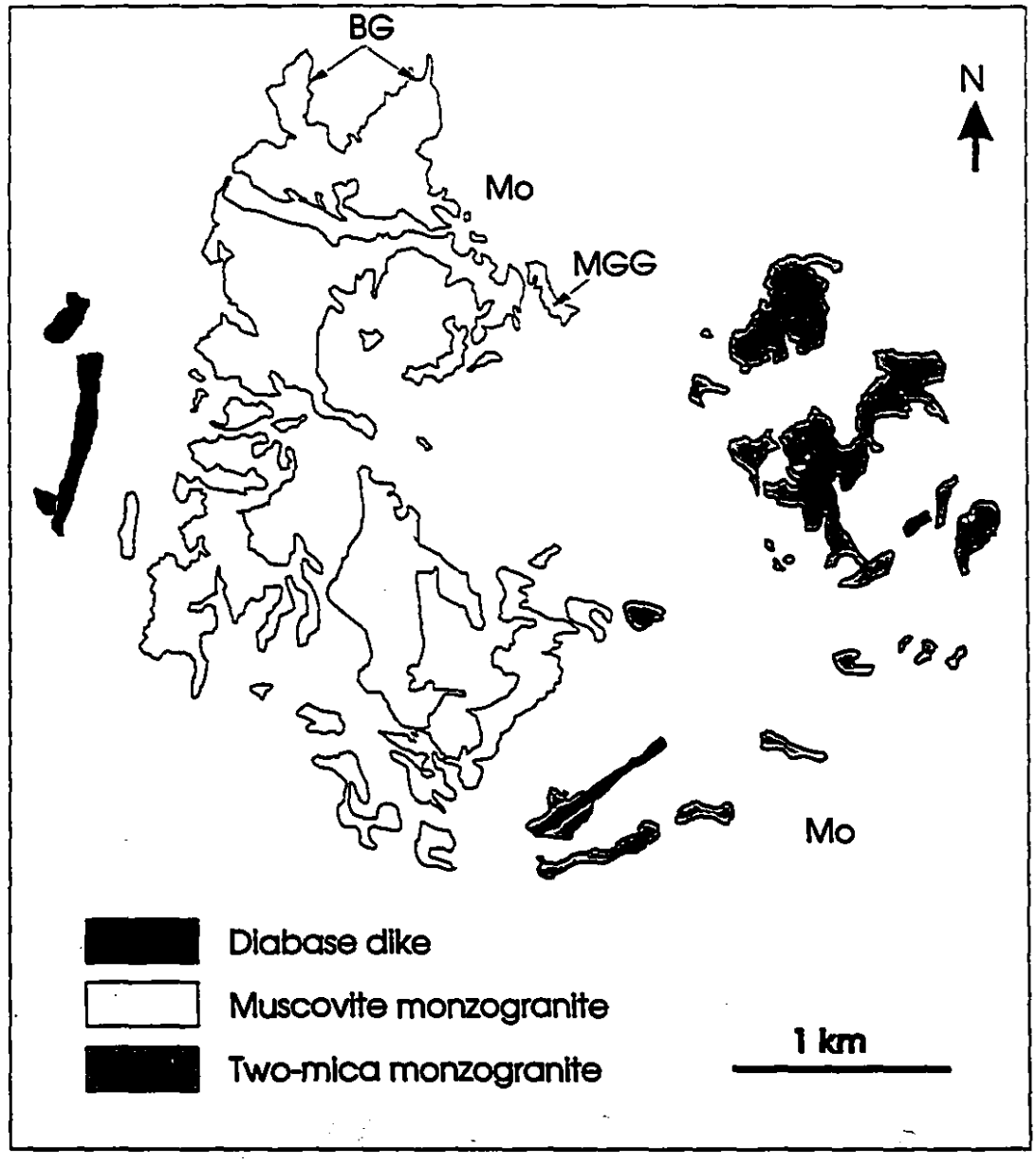
BG
N
Mo
MGG
Mo
Diabase dike
Muscovite monzogranite
Two-mica monzogranite
1 km

Figure 2A

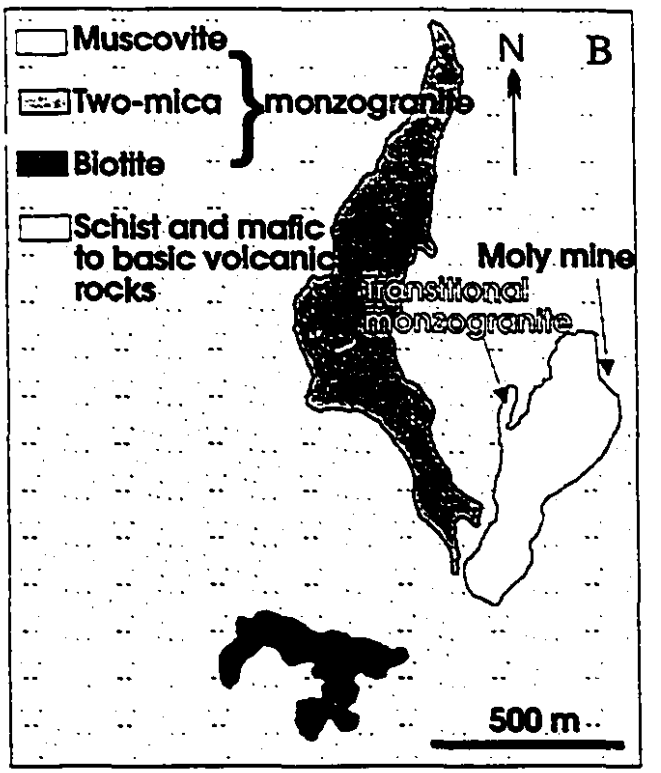
Muscovite
Two-mica
monzogranite
Biotite
Schist and mafic
to basic volcanic
rocks
N
B
Moly mine
Transitional
monzogranite
500 m

Figure 2B

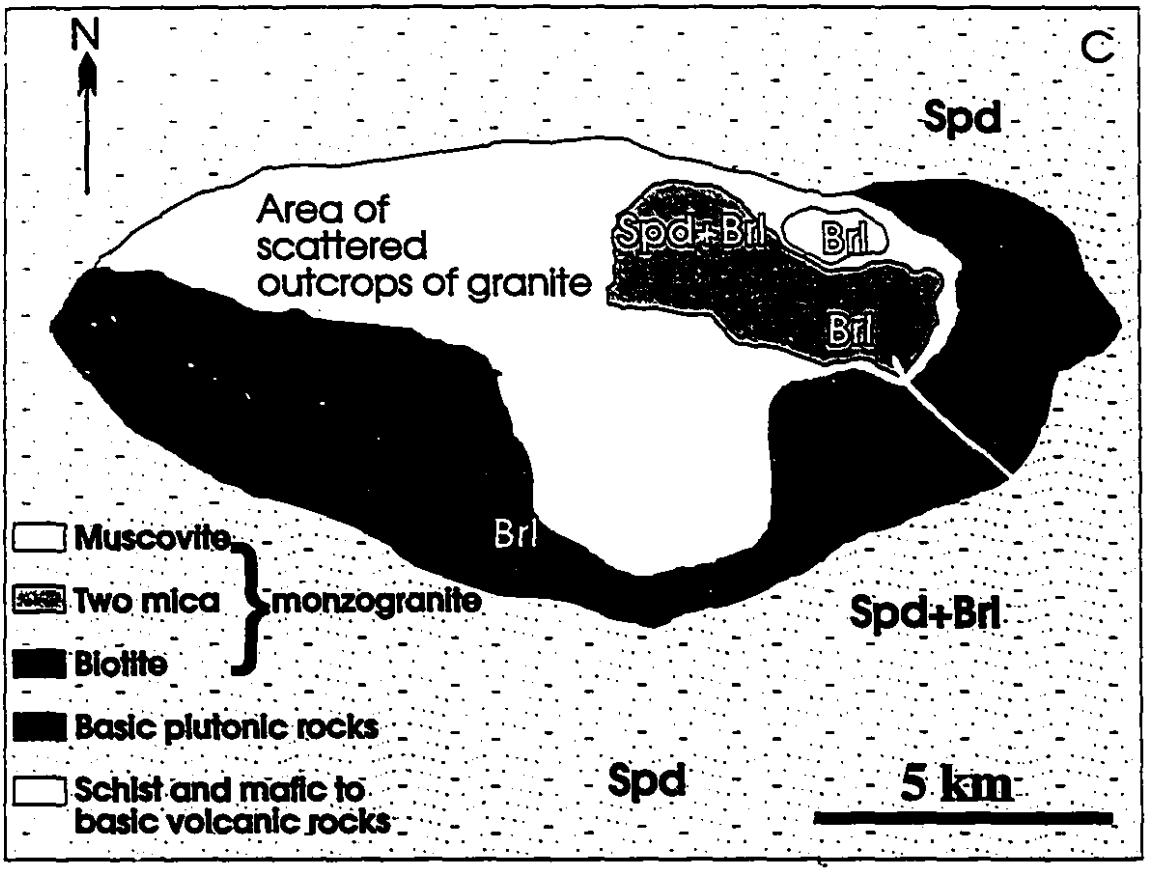
N
C
Spd
Area of
scattered
outcrops of granite
Spd+Brl
Brl
Brl
Brl
Spd+Brl
Muscovite
Two mica
monzogranite
Biotite
Basic plutonic rocks
Schist and mafic to
basic volcanic rocks
Spd
5 km

Figure 2C

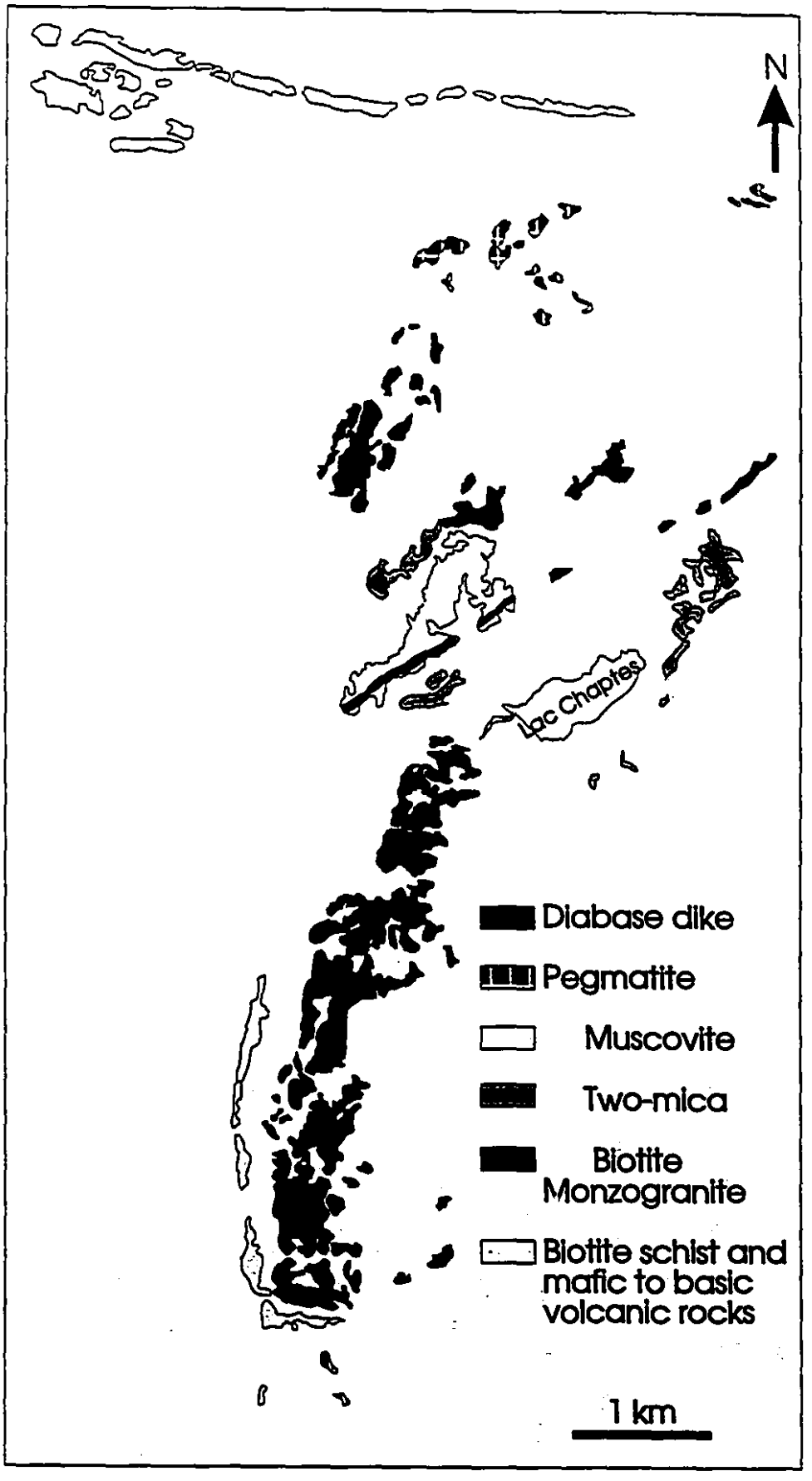
N
Lac Chaptes
Diabase dike
Pegmatite
Muscovite
Two-mica
Biotite
Monzogranite
Biotite schist and
mafic to basic
volcanic rocks
1 km

Figure 2D

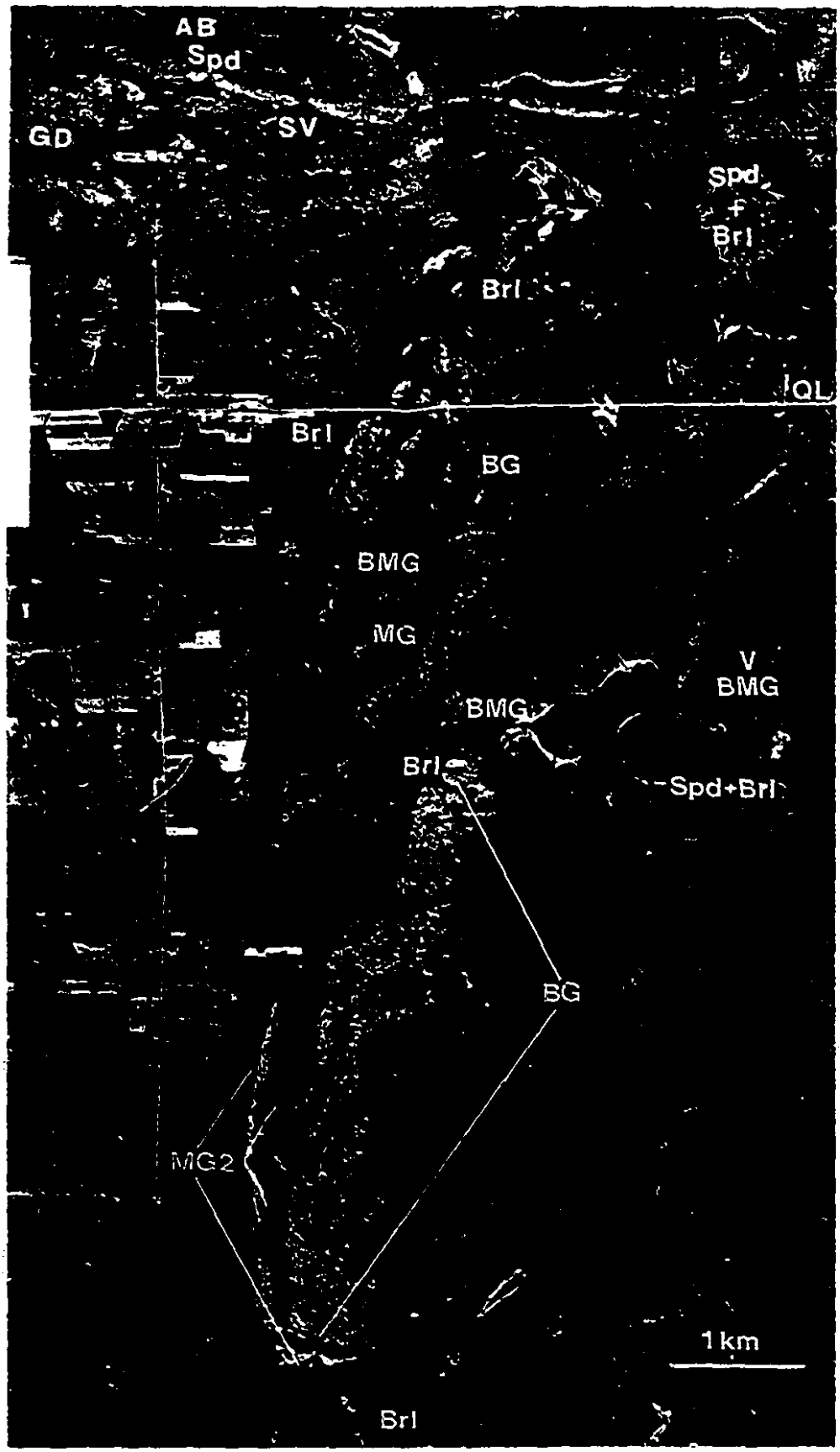
AB
Spd
SV
GD
Spd
+
Brl
Brl
QL
Brl
BG
BMG
MG
V
BMG
BMG
Brl
Spd+Brl
BG
MG2
1 km
Brl

Fig. 3. Photomicrographs of minor and accessory minerals (determined with an EDS-SEM) in the monzogranites. A. Inclusion biotite (Bt) in sharp contact with muscovite (Ms) in quartz (Qtz) (TM-766). To the right of the micas is a plane of fluid inclusions. B. Cross-cutting biotite and muscovite, and interstitial epidote (Ep) (TM-782). Zircon (Zrn) inclusions with halos are present in the micas. Relict biotite is contained in the cross-cutting secondary muscovite (see text for explanation). C. Coarse-grained euhedral magmatic muscovite displaying sharp contacts with the adjacent quartz, plagioclase (Pl) and K-feldspar (Kfs) (TM-652). D. Euhedral interstitial garnet (Grt) in biotite monzogranite (TM-672). E. Anhedral, skeletal garnet intergrown with quartz in two-mica monzogranite located near a fracture (TM-797). F. Subhedral magnetite (Mag) partly enclosed in K-feldspar and adjacent albite (Ab) (TM-40). G. A euhedral inclusion of ilmenite (Ilm) in quartz. Planes of fluid inclusions occur nearby. H. A corroded spodumene xenocryst enclosed in plagioclase. All scale bars are 100 μm.

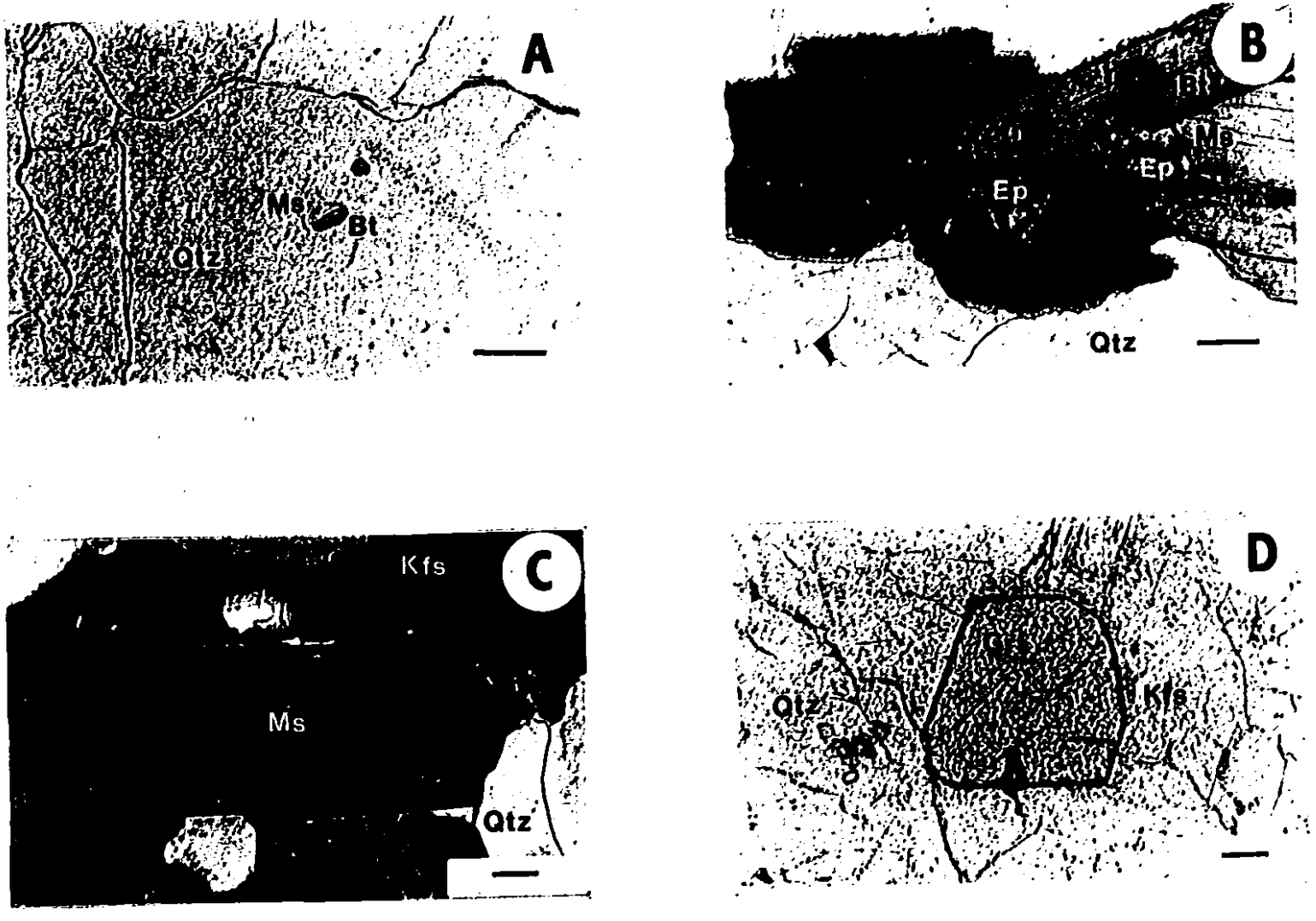
A
Ms
Bt
Qtz
B
Ep
Ep
Ms
Qtz
C
Kfs
Ms
Qtz
D
Qtz
Kfs


E
Qtz

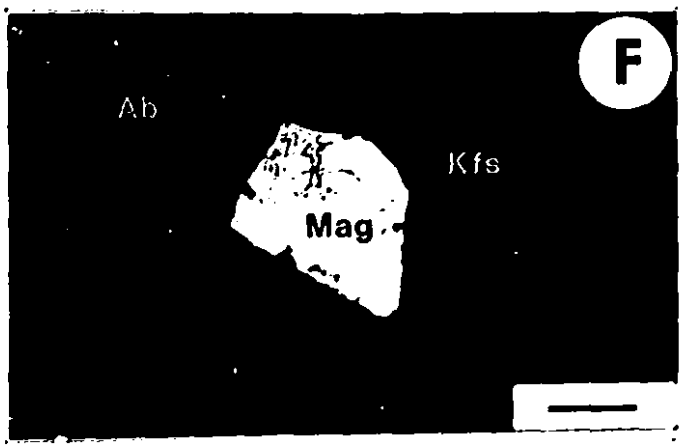
F
Ab
Kfs
Mag

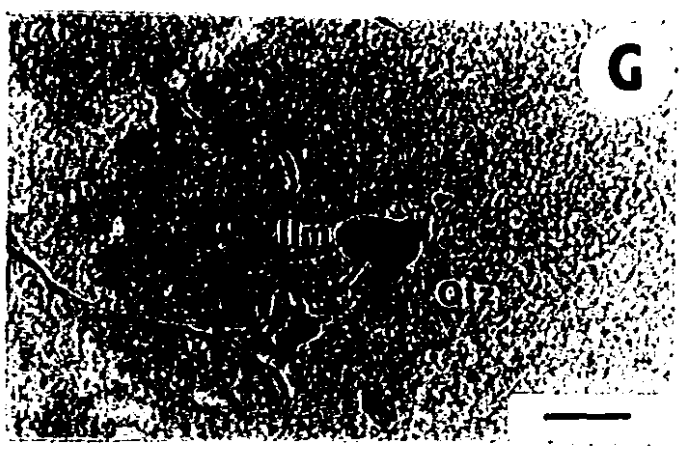
G
Ilm
Qtz

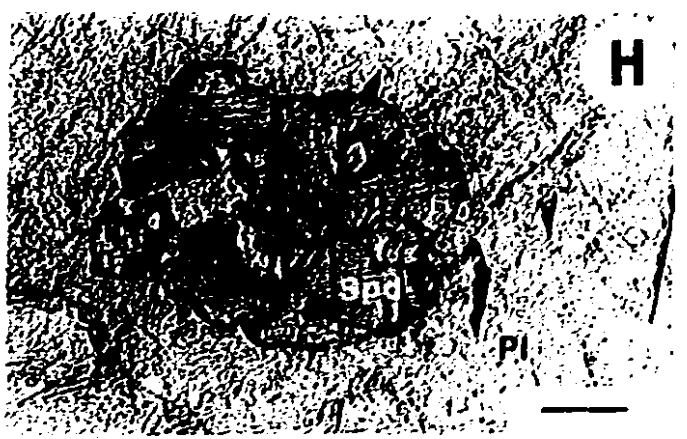
H
Spg
Pl

Fig. 4. The paragenesis of minor and accessory minerals commonly found in the monzogranites, pegmatites, albitites and quartz veins. The widths of the lines indicate the relative abundance (point-counting) of the minerals. Bt: biotite, Ep: epidote, Grt: garnet, Ms: muscovite, Mag: magnetite, Ilm: ilmenite, Ap: apatite, Zrn: zircon, Mnz: monazite, Xe: xenotime, Ttn: titanite, Mo: molybdenite, Ct: columbite-tantalite, Brl: beryl, Spd: spodumene. Dashed lines for spodumene indicate that the mineral is a xenocryst. Not shown are traces of hematite, which occurs with quartz in veinlets that cut the plutons, allanite in the Lamotte biotite monzogranite, rutile, and small grains of tourmaline, pyrophanite ($MnTiO_3$) and gahnite ($ZnAl_2O_4$) in pegmatites.

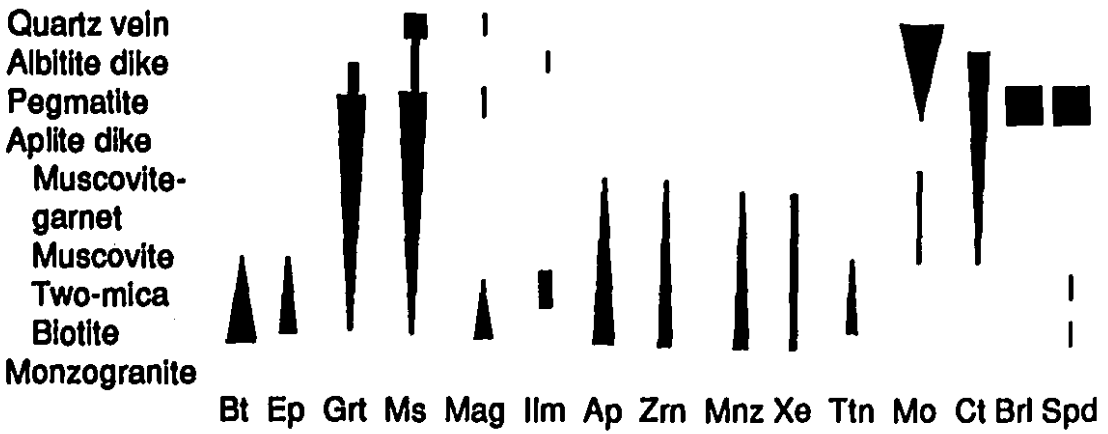
Quartz vein
Albitite dike
Pegmatite
Aplite dike
Muscovite-garnet
Muscovite
Two-mica
Biotite
Monzogranite
Bt Ep Grt Ms Mag Ilm Ap Zrn Mnz Xe Ttn Mo Ct Brl Spd

Figure 4

zircon, monazite, and titanite (in some cases titanite is Nb-bearing) decrease gradually, whereas those of muscovite and garnet increase, from the biotite monzogranite, through the two-mica monzogranite, to the muscovite monzogranite. Molybdenite, columbite-tantalite, and sphalerite were observed only in the muscovite and muscovite-garnet monzogranites and in pegmatites. Some plagioclase and K-feldspar crystals are replaced partially by muscovite, and some biotite flakes by chlorite ± ilmenite ± rutile, muscovite, or epidote.

The Preissac pluton is exposed as an asymmetrical dome having dips which are steeper to the west and north than to the east and south (Fig. 2A). The pluton is composed mostly of two-mica and muscovite monzogranites: the former ranges from coarse- to medium-grained, and the latter is generally medium-grained in the south and fine-grained in the north; these two major outcrops of muscovite monzogranite are separated by a wide fracture (see below). Contacts between the two subtypes of monzogranite are not exposed. At the margins of the pluton, monzogranite lenses locally intermingle with biotite schist, which was recrystallized as a result of contact metamorphism. A subtle foliation has been observed along the northeastern margin, where muscovite in the pluton is oriented parallel to the contact. Fine-grained biotite monzogranite occurs as a thin marginal facies at the northern tip of the pluton, where it grades sharply into the muscovite monzogranite or is separated from the latter by irregular quartz + K-feldspar veins. Dikes (up to 3-m wide) of muscovite-garnet monzogranite, with vugs containing molybdenite and pyrite, intruded the northeastern margin of the pluton (Fig. 2A). The dikes appear to represent the youngest phase of monzogranite-related igneous activity, as they cut both the Mo-bearing quartz veins and pod-shaped pegmatites.

The muscovite monzogranite developed extensive fractures or joints that strike mostly east and southeast with steep dips (Fig. 2A). No slickensides were observed in most of the major fractures. Dawson (1966) suggested that these nearly parallel fractures were formed by tension in a north-south direction. Some of the fractures are occupied by barren pegmatites, and barren and Mo-bearing quartz veins. Economic molybdenite-bearing quartz veins form a stockwork immediately north of the dikes

(Preissac Mine), and another close to the southern margin of the pluton (Cadillac Mine).

The Moly Hill pluton is exposed in three main separated outcrops, consisting of massive fine - to medium- grained biotite monzogranite, foliated medium-grained two-mica monzogranite and muscovite monzogranite (Fig. 2B). The muscovite monzogranite includes a small body of two-mica monzogranite with gradational contacts. The boundary with the biotite schist in the northern two-mica monzogranite varies from sharp to irregular as a result of randomly oriented networks of quartz veinlets in the monzogranite and biotite schist. At their present level of exposure, the three rock types form a horst and graben-like structure, in which the two-mica monzogranite is the down-thrown block. However, cataclastic texture was not observed in the marginal part of any of three monzogranites, indicating that the field relations among the monzogranites are not due to faults. Instead, thermally metamorphosed biotite schist and basalt occur along the contacts between the two-mica monzogranite and the muscovite monzogranite, and a foliation defined by the micas developed in the two-mica and muscovite monzogranites. The field relationships and mineral fabric suggest that intrusion of the monzogranitic magma was fracture-controlled.

A quartz-vein type of Mo deposit is situated between the eastern margin of the muscovite monzogranite and mafic volcanic rocks. This muscovite monzogranite is finer-grained than that in the main mass. Although the mafic rocks are not exposed, its existence can be inferred from inclusions of altered mafic rocks along the walls of subhorizontal quartz veins. Irregularly zoned, east-west-trending pegmatite and aplite dikes cut the biotite monzogranite.

The Lamotte pluton is asymmetrically zoned, and grades inwards from porphyritic to coarse-grained biotite monzogranite at the margins to medium-grained two-mica monzogranite and muscovite monzogranite (Fig. 2C). Contacts between the various subtypes of monzogranite were not observed. The contact with the biotite schist is characterized by complex mixing of aplites and pegmatites in the east, by a concentration of irregular Mo-bearing quartz veins in the south, and by a contact metamorphic zone containing cordierite, garnet, staurolite and sillimanite in the north (Dawson 1966). Xenoliths of partially digested biotite schist are present along the

eastern margin of the two-mica monzogranite.

Samples of biotite and two-mica monzogranite taken near the contact with the biotite schist contain anhedral crystals of spodumene (Fig. 4H) and anhedral aggregates of spodumene, altered biotite, K-feldspar, and quartz. The modes of occurrence of these crystals and crystal aggregates, and disequilibrium textural relationships with other minerals in the rocks, suggest that they are xenocrysts and xenoliths, respectively.

The Lacorne pluton has a north-south oriented elliptical plan, and is dominated by biotite monzogranite, which gives way inwards, to two-mica and muscovite monzogranite (Fig. 2D). No contacts between these subtypes of monzogranite were observed, except that between the biotite and two-mica monzogranite in the north, which is gradational; contacts with the biotite schist are sharp. A dike-like muscovite monzogranite intrusion, separated from the main mass by faults, crops out in the southern part of the pluton. The various subtypes of monzogranite are generally medium-grained, except along the northwestern margin, where the biotite monzogranite is fine-grained and foliated, and probably represents a chilled margin, and in the east where the discrete two-mica monzogranite (labeled Valor, Fig. 2D) is finer-grained and has a whiter hue. In addition, the dike-like muscovite monzogranite differs from the muscovite monzogranite in the main body by the absence of biotite and heterogeneous texture. Xenoliths of diorite and biotite schist occur in the pegmatites in the northwest, and in the dike-like muscovite monzogranite in the south, respectively.

Pegmatites and albitites. Over 1600 barren and mineralized pegmatites have been recorded in the study area (Dawson 1966), and they cut all subtypes of monzogranite and adjacent country rocks. The pegmatites generally strike east-west and range in dip from vertical to subhorizontal. The mineralogy of the barren pegmatites is similar to that of the muscovite monzogranite, except that biotite is absent and garnet is more abundant. Mineralized or rare element-bearing pegmatites are associated with the Lamotte and Lacorne plutons and vary from beryl-bearing at the margins of the plutons, to spodumene-bearing in the country rocks (Figs. 2C & D). In addition, the pegmatites host significant amounts of columbite-tantalite, and subordinately, tourmaline and molybdenite.

The rare-element pegmatites display internal textural variations. A simple zoned pegmatite typically consists of an aplite border zone and a pegmatite core. In a very rare case the two units form a layered-like intrusion, in which each pegmatite consists of an aplite footwall and a pegmatite hanging wall. Complex beryl pegmatites are typically zoned from the margin to center as follows: (1) border zone aplite, (2) muscovite + albite + quartz + beryl, (3) perthite + quartz + beryl, (4) perthite + quartz, (5) massive quartz. Spodumene pegmatites, which normally do not contain beryl or have very little beryl, are massive (i.e. no clear internal zonation) or zoned. The latter pegmatites, which have mineralogical zonation similar to that of the beryl pegmatite, contain spodumene in zones 2 to 5. A transitional spodumene-beryl pegmatite is characterized by beryl fringes only along the border between zones 1 and 2, spodumene in zones 2 to 5, cleavelandite and lepidolite in zones 3-4.

Molybdenite- and columbite-tantalite-bearing albitite dikes and Mo-bearing quartz veins occur beyond the spodumene pegmatite zone to the north and south of the Lacorne pluton, respectively. The dikes vary from 20 cm to 1 m wide, have an east-west strike (parallel to the joints of the country rocks) and dip steeply (about 75 degrees to the south). They consist almost of entirely of albite (Ab_{99}), appreciable amounts of molybdenite and columbite-tantalite, and traces of zircon and Ta-bearing ilmenite.

MINERAL CHEMISTRY

Analytical methods: The compositions of silicate and oxide minerals were determined with an automated CAMECA electron microprobe. The operating conditions were 15 kV acceleration voltage, 8 nA (10 nA for garnet) beam current, a 2 μm spot size (defocused to about 6 μm for feldspar), and 25 second counting times (60-75 seconds for fluorine). Mineral standards used were albite (Na), orthoclase (Al, K, Si), diopside (Ca, Mg), andradite and magnetite (Fe), spessartine (Mn, Si, Al in garnet analyses), fluorite (F), and synthetic MnTi (Mn, Ti). Data reduction was accomplished with full PAP correction procedures (Pouchou & Pichoir 1984).

Muscovite separates were analyzed by Bondar-Clegg laboratory, Ottawa, for Cs, Ta, Sc, and Rb using instrumental neutron activation analysis, Li using atomic absorption spectrometry, and F using an ion-selective electrode.

Plagioclase

Plagioclase compositions typically range from An_{15} in the biotite monzogranite to An_7 in the muscovite monzogranite, and less than An_5 in the pegmatites (Table 1; Fig. 5). Exceptions to this are plagioclase phenocrysts in the Lamotte biotite monzogranite which have a composition of $An_{17.5}$, and plagioclase in both the biotite monzogranite and muscovite monzogranite of the Preissac pluton, which have compositions of An_8, and $An_{3.7}$, respectively. Muscovite-garnet monzogranite which, as noted above, occurs only in the Preissac pluton, contains plagioclase which has an average composition of An_3.

In addition to the composition of the plagioclase varying with the subtype of monzogranite, it also varies spatially, i.e., in the Lacorne biotite monzogranite the An content of plagioclase decreases from the margins inward (Fig. 6), and in the Preissac muscovite monzogranite and the Moly Hill two-mica monzogranite, plagioclase generally becomes more sodic northwards and eastwards, respectively.

K-feldspar

As noted earlier, the K-feldspar is perthitic. K-feldspar domains in perthite have a narrow range of composition, from $Or_{95}Ab_4An_1$ to $Or_{98}Ab_2$ (Table 2), and do not show any significant compositional variations with rock type, sample location, or paragenesis. Most contain less than 0.1 wt. % CaO. Bread beam (10 μm) analyses of perthite including the albite lamellae yielded a composition of $Or_{89}Ab_{11}$ (Sample 24, Table 2). The high Or-content of the K-feldspar indicates that it re-equilibrated at post-magmatic conditions.

Biotite

Biotite is either early, forming inclusions in quartz and to a lesser extent

TABLE 1. REPRESENTATIVE COMPOSITIONS OF PLAGIOCLASE

	Biotite monzogranite				Two-mica monzogranite				Muscovite monzogranite				MGG*
Pluton**	PR	MH	LM	LC	PR	MH	LM	LC	PR	MH	LM	LC	PR
Sample	402	29	782	614	903	31	766	652	302	12	101	684	473
SiO_2	67.28	65.41	65.31	65.07	66.31	66.46	66.1	66.46	67.44	66.05	66.12	66.94	67.45
Al_2O_3	20.35	21.61	22.29	21.43	20.87	20.98	22.11	21.31	20.56	20.89	21.6	20.83	20.27
Na_2O	10.71	9.86	9.51	10.07	10.05	9.95	9.68	10.3	10.81	10.68	10.28	10.45	11.18
K_2O	0.06	0.15	0.2	0.09	0.19	0.13	0.1	0.12	0.14	0.14	0.19	0.07	0.07
CaO	1.38	3.15	3.68	2.75	2.22	3.15	2.33	2.5	1.87	1.31	2.47	1.77	0.97
Total	99.78	100.2	100.9	99.41	99.64	100.7	100.3	100.7	100.8	99.07	100.7	100.1	99.94
Number of cations on the basis of 8 oxygen atoms													
Si	2.949	2.874	2.85	2.879	2.917	2.902	2.885	2.998	2.935	2.919	2.887	2.929	2.953
Al	1.052	1.119	1.463	1.118	1.083	1.08	1.137	1.096	1.055	1.088	1.112	1.074	1.046
Na	0.911	0.84	0.804	0.864	0.858	0.842	0.819	0.872	0.912	0.915	0.870	0.887	0.949
K	0.004	0.008	0.011	0.005	0.011	0.75	0.005	0.007	0.008	0.008	0.010	0.004	0.004
Ca	0.065	0.148	0.172	0.13	0.105	0.147	0.109	0.117	0.087	0.062	0.115	0.083	0.045
End members Mol. %													
Ab	93	84	81	86	88	84	88	87	90	93	87	91	95
Or	0.4	1	1	1	1	1	1	1	1	1	1	0.5	0.5
An	6.6	15	18	13	11	15	11	12	9	6	12	8.5	4.5

* Muscovite-garnet monzogranite

** PR: Preissac, MH: Moly Hill, LM: Lamotte, LC: Lacorne

Fig. 5. Molecular proportions of albite (Ab), anorthite (An) and orthoclase (Or) in plagioclase.

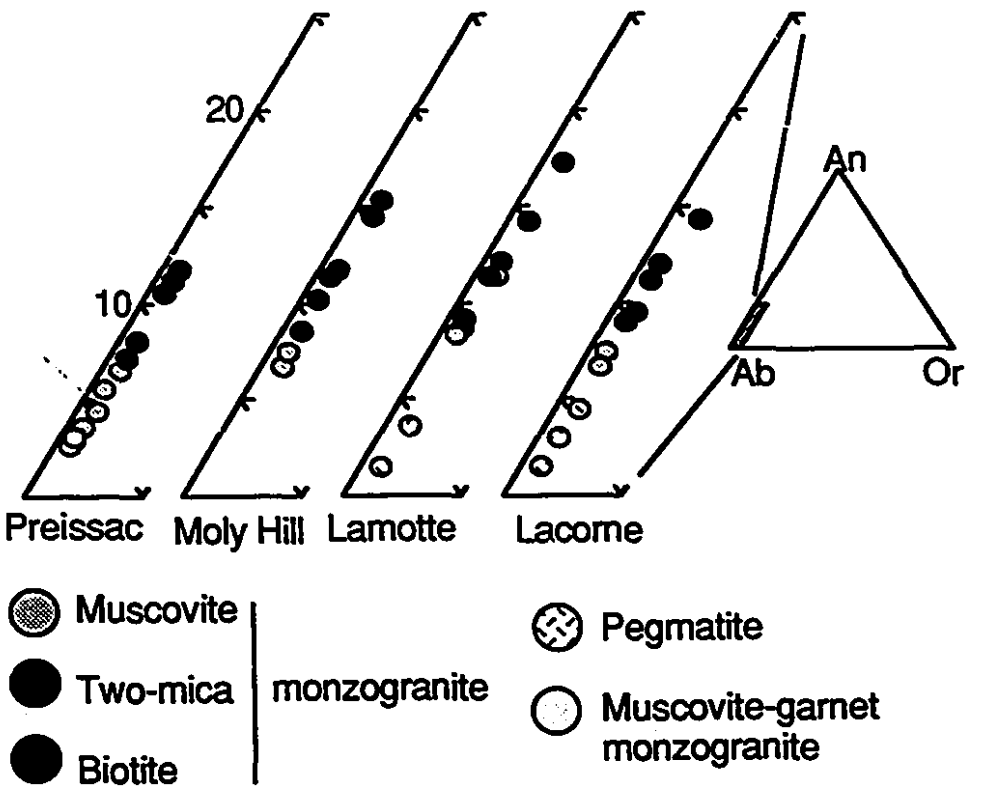
20
10
An
Ab
Or
Preissac
Moly Hill
Lamotte
Lacorne
Muscovite
Two-mica
Biotite
monzogranite
Pegmatite
Muscovite-garnet monzogranite

Figure 5

Fig. 6. Compositional variations in plagioclase and biotite along a north-south traverse across the Lacorne monzogranite pluton. Solid square: biotite monzogranite, open square: two-mica monzogranite, and open circle: muscovite monzogranite.

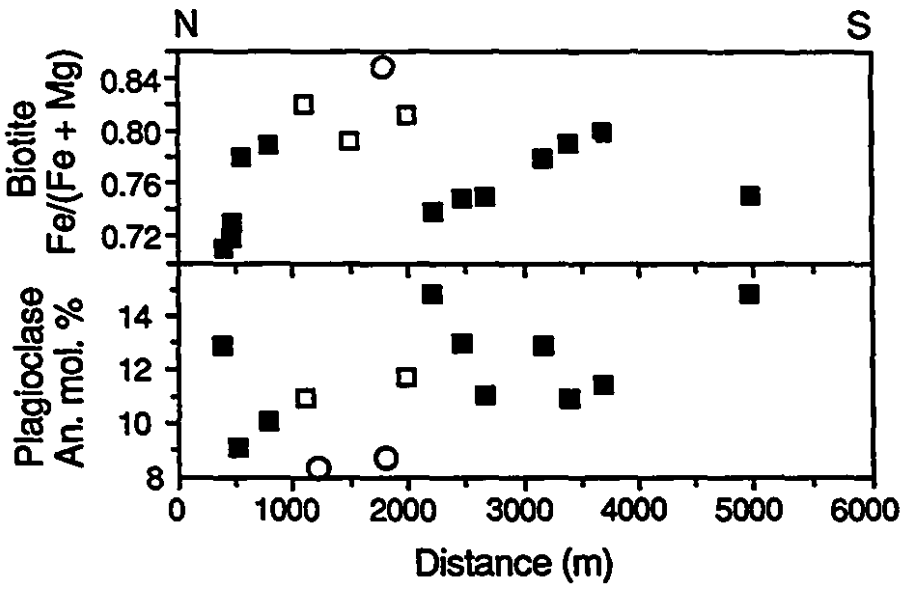
N
S
Biotite
Fe/(Fe + Mg)
0.84
0.80
0.76
0.72
Plagioclase
An. mol. %
14
12
10
8
0
1000
2000
3000
4000
5000
6000
Distance (m)

Figure 6

TABLE 2 REPRESENTATIVE COMPOSITIONS OF K-FELDSPAR

	Biotite monzogranite				Two-mica monzogranite				Muscovite monzogranite				MGM**
Pluton*	PR	MH	LM	LC	PR	MH	LM	LC	PR	MH***	LM	LC	1a
Sample	402	29	767	614	903	31	766	652	302	24	101	633	477
SiO_2	64.11	65.13	66	64.65	65.1	65.00	65.33	65.68	65.13	65.05	65.41	64.56	64.30
Al_2O_3	17.94	18.18	18.39	17.96	17.65	17.62	18.44	17.05	17.96	18.30	18.14	17.80	18.15
Na_2O	0.45	0.39	0.40	0.33	0.62	0.36	0.37	0.36	0.34	1.24	0.29	0.41	0.28
K_2O	16.67	17.12	15.90	16.99	16.66	17.11	16.73	16.78	16.89	15.86	17	16.79	16.97
CaO	0.09				0.01			0.01					
Total	99.26	100.8	100.7	99.93	100	100.1	101	99.88	100.3	100.40	100.8	99.56	99.70
Number of cations on the basis of 8 oxygen atoms													
Si	2.997	3.000	3.016	3.003	3.015	3.012	2.999	3.044	3.009	2.993	3.005	3.008	2.992
Al	0.989	0.987	0.991	0.983	0.964	0.962	0.998	0.931	0.978	0.992	0.982	0.977	0.996
Na	0.041	0.035	0.035	0.030	0.055	0.033	0.033	0.032	0.031	0.111	0.026	0.037	0.026
K	0.994	1.006	0.927	1.007	0.985	1.012	0.980	0.992	0.996	0.931	1.000	0.998	1.007
Ca	0.004	0.000	0.000	0.000	0.001	0.000	0.000	0.001	0.000	0.000	0.000	0.000	0.000
End members Mol. %													
Ab	4	3.4	4	3	5	3	3	3	3	11	2.5	4	2.5
Or	95.5	96.6	96	97	95	97	97	97	97	89	97.5	96	97.5
An	0.5												

*Pluton headings as in Table 2.
**Muscovite-garnet monzogranite
***Including albite lamella

feldspar, or late, occurring in interstices between the major silicate phases (Figs. 3A-B). Compositionally, it is higher in Fe/(Fe + Mg), which ranges from 0.69 to 0.85, and less aluminous (^{IV}Al: 2.1-2.5) than biotite in other peraluminous granites (compiled by Clarke 1981). The atomic proportions of Si-$\sum$Al-M^{2+}(Fe + Mg + Mn) show that it has a significant dioctrahedral mica content, which is higher in the interstitial biotite than in included biotite (Fig. 7). In the Lamotte and Lacorne biotite monzogranites, included biotite is consistently lower in SiO_2, TiO_2 and Al_2O_3, generally lower in Na_2O, and always higher in $FeO_{(t)}$ than the interstitial variety (Table 3), and has similar ranges of MnO, MgO and K_2O, and F. As a result, there is a slight overlap in the Fe/(Fe + Mg) of biotite, which ranges from 0.69-0.76 in interstitial biotite to 0.72-0.80 in included biotite. This is opposite to the compositional behavior of biotite in the Cuffytown Creek pluton, South Carolina, where the interstitial biotite has the higher Fe/(Fe + Mg) (Speer & Becker 1992). A trend of decreasing Fe/(Fe + Mg) of biotite during crystallization of plutonic rocks is common (e.g. Czamanske & Wones 1973, Chivas 1981, Parsons 1981), and is attributed to an increase in oxygen fugacity and a drop in temperature. According to these authors, the increasing oxidation is caused by the increased partial pressure of water, which is enhanced by higher amounts of fluid exsolved from the crystallizing magma.

Included biotite is rare in the Lamotte and Lacorne two mica monzogranites, and analyses are too few to permit meaningful comparisons with those of interstitial biotite. Therefore, unless otherwise stated, the following discussion refers to interstitial biotite. The Fe/(Fe + Mg) of biotite in the Moly Hill, Lamotte and Lacorne plutons increases from approximately 0.69 in the biotite monzogranite to 0.85 in the muscovite monzogranite. However, this trend is reversed in the Preissac monzogranites with the Fe/(Fe + Mg) ratio decreasing from approximately 0.78 in the biotite monzogranite to 0.69 in the two-mica monzogranite. Within the biotite monzogranite of the Lamotte pluton, this ratio generally increases with decreasing distance toward the two-mica monzogranite. This trend is also observed in the northern part of the Lacorne pluton. Biotite in the southern body of biotite monzogranite in this pluton, however, increases its Fe/(Fe + Mg) value toward the center of the mass (Figs. 2D & 6). There is no

Fig. 7. Average compositions of biotite and muscovite for each of the subtypes of monzogranite and pegmatite plotted in atomic proportions of $\sum$Al-M^{2+}-Si (diagram after Monier & Robert 1986). Although the plot suggests dioctahedral-trioctahedral substitution for the biotite, and Al-Tschermak substitution for the muscovite, the absence of Li analyses precludes corroboration of the mechanism of exchange. M^{2+}: Fe + Mn + Mg. East: eastonite, Phl/Ann: phlogopite/annite, Ms: muscovite, Ph: phengite, Cel: celadonite.

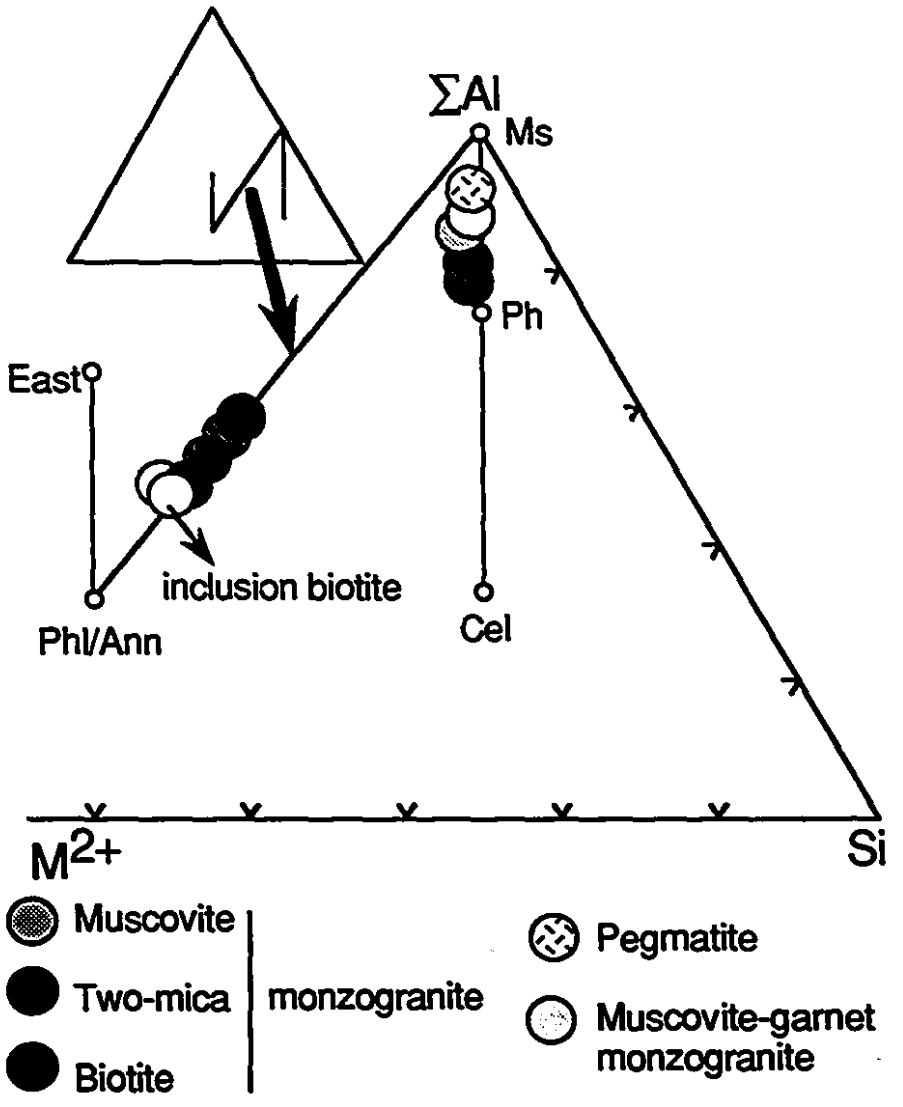
ΣAl
Ms
Ph
East
inclusion biotite
Phl/Ann
Cel
M2+
Si
Muscovite
Two-mica
Biotite
monzogranite
Pegmatite
Muscovite-garnet monzogranite

Figure 7

TABLE 3. REPRESENTATIVE COMPOSITIONS OF BIOTITE

	Biotite monzogranite							Two-mica monzogranite							MG*
Pluton	PR	PR	MH	LM	LM	LC	LC	PR	MH	MH	LM	LM	LC	LC	LC
Sample	402**	402+	29	768*	908	613	673+	903	26	41**	766	791**	672+	672	648+
SiO_2	36.37	35.89	36.61	34.76	36.84	37.76	36.91	37.00	36.85	35.86	36.29	36.22	35.42	36.87	37.13
TiO_2	2.56	2.90	2.71	2.43	1.33	1.79	2.45	2.80	2.20	2.86	1.16	1.05	2.12	2.00	1.93
Al_2O_3	16.76	16.39	16.57	17.83	20.03	21.43	17.99	17.07	17.94	16.85	18.63	20.24	17.22	19.64	18.72
FeO	25.33	25.92	23.72	25.3	20.62	19.15	23.24	22.31	23.15	23.00	21.18	20.46	26.41	23.81	22.84
MnO	0.69	0.95	0.60	0.68	0.61	0.80	1.09	0.77	0.94	2.26	1.02	0.7	0.76	0.60	0.68
MgO	4.15	3.89	6.02	4.89	3.29	2.66	4.07	5.40	4.13	4.78	4.74	3.69	3.15	2.91	2.22
Na_2O	0.14	0.02	0.09	0.02	0.01	0.01	0.03	0.04	0.06	0.05	0.04	0.06	0.02	0.05	0.06
K_2O	9.84	10.05	9.90	9.3	9.81	10.08	9.73	10.24	9.63	9.70	9.13	9.9	10.02	10.13	9.81
F	0.69	0.62	0.83	0.72	0.93	1.02	0.96	1.34	0.77	0.51	0.9	0.77	0.97	0.51	1.23
	96.75	96.63	97.25	95.93	95.47	94.70	96.47	96.97	95.67	95.87	95.09	95.09	96.09	96.52	94.62
F=O	0.29	0.26	0.35	0.30	0.39	0.43	0.4	0.56	0.32	0.21	0.38	0.32	0.41	0.21	0.52
Total	96.46	96.37	96.90	95.63	95.08	94.27	96.07	96.41	95.35	95.66	94.71	94.77	95.68	96.31	94.10
	Number of cations on the basis of 22 oxygen atoms														
Si	5.680	5.647	5.674	5.481	5.932	5.801	5.718	5.719	5.739	5.621	5.900	5.864	5.657	5.696	5.853
^{iv}Al	2.320	2.353	2.327	2.519	2.068	2.199	2.282	2.281	2.261	2.379	2.100	2.136	2.343	2.304	2.147
^{vi}Al	0.765	0.667	0.684	0.795	1.537	1.681	1.003	0.829	1.032	0.735	1.284	1.523	0.878	1.239	1.33
Ti	0.303	0.343	0.314	0.277	0.153	0.206	0.285	0.325	0.258	0.338	0.134	0.121	0.253	0.232	0.229
Fe	3.308	3.411	3.057	3.336	3.633	2.461	3.011	2.884	3.016	3.016	2.729	2.625	3.505	3.075	3.011
Mn	0.118	0.126	0.078	1.149	0.749	0.104	0.144	0.101	0.124	0.301	1.090	0.844	0.102	0.078	0.091
Mg	0.966	0.912	1.383	0.091	0.078	0.610	0.939	1.244	0.958	1.116	0.133	0.091	0.745	0.670	0.521
Na	0.043	0.007	0.027	0.005	0.004	0.003	0.009	0.013	0.017	0.016	0.011	0.016	0.006	0.014	0.018
K	1.961	2.016	1.947	1.670	1.911	1.976	1.922	2.020	1.914	1.939	1.795	1.937	2.018	1.996	1.973
F	0.339	0.309	0.404	0.359	0.447	0.490	0.471	0.653	0.381	0.255	0.437	0.376	0.487	0.251	0.614
FM	0.77	0.79	0.69	0.97	0.98	0.80	0.76	0.70	0.76	0.73	0.95	0.97	0.82	0.82	0.85

Pluton headings as in Table 2. *Muscovite monzogranite +Inclusion biotite ~Inclusion biotite co-existing with muscovite
**Co-existing with muscovite FM: Fe/(Fe+Mg)

apparent trend in the Fe/(Fe + Mg) ratio of biotite in the biotite monzogranite of the Moly Hill pluton, and no trend can be determined for this ratio in the Preissac pluton, because the biotite monzogranite occurs only as a narrow marginal facies.

The fluorine content of biotite in both biotite and two-mica monzogranite has a similar range from 0.6 to 1.4 wt.%, except for the Preissac pluton, where the F content varies very little and averages 0.65 and 1.35 wt.% in the two rock types, respectively. The average F content of biotite in the biotite monzogranite is marginally higher than that of biotite in the two-mica monzogranite of the Moly Hill, Lamotte, and Lacorne plutons (0.93 vs. 0.78 wt.%).

Muscovite

On the basis of textural relationships, muscovite can be subdivided into primary and secondary varieties (cf. Miller et al 1981, Speer 1984). Primary muscovite forms discrete, randomly distributed euhedral crystals, many of which are similar in size to other major silicate phases (Fig. 4C). Less commonly, this muscovite occurs as inclusions in quartz. The primary muscovite is characterized by its higher Ti and Na contents and lower Mg content than secondary muscovite, which has a composition similar to hydrothermal muscovite in quartz veins (this study). Secondary muscovite occurs mostly as cross-cutting grains containing relicts of biotite, intergrowths of ilmenite or rutile, and inclusions of zircon (Fig. 4B). Muscovite in the muscovite and biotite monzogranites is dominantly primary and secondary, respectively. By contrast, both varieties of muscovite are common in the two-mica monzogranite. Muscovite in the pegmatites occurs as large books concentrated mostly near the contact with the host monzogranite or with aplitic phases in the pegmatites.

The atomic proportions of Si-$\sum$Al-M^{2+}(Fe+Mg+Mn) in the primary muscovite in the different subtypes of monzogranite suggest that the muscovite becomes progressively less phengitic and approaches the end-member composition in the muscovite monzogranite and the pegmatites (Fig. 7). As with biotite, the Fe/(Fe + Mg) of muscovite increases from 0.65 to 0.85 from the biotite to the muscovite monzogranite and pegmatites (Table 4). The fluorine content of muscovite ranges from

TABLE 4. REPRESENTATIVE COMPOSITIONS OF PRIMARY MUSCOVITE

	Biotite monzogranite				Two-mica monzogranite				Muscovite monzogranite				MGG**
Pluton	PR	MH	LM	LC	PR	MH	LM	LC	PR	MH	LM	LC	PR
Sample	402*	29	782*	613	902	32	791	652	302	17	101	648	479
SiO_2	46.93	46.67	47.30	46.85	47.24	46.46	47.63	48.49	46.95	46.49	46.78	46.01	46.75
TiO_2	0.91	1.77	0.23	0.40	0.97	0.61	0.12	0.27	0.62	0.43	0.3	0.34	0.22
Al_2O_3	27.82	27.39	29.38	28.49	28.87	30.49	31.35	31.35	27.14	30.83	31.14	31.43	31.47
FeO	6.11	5.84	5.07	7.77	5.58	5.06	4.10	4.66	6.21	5.27	3.7	5.28	5.22
MnO	0.11	0.14	0.11	0.36	0.10	0.17	0.1	0.09	0.15	0.06	0.05	0.10	0.12
MgO	1.45	1.50	1.62	1.09	1.42	0.92	1.41	1.06	1.73	0.71	0.68	0.72	0.71
Na_2O	0.15	0.23	0.26	0.06	0.23	0.34	0.21	0.23	0.20	0.22	0.3	0.37	0.31
K_2O	11.38	11.49	10.93	10.04	11.44	11.44	10.79	10.19	11.25	11.52	11.12	11.34	11.02
F		0.71	0.53	1.20		1.59							
		95.74	95.43	96.26		97.08							
O-F=O		0.30	0.22	0.51		0.67							
Total	94.86	95.44	95.21	95.75	95.85	96.41	95.71	96.34	94.25	95.53	96.41	95.59	95.82
Number of cations based on 22 oxygen atoms													
Si	6.484	6.446	6.468	6.453	6.439	6.246	6.406	6.462	6.534	6.344	6.271	6.276	6.335
^{iv}Al	1.516	1.554	1.532	1.547	1.561	1.754	1.594	1.538	1.466	1.656	1.729	1.724	1.665
^{vi}Al	3.013	2.908	3.205	2.713	3.078	3.078	3.376	3.385	2.985	3.303	3.507	3.328	3.360
Ti	0.095	0.185	0.024	0.041	0.100	0.062	0.012	0.027	0.064	0.045	0.028	0.035	0.022
Fe	0.706	0.675	0.58	0.895	0.636	0.569	0.461	0.519	0.723	0.601	0.415	0.602	0.591
Mn	0.013	0.016	0.012	0.042	0.012	0.019	0.011	0.010	0.018	0.007	0.006	0.012	0.014
Mg	0.298	0.310	0.33	0.224	0.288	0.184	0.282	0.211	0.359	0.144	0.137	0.146	0.143
Na	0.039	0.062	0.069	0.016	0.060	0.089	0.056	0.060	0.053	0.058	0.078	0.098	0.082
K	2.005	2.025	1.906	1.764	1.960	1.962	1.852	1.732	1.998	2.006	1.902	1.973	1.905
F		0.310	0.23	0.523		0.676							

Pluton headings as in Table 2 Fluorine concentration less than 0.4 wt. percent is not listed *cross-cutting with biotite

< 0.3 to 1.6 wt.%; the lower value is considered to represent the detection limit of F using the electron microprobe. The most F-enriched muscovite occurs in the Lacorne biotite monzogranite and has an average of 0.8 wt.% F. There is, moreover, a clear trend of decreasing average F content of muscovite from biotite through two-mica (0.6 wt.%) to muscovite monzogranite (0.4 wt.%). The muscovite in the monzogranites of the other plutons has significantly less F, but nevertheless also displays trends of decreasing F content from biotite or two-mica to muscovite monzogranite (Preissac: 0.45, < 0.3, < 0.3; Moly Hill: <0.3, 0.55, 0.4; Lamotte: 0.52, 0.54, 0.36). Somewhat surprisingly, this trend is not continued into the pegmatites; muscovite in these rocks shows a wide range of F contents (Lamotte, < 0.3 to 1.0 wt.%; Lacorne < 0.3 to 2.1 wt.%).

Lithium, which was only analyzed in muscovite from pegmatites and in two samples of muscovite monzogranite (one each from the Lamotte and Lacorne plutons), shows a strong positive correlation with F. The Li_2O content of muscovite in the muscovite monzogranite samples is 0.4 and 0.6 wt.%. The Cs content of muscovite from the muscovite monzogranite and rare-metal pegmatites in the Lamotte and Lacorne plutons correlates positively with Ta and Rb, and negatively with Sc and K/Rb (Table 5; Fig. 8).

Garnet

Garnet forms small, randomly distributed, euhedral to subhedral interstitial crystals and anhedral aggregates or clots concentrated near fractures, and quartz veins (Figs. 4D-E). The first mode of occurrence suggests magmatic crystallization, whereas the second mode of occurrence is interpreted to reflect a sub-solidus origin; the texture resembles that of metasomatic garnet described by Kontak and Corey (1988) from monzogranites in the South Mountain Batholith, Nova Scotia.

The primary garnet is a spessartine-almandine solid solution ($Sp_{30-60}Al_{37-59}$; Table 6), which in most cases is normally zoned, i.e., Mn decreases toward the rim; less than 5 % of the garnet crystals analyzed are reversely zoned. In both types of garnet, the average variation in MnO is 4 wt. %. Primary and secondary garnets in the

TABLE 5. TRACE ELEMENT CONTENTS OF MUSCOVITE SEPARATES (ppm)

LAMOTTE PLUTON					
Host rock	MG	Brl	Brl	Spd-brl	Spd
Sample No.	101*	912	798	TMC-2	HP9-5
ppm					
Cs	18	213	n.a	234	497
Sc	84	7.7	2.2	1.6	0.9
Ta	10	44	n.a	57	103
Rb	1080	4620	6230	9040	7300
Li	2060	5365	1690	4030	1520
F	2050	9630	5430	7140	875

LACORNE PLUTON								
Host rock	MG	MG	Brl	Brl	Spd-brl	Spd-brl	Spd-brl	Spd
Sample No.	648*	633*	952	1008	708	711	753	756**
ppm								
Cs	46	120	200	422	532	632	390	3680
Sc	83	72	4.4	5	5.5	3.4	2.5	0.9
Ta	35	78	64	207	113	98	110	160
Rb	2100	3100	6540	8290	10600	10700	14900	24600
Li	2890	n.a	1520	1090	12400	3730	990	27500
F	3376	2804	2797	2804	11220	7245	1697	20780

Host rock. MG: muscovite monzogranite; Brl, Spd: beryl, spodumene pegmatite
*Samples 101 and 648 contain small amounts of biotite, whereas Sample 633 has none
**Lepidolite

Fig. 8. Plots illustrating the variations of K/Rb, Sc, Rb and Ta with Cs in muscovite. The muscovite samples from the pegmatites are from border zones, along which the mineral occurs as cumulate-like aggregates, with the exception of Sample HP9-5 (Table 5), where it is disseminated throughout the pegmatite. The sample with the highest Cs content is lepidolite, which was collected from a spodumene pegmatite in the Lacorne pluton.

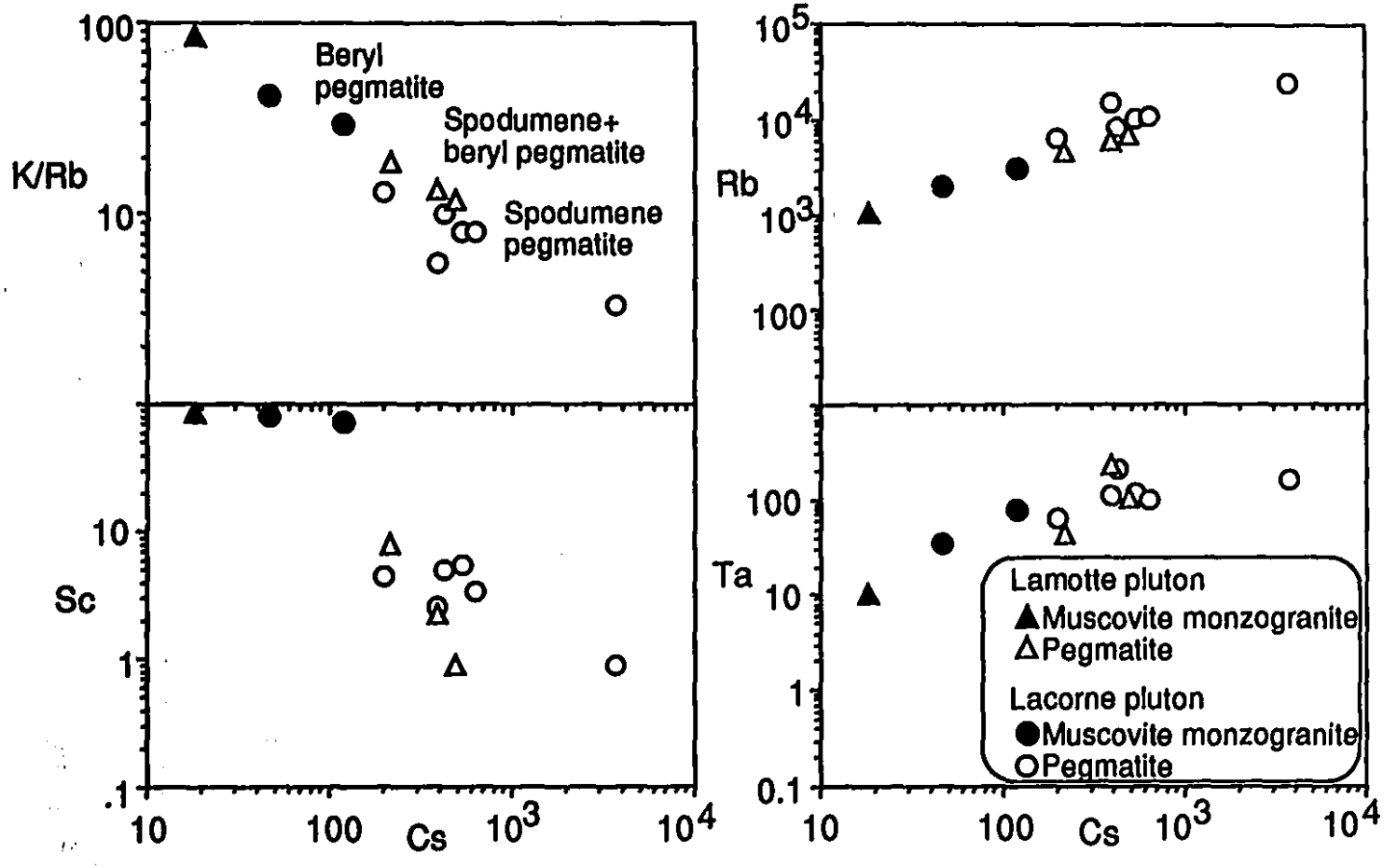
100
10
K/Rb
Beryl
pegmatite
Spodumene+
beryl pegmatite
Spodumene
pegmatite
10
1
.1
Sc
10
100
Cs
10^3
10^4
10^5
10^4
10^3
100
Rb
100
10
1
0.1
Ta
10
100
Cs
10^3
10^4
Lamotte pluton
▲Muscovite monzogranite
△Pegmatite
Lacorne pluton
●Muscovite monzogranite
○Pegmatite

Figure 8

TABLE 6. REPRESENTATIVE COMPOSITIONS OF GARNET

	Biotite monzogranite			Two-mica monzogranite				Muscovite monzogranite			MGG	Aplite	Peg
Pluton	LM		LC	MH	LM	LM	LC	PR	MH	LC	PR	MH	LC
Sample	797		631	35	796	907	672	314	17	637	473	30	1001
	core	rim	n=6			n=4				n=4			
SiO_2	37.00	36.85	36.6	36.17	36.80	36.97	36.67	36.27	36.70	36.56	35.83	36.31	36.63
Al_2O_3	19.69	19.66	20.15	20.13	20.30	20.50	19.80	19.96	20.43	19.57	20.00	20.31	19.89
TiO_2	0.29	0.19		0.14			0.12		0.11		0.16		
FeO	21.89	25.72	19.75	17.52	28.72	25.96	20.50	20.58	20.18	19.39	16.37	21.08	18.25
Fe_2O_3	1.26	1.36	0.70	0.68			1.05	0.61		1.27	1.19		0.80
MgO	0.55	0.42	0.42	0.28	0.49	0.34	0.51	0.23	0.29	0.24	0.16	0.30	0.11
MnO	16.32	15.07	20.62	23.99	13.05	15.55	19.87	20.66	20.87	20.24	26.14	20.33	23.29
CaO	1.30	1.28	1.73	1.11	0.67	1.00	0.78	0.66	1.14	1.75	0.75	1.30	0.38
Total	100.3	100.5	99.97	100	100	100.3	99.50	98.97	99.72	99.02	100.6	99.63	99.35
Number of cations based on 24 oxygen atoms													
Si	6.073	6.056	6.021	5.977	6.029	6.049	6.091	6.040	6.017	6.079	5.928	5.979	6.062
Al	3.809	3.808	3.961	3.921	3.919	3.953	3.855	3.917	4.001	3.835	3.904	3.942	3.879
Ti	0.036	0.024		0.017			0.015		0.014		0.020		
Fe^{2+}	3.004	3.535	2.718	2.422	3.935	3.547	2.832	2.866	2.794	2.696	2.265	2.903	2.525
Fe^{3+}	0.156	0.169	0.088	0.058			0.130	0.760		0.159	0.149		0.100
Mg	0.135	0.103	0.103	0.069	0.120	0.083	0.126	0.057	0.072	0.060	0.040	0.073	0.026
Mn	2.550	2.098	2.874	3.358	1.811	2.155	2.781	2.914	2.934	2.851	3.663	2.834	3.264
Ca	0.229	0.225	0.305	0.197	0.118	0.175	0.138	0.118	0.203	0.332	0.133	0.230	0.068
End members Mol. %													
Alm	51	59	45	40	66	59	48	48	47	46	37	48	43
Prp	2	2	2	1	2	1	2	1	1	1	1	1	0
Grs			3	1		2			3	1		2	
Adr	4	4	2	3	2	1	2	2	0	4	2	2	1
Sps	43	35	48	56	30	36	47	49	49	48	60	47	56

Pluton headings as in Table 2 Peg: pegmatite n: number of analyses

monzogranites are indistinguishable on the basis of the major element compositions, whereas secondary garnets in pegmatite are strongly enriched in Mn (85-90 mol. % Sp). The primary garnet in most of the monzogranites has a wide compositional range but only in the Preissac pluton is there any evidence of systematic change in garnet composition with subtype of monzogranite: the garnet in the muscovite-garnet monzogranite is richer in Mn than that in the muscovite monzogranite (Fig. 9).

Epidote

Coarse-grained, euhedral to subhedral crystals of epidote are invariably intergrown with biotite or chloritized biotite, and the contacts between the two minerals vary from sharp to corroded (Fig. 4B). Smaller grains replaced plagioclase and muscovite. Epidote, which replaced biotite, is richer in ferric iron than epidote which replaced plagioclase or muscovite: the atomic ratio $Fe^{3+}/(Fe^{3+} + Al)$ varies from 0.26 to 0.33 vs. 0.22 to 0.24, respectively (Table 7). Epidote from biotite schist in contact with the Preissac two-mica monzogranite has a consistent $Fe^{3+}/(Fe^{3+} + Al)$ ratio of 0.24. The higher ratio, according to Naney (1983) and Tulloch (1979), reflects a magmatic origin, and the lower ratio a hydrothermal origin. On textural grounds, we conclude that epidote in the Preissac-Lacorne monzogranites is secondary and that the $Fe^{3+}/(Fe^{3+} + Al)$ ratio depends simply on the nature of the mineral replaced, i.e., we do not believe that this chemical criterion can be used to distinguish primary from secondary epidote. This opinion is supported by data for epidote in granitic rocks from Nova Scotia and the southern Appalachians. This epidote is believed to be magmatic on textural grounds, yet its $Fe^{3+}/(Fe^{3+} + Al)$ ratio ranges from 0.23 to 0.29 (Farrow & Barr 1992), and from 0.24 to 0.33 (Vyhnal et al. 1991), respectively.

Iron-titanium oxides and titanite

The composition of magnetite does not vary from one monzogranite subtype to the next, and is very close to Fe_3O_4. Primary and secondary crystals of ilmenite have essentially the same compositions, and contain significant amounts of MnO (from 4 to

Fig. 9. Compositions of garnet recalculated to 100 mol. % in terms of end-members almandine (Alm), pyrope (Prp), and spessartine (Sps). The shaded area shows the range of garnet compositions compiled by Clarke (1981) for other peraluminous granites.

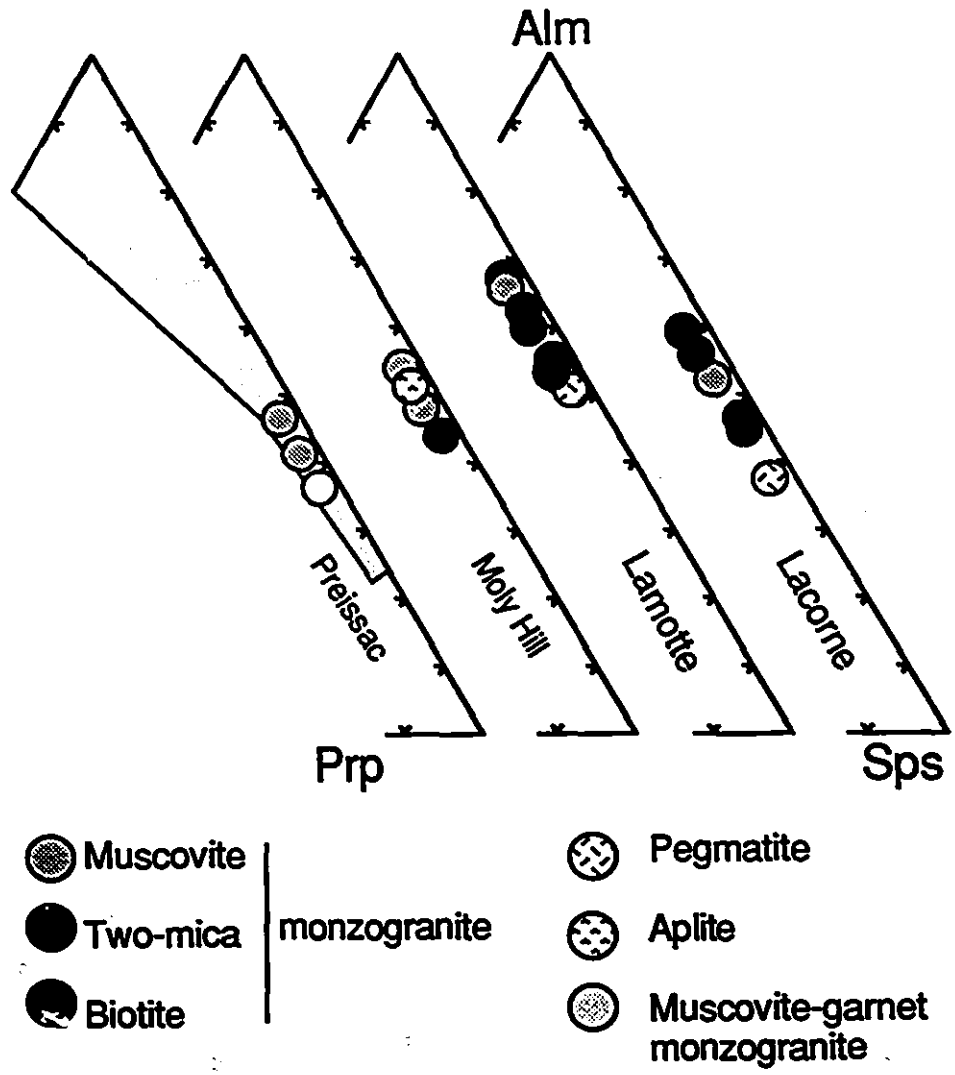
Alm
Preissac
Moly Hill
Lamotte
Lacorne
Prp
Sps
Muscovite
Two-mica
Biotite
monzogranite
Pegmatite
Aplite
Muscovite-garnet monzogranite

Figure 9

TABLE 7. REPRESENTATIVE COMPOSITIONS OF EPIDOTE

Host rock	BG			2MG					MG	BG	MG	SC
Pluton	LM	LC	LC	PR	MH	LM	LC	LC	PR	LC	LC	
Sample	908	613	620	902	26	791	673	707	302	614	603	921
Texture	1	1	1	2	1	1	1	2	2	3	4	1
SiO_2	38.10	38.44	38.32	39.23	38.06	38.00	38.05	38.30	38.88	39.57	39.20	38.76
TiO_2	0.12	1.16	0.30		0.13	0.22		0.19				
Al_2O_3	22.26	22.31	21.83	23.68	22.77	22.48	21.69	22.58	23.00	23.79	24.83	23.85
Fe_2O_3	13.68	12.86	14.40	12.78	13.16	14.10	15.20	13.44	13.34	11.72	10.95	11.52
MnO	0.26	0.46	0.25	0.61	0.61	0.23	0.27	0.46	0.45	0.85	0.16	0.31
CaO	23.05	22.67	22.10	22.52	22.37	23.05	22.77	22.77	22.53	22.17	22.98	22.15
Total	97.47	97.90	97.20	98.82	97.10	98.08	97.98	97.74	98.20	98.10	98.12	96.59
	Number of cations based on 13 oxygen atoms											
Si	3.051	3.177	3.197	3.297	3.277	3.029	3.163	3.176	3.303	3.237	3.196	3.214
Ti	0.007	0.072	0.019		0.008	0.013		0.012				
Al	2.101	2.174	2.147	2.345	2.311	2.110	2.126	2.207	2.304	2.294	2.387	2.331
Fe^{3+}	0.825	0.800	0.904	0.809	0.853	0.845	0.951	0.839	0.853	0.721	0.672	0.719
Mn	0.017	0.032	0.018	0.043	0.044	0.016	0.019	0.032	0.033	0.059	0.011	0.022
Ca	1.978	2.008	1.974	2.028	2.064	1.967	2.028	2.023	2.050	1.943	2.008	1.968
^	0.28	0.27	0.30	0.26	0.27	0.28	0.31	0.28	0.27	0.24	0.22	0.24

^^ $Fe^{3+}/(Fe^{3+}+Al)$

Pluton headings as in Table 1

Host rock: BG, biotite monzogranite; 2MG, two-mica monzogranite; MG, muscovite monzogranite, SC, schist

Texture: 1, coexist with biotite and feldspar; 2, coexist with primary muscovite; 3, interstitial; 4, replacing plagioclase

11.5 wt.%). In albitite dikes, this mineral contains up to 1.2 wt.% Ta_2O_5. Neither magnetite nor ilmenite hosts any exsolved phases (Figs. 4F-G). Primary titanite contains very little or negligible amounts of MnO, higher SiO_2 and lower TiO_2 than secondary titanite. The latter, together with chlorite, replaced biotite. The primary titanite crystals contain minor niobium.

DISCUSSION

Evolution of the AFM minerals

We have used the parageneses and compositions of the AFM mineral assemblages (biotite, muscovite, garnet) in the various subtypes of the monzogranite and the corresponding AFM liquidus topologies of Abbott (1985) to trace the reactions which are believed to have taken place during the course of crystallization of the monzogranitic magma (cf. Speer & Becker 1992) (Fig. 10).

The presence of included biotite in the Lamotte and Lacorne biotite monzogranite (Preissac pluton only). The initial composition of the liquid is indicated by the number 1, and the paths of the crystallization are shown with arrows.
monzogranite suggests the reaction liquid → Bio. By contrast, evidence for contemporaneous crystallization of included biotite and muscovite in the Preissac two-mica monzogranite and in the Moly Hill biotite monzogranite indicate that the liquid of these intrusions was on the three-phase surface, liquid-Bio-Mus, precipitating the two micas by the reaction liquid → Bio + Mus. The final assemblage in the Moly Hill biotite monzogranite consisted of biotite and muscovite, indicating that the reaction continued until the consolidation of the monzogranite (Fig. 10B). After the inclusion micas had formed in the Preissac, Lamotte and Lacorne plutons, the liquid crystallized the more abundant interstitial biotite and isolated muscovite. The final AFM minerals to crystallize were muscovite and garnet. The appearance of late garnet was a consequence of the crystallization of the micas and Mn-poor magnetite, which increased the Mn/(Mn + Fe + Mg) of the liquid, because of the intolerance of biotite for high Mn^{2+} (Abbott 1985).

Fig. 10 A. Compositions of the liquidus AFM minerals (biotite, muscovite, garnet) plotted on an A (Al_2O_3-CaO-Na_2O-K_2O) F (FeO + MnO) M (MgO) ternary diagram, and the corresponding liquidus AFM diagram, B, (after Abbott 1985). Coexisting minerals are indicated by tie lines. Solid square: biotite monzogranite, open square: two-mica monzogranite, open circle: muscovite monzogranite, triangle: muscovite-garnet monzogranite (Preissac pluton only). The initial composition of the liquid is indicated by the number 1, and the paths of the crystallization are shown with arrows.

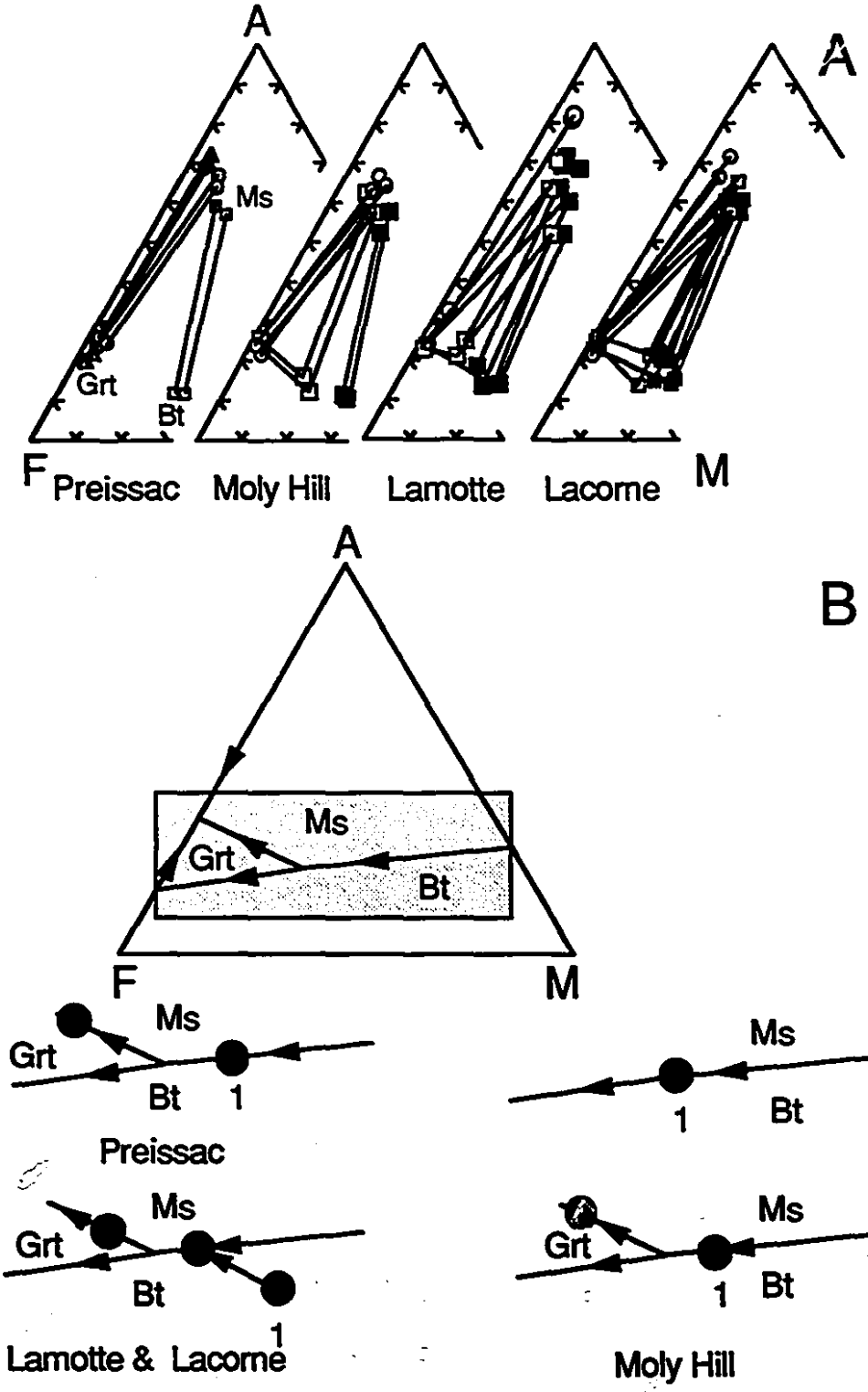
A
A
Ms
Grt
Bt
F
Preissac
Moly Hill
Lamotte
Lacorne
M
A
B
Ms
Grt
Bt
F
M
Ms
Grt
Bt
1
Preissac
Ms
1
Bt
Ms
Grt
Bt
1
Lamotte & Lacorne
Ms
Grt
1
Bt
Moly Hill

Figure 10

The occurrence of Mus + Gar suggests that the remaining liquid only moved onto the Mus + Gar eutectic surface from the three-phase eutectic, liquid + Bio + Mus, through the four-phase peritectic, liquid + Bio + Mus + Gar. There is no evidence to indicate whether the reaction, liquid → Bio + Mus + Gar, or liquid + Bio + Mus → Gar, occurred. It thus follows that after crystallization of biotite, the final liquid must have been on the Mus + Gar eutectic surface, precipitating both minerals by the reaction, liquid → Mus + Gar, until the final consolidation of the monzogranitic magma.

In conclusion, crystallization of the monzogranites in the Preissac-Lacorne plutons proceeded by the same sequence of reactions: liquid → Bio, liquid → Bio + Mus, liquid → Mus + Gar, with the exception of the Moly Hill biotite monzogranite and Preissac muscovite monzogranite, in which crystallization involved only one reaction, liquid → Bio + Mus, and liquid → Mus + Gar, respectively.

P-T conditions of crystallization

The pressure of emplacement of the Preissac-Lacorne monzogranites, based on phase equilibrium estimates of the contact metamorphic conditions (Powell et al. 1994) was probably in the order of 3.5 kbar. A minimum estimate of the pressure is 2.1 kbar, which corresponds to the lower pressure stability limit of the assemblage spodumene + quartz (London 1984). The temperature of emplacement has been estimated from mineral-mineral exchange reactions, experimental data for the saturation of monazite and zircon in felsic magmas, and oxygen isotopic fractionation between mineral pairs (Table 8). The muscovite-biotite (Hoisch 1989), garnet-biotite (Williams & Grambling 1990), and plagioclase-K-feldspar (Brown & Parsons 1981) geothermometers, applied to mineral pairs in the various subtypes of monzogranite, all yield similar subsolidus temperatures of 320-450°C. By contrast, the monazite and zircon "geothermometers", which are based on the solubility of these minerals in the magma (Rapp et al. 1987, Watson & Harrison 1983), yield temperatures of 680 and 780°C in the biotite monzogranite and about 665°C and 660-750°C in the muscovite monzogranite, respectively.

TABLE 8. INFERRED TEMPERATURE OF CRYSTALLIZATION BASED ON OXYGEN ISOTOPE AND SATURATION OF MONAZITE AND ZIRCON

Pluton	Mineral pair	Temperature in °C			
		Biotite	Two-mica monzogranite	Muscovite	Vein
Preissac	Δqtz-mus				514-576
	Δqtz-gar		695		
	Monazite	nc	680		
	Zircon	nc	765	750	
Moly Hill	Δqtz-mus				540-593
	Δqtz-gar			580	
	Monazite	690	700	675	
	Zircon	777	750	730	
Lamotte	Monazite	680	680	670	
	Zircon	780	740	660	
Lacorne	Monazite	685	670	665	
	Zircon	780	750	750	

qtz: quartz, grt: garnet, ms: muscovite
Source of data: Preissac vein (Taner 1989); Moly Hill vein (Mulja et al. 1990); others (Feng 1992)
nc: not calculated due to the altered nature of the rock (described in text)

The higher temperature given by the zircon geothermometer can be attributed to the fact that zircon is one of the earliest minerals to crystallize, i.e. the 780 °C temperature is probably close to that of the liquidus of the monzogranitic magma. The lower temperature for the monazite geothermometer reflects crystallization closer to the solidus or *LREE* undersaturation of the melt (Scaillet et al. 1990). This deduction is consistent with the paragenesis of monazite, which occurs mostly as an interstitial phase. Furthermore, the lower temperature is similar to the isotopic temperature of 695°C (quartz-garnet) obtained for the two-mica monzogranite of the Preissac pluton. Since both garnet and quartz are late minerals, the isotopic temperature most likely reflects the near solidus temperature of the monzogranite. A minimum for the solidus temperature is provided by the isotopic temperature of 593°C (quartz-muscovite) for the quartz vein (Table 8). The solidus temperature of the muscovite monzogranite must have been higher than that of vein formation, i.e., > 593°C. This minimum estimate of the solidus temperature is about 40°C lower than that experimentally determined for H_2O-saturatedgranite by Johannes and Holtz (1991). Although experimental studies by Manning (1981) and Martin (1983) showed that F and Li lower the liquidus and solidus temperatures of granitic melts (e.g. 35°C with 1 wt.% F and 25°C with 1 wt.% Li_2O), this would not have been a factor for the Preissac-Lacorne monzogranites, which contain low contents of F and Li, 0.05 and 0.1 wt.%, respectively (Mulja et al. 1995).

Thus, in summary, the above data suggest that the monzogranites in the Preissac-Lacorne batholith were emplaced at temperatures of 750 to 650 °C and a pressure of 3.5 kbar.

Processes controlling monzogranite crystallization and emplacement

From the data which have been presented above, it is clear that the biotite monzogranite is the least differentiated and the muscovite monzogranite the most differentiated of the principal intrusive phases in the Preissac-Lacorne plutons. In going from biotite to muscovite monzogranite there is a change in mineralogy from biotite to garnet, oligoclase to albite, and niobium-bearing titanite to columbite-tantalite. Parallel with these mineralogical changes, the An content of plagioclase decreases, the Fe/(Fe

+ Mg) of biotite increases, and the Al content of muscovite increases. The only exception to this is in the Preissac pluton where the biotite monzogranite is anomalous relative to the other subtypes of monzogranite. As mentioned earlier, the biotite monzogranite occurs only as a thin marginal facies of the muscovite monzogranite, and the extent of the intrusion is unknown. Its contacts with the muscovite monzogranite are sharp in some localities and are separated by quartz + K-feldspar veins in others. These field relationships imply two separate pulses of magma. However, due to the absence of cross-cutting relationships, the sequence of intrusion is not known. The Preissac biotite monzogranite is therefore excluded from the following discussion.

In the Lamotte pluton, and to a lesser extent in the Lacorne pluton, there is a clear inward zonation from biotite monzogranite (least evolved) to muscovite monzogranite (most evolved) in the core. Similar zonal distributions of intrusive facies have been documented for a number of granitic intrusions, e.g. the Tuolumne Intrusive Series, California (Bateman & Chappell 1979), the Blue Tier batholith, Tasmania (McCarthy & Groves 1979), and the Loch Doon pluton, Scotland (Tindle & Pearce 1981), and in each of these intrusions the sequence of crystallization was from a marginal biotite facies to a muscovite facies. These spatial and temporal relationships have been interpreted as evidence for side-wall fractional crystallization being the main mechanism of differentiation. While we believe that the process of fractional crystallization also explains various mineralogical and petrological characteristics of the monzogranite plutons in the Preissac-Lacorne batholith, we do not think that this mechanism was restricted to side-wall crystallization. The reasons are the lack of biotite monzogranite in the northern part of the Lamotte pluton and the trends of Fe/(Fe + Mg) of biotite and An content of plagioclase across the Lacorne pluton (Fig. 6). The latter suggests that the direction of the crystallization did not occur uniformly across the pluton. Independent side-wall crystallization seems to have taken place in both ends of the pluton.

The Preissac and Moly Hill plutons are not concentrically zoned. However, the variations in mineralogy and mineral chemistry are similar to those observed in the Lamotte and Lacorne plutons. Moreover, in the case of the Moly Hill pluton, there is

a gradual transition from the two-mica monzogranite to the muscovite monzogranite. Gradual transitions from one subtype of monzogranite to another are also observed in the northern part of the Lacorne pluton where the biotite monzogranite grades imperceptibly into two-mica monzogranite. Such transitions are consistent with the model of fractional crystallization proposed above.

In all four plutons, biotite was the earliest AFM mineral to crystallize, thereby depleting the magma in Mg/(Mg + Fe) and in F. Such depletions are documented by the increase in the Fe/(Fe + Mg) ratio and decrease in the F content of biotite, from biotite monzogranite to two-mica monzogranite, and the decrease in Ti from included to interstitial biotite. They are also documented by similar trends of Fe/(Fe + Mg) and F for muscovite from two-mica to muscovite monzogranite. Early biotite was accompanied by crystallization of the most calcic plagioclase (oligoclase), which served to deplete the magma in Ca. Crystallization of biotite and oligoclase caused higher Fe/(Fe + Mg) and Na/(Na + K), thereby promoting the crystallization of muscovite, garnet, and albitic plagioclase.

Although the process of fractional crystallization is supported by the geochemistry of the monzogranite (Mulja et al. 1995) and the preceding paragraphs have stressed the importance of gradational boundaries between monzogranite subtypes, many of the contacts are fracture-bounded or unexposed, and at least one, between muscovite-garnet monzogranite and muscovite monzogranite (Preissac pluton), is clearly intrusive. The two-mica monzogranite in the northeastern part of the Lacorne pluton (labeled Valor) differs texturally from, and has an uncertain spatial relationship to, the two-mica monzogranite in the main mass (Fig. 2D). Thus, the muscovite-garnet monzogranite and the Valor two-mica monzogranite in the Preissac and Lacorne plutons, respectively, are likely to represent different pulses of magma.

If the various subtypes of monzogranite were the products of fractional crystallization as proposed above, then differentiation must have preceded local fracturing and magma emplacement. While plutonism can induce emplacement fractures (Castro 1987), there is no simple explanation available in the literature for how each body of magma is segregated into a fracture-bounded mass. A possible explanation is

that of McCarthy and Groves (1979), who proposed that the fault-bounded cogenetic rocks in the Blue Tier batholith (Tasmania) were the result of periodic tectonic disturbances which caused the rest magma to locally reintrude earlier crystallized units. In this scenario, the separated melts began to crystallize independently, e.g. the Lacorne biotite monzogranite.

Relationships between monzogranite and rare-element pegmatites

The most evolved members of the plutons are the pegmatites, which are characterized by plagioclase with the lowest An content, muscovite with the highest Al content, the most spessartine-rich garnet, and the absence of biotite. Trace element contents of the muscovite from the muscovite monzogranite to various subtypes of rare-element pegmatite form a systematic trend that suggests petrogenetic linkage between the two rock types by differentiation (Table 5; Fig. 8). These trends are consistent with a process of differentiation in which the residual liquid is progressively enriched in Cs, Rb, and Ta, and depleted in Sc. This, in turn, suggests that the muscovite monzogranite and pegmatites are co-magmatic. The above trends are also evident among the different types of rare-element pegmatites, i.e., beryl-bearing pegmatites have higher K/Rb, Sc, and lower Cs, Rb, and Ta contents than spodumene-bearing pegmatites; these components have intermediate concentrations in the spodumene-beryl-bearing pegmatites. This interpretation is corroborated by the chemical composition of columbite-tantalite which evolved from ferrocolumbite in beryl pegmatite to manganotantalite and ixiolite in spodumene pegmatites (Mulja et al. 1993), and by the whole rock geochemistry of the pegmatites (Mulja et al. 1995). Therefore, the residual melts from fractional crystallization of the monzogranitic magma continued to differentiate to form the pegmatites.

CONCLUSIONS

1. The monzogranitic plutons (Preissac, Moly Hill, Lamotte, Lacorne) of the Preissac-Lacorne batholith were emplaced at a pressure of 3.5 kbar, and crystallized

over a temperature range from 750 to 650°C.

2. These plutons vary from biotite through two-mica to muscovite monzogranite subtypes, which display gradational, intrusive, and fracture-bounded contacts.

3. Field relations and systematic mineralogical and mineral-chemical variations within and between the monzogranite subtypes are interpreted to have been produced mainly by fractional crystallization, and subordinately by intrusion of different batches of magma. The former process caused the early fractionation of oligoclase, biotite and Fe-Ti oxides, and the later crystallization of albite, garnet and muscovite.

4. The end stage of fractional crystallization was marked by the occurrence of beryl, spodumene and columbite-tantalite in pegmatites.

ACKNOWLEDGMENTS

This study was supported by a FCAR team grant, a MERQ contract, and NSERC operating grants to A. E. W-J. and S.A.W., and a NATO travel grant to S. A. W and A. E. W-J. Field work was assisted by D. Ahmad and A. Fournier. The Ministére de l'Enérgie et des Resources of the Government of Québec kindly permitted us to reproduce their airphotos. We thank P. Černy, F. Holtz, C. Miller, J. Bourne, D. Kontak, R. F. Martin, and an anonymous reviewer for their constructive criticisms and corrections, which improved the manuscript.

REFERENCES

ABBOTT, R.N Jr. (1985): Muscovite-bearing granites in the AFM liquidus projection. *Can. Mineral.* **23**, 553-561.

BATEMAN, P.C. & CHAPPELL, B.W. (1979): Crystallization, fractionation, and solidification of the Tuolumne Intrusive series, Yosemite National Park, California. *Geol. Soc. Am. Bull.* **90**, 465-482.

BREAKS, F.W. & MOORE JR, J.M. (1992): The Ghost Lake batholith, Superior Province of northwestern Ontario: a fertile, S-type, peraluminous granite-rare-element pegmatit system. *Can. Min.* **30**, 835-876.

BROWN, W.L. & PARSONS, I. (1981): Towards a more practical two-feldspar geothermometer. *Contrib. Mineral. Petrol.* **76**, 369-377

CASTRO, A. (1987): On granitoid emplacement and related structures. A review. *Geol Rundsch.* **76**, 101-124.

ČERNÝ, P., GOAD, B.E., HAWTHORNE, F.C. & CHAPMAN, R (1986): Fractionation trends of the Nb- and Ta-bearing oxide minerals in the Greer lake pegmatitic granite and its pegmatite aureole, southeastern Manitiba. *Am. Mineral.* **71**, 501-517.

CHAPPELL, B.W., WHITE, A.J.R. & WYBORN, D. (1987): The importance of residual source material (restite) in granite petrogenesis. *J. Petrol.* **28**, 1111-1138.

CHIVAS, A.R. (1981): Geochemical evidence for magmatic fluids in porphyry copper mineralization. Part I. Mafic silicates from the Koloula igneous complex. *Contrib. Mineral. Petrol.* **78**, 389-403.

CLARKE, D.B. (1981): The mineralogy of the peraluminous granites: a review. *Can. Min.* **19**, 3-19.

CORFU, F. (1993): The evolution of the Southern Abitibi Greenstone Belt in light of precise U-Pb geochronology. *Econ. Geol.* **88**, 1323-1340.

CZAMANSKE, G.K., & WONES, D.R. (1973): Oxidation during magmatic differentiation, Finnmarka complex, Oslo area, Norway, Part 2, the mafic silicates. *J. Petrol.* **14**, 349-380.

DAWSON, K.R. (1966): *A comprehensive study of the Preissac-Lacorne batholith, Abitibi county, Quebec.* Geol. Surv. Can. Bull. 142. p76.

DIMROTH, E., IMREH, L., GOULET, N., & ROCHELEAU, M. (1983): Evolution of the south-central segment of the Archean Abitibi belt, Quebec. Part. III. Plutonic and metamorphic evolution and geotectonic model. *Can. Jour. Earth. Sci.* **20**, 1374-1388.

FARROW, C.E.G. & BARR, S.M. (1992): Petrology of high-Al-hornblende and magmatic-epidote-bearing plutons in the southeastern Cape Breton highlands, Nova Scotia. *Can. Min.* **30**, 377-392

FENG, R. & KERRICH, R. (1991): Single zircon age constraints on the tectonic juxtaposition of the Archean Abitibi Greenstone Belt and Pontiac Subprovince, Quebec, Canada. *Geochim. Cosmochim. Acta* **55**, 3437-3441.

FENG, R. & KERRICH, R. (1992): Geochemical evolution of granitoids from the Archean Abitibi southern volcanic zone and the Pontiac Subprovince, Superior Province, Canada: implications for tectonic history and source regions. *Chem. Geol.* **98**, 23-70.

GARIÉPY, C. & ALLÈGRE, C.J. (1985): The lead isotope geochemistry and geochronology of late kinematic intrusives from the Abitibi Greenstone Belt and the implications for late Archean crustal evolution. *Geochim. Cosmochim. Acta* **49**, 2371-2383.

GOAD, B.E. & ČERNÝ, P. (1981): Peraluminous pegmatitic granites and their pegmatite aureoles in the Winnipeg River district, southeastern Manitoba. *Can. Mineral.* **19**, 177-194.

HOISCH, T.H. (1989): A muscovite-biotite geothermometer. *Am. Mineral.* **74**, 565-572.

JOHANNES, W & HOLTZ, F. (1991): Formation and ascent of granitic magmas. *Geol. Rund.* **80**, 225-231.

KONTAK, D.J. & COREY, M. (1988): Metasomatic origin of spessartine-rich garnet in the south Mountain Batholith, Nova Scotia. *Can. Mineral.* **26**, 315-334.

LONDON, D. (1984): Experimental phase equilibria in the system $LiAlSiO_4$-SiO_2-H_2O:

a petrogenetic grid for lithium-rich pegmatites. *Am. Mineral.* **69**, 995-1004.

MANNING, D.A.C (1981): The effects of fluorine on liquidus phase relationships in the system Qz-Ab-Or with excess water at 1 kbar. *Contrib. Mineral. Petrol.* **76**, 206-215.

MARTIN, J.S. (1983): An experimental study of the effects of lithium on the granite system. *Proc. Ussher. Soc.* **5**, 417-420.

MCCARTHY, T.S. & GROVES, D.I. (1979): The Blue Tier Batholith, Northeastern Tasmania, a cumulate-like product of fractional crystallization. *Contrib. Mineral. Petrol.* **71**, 193-209.

MILLER, C.F., STODDARD, E.F., BRADFISH, L.J., & DOLLASE, W.A. (1981): Composition of plutonic muscovite: genetic implications. *Can. Mineral.* **19**, 25-34.

MONIER, G. & ROBERT, J-L. (1986): Muscovite solid solution in the system K_2O-MgO-FeO-Al_2O_3-SiO_2-H_2O: an experimental study at 2 kbar PH_2O and comparison with natural Li-free white micas. *Mineral. Mag.* **50**, 257-266.

MULJA, T., WILLIAMS-JONES, A.E., MARTIN, R.F., & WOOD, S.A. (1993): Compositional variations of Nb-Ta oxide minerals in rare-metal granitic pegmatites: examples from the Preissac-Lacorne batholith, Québec, Canada. *Geol. Soc. Am. Abstracts with Programs.* **25**, A-381.

_____, _____ WOOD, S.A., & BOILY, M. (1995): Petrogenesis of zoned monzogranite and associated rare-element granitic pegmatites and quartz veins: the Preissac-Lacorne batholith, Québec, Canada. *Can. Mineral.* **33**, 000-000.

NANEY, M.T. (1983): Phase equilibria of rock-forming ferromagnesian silicates in granitic systems. *Am. J. Sci.* **283**, 993-1033.

PARSON, I. (1981): The Klokken gabbro-syenite complex, South Greenland: quantitative interpretation of mineral chemistry. *J. Petrol.* **22**, 233-260.

POUCHOU, J.L. & PICHOIR, F. (1984): A new model for quantitative X-ray microanalyses. Part I: application to the analysis of homogeneous samples. *La*

Rech Aeros. **3**, 13-38.

POWELL, W.C, CARMICHAEL, D.M. & HODSON, J.C (1994) Conditions and relative timing of metamorphism during the evolution of the southwest Abitibi Greenstone Belt. *Geol./Mineral. Assc. Can.* Program with Abstracts, **19**, A90.

RAPP, R.P. & WATSON, E.B. (1986): Monazite solubility and dissolution kinetics: implications for the thorium and light rare earth chemistry of felsic magmas. *Contrib. Mineral. Petrol.* **94**, 304-316.

SCAILLET, B., FRANCE-LANORD, C., & LE FORT, P. (1990): Badrinath-Gangotri plutons (Garhwal, India): petrological and geochemical evidence for fractionation processes in a high Himalayan leucogranite. *J. Vol. Geotherm. Res.* **44**, 163-188.

SUTCLIFFE, R.H., BARRIE, C.T., BURROWS, D.R., & BEAKHOUSE, G.P. (1993): Plutonism in the Southern Abitibi Subprovince: a tectonic and petrogenetic framework. *Econ. Geol.* **88**, 1359-1375.

SHEARER, C.K., PAPIKE, J.J. & LAUL, J.C. (1987): Mineralogical and chemical evolution of a rare-earth granite-pegmatite system: Harney Peak granite, Black Hills, South Dakota. *Geochim. Cosmochim. Acta* **51**, 473-486.

_____, _____, & JOLLIFF B.L. (1992): Petrogenetic links among granites and pegmatites in the Harney Peak rare-element granite-pegmatite system, Black Hills, South Dakota. *Can Mineral.* **30**, 785-809.

SIMMONS, WM.B., LEE, M.T. & BREWSTER, R.H. (1987): Geochemistry and evolution of the south Platte granite-pegmatite system, Jefferson County, Colorado. *Geochim. Cosmochim. Acta.* **51**, 455-471.

SPEER, J.A. (1984): Micas in igneous rocks. *In* Micas (SA Baily, ed.), M.S.A Reviews in Mineralogy. **13**, 299-356.

_____, & BECKER, S.W. (1992): Evolution of magmatic and subsolidus AFM mineral assemblages in granitoids rocks: biotite, muscovite, and garnet in the Cuffytown Creek pluton, South Carolina. *Am. Mineral.* **77**, 821-833.

STEIGER, R.H. & WASSERBURG, G.J. (1969): Comparative U-Th-Pb systematics in 2.7 x 10^6 yr. plutons of different geologic histories. *Geochim. Cosmochim. Acta* **33**,

1213-1232.

TINDEL, A.G. & PEARCE, J.A. (1981): Petrogenetic modeling of in situ fractional crystallization in the zoned Loch Doon pluton, Scotland. *Contrib. Mineral. Petrol.* **78**, 196-207.

TULLOCH, A.J. (1979): Secondary Ca-Al silicates as low-grade alteration products of granitoid biotite. *Contrib. Mineral. Petrol.* **69**, 105-117.

VYHNAL, C.R., MCSWEEN JR., H.Y. & SPEER, J.A. (1991): Hornblende chemistry in southern Appalachian granitoids: implications for aluminum hornblende thermobarometry and magmatic epidote stability. *Am. Mineral.* **76**, 176-188.

WALL, V.J., CLEMENS, J.D., & CLARKE, D.B. (1987): Models for granitoid evolution and source composition. *J. Geol.* **6**, 731-750.

WATSON, E.B. & HARRISON, T.M. (1983): Zircon saturation revisited: temperature and composition effects in a variety of crustal magma types. *Earth Planet. Sci. Lett.* **64**, 295-304.

WILLIAMS, M.L. & GRAMBLING, J.A. (1990): Manganese, ferric iron, and the equilibrium between garnet and biotite. *Am. Mineral.* **75**, 886-908.

CHAPTER 3

PETROGENESIS OF ZONED MONZOGRANITIC PLUTONS AND ASSOCIATED RARE-ELEMENT-ENRICHED GRANITIC PEGMATITES AND QUARTZ VEINS: THE PREISSAC-LACORNE BATHOLITH, QUEBEC

Thomas MULJA, Anthony E. WILLIAMS-JONES,

Scott A. WOOD[1], and Michel BOILY[2]

Department of Earth and Planetary Sciences, McGill University,

3450 University St., Montreal, Quebec H3A 2A7

[1]Department of Geology and Geological Engineering,

University of Idaho, Moscow, Idaho 83843, U.S.A.

[2] 2121 De Romagne, Laval, Quebec H7M 5P8

ABSTRACT

The Archean Preissac-Lacorne batholith in northwestern Québec includes four felsic plutons (Preissac, Moly Hill, Lamotte, Lacorne), which are zoned from biotite to muscovite monzogranite. The Lamotte and Lacorne plutons are also associated spatially with rare-element pegmatites, whereas pegmatites are absent from the Moly Hill pluton and do not contain rare-element minerals in the Preissac pluton. The rare-element pegmatites are zonally distributed from beryl-bearing in the plutons to spodumene-bearing in the country rocks. Molybenite-bearing quartz veins are associated with all four plutons, and in the case of the Lamotte and Lacorne plutons, occur beyond the spodumene pegmatites. Molybdenite-bearing albitite dikes occur north of the Lacorne pluton.

All the plutons are weakly to moderately peraluminous (A/CNK: 1.0-1.3) and exhibit a compositional continuum in major- and trace-element contents from biotite to muscovite monzogranite. This compositional continuum extends into the rare-element pegmatites, indicating that the monzogranites and pegmatites are comagmatic. The chemistry of the pegmatites suggests that they underwent further evolution from beryl-bearing to spodumene-bearing varieties. The monzogranites and pegmatites have $\delta^{18}O_{(SMOW)}$ values (8.6 ± 0.3 ‰).

The zonation of the plutons, the geochemical trends, and the oxygen isotopic compositions indicate that the various types of monzogranite were mainly the products of fractional crystallization. Trace element (Rb, Ba, Sr) modeling of the Lamotte and Lacorne plutons suggests that the most fractionated monzogranite could have been formed by 80-90 % crystallization of the magma that formed the biotite monzogranite. A model is proposed for the evolution of the Lamotte and Lacorne plutons, in which side-wall crystallization produced the observed quasi-concentric zonation, and created volatile-rich residual melts. These melts were subsequently injected sequentially into the overlying parental monzogranite and later the country rocks, producing zonally distributed beryl and spodumene pegmatites, respectively. Fluids exsolved from the most evolved pegmatites back-reacted with earlier-crystallized spodumene-bearing aplite to form albitite, or separated from the melts, filling fractures as molybdenite-bearing quartz veins. The

smaller Preissac and Moly Hill plutons, which host molybdenite-bearing quartz veins, did not evolve sufficiently to form rare-element pegmatites. Vapor saturation occurred during late crystallization of the muscovite monzogranite, and culminated in the formation of molybdenite-bearing quartz veins, which filled fractures in the overlying crust of previously solidified magma.

Keywords: rare-element monzogranite, beryl and spodumene pegmatites, molybdenite-bearing albitite and quartz veins, geochemistry, fractional crystallization, Preissac-Lacorne batholith, Archean, Québec.

INTRODUCTION

Recent investigations of rare-element-enriched granites and granitic pegmatites have been concerned mainly with the very late stages of the evolution of the magma, particularly the transition to subsolidus processes (e.g., Černý et al. 1986, London 1986, Trumbull 1993, Linnen & Williams-Jones 1994). However, comparatively few studies have focused on the early history of magmatic crystallization (e.g., Goad & Černý 1981, Breaks & Moore 1992, Shearer et al. 1992), which controls the pattern of subsequent enrichment of the residual melt in elements of economic importance (Burnham & Ohmoto 1980). Another feature that is poorly documented is the zonal distribution of bodies of granitic pegmatite with respect to their predominant rare-element-bearing minerals, e.g., the occurrence of beryl-bearing granitic pegmatite within and close to the parental pluton, and of spodumene-bearing granitic pegmatite further away, in the country rocks.

The Preissac-Lacorne batholith in Québec (Fig. 1) contains several excellent examples of zoned monzogranitic intrusions and associated bodies of rare-element-enriched granitic pegmatite and Mo-bearing quartz veins. The monzogranites vary from biotite- to muscovite-bearing varieties, and show continuous variations in plagioclase, biotite and muscovite compositions, suggesting that the various subtypes of monzogranite are comagmatic (Mulja et al. 1995b). This compositional continuity extends to the bodies of rare-element pegmatite, thereby linking the evolution of the monzogranite to the formation of the Be-, Li-, Nb- and Ta-enriched pegmatites. The distribution of pegmatite bodies is zoned from beryl-bearing varieties within the monzogranitic plutons to spodumene-bearing varieties in the country rocks (Figs. 1A-D). Previous investigators (Dawson 1966, Bourne & Danis 1987, Feng & Kerrich 1992) have presented some geochemical data on the Preissac-Lacorne monzogranites, but have not distinguished between monzogranite types (cf. Mulja et al. 1995b) or analyzed the associated pegmatites. In this study, results of 85 chemical analyses of samples representing the various subtypes of monzogranite and pegmatite are used to decipher the geochemical evolution of the plutons. These data are integrated with geological and mineralogical

Fig. 1. Geological map of the Preissac-Lacorne batholith in northwestern Quebec, showing the locations of four monzogranitic plutons (after Dawson 1966) and the various subtypes of monzogranite and pegmatite (after Mulja et al. 1995b) The exposure of biotite (B) and muscovite-garnet (MGG) monzogranites in the Preissac pluton (B) are too small to be shown; the biotite monzogranite occurs as a narrow marginal facies of the muscovite monzogranite (MG), and the muscovite-garnet monzogranite occurs as dikes cutting the muscovite monzogranite in the northeast. A north-south (N-S) traverse along the length of the Lacorne pluton (D) is a reference for Figure 4. The boundaries of the plutons are based on the locations of the outermost occurrences of granitic rocks (Dawson 1966). Abbreviations are: Ab, Albitite; Brl, beryl pegmatite; Mo, molybdenite-bearing quartz veins; Spd, spodumene pegmatite; MBP, Mass Beryl Pegmatite (name of a prospect); QL-Spd, former Québec Lithium mine, about 7 km from the margin of the map.

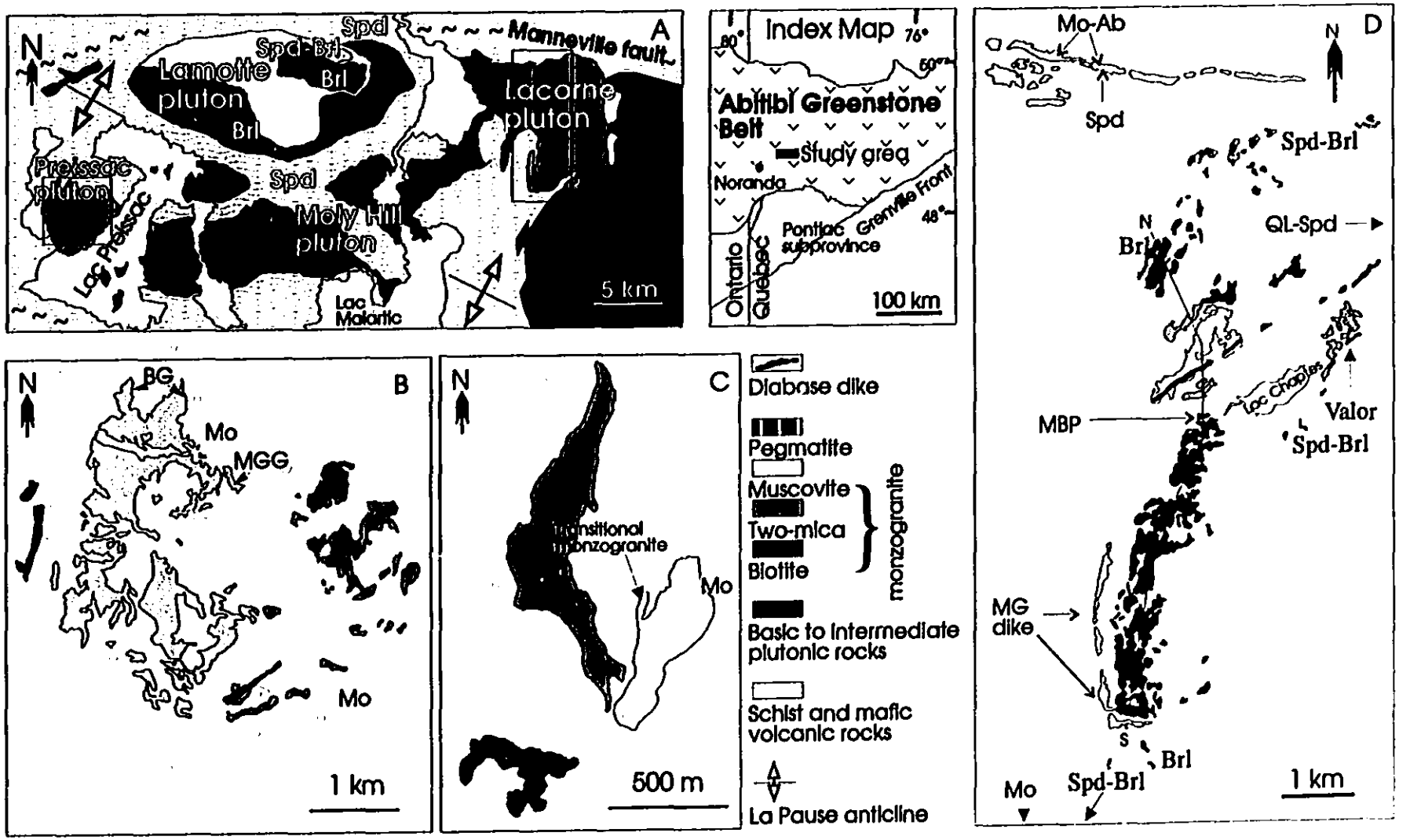
A
N
Spd
Manneville fault
Spd-Brl
Lamotte pluton
Brl
Lacorne pluton
Preissac pluton
Spd
Moly Hill pluton
Lac Preissac
Lac Malartic
5 km
Index Map
Abitibi Greenstone Belt
Study area
Noranda
Pontiac subprovince
Grenville Front
Ontario
Québec
100 km
B
N
BG
Mo
MGG
Mo
1 km
C
N
Transitional monzogranite
Mo
500 m
Diabase dike
Pegmatite
Muscovite
Two-mica
Biotite
monzogranite
Basic to intermediate plutonic rocks
Schist and mafic volcanic rocks
La Pause anticline
D
Mo-Ab
N
Spd
Spd-Brl
N
Brl
QL-Spd
Lac Chapais
Valor
Spd-Brl
MBP
MG dike
S
Brl
Mo
Spd-Brl
1 km

Figure 1

data (Mulja et al. 1995b) to develop a model that explains the processes responsible for the development of zoned rare-element-enriched granitic systems in and around the Preissac-Lacorne batholith.

GEOLOGICAL SETTING AND MINERALOGY OF THE MONZOGRANITE

The Preissac-Lacorne batholith crops out over an area of approximately 600 km^2 in the southern Abitibi subprovince of the Superior province, and was emplaced in mafic to felsic volcanic rocks of the Kinojevis and Malartic groups, and biotite schist of the Kewagama Group (Fig. 1; Dawson 1966). Intrusive activity took place in two stages; the first stage at 2671-2675 Ma (Feng & Kerrich 1991) was marked by the emplacement of syntectonic gabbro to granodiorite, and the second stage at 2630-2655 Ma (Gariépy & Allègre 1985, Feng & Kerrich 1991, Feng et al. 1993) by the emplacement of post-tectonic monzogranite and pegmatite. This plutonism is believed to have occurred late in the development of the Abitibi Greenstone belt, and to have involved collision of continents in a convergent-plate setting (Dimroth et al. 1983). The early Preissac-Lacorne intrusions are interpreted to represent partial melting of a mantle wedge above a subduction zone, and the later intrusions, to be products of the melting of sedimentary rocks, which were part of a continental crust thickened by collision (Feng & Kerrich 1992).

The monzogranite forms four plutons, two of which, Lamotte and Lacorne, host and are surrounded by numerous rare-element-enriched pegmatite bodies. The other plutons, Preissac and Moly Hill, are associated with fewer bodies of pegmatite, most of which do not contain rare-element-bearing minerals. Molybdenite-bearing quartz veins and stockworks occur in or near all of the plutons.

Detailed mapping by Mulja et al. (1995b) has shown that each of the monzogranite plutons comprises biotite, two-mica and muscovite subtypes. The most westerly pluton, Preissac, is dominated by two-mica and muscovite monzogranites; biotite monzogranite occurs only as a narrow marginal facies adjacent to muscovite monzogranite in the northern part of the pluton. In addition to the principal subtypes of monzogranite, there

are also fine-grained dikes of muscovite-garnet monzogranite (Fig. 1A). Contacts between the principal subtypes of monzogranite are not exposed, except for that between biotite and muscovite monzogranite, which is marked by narrow, anastomosing veins (< 20 cm wide) containing quartz and K-feldspar. The three subtypes of monzogranite in the Moly Hill pluton form discrete bodies, which are separated by screens of mafic volcanic rocks and biotite schists. The contact relationships among the monzogranite subtypes are hidden, except at one locality, near the edge of the muscovite monzogranite, where there is a gradual transition from two-mica to muscovite monzogranite (Fig. 1B). Both the Lamotte and Lacorne plutons are quasi-concentrically zoned, with the outer unit of biotite monzogranite giving way inward to two-mica and muscovite monzogranites. A separate intrusion of muscovite monzogranite forms an L-shaped dike in the southern part of the Lacorne pluton. Contacts between subtypes of monzogranite are not exposed, except in the northern part of the Lacorne pluton, where the biotite monzogranite grades imperceptibly into two-mica monzogranite.

All subtypes of monzogranite vary from fine- to coarse-grained (crystals up to 0.5 cm across) and consist essentially of quartz (25-35 vol.%), plagioclase (30-45 %) and perthitic microcline (25-45 %), approximately 5 % biotite + muscovite, up to 3 % garnet, and minor epidote. Biotite monzogranite is distinguished from the other types of monzogranite by the presence of biotite and a lack of primary muscovite; the two-mica monzogranite contains muscovite and biotite roughly in the proportion 2:1, and muscovite monzogranite contains little or no biotite. Biotite and garnet show an antithetic relationship in the transition from biotite to muscovite monzogranite. In the compositional range from biotite to muscovite monzogranite, the plagioclase composition varies from $An_{17.5}$ to An_5, the Fe/(Fe+Mg) of biotite increases from 0.69 to 0.85, and the Fe/(Fe+Mg) and ^{IV}Al of muscovite increase from 0.65 to 0.85 and from 1.55 to 1.72, atoms per molar unit, respectively. The garnet is a normally zoned spessartine-almandine solid solution ($Sps_{30-60}Alm_{37-59}$) and does not show systematic compositional variations with monzogranite subtypes. The accessory minerals are xenotime, apatite, zircon, monazite, titanite, magnetite and ilmenite. In the muscovite and muscovite-garnet monzogranite subtypes, columbite-tantalite and molybdenite also are present as accessory

minerals. With the exceptions of xenotime and ilmenite, which are present in similar amounts (≤ 0.1 vol.%) in the main subtypes of monzogranite (xenotime is not present in the muscovite-garnet monzogranite dike), the abundances of all accessory minerals decrease systematically from biotite to muscovite monzogranite.

The rare-element-enriched pegmatite occurs as vertical to subhorizontal dikes (up to 8 meters wide and about 200 meters long), which generally strike east-west and randomly in the Lacorne and Lamotte plutons, respectively. On the basis of the predominant rare-element-hosting minerals, the pegmatite is subdivided into beryl-bearing, spodumene-beryl-bearing and spodumene-bearing types. In the text that follows, these types of pegmatite are referred to as beryl, spodumene-beryl and spodumene pegmatites. These bodies of pegmatite are zonally distributed from beryl pegmatite in the monzogranite through spodumene-beryl pegmatite at and near the margins of the monzogranite to spodumene pegmatite in the country rocks (Figs. 1A-D). Beyond the spodumene pegmatite to the north of the Lacorne pluton is a set of east-west-trending dikes of molybdenite-bearing albitite, which occupy fractures in the intercalated schist and basalt. The albitite dikes vary from 20 cm to 1 m wide and dip steeply 75° to the south.

The beryl pegmatite and muscovite monzogranite are mineralogically similar, except that the pegmatite contains beryl, more garnet (up to 10 vol.%), considerably more columbite-tantalite (up to 1 vol.%), and traces of gahnite. Spodumene-beryl pegmatite in the Lamotte pluton is distinguished from beryl pegmatite only by the presence of spodumene in the center of the pegmatite. In contrast, spodumene-beryl pegmatite associated with the Lacorne pluton has spodumene throughout, variable amounts of lepidolite (up to 5 vol.%), and traces of schorl and pyrophanite. The spodumene pegmatite differs mineralogically from the spodumene-beryl pegmatite by containing much more spodumene (up to 30 vol.%), much less microcline (<10 vol.%), less garnet, and generally no beryl or lepidolite. Both beryl and spodumene-beryl pegmatites are zoned from a garnet-rich aplite border through an albite-perthite-quartz-muscovite zone to a massive quartz core. In contrast, spodumene pegmatite bodies are not zoned, or subtly zoned where large crystals of perthite occur in the innner part of the pegmatite. The albitite is an almost monomineralic rock, composed mainly of euhedral to subhedral

albite, variable amounts of molybdenite, and traces of zircon, Ta-enriched ilmenite and garnet.

The plagioclase composition in the pegmatite is An_{1-5}, and the Fe/(Fe+Mg) and ^{IV}Al of muscovite are similar to those of muscovite monzogranite. The Cs content of muscovite in the muscovite monzogranite and rare-element pegmatites correlates positively with the contents of Ta and Rb, and negatively with those of Sc and K/Rb. The composition of columbite-tantalite ranges from ferrocolumbite in beryl pegmatite to manganotantalite in spodumene pegmatite (Mulja et al. 1995a).

GEOCHEMISTRY OF THE MONZOGRANITE

Analytical methods

Concentrations of the major and trace elements were determined with X-ray fluorescence spectrometry at McGill University, the Université de Montréal, and the Centre de Recherches Minérales du Québec. The concentrations of rare-earth elements in selected samples were determined by instrumental neutron-activation analyses at the Université de Montréal, and by inductively coupled plasma mass spectrometry (ICP-MS) at Memorial University of Newfoundland. Twelve whole-rock compositions from Bourne & Danis (1987) and Feng (1992) were included in this study.

Major and trace elements

The Preissac-Lacorne monzogranites are siliceous (72.4-76.5 wt.% SiO_2, Tables 1A, B), and weakly to moderately peraluminous [molar ratio $Al_2O_3/(CaO + Na_2O + K_2O)$: 1.1-1.3, and 1.2-2.8% normative corundum]. Although there is considerable scatter in the data, generally, the SiO_2 content increases from biotite to muscovite monzogranite (to muscovite-garnet monzogranite in the Preissac pluton), whereas the K_2O, CaO, MgO, Fe_2O_3 and TiO_2 contents decrease (Fig. 2); the Na_2O, MnO and Al_2O_3 contents are invariant. Two exceptions to these generalizations are shown by the Lacorne monzogranites, where the CaO content is inconsistent with monzogranite types, and the SiO_2 content in the muscovite monzogranite dike is lower than that in the main muscovite

TABLE 1A. BULK COMPOSITION OF THE PREISSAC AND MOLY HILL PLUTONS

Rock	Preissac monzogranite							Moly Hill monzogranite				
	Biotite	Two-mica		Muscovite		MG		Biotite	Two-mica		Muscovite	
		x	n	x	n	x	n		x	n	x	n
Major-element oxides (wt. %)												
SiO_2	72.4	74.8	7	75.5	10	76.1	3	73.8	74.2	2	75.4	7
TiO_2	0.16	0.10	7	0.04	10	0.02	3	0.16	0.09	2	0.03	7
Al_2O_3	15.4	14.4	7	14.4	10	14.2	3	14.6	14.6	2	14.5	7
Fe_2O_3	1.75	0.86	7	0.40	10	0.44	3	1.33	1.60	2	0.41	7
MnO	0.06	0.04	7	0.02	10	0.26	2	n.a	0.05	2	n.a	7
MgO	0.03	0.19	7	0.10	10	0.06	3	0.31	0.14	2	0.05	7
CaO	0.5	0.73	7	0.50	10	0.29	3	1.26	1.10	2	0.61	7
Na_2O	4.21	4.16	7	4.27	10	4.70	3	3.73	4.33	2	4.2	7
K_2O	5.63	4.20	7	4.10	10	3.63	3	4.37	4.47	2	4.24	7
P_2O_5	0.03	0.03	7	0.04	10	0.04	3	0.07	0.03	2	0.03	7
Trace-elements (ppm)												
Ba	6.76	419	5	10	6	4.62		788	236	3	9.5	
Rb	450	365	7	496	13	476	2	350	348	3	465	4
Sr	10.5	98	7	9.5	13	7.81	2	165	57	3	19	4
Zr	33	69	7	58	13	16	2	80	53	2	40	4
Nb	28	22	7	37	13	73	2	15	23	2	22.5	4
Y	24	12	7	26	13	24	2	8.7	11	3	33	4
Ta	4.82	6.3	2	5.6	2	9.6	2	4	3.8	3	5.6	
Hf	2.76	2.9	2	1.75	2	2.6	2	4.5	2.3	3	1.43	
Th	10.4	13	2	7.89	2	1.2	2	19.5	14	3	12	
Li	91	92	3	30	3	44		134	118		18	
Be	n.d	5	3	3		2.25		2.6	3.8	2	3	

Continued

Table 1A (continued)

Rare-earth elements (ppm)										
La	5.22	21.2	2	4.69	2	0.64	50.32	9.4	2	7.46
Ce	15.7	36	2	11.7	2	1.67	91.5	17.7	2	15.6
Pr	1.51			1.69	2	0.23	9.72	2	2	1.92
Nd	6.23	13.3	2	6.27	2	0.9	31.7	7.1	2	7.44
Sm	2.47	2.3	2	2.1	2	0.88	4.57	1.8	2	2.38
Eu	0.09	0.2	2	0.12	2	0.02	0.67	0.31	2	0.14
Gd	3.05			1.97	2	2.08	3.1	1.8	2	2.61
Tb	0.49	0.35	2	0.35	2	0.62	0.34	0.26	2	0.4
Dy	3.14			2.1	2	4.22	1.84	1.53	2	2.53
Ho	0.6	0.9	2	0.36	2	0.7	0.31	0.27	2	0.43
Er	1.51			0.97	2	1.87	0.74	0.77	2	1.18
Tm	0.23	0.8	2	0.15	2	0.35	0.12	0.12	2	0.17
Yb	1.55	1.05	2	0.91	2		0.64	0.76	2	1
Lu	0.2	0.15	2	0.12	2	0.36	0.1	0.11	2	0.14
Σ REE	42	76.3		33.5		14.5	196	43.9		43.4
Eu/Eu	0.03	0.08		0.06		0.01	0.17	0.17		0.06
$\delta^{18}O$		8.50		8.50	9					

*Including two samples, LC-5 and 6, from Feng (1992), with the exception of the REE

MG: muscovite-garnet monzogranite

E* = (Sm + Gd)/2. Where no data for Gd are reported, its value is approximated by the intersection of a straight line interpolated values for Sm and Tb.

X: mean; n: number of analyses (blank: one analysis)

Complete REE analyses (14 elements) were determined with the ICP-MS methods, partial REE analyses were determined with the NAA methods.

TABLE 1B. BULK COMPOSITION OF THE LAMOTTE AND LACORNE PLUTONS

	Lamotte monzogranite						Lacorne monzogranite							
	Biotite		Two-mica		Muscovite		Biotite		Two-mica		MG 1		MG 2	
	x	n	x	n	x	n	x	n	x	n	x	n	x	n
Major-element oxides (wt. %)														
SiO_2	74.4	6	75.1	4	76.1	2	74.5	10	75.4	8	76.5	2	75.2	3
TiO_2	0.08	6	0.04	4	0.03	2	0.09	10	0.06	8	0.03	2	0.06	3
Al_2O_3	14.2	6	14.4	4	14.6	2	14.1	10	13.8	8	14.0	2	14.8	3
Fe_2O_3	0.74	6	0.68	4	0.6	2	1.37	10	0.82	8	0.4	2	0.6	3
MnO	0.05	6	0.01	4	0.16	2	0.04	10	0.04	8	0.07	2	0.06	3
MgO	0.07	6	0.11	4	0.09	2	0.16	10	0.10	8	0.08	2	0.04	3
CaO	0.92	6	0.78	4	0.33	2	0.91	10	0.67	8	0.55	2	0.55	3
Na_2O	3.82	6	4.0	4	4.69	2	3.95	10	4.17	8	4.21	2	4.56	3
K_2O	4.36	6	4.43	4	3.39	2	4.63	10	4.28	8	4.3	2	4.16	3
P_2O_5	0.03	6	0.04	4	0.02	2	0.03	10	0.02	8	0.01	2	0.03	3
Trace-elements (ppm)														
Ba	502	6	145	5	12.5	2	550	11	154	8	69	2	28	3
Rb	284	6	367	8	455	2	391	11	641	8	488	2	703	3
Sr	110	6	46.1	8	10.5	2	118	11	59	8	36.5	2	18.3	3
Zr	88	6	52.9	7	18.5	2	79	10	61	8	60	2	40	3
Nb	16	6	17.9	7	42	2	16	10	22.7	8	24.5	2	48.5	3
Y	17	6	19.2	8	42.5	2	17.2	11	29	8	30.5	2	33	3
Ta	6.13	4	6	4	12	2	5	8	5.5	4	4.5	2	6.7	3
Hf	2.93	4	2.1	4	2.15	2	3.35	8	1.8	3	2		2.4	2
Th	16	5	16.2	5	4.55	2	22	8	21	5	15.5	2	8.3	3
Li	232	5	340	3	78	2	247	8	150	6	165	2	179	3
Be	3.6	5	5.75	4	4.5	2	4.22	8	5.8	5	6.5	2	8	3
U	4.13	4	8	5	7.3	2	3.21	8	5.5	5	4.6	2	11.3	3
Ga	21	5	24	3	34		20	3	23	3	26.5	2	26	

Continued

Table 1B (continued)

Rare-earth elements (ppm)										
La	19.5	5	11.7	6	5.1	24.3	3	12.8	2	9.35	5.54
Ce	37.5	5	21	6	16	41.7	3	27.4	2	19.2	11.7
Pr						4.62	3	3.15	2	2.4	1.34
Nd	14	5	8.12	6	8	12.7	3	11.6	2	8.93	4.73
Sm	2.1	5	2.33	6	2.6	2.4	3	3.23	2	2.62	1.63
Eu	0.36	5	0.23	6	0.1	0.38	3	0.24	2	0.19	0.14
Gd						2.22	3	3.28	2	2.9	1.93
Tb	0.36	5	0.4	6	0.9	0.25	3	0.55	2	0.51	0.35
Dy						1.5	3	3.85	2	3.7	2.4
Ho	0.7	5	0.85	6	1.5	0.31	3	0.73	2	0.7	0.46
Er						0.7	3	2.17	2	2.1	1.36
Tm			0.13	6	1.3	0.11	3	0.35	2	0.34	0.2
Yb	0.86	5	1.85	6	2.2	0.76	3	2.44	2	2.42	1.32
Lu	0.3	5	0.25	6	0.3	0.12	3	0.36	2	0.35	0.16
Σ REE	75.7		46.9		38	92.1		72.2		55.7	33.3
Al/Ga	3639		3150		2272	3852		3196		2796	3012
Th/U	4.15		2.23		0.55	7		3.75		3.4	1.45
Eu/E	0.23		0.13		0.03	0.16		0.07		0.07	0.08
$\delta^{18}O$	8.6		8.5	2	9.3	8.60	3	8.40	2	8.30	9.60

*Including three samples, BD-3060, 3061 and 3062, from Danis (1985), and one sample LC-30 from Feng (1992), with the exception of the REE

MG 1: main muscovite monzogranite; MG 2: muscovite monzogranite dike (see Figure 1D)

Fig. 2. Plot of major element oxides (wt %) versus SiO_2 for all types of monzogranite in the Preissac, Moly Hill, Lamotte and Lacorne plutons. In this and subsequent diagrams, the symbols of the monzogranite, unless otherwise indicated, are: black square, biotite monzogranite; white square, two-mica monzogranite; black circle, muscovite monzogranite; white triangle, dikes of muscovite-garnet monzogranite (Preissac pluton) and muscovite monzogranite (Lacorne pluton). There is only one data point for biotite monzogranite of the Preissac pluton owing to the small exposure of the rock (Fig.1, and Mulja et al. 1985b). The bulk-rock chemistry of the biotite monzogranite therefore cannot be assessed in the present paper.

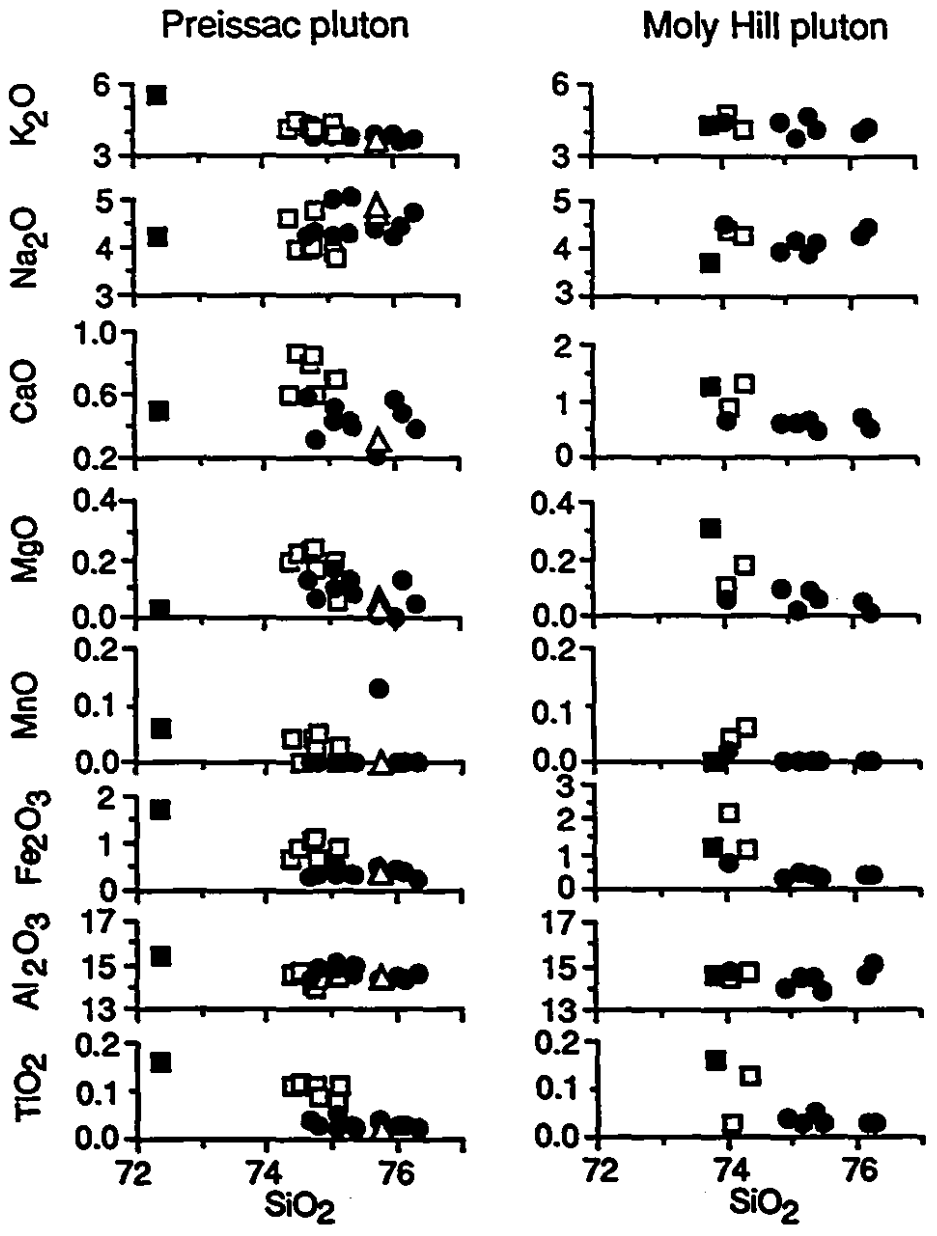
Preissac pluton
Moly Hill pluton
K2O
Na2O
CaO
MgO
MnO
Fe2O3
Al2O3
TiO2
SiO2
SiO2

Figure 2

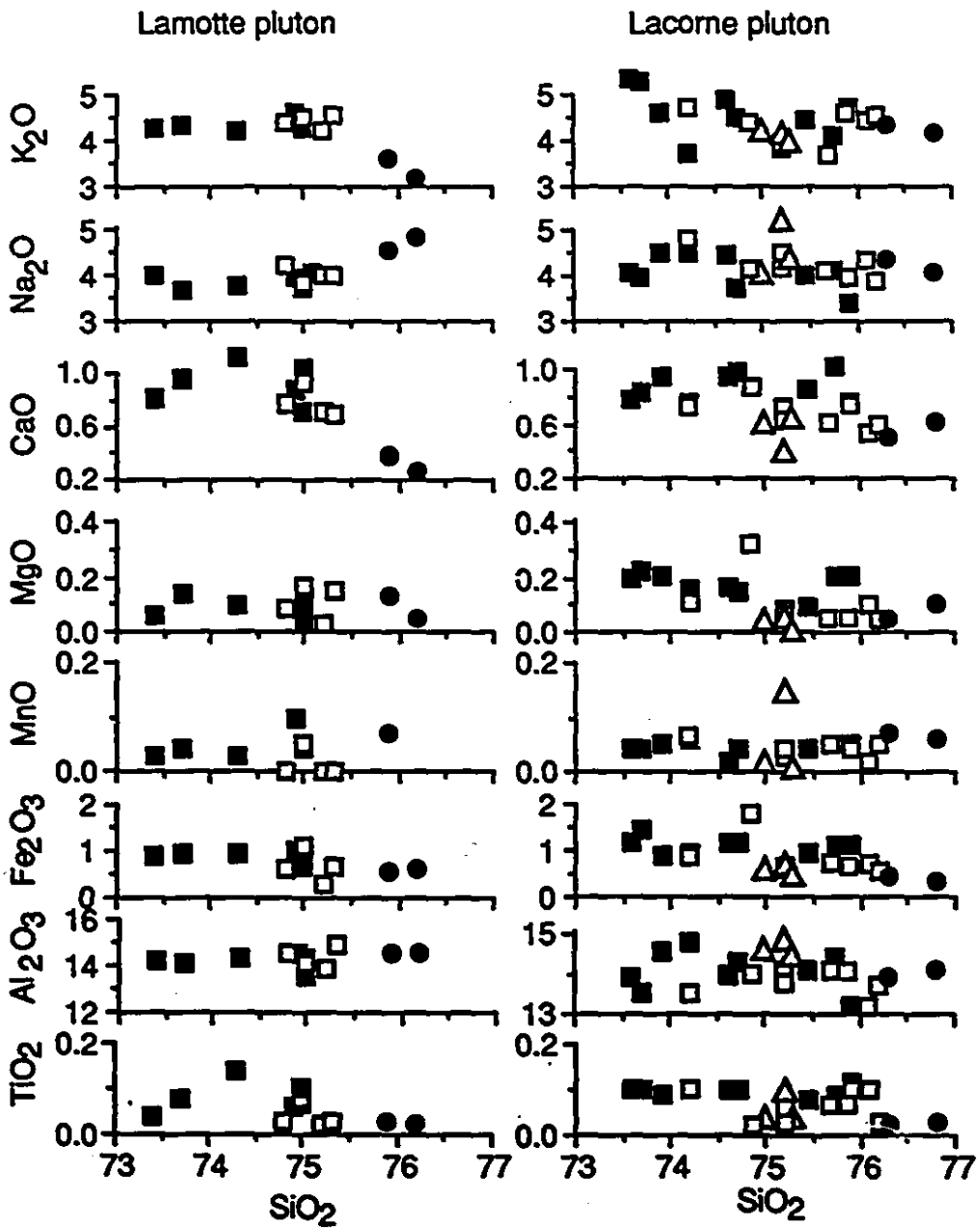
Lamotte pluton
Lacorne pluton
K2O
Na2O
CaO
MgO
MnO
Fe2O3
Al2O3
TiO2
SiO2
SiO2

Figure 2

monzogranite. The concentration of Ba, Sr and Th decreases from biotite to muscovite monzogranite (Fig. 3). The Zr content also decreases, but only in the Lamotte and Lacorne plutons. In contrast, the Rb content increases from biotite to muscovite monzogranite, and the content of Nb is highest in muscovite monzogranite. The concentration of trace elements, other than those mentioned above, and of Li, Be, U, Ga, F and *REE*, which are discussed below, do not exhibit systematic trends with monzogranite type.

Besides varying with monzogranite type, the contents of Ba and Sr also vary spatially within the Lacorne pluton. In the northern part of the pluton, their contents decrease toward the two-mica monzogranite (Fig. 4). On the other hand, in the southern biotite monzogranite, Ba and Sr contents decrease inward from the margins of the intrusion.

The distribution of bodies of spodumene pegmatite, i.e., their restriction to the Lamotte and Lacorne plutons, is reflected in the relative contents of Li in the monzogranites of the four plutons. The content of this element in each of the monzogranite types in the Preissac and Moly Hill plutons is low relative to that in the corresponding monzogranites in the Lamotte and Lacorne plutons. Moreover, the content of Li in the muscovite monzogranite of each pluton is markedly lower than that of the other types of monzogranite. In the Preissac and Moly Hill plutons, the contents of Li averaged over biotite and two-mica monzogranites are 92 ± 12 ppm and 126 ± 11 ppm, respectively. In contrast, the corresponding values in the Lamotte and Lacorne plutons are 265 ± 107 and 202 ± 124 ppm. The contents of Li in muscovite monzogranite for the four plutons are 30 ± 2 ppm (Preissac), 18 ppm (Moly Hill), 78 ± 32 ppm (Lamotte) and 173 ± 70 ppm (Lacorne, including the muscovite monzogranite dike). The distribution of Be is much more uniform among the four plutons, and does not vary appreciably with monzogranite type. However, it may be significant that the Be content is lowest in the Moly Hill pluton (3 ± 0.6 ppm versus 4 ± 1.4, 4.5 ± 1.8 and 5.5 ± 1.8 ppm in the Preissac, Lamotte and Lacorne plutons, respectively); the Moly Hill pluton is the only one that does not contain beryl.

Fig. 3. Plot of trace-element contents (ppm) versus SiO_2 for all types of monzogranite in the Preissac, Moly Hill, Lamotte and Lacorne plutons.

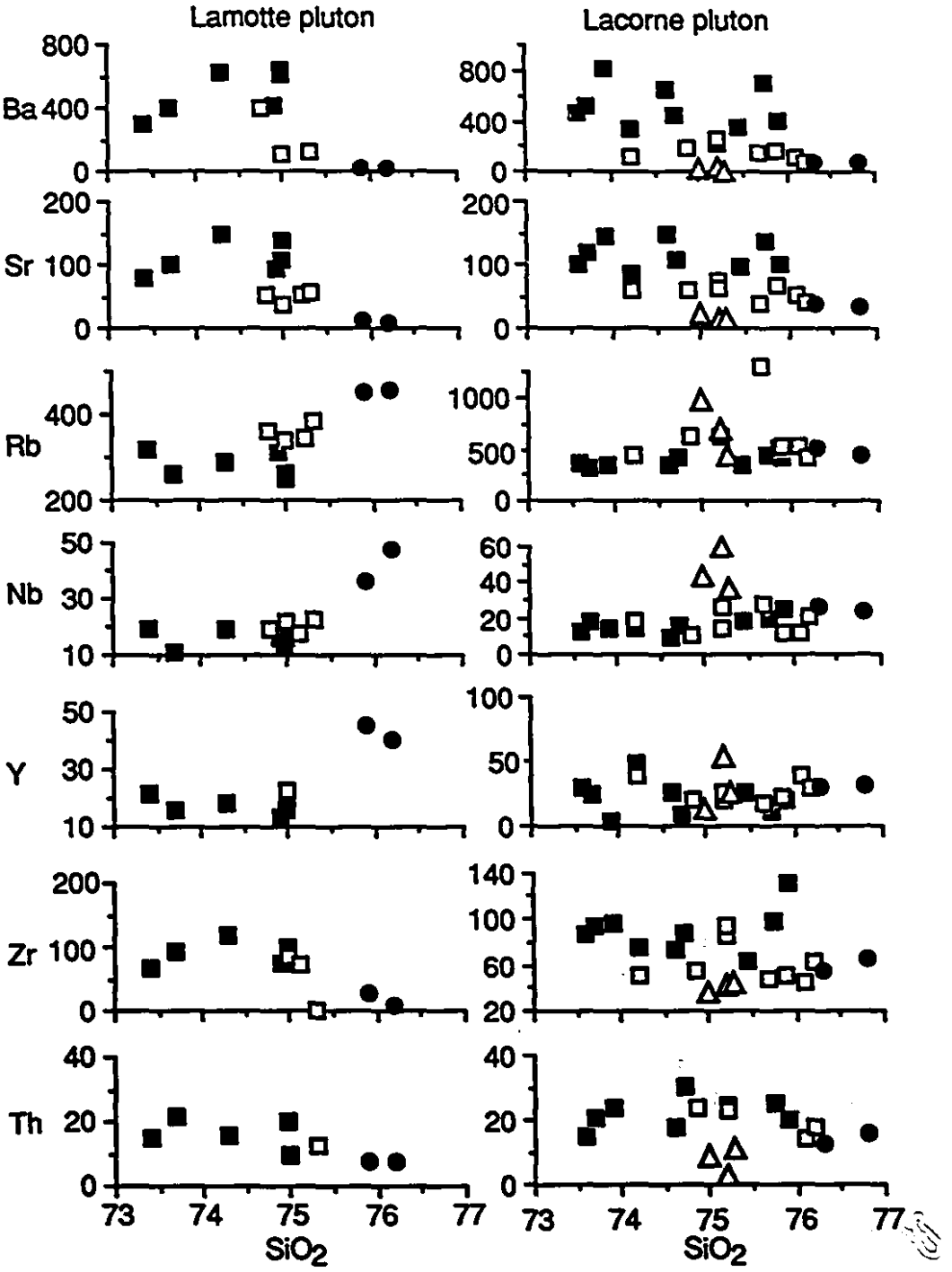
Lamotte pluton
Lacorne pluton
Ba
Sr
Rb
Nb
Y
Zr
Th
800
400
0
200
100
1000
500
60
40
20
140
50
73
74
75
76
77
SiO2

Figure 3

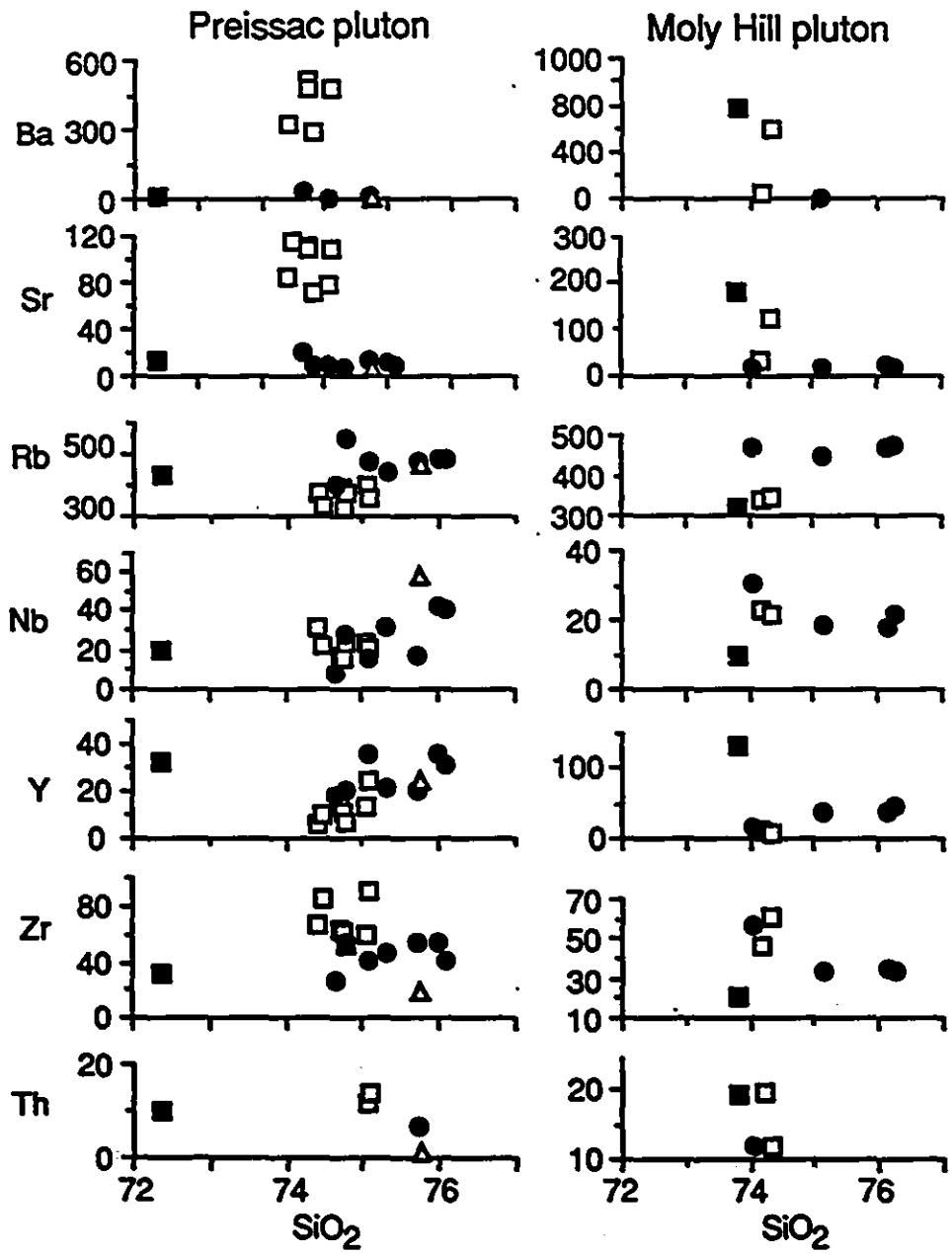
Preissac pluton
Moly Hill pluton
Ba
Sr
Rb
Nb
Y
Zr
Th
600
300
0
1000
800
400
120
80
40
300
200
100
500
400
60
20
70
50
30
10
72
74
76
SiO2

Figure 3

Fig. 4. Bulk-rock contents of Ba and Sr along a north-south traverse (N-S) in the Lacorne-pluton (Fig. 1), showing chemical trends from biotite to muscovite monzogranite in the northern part of the pluton, and from the margins to the center of the southern biotite monzogranite.

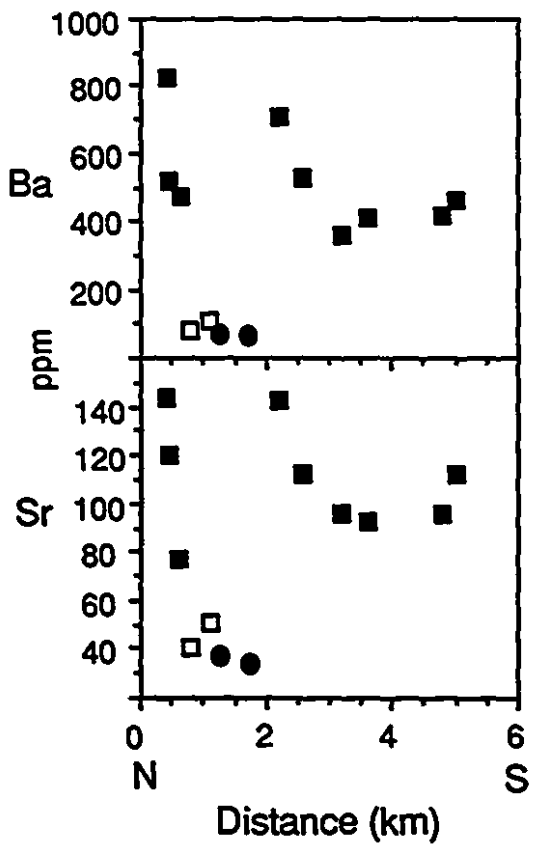
1000
800
600
Ba
400
200
ppm
140
120
Sr
100
80
60
40
0
2
4
6
N
S
Distance (km)

Figure 4

Concentrations of U and Ga were determined only for the Lamotte and Lacorne monzogranites, and were found to increase systematically from biotite to muscovite monzogranite (Table 1B). The average Th/U values in the Lamotte and Lacorne plutons decrease from 5.4 and 7 in biotite monzogranite, through 2.2 and 3.9 in two-mica monzogranite, to 0.55 and 0.4 in muscovite monzogranite, respectively. In the same order of types of monzogranite, the mean values of Al/Ga decrease: 3639 → 3150 → 2272 in the Lamotte pluton, and 3852 → 3196 → 2796 in the Lacorne pluton.

The fluorine content was established in only three samples of two-mica monzogranite and two samples of muscovite monzogranite, all from the Lacorne pluton. The average F content is 0.03 wt.%, and does not vary with rock type.

The sum of the rare-earth elements is low, less than 100 ppm, in all subtypes of monzogranite, except for the Moly Hill biotite monzogranite, where it is approximately 200 ppm (Tables 1A, B). Chondrite-normalized profiles display light rare-earth enrichment and negative Eu anomalies, and there is a general tendency for the profiles to flatten and the Eu anomaly to become increasingly negative from biotite to muscovite monzogranite (Fig. 5).

GEOCHEMISTRY OF THE PEGMATITES AND ALBITITES

Major and trace elements

Only a small number of the occurrences of spodumene pegmatite in the Lamotte pluton, and of beryl and spodumene pegmatites in the Lacorne pluton, could be analyzed (rare-element pegmatites do not occur in the Preissac and Moly Hill plutons), owing to the difficulty of obtaining representative bulk-samples of these very coarse-grained rocks. In order to minimize the problem of sample heterogeneity, approximately 4 kg of material were collected from channels cut across small bodies of pegmatite (< 1 m wide).

The beryl pegmatite in the Lacorne pluton contains 73.5 to 77 wt.% SiO_2 (most samples contain between 76 and 77 wt% SiO_2), and thus is indistinguishable in terms of SiO_2 content from the muscovite monzogranite (Tables 1B, 2). The spodumene pegmatite in the Lacorne and Lamotte plutons contains 73-74 wt.% and 74 wt.% SiO_2, respectively.

Fig. 5. Chondrite-normalized *REE* profiles for the subtypes of monzogranite in all four plutons. The chondrite values are those recommended by Boynton (1984).

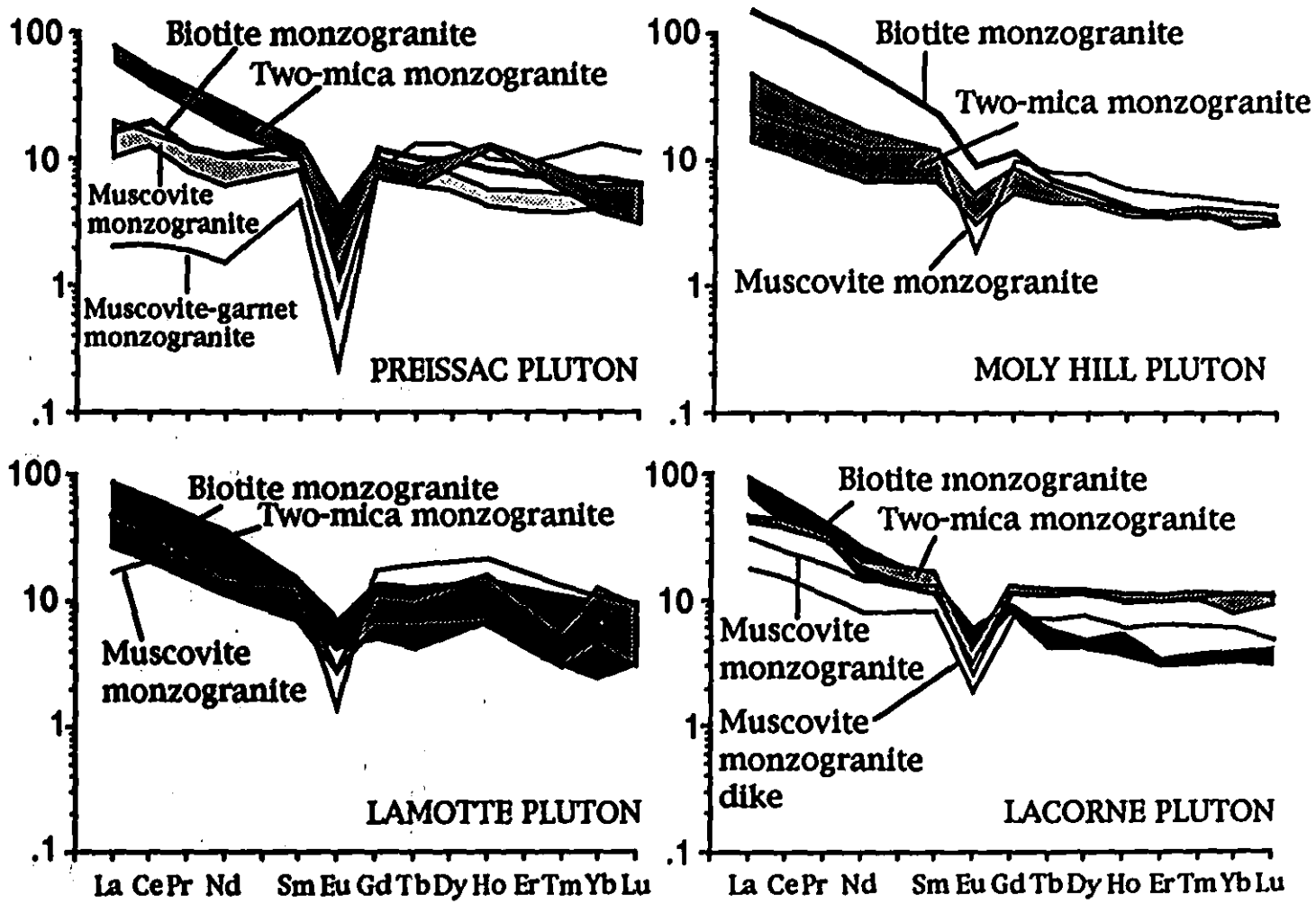
100
10
1
.1
Biotite monzogranite
Two-mica monzogranite
Muscovite monzogranite
Muscovite-garnet monzogranite
PREISSAC PLUTON
Biotite monzogranite
Two-mica monzogranite
Muscovite monzogranite
MOLY HILL PLUTON
Biotite monzogranite
Two-mica monzogranite
Muscovite monzogranite
LAMOTTE PLUTON
Biotite monzogranite
Two-mica monzogranite
Muscovite monzogranite
Muscovite monzogranite dike
LACORNE PLUTON
La Ce Pr Nd Sm Eu Gd Tb Dy Ho Er Tm Yb Lu

Figure 5

TABLE 2. BULK COMPOSITION OF PEGMATITE AND ALBITITE

Pluton	Lamotte		Lacorne						
Rock	Spd		Brl		Spd	Ab 1		Ab 2	
	x	n	x	n		x	n	x	n
Major-element oxides (wt. %)									
SiO_2	74.4	2	75.9	4	73.6	69	4	68	2
TiO_2	0.01	2	0.02	4	0.01	0.01	4	0.02	2
Al_2O_3	16	2	14.6	4	16	19.4	4	20.1	2
Fe_2O_3	0.97	2	0.51	4	0.16	0.16	4	0.11	2
MnO	0.16	2	0.3	4	0.13	0.07	4	0.2	2
MgO	0.24	2	0.03	4	0.01	0.01	4	0.01	2
CaO	0.27	2	0.3	4	0.06	0.53	4	0.13	2
Na_2O	3.91	2	5.13	4	4.31	10.1	4	10.8	2
K_2O	2.02	2	3.12	4	4	0.09	4	0.3	2
P_2O_5	0.01	2	0.02	4	0.04	0.03	4	0.05	2
Trace-elements (ppm)									
Ba	10	2	26.3	4	3.2	48	4	67	2
Rb	1104	2	853	4	4875	13.6	4	2.25	2
Sr	22	2	31.3	4	53	72	4	511	2
Zr	26	2	42	4	7	31	4	55	2
Nb	60	2	95	4	50	45.7	4	44	2
Y	14.5	2	15	4	0.6	2.55	4	2.25	2
Ta	43		60	4	67	225	2	122	2
Th	2.4		9.5	4	2	4		5	
U	1.7		18	4		5.5		12	
Ga	46	2	43	4		57	2	60	2
Li	6735	2	257	4		6.5	2	6	2

Continued

Table 2 (continued)

						Aplite
Rare-earth elements (ppm)						
La	0.8	2	5.72	0.2	1.86	0.96
Ce	1.75	2	18	0.52	3.35	3.22
Pr			2.71	0.06	0.37	0.51
Nd	3.5	2	10.5	0.24	1.63	2
Sm	0.65	2	8.68	0.34	1.18	1.81
Eu	0.1	2	0.03	0.01	0.06	0.05
Gd			5.63	0.33	1.02	1.43
Tb	0.15	2	0.63	0.06	0.19	0.16
Dy			1.62	0.18	0.68	0.47
Ho	0.35	2	0.13	0.02	0.06	0.05
Er			0.19	0.02	0.11	0.1
Tm			0.02	0.01	0.02	0.01
Yb	0.2		0.12	0.06	0.16	0.05
Lu	0.1	2	0.02	0.01	0.03	0.02
Σ REE	7.6		54	2.06	10.7	10.8
Al/Ga	1806		1826			
Th/U	1.4		0.58			
Eu/Eu	0.21		0.004	0.03	0.05	0.031
$\delta^{18}O$	8.8		8.7-9.5	7.6-10.3	8.8	2

Brl: beryl pegmatite; Spd: spodumene pegmatite; Ab: albitite

Harker diagrams of major-element oxides against SiO_2 for the muscovite monzogranite and the pegmatites do not show any significant variations except for Na/K, which is slightly higher in beryl pegmatite. The contents of Ba, Y and Th decrease, whereas those of Rb and Ga increase, from muscovite monzogranite to spodumene pegmatite in both plutons (Fig. 6). The contents of Zr and Hf decrease in the Lacorne pluton but increase in the Lamotte pluton from muscovite monzogranite to spodumene pegmatite. The content of Sr decreases initially from the monzogranite to the beryl pegmatite, but then increases in the spodumene pegmatite, in the Lacorne pluton. A possible explanation for the high Sr content of the spodumene pegmatite is the breakdown of radiogenic Rb (cf. Clark & Černý 1987). In the Lamotte pluton, the Sr content is higher in the spodumene pegmatite than in the muscovite monzogranite. The content of Nb increases from the monzogranite to the beryl pegmatite, and then drops in the spodumene pegmatite. This sharp decrease is reflected by the presence of tantalite as opposed to columbite in the latter pegmatite (Mulja et al. 1995b). In the Lamotte pluton, the Nb content is higher in the spodumene pegmatite than in the muscovite monzogranite.

The Σ *REE* content of beryl pegmatite (Lacorne pluton) is similar to that of muscovite monzogranite (54 versus 56 ppm). However, the Σ *REE* content of spodumene pegmatite in both plutons is sharply lower at 2.06 ppm (Lacorne) and 7.6 ppm (Lamotte). Both beryl and spodumene pegmatites display chondrite-normalized gull-wing profiles as a result of depletions of *LREE* and *HREE* (Figs. 7A, B). An aplite dike, which cuts the L-shaped muscovite monzogranite dike in the Lacorne pluton, has a chondrite-normalized *REE* pattern similar to that of the pegmatites (Fig. 7B).

The albitite dikes, which occur only in association with the Lacorne pluton, have a uniform major-element composition, but form two distinct populations with respect to their trace-element concentrations (Table 2). Group-1 albitite has much higher Rb and Ta contents, and Group-2 albitite has a much higher content of Sr. The Σ *REE* content of the albitite (Group 1) is 10.7 ppm, a value intermediate between those of the beryl and spodumene pegmatites in the Lacorne pluton. It is worth noting that its REE_N profile is almost identical to that of aplite (Fig. 7B).

Fig. 6. Selected trace-element (ppm) concentrations in the muscovite monzogranite and types of pegmatite in the Lamotte and Lacorne plutons. The elevated Sr contents of beryl and spodumene pegmatites in the Lacorne pluton could be due to the decay of ^{87}Rb (see text).

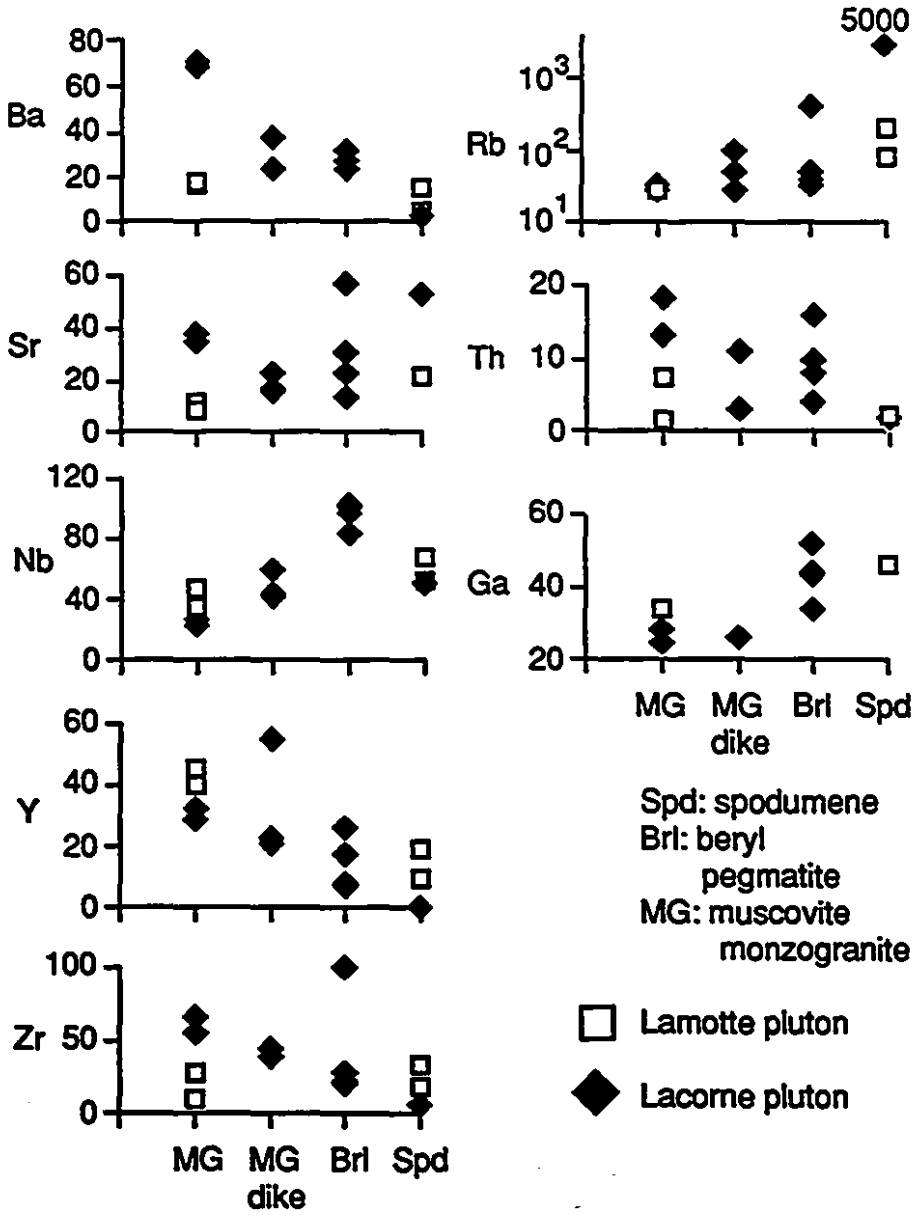
Ba
Rb
Sr
Th
Nb
Ga
Y
Zr
MG
MG dike
Brl
Spd
Spd: spodumene
Brl: beryl pegmatite
MG: muscovite monzogranite
Lamotte pluton
Lacorne pluton

Figure 6

Fig. 7. REE_N profiles of rare-element pegmatites in the Lamotte and Lacorne plutons. Also shown are the REE_N profiles for dikes of aplite and albitite. The stippled area indicates the range of REE_N in the monzogranite.

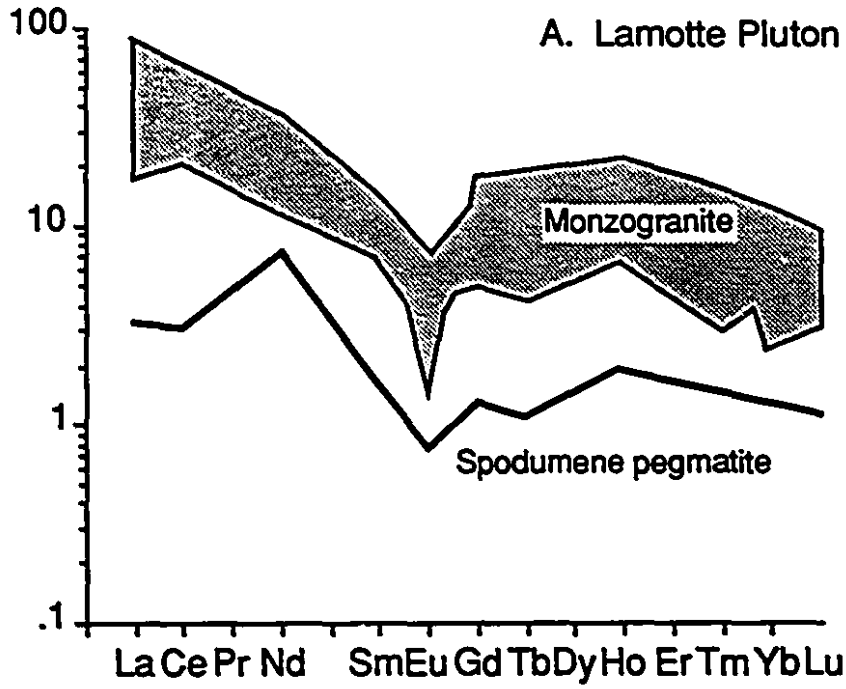
A. Lamotte Pluton
100
10
1
.1
Monzogranite
Spodumene pegmatite
La Ce Pr Nd Sm Eu Gd Tb Dy Ho Er Tm Yb Lu

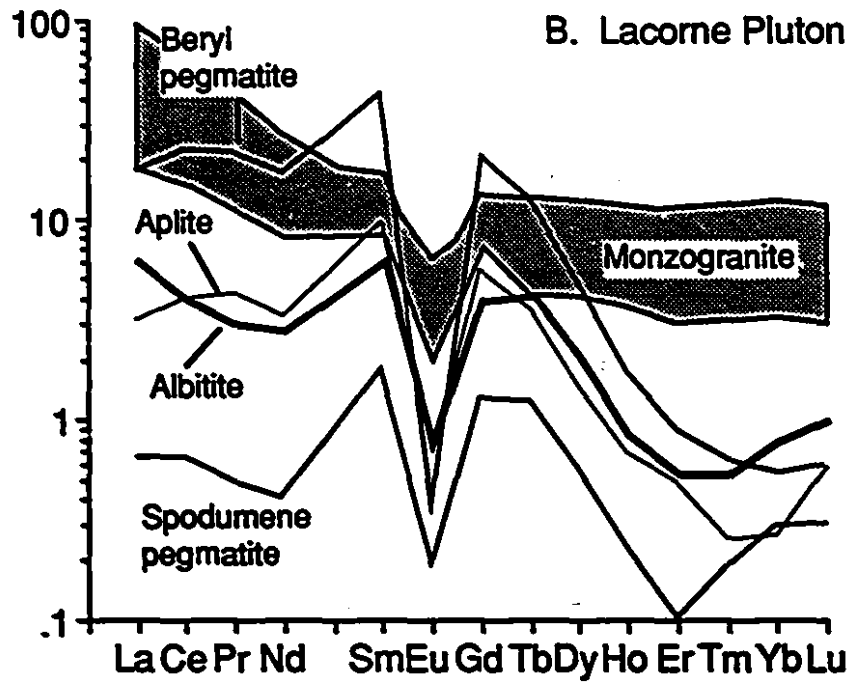
B. Lacorne Pluton
100
10
1
.1
Beryl pegmatite
Aplite
Albitite
Monzogranite
Spodumene pegmatite
La Ce Pr Nd Sm Eu Gd Tb Dy Ho Er Tm Yb Lu

Figure 7

OXYGEN ISOTOPE ANALYSES

Oxygen isotope analyses (whole rock) of representative samples of monzogranite, pegmatite, and albitite were performed at the Université de Montréal and the University of Saskatchewan. Details of the analytical technique are given in Hoy (1993). All $\delta^{18}O$ values are reported relative to Standard Mean Ocean Water (SMOW).

The whole-rock $\delta^{18}O$ values of the Preissac, Lamotte and Lacorne monzogranites (the Moly Hill monzogranite was not analyzed) range from 8.1 to 9.8‰, with most values lying between 8.1 and 8.8‰ (Tables 1, 2, Fig. 8). This range is typical of fresh granitic rocks, which show a range of $\delta^{18}O$ from 7 to 10‰ (Taylor 1978). The monzogranites are isotopically indistinguishable from one type of monzogranite to another within each of the plutons, or from one pluton to another, i.e., they have not undergone significant interaction with meteoric water. A similar range of $\delta^{18}O$ values is also displayed by the four samples of beryl pegmatite, whereas the spodumene pegmatites show a somewhat wider range of $\delta^{18}O$ values (7.4 to 10.3‰). Interestingly, the mean $\delta^{18}O$ values of monzogranite, beryl and spodumene pegmatites are almost identical (Tables 1, 2), and similar to the $\delta^{18}O$ values of the two samples of albitite analyzed.

DISCUSSION

Geochemical evolution

The systematic chemical trends described above and the geological relationships discussed earlier, and in Mulja et al. (1995b), provide strong evidence of the evolution of the Preissac-Lacorne plutons from early biotite through two-mica and muscovite monzogranite to beryl and spodumene pegmatites. The most plausible explanation for this evolution is fractional crystallization of a parental monzogranitic magma.

Depletion of Ti, Fe, Ca, Ba, Sr, Zr and Th, and concomitant enrichment of Rb, Nb and U from biotite to muscovite monzogranite (Figs. 2, 3, 5) are consistent with early fractionation of plagioclase, biotite, zircon, monazite and apatite, and late crystallization of albite, muscovite, garnet, and columbite-tantalite. Similarly, the systematic increase in

Fig. 8. Results of oxygen isotope analyses of monzogranite, pegmatite (white and black symbols are for Lamotte and Lacorne plutons, respectively), and albitite in the Preissac-Lacorne batholith. The values are quoted with respect to SMOW.

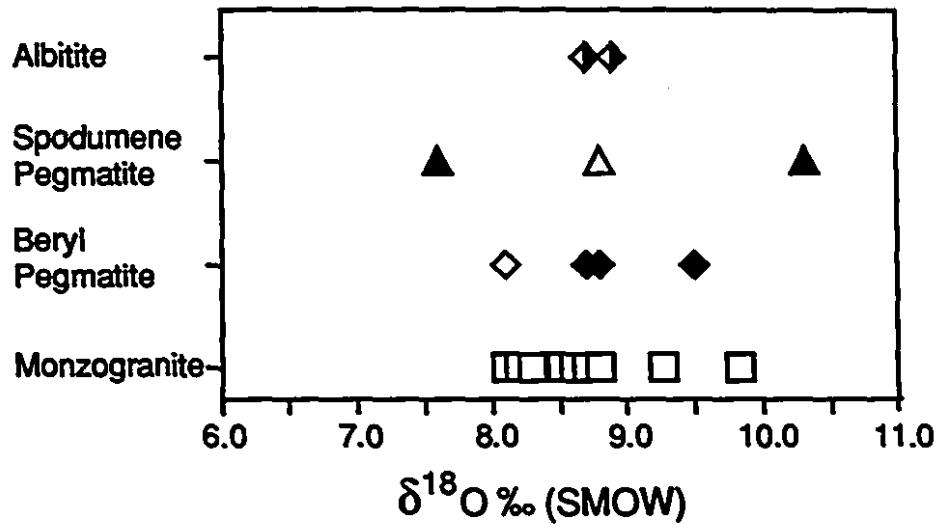
Albitite
Spodumene Pegmatite
Beryl Pegmatite
Monzogranite
6.0
7.0
8.0
9.0
10.0
11.0
δ18O ‰ (SMOW)

Figure 8

the negative Eu anomaly with magma evolution is consistent with fractionation of early, more calcic plagioclase (cf. Cullers & Graf 1984); the corresponding decrease in total *REE*, particularly in the *LREE*, can be explained by early fractionation of monazite and apatite (Fig. 5). Finally, the linear relationship between Ba and Sr, and the marked decrease in Ba from biotite to muscovite monzogranite (Fig. 9), are strong evidence for fractional crystallization of plagioclase and K-feldspar.

Other processes that have been proposed to explain monzogranitic plutons similar in zonation to that observed in the Preissac-Lacorne plutons are restite unmixing (Chappell et al. 1987), source-rock heterogeneity (Nabelek et al. 1992), and sequential partial melting (Holtz 1989). We can rule out restite unmixing as the cause of the monzogranite zonation, because of the conspicuous absence of xenoliths or xenocrysts that could represent restite, and the requirement that the contents of all elements vary linearly with SiO_2 contents (Chappell et al. 1987). Although many of the major and trace elements do show such linear variations (Figs. 2, 3), a significant number shows trends that are clearly nonlinear, e.g., Nb, Y, and Rb. Source-rock heterogeneity also can be ruled out because of the remarkable consistency of $\delta^{18}O$ values from biotite (8.6 ± 0.1‰) through two-mica (8.5 ± 0.1‰) to muscovite (8.6 ± 0.4‰) monzogranite. Finally, sequential partial melting can be eliminated because this process tends to produce relatively constant concentrations of compatible elements (Hanson 1978). In the Preissac-Lacorne plutons, several of the compatible elements display wide variations in concentrations, e.g., Ba and Sr. The relatively high contents of Ba and Sr in tne biotite monzogranite and their extreme depletion in the muscovite monzogranite simply cannot be explained by partial melting (cf. Mittlefehldt & Miller 1983).

Trace element modeling

In order to test the hypothesis that fractional crystallization was the principal process responsible for the compositional diversity of the Preissac-Lacorne monzogranites, we applied Rayleigh fractionation calculations to simulate the behavior of Ba, Sr and Rb, which are generally considered to be petrogenetic indicators in granitic rocks (e.g., McCarthy & Hasty 1976, Tindle & Pearce 1981). This modeling was restricted to the

Fig. 9. Plots illustrating Ba versus Sr in the four monzogranite plutons of the Preissac-Lacorne batholith. All values are in ppm.

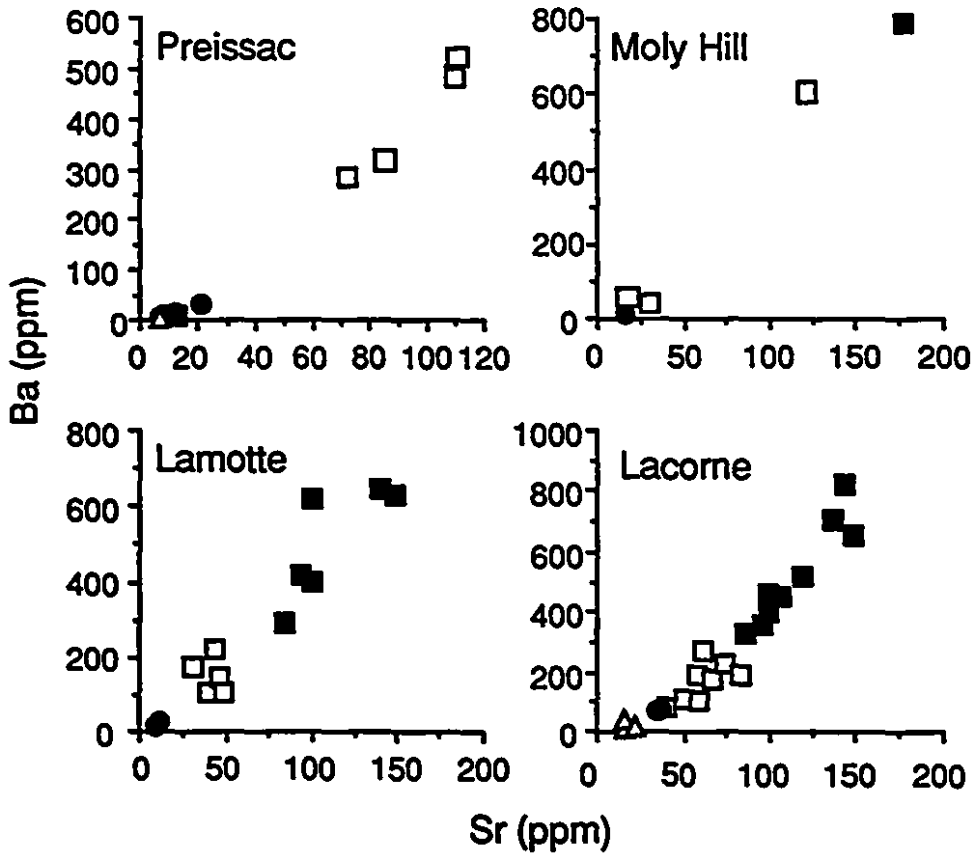
Preissac
Moly Hill
Lamotte
Lacorne
Ba (ppm)
Sr (ppm)
600
500
400
300
200
100
0
800
600
400
200
0
1000
800
600
400
200
0
0 20 40 60 80 100 120
0 50 100 150 200

Figure 9

Lamotte and Lacorne plutons because the data for the Preissac and Moly Hill plutons are inadequate. The following equation was used to describe fractional crystallization (after Hanson 1978) in the calculation:

$$C^l/C^o = F^{(D-1)},$$

where C^l and C^o are weight concentrations of a trace element in the derived melt, and in the parental melt, respectively, F is the fraction of melt, and D is the bulk distribution-coefficient. The concentration of a trace element in the residual mineral phases, C^s, relative to the parent, C^o, was calculated from the relationship $C^s = C^l * D$. Barium, Sr, and Rb were used in the modeling; among the trace elements whose concentration was established these are the elements for which the mineral/melt distribution coefficients (K_D) are best known (Table 3). The values of K_D used in the calculations were selected because the rocks from which they were estimated have compositions similar to those of the Preissac-Lacorne monzogranites. Because the initial composition of the melt, C^o, cannot be determined at present, we assume that biotite monzogranite with the smallest negative Eu anomaly has the composition of an unfractionated magma, and therefore its Ba, Sr and Rb contents are used as inputs for the C^o in the above equation. The results of the modeling suggest that the various subtypes of monzogranite in the Lamotte and Lacorne plutons can be produced by moderate to high degrees of fractional crystallization (60-95%) from such a biotite monzogranite parent (Fig. 10). Such high degrees of fractionation are consistent with the relatively small volumes of the more evolved monzogranites relative to those of biotite monzogranite. Although the calculations also produce good correspondence between the model and observed compositions of some of the occurrences of beryl pegmatite in the Lacorne pluton (over 90% fractional crystallization, Fig. 10), other occurrences of the same type of pegmatite and examples of spodumene pegmatite have substantially higher Rb, Ba and Sr contents than predicted. A possible explanation for the elevated contents of these elements is local contamination of the magma by the host rock, biotite schist. Another possibility is that the distribution coefficients for these elements were different in the latter pegmatites because of the high contents of volatiles, as indicated by the presence of magmatic lepidolite, tourmaline and fluorine-rich muscovite (Mulja et al. 1995b); it is known that volatiles such as H_2O, F and

TABLE 3. MINERAL/MELT DISTRIBUTION COEFFICIENTS (KD) USED IN TRACE-ELEMENT MODELING, AND VOLUME % OF PHASES FRACTIONATED FROM BIOTITE TO MUSCOVITE MONZOGRANITE

Mineral	Ba	Sr	Rb	Vol. %
Plagioclase	1.3	2.8	0.09	31
K-feldspar	6.12	3.6	1.6	32
Biotite	6.4	0.12	4.3	5
Muscovite	12	0.4	1.5	1
C^o: Lamotte	635	131	265	
C^o: Lacorne	822	144	360	

Source of K_D data:Hanson (1978), Nash & Crecraft (1985), Mahood & Hildreth (1983)

C^o: original concentration of element in "parent" melt (see text)

Fig. 10. Comparisons of the Rayleigh fractionation model (solid line) and observed data of all subtypes of monzogranite and pegmatites in the Lamotte and Lacorne plutons. The agreement between the theoretically calculated and measured compositions strongly supports the conclusion that fractional crystallization was the main process responsible for the compositional diversity of the monzogranite. Deviation of some measured values for some of the pegmatites suggest that the distribution coefficients used for the monzogranite are not applicable to volatile-rich batches of pegmatite-forming liquid.

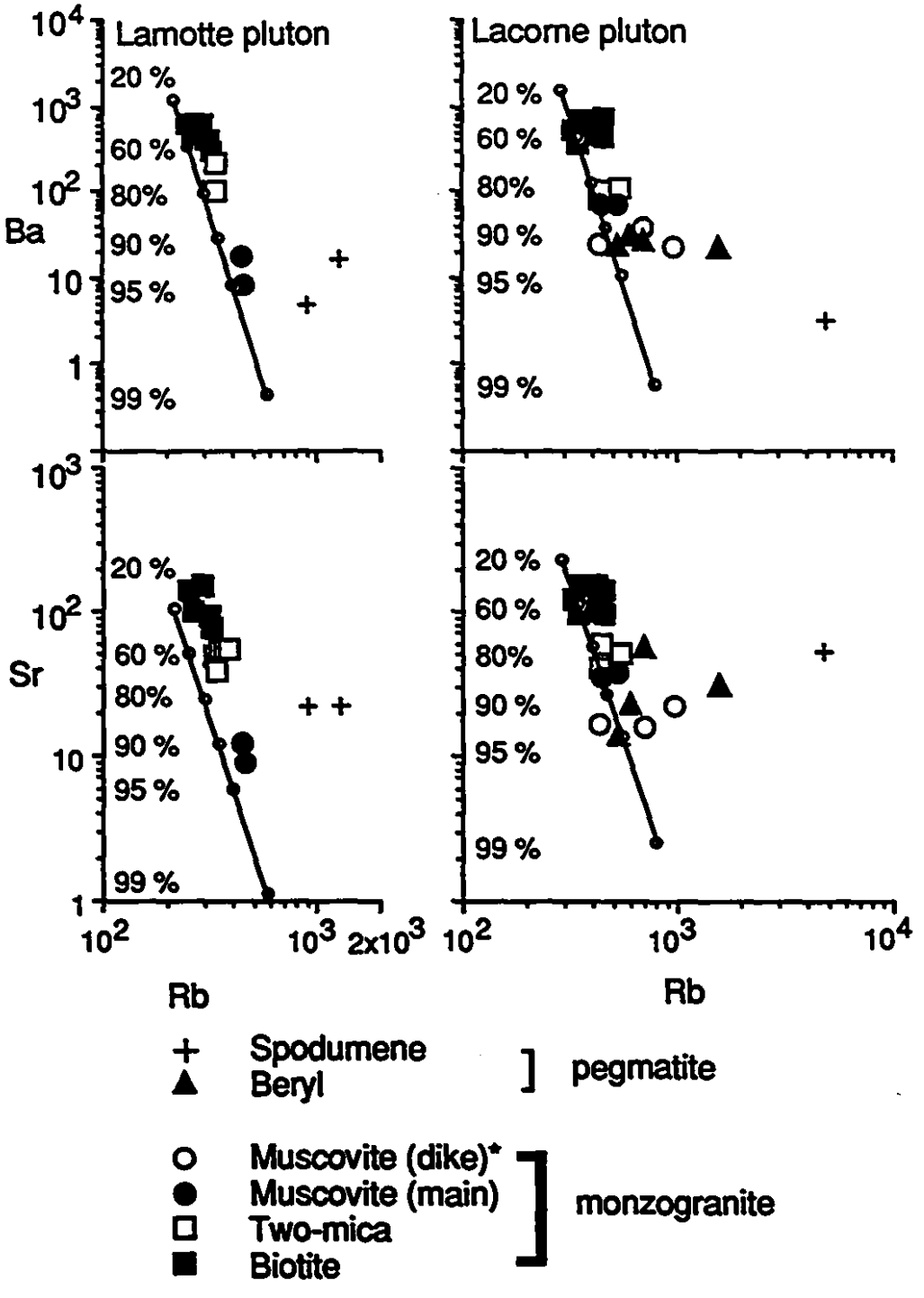
Lamotte pluton
Lacorne pluton
Ba
Sr
Rb
Rb
20 %
60 %
80%
90 %
95 %
99 %
Spodumene
Beryl
pegmatite
Muscovite (dike)*
Muscovite (main)
Two-mica
Biotite
monzogranite

Figure 10

B increase the concentration of Group-I elements including Rb in the melts (London 1987, Manning & Pichavant 1988). These arguments, the coherent relationships among trace elements between the monzogranite and pegmatites (Figs. 6, 7), and the evidence from the trace-element data for muscovite (Fig. 8; Mulja et al. 1995b) illustrating a linear relationship of Sc, Rb and Ta against Cs, demonstrate the genetic link of the monzogranite to the rare-element pegmatites.

Behavior of REE during pegmatite evolution

The concentrations of Eu, and of the light and heavy *REE* decrease progressively from beryl to spodumene pegmatite in the Lacorne pluton (Fig. 7). The large negative Eu anomaly is most reasonably interpreted by fractionation of plagioclase, as discussed previously. Given the relative abundance of xenotime in the muscovite monzogranite (Mulja et al. 1995b) and the absence of this mineral in the beryl pegmatite, we interpret the strong depletion of *HREE* in the latter rock to be a result of xenotime fractionation (in view of its well-established tendency to concentrate the *HREE*). The depletion in *HREE* may also be due partly to garnet fractionation in the muscovite-monzogranite-forming magmas. The depletion of *LREE* in the beryl pegmatite can be interpreted to reflect fractionation of monazite; monazite is considerably more abundant in the muscovite monzogranite than in the beryl pegmatite (Mulja et al. 1995b). The extreme depletion of both *LREE* and *HREE* in the spodumene pegmatite can be explained by the continued fractionation of monazite and garnet in the beryl-pegmatite-forming magma, and the absence of these minerals in the spodumene pegmatite. Other explanations that have been proposed for extreme depletion of *REE* in pegmatites are magmatic fluxing, i.e., F-*REE* complexing (Flynn & Burnham 1978), and subsolidus mobilization of *REE* by hydrothermal processes (e.g., Sverjensky 1984). Although we do not have a means to test the former hypothesis, replacement of amphibolite by biotite near the spodumene pegmatite and replacement of hornblende by holmquistite [$Li_2(Fe,Mg)_3Al_2Si_8O_{22}(OH,F)_2$] indicate there was significant transfer of materials from the spodumene pegmatite to the country rocks. Moreover, altered amphibolite within a centimeter of the contact commonly

contains abundant apatite. It is thus possible that some *REE* may have been hydrothermally transported out of the pegmatite and concentrated in apatite in the country rocks.

Formation of albitite dikes

The almost monomineralic nature of the albitite dikes (97% albite and minor molybdenite) rules out their formation by equilibrium magmatic crystallization. A purely metasomatic replacement of the host basalt or biotite schist is unlikely because of the sharp contact between the albitite and the country rocks. Moreover, the REE_N pattern of the albitite does not resemble that of the biotite schist (cf. Feng 1992). On the other hand, the albitite could represent a felsic dike that has been metasomatically altered. This interpretation is supported by the similarity of the REE_N profile of the albitite to that of aplite (Fig. 7B). We therefore propose that the dikes are the products of a complete replacement of highly evolved granitic rocks by residual aqueous fluids, which evolved during the late-stage crystallization of the magma, i.e., the precursor magmatic rock stewed in its own residual fluids. A question that needs to be addressed, however, is why quartz was removed completely from the rock, given that the residual fluids would have been quartz-saturated. The precursor may have been a spodumene-rich aplite, in which spodumene and quartz reacted with the fluid phase to form albite. This process has been predicted thermodynamically by Wood & Williams-Jones (1993) to be an inevitable consequence of the cooling of a fluid initially in equilibrium with spodumene-bearing pegmatite.

THE MAGMA CHAMBER

The (quasi-) concentric zonation displayed by the Lamotte and Lacorne plutons, i.e., less evolved biotite monzogranite along the margin of the intrusions and the most evolved muscovite monzogranite in the center, suggests that the magma underwent side-wall crystallization, in which the earliest solidification occurred at the contact between the liquid and the intruded country-rocks. In the Lacorne pluton, the geochemical (Fig.

4) and mineral-chemical (Fig. 6, Mulja et al. 1995b) trends corroborate strongly the process of side-wall crystallization. The Lamotte pluton, which lacks observable systematic chemical variations across the monzogranites, could have been formed in a regime of slow solidification, as is the case for homogeneous plutonic rocks (Sawka et al. 1990). Furthermore, the comagmatic beryl and spodumene pegmatites, which represent the more and most evolved felsic liquids, respectively, cut all types of monzogranite, indicating that the liquids must have evolved toward the interior of the body of magma. On the basis of these geological and geochemical observations, we envisage an initial stage of side-wall crystallization that produced crystal-mush (biotite monzogranite) and a less dense boundary-layer liquid (Fig. 11A) [see McBirney et al. (1985) for a discussion of the dynamics of magma chambers]. According to this model, boundary-layer liquid rises buoyantly to the top of the chamber, displacing earlier-formed, denser crystal-mush layers from the roof. Convection and high density eventually drive these layers into the lower part of the chamber, where they undergo further upward crystallization. This latter crystallization and continued crystallization along the walls produced more evolved two-mica monzogranite, which led to the ascent of an even more differentiated boundary-layer (Fig. 11B). In the Lacorne pluton, a portion of the biotite monzogranitic crystal-mush layer (southern biotite monzogranite) must have separated from the other layers prior to its complete consolidation, and must have begun its own pattern of side-wall crystallization. The separation and independent crystallization were necessary to produce the observed geochemical and mineral-chemical trends mentioned above. One cause for the separation of the southern biotite monzogranite was perhaps the emplacement of the magma along reactivated pre-existing fractures or along new ones. This tectonically induced emplacement of magma seems applicable also to the emplacement of the L-shaped muscovite monzogranite dike (labelled MG-dike, Fig. 1D), which suggests that a batch of somewhat evolved felsic liquid breached the walls of the magma chamber through fractures.

A consequence of the inward crystallization was the accumulation of more differentiated and volatile-rich residual liquids, which were below an already lithified carapace. Fractures in the roof rocks, produced tectonically or by overpressures, provided

Fig. 11. Sketches depicting the proposed history of crystallization of the rare-element-enriched granitic magma chamber of the Lamotte and Lacorne plutons. A) Early side-wall crystallization produces marginal biotite monzogranite and less dense boundary-layer melts, which ascend to the roof of the magma chamber. These melts displace downward the denser crystal-mushes that formed earlier. B) Continued fractional crystallization forms successive two-mica and muscovite monzogranite layers and more differentiated melts. Late-stage crystallization moves toward the center of the chamber, where the residual magma continues to differentiate. A small portion of the more differentiated muscovite-bearing monzogranitic melt breaches the chamber and intrudes the country rocks as a dike (MG) in the Lacorne pluton. C) Expulsion of pegmatite-forming volatile-rich magma from the chamber owing fluid overpressure results in the emplacement of the beryl (Brl) pegmatite in the overlying monzogranite. D) Later contraction of the pluton, partly due to its advanced stage of crystallization, and to the cooling of magma, reactivates fractures in the country rocks and produces new fractures, into which the more evolved melts are intruded. This gives rise to the spodumene-beryl (Spd-Brl) and spodumene (Spd) pegmatites. Aqueous fluids exsolve from the spodumene pegmatites; some back-react with earlier-formed aplite and pegmatite to form Mo-bearing albitite (Mo-Ab), and some precipitate quartz and molybdenite as veins (Mo-qtz), in the country rocks.

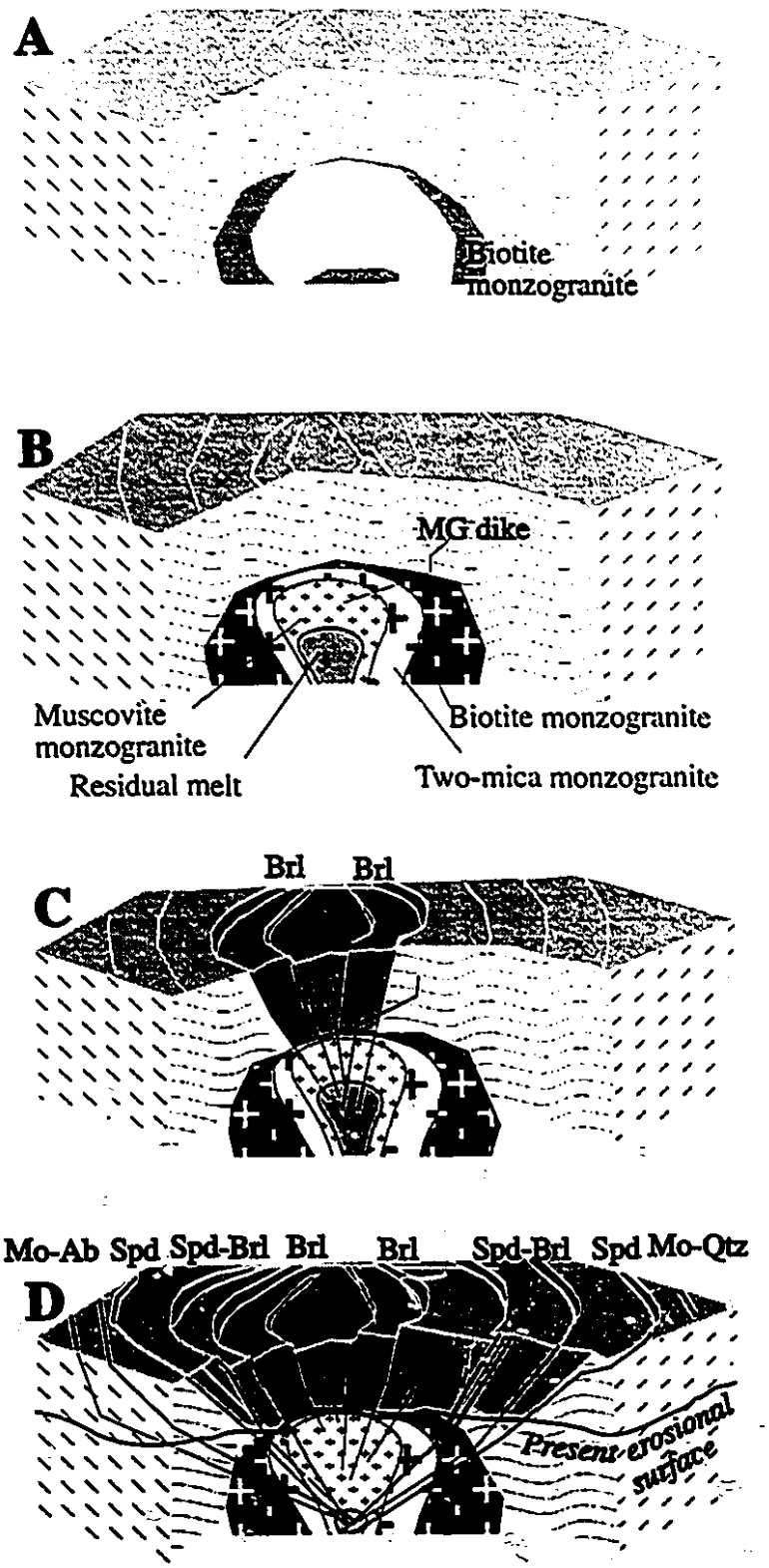
A
Biotite
monzogranite
B
MG dike
Muscovite
monzogranite
Residual melt
Biotite monzogranite
Two-mica monzogranite
C
Brl
Brl
D
Mo-Ab Spd Spd-Brl Brl
Brl
Spd-Brl Spd Mo-Qtz
Present erosional
surface

Figure 11

the conduits for the early, beryl-pegmatite-producing liquid (Fig. 11C). At an advancedstage of crystallization, corresponding to the onset of withdrawal of the above liquid from the chamber, the pluton underwent contraction, producing conical fractures, analogous to those associated with the main events of caldera formation, and reactivated pre-existing east-west-trending fractures in the country rocks. These fractures tapped deep pockets of more evolved liquid, which was drawn upward and outward, solidifying as spodumene-beryl pegmatite along the margins of the plutons, and eventually as spodumene pegmatite in the country rocks (Fig. 11D). Crystallization of the spodumene pegmatite terminated with the exsolution of aqueous fluids from the melt, which formed systems of quartz veins or, in some cases, caused the albitization of the associated aplites. Molybdenum, which has a fluid/melt distribution coefficient greater than 1 (Candela & Holland 1984), partitioned into the residual fluid and concentrated as molybdenite in the veins and albitite. The proposed evolution of granite-related mineralization is consistent with the spatial distribution of pegmatites, and the proximity of the most evolved spodumene pegmatites to the dikes of albitite and the veins of quartz.

ORIGIN OF MOLYBDENITE-BEARING QUARTZ VEINS IN THE PREISSAC AND MOLY HILL PLUTONS

In contrast to the Lamotte and Lacorne plutons, where molybdenite is concentrated in albitite dikes and quartz veins that are spatially associated with spodumene pegmatite in the country rocks, molybdenite in the Preissac and Moly Hill plutons occurs almost exclusively in quartz veins in the muscovite monzogranite. Pegmatites are relatively uncommon in these latter plutons, rarely contain beryl, never contain spodumene, and show no obvious spatial association with molybdenite-bearing quartz veins. The small size of the plutons and the fact that they did not undergo differentiation to the same extent as the Lamotte and Lacorne plutons are considered responsible for these characteristics. Consequently, vapor saturation occurred during crystallization of the muscovite monzogranite under a relatively thin crust of solidified magma, which was readily fractured. The exsolved fluid phase escaped through these fractures and formed

molybdenite-bearing quartz veins in the muscovite monzogranite. This exsolution is reflected in the finer-grained nature of the monzogranite around the veins (Mulja et al. 1995b), which developed as a result of compositional quenching of the melt. Support for the above interpretation is provided by the fine-grained muscovite-garnet monzogranite dike, which contains small molybdenite-bearing vugs that probably represent the site of vapor-phase exsolution. Significantly, this dike crystallized late in the history of the pluton, and in fact cuts molybdenite-bearing quartz veins.

CONCLUSIONS

Field, petrochemical and oxygen isotope data for four peraluminous monzogranitic plutons in the Preissac-Lacorne batholith, taken in conjunction with geological and mineralogical indicators (Mulja et al. 1995b) have distinguished suites of comagmatic monzogranite and pegmatite subtypes, and shown that their compositional diversity was mainly the result of fractional crystallization. The Lamotte and Lacorne magmas underwent the most extensive differentiation, and evolved to the stage of producing rare-element-bearing pegmatites. The mechanism of fractionation in these plutons was side-wall crystallization, which developed quasi-concentrically zoned intrusive bodies. The rare-element-enriched pegmatites were derived from batches of residual melt trapped in the interior of the cooling plutons. Beryl and spodumene pegmatites were emplaced sequentially, the former filling pressure-induced fractures in the overlying parental monzogranites, and the latter filling extension fractures in the country rocks, reactivated and produced by contraction of the adjacent solidified plutons. The terminal stage of pegmatite evolution was marked by exsolution of an aqueous fluid, which in some places back-reacted with earlier-formed spodumene-bearing aplite to form albitite, and in other places separated from the parental bodies of pegmatite to precipitate quartz, muscovite and molybdenite in veins.

The Preissac and Moly Hill plutons underwent much less extensive differentiation than the Lamotte and Lacorne plutons, probably owing to their small size. Consequently, they did not evolve magmas capable of crystallizing rare-element-enriched pegmatite.

Vapor saturation occurred during crystallization of the muscovite monzogranite under a relatively thin crust of solidified magma. The latter was readily fractured, allowing the exsolved fluid to escape into the overlying muscovite monzogranite, and there to form molybdenite-bearing quartz veins.

ACKNOWLEDGEMENTS

This study was supported financially by NSERC operating grants to AEW-J and SAW, a FCAR team grant to AEW-J, SAW and MB, and an MERQ contract to MB. Reviews by D. Kontak, R.F. Martin, D.B. Clarke and an anonymous referee helped improve the presentation of this manuscript.

REFERENCES

BOURNE, J. & DANIS, D. (1987): A proposed model for the formation of the reversely zoned pluton based on a study of the Lacorne complex, Superior Province, Québec. *Can. J. Earth Sci.* **24**, 2506-2520.

BOYNTON, W.C. (1984): Cosmochemistry of the rare earth elements: meteorite studies. *In* Geochemistry of Rare-Earth Elements (P. Henderson, ed.). Elsevier, Amsterdam, The Netherlands (63-107).

BREAKS, F.E. & MOORE, J.M., JR. (1992): The Ghost Lake Batholith, Superior Province of northwestern Ontario: a fertile, S-type, peraluminous granite-rare-element pegmatite system. *Can. Mineral.* **30**, 835-875.

BURNHAM, C.W. & OHMOTO, H. (1980): Late-stage processes in felsic magmatism. *Mining Geol., Spec. Issue* **8**, 1-11.

CANDELA, P. & HOLLAND, H. (1984): The partitioning of copper and molybdenum between silicate melts and aqueous fluids. *Geochim. Cosmochim. Acta* **48**, 373-380.

ČERNÝ, P., GOAD, B.E., HAWTHORNE, F.C. & CHAPMAN, R. (1986): Fractionation trends of the Nb- and Ta-bearing oxide minerals in the Greer Lake pegmatitic granite and its pegmatite aureole, southeastern Manitoba. *Am. Mineral.* **71**, 501-517.

CHAPPELL, B.W., WHITE, A.J.R. & WYBORN, D. (1987): The importance of residual source material (restite) in granite petrogenesis. *J. Petrol.* **28**, 1111-1138.

CLARK, G.S. & ČERNÝ, P. (1987): Radiogenic ^{87}Sr, its mobility, and the interpretation of Rb-Sr fractionation trends in rare-element granitic pegmatites. *Geochim. Cosmochim. Acta* **51**, 1011-1018.

CULLERS, R.L. & GRAF, J.L. (1984): Rare earth elements in igneous rocks of the continental crust: intermediate and silicic rocks, ore petrogenesis. *In* Rare Earth Element Geochemistry (P. Henderson, ed.). Elsevier, Amsterdam, The Netherlands (275-308).

DANIS, D. (1985): *Pétrologie et géochimie du batholite de Lacorne*. Thèse de maîtrise, Univ. du Québec, Montréal, Québec.

DAWSON, K.R. (1966): A comprehensive study of the Preissac-Lacorne batholith, Abitibi County, Québec. *Geol. Surv. Can., Bull.* **142**.

DIMROTH, E., IMREH, L., GOULET, N. & ROCHELEAU, M. (1983): Evolution of the south-central segment of the Archean Abitibi belt, Quebec. III. Plutonic and metamorphic evolution and geotectonic model. *Can. J. Earth Sci.* **20**, 1374-1388.

FENG, R. (1992): *Tectonic Juxtaposition of the Archean Abitibi Greenstone Belt and Pontiac Subprovince: Evidence from Geobarometry, Geochemistry, and Ar-Ar Geochronology of Metasedimentary Rocks and Granitoids*. Ph.D. thesis, Univ. of Saskachewan, Saskatoon, Saskachewan.

FENG, R. & KERRICH, R. (1991): Single zircon age constraints on the tectonic juxtaposition of the Archean Abitibi greenstone belt and Pontiac Subprovince, Québec, Canada. *Geochim. Cosmochim. Acta* **55**, 3437-3441.

_____ & _____ (1992): Geochemical evolution of granitoids from the Archean Abitibi Southern Volcanic Zone and the Pontiac subprovince, Superior Province, Canada: implications for tectonic history and source regions. *Chem. Geol.* **98**, 23-70.

_____, FAN, J., & KERRICH, R. (1993): Noble metal abundances and characteristics of granitic magma series, Archean Abitibi belt, Pontiac subprovince: relationships to metallogeny and overprinting of mesothermal gold deposits. *Econ. Geol.* **88**, 1376-1401.

FLYNN, R.T. & BURNHAM, C.W. (1978): An experimental determination of rare-earth partition coefficients between a chloride containing vapor phase and silicate melts. *Geochim. Cosmochim. Acta* **42**, 685-701.

GARIÉPY, C. & ALLÈGRE, C.J. (1985): The lead isotope geochemistry and geochronology of late kinematic intrusives from the Abitibi Greenstone Belt and the implications for late Archean crystal evolution. *Geochim. Cosmochim. Acta*

49, 2371-2383.

GOAD, B.E. & ČERNÝ, P. (1981): Peraluminous pegmatitite granites and their pegmatite aureoles in the Winnipeg River district, southeastern Manitoba. *Can. Mineral.* **19**, 177-194.

HANSON, G.N. (1978): The application of trace elements to the petrogenesis of igneous rocks of granitic composition. *Earth Planet. Sci. Lett.* **38**, 26-43.

HOLTZ, F. (1989): Importance of melt fraction and source rock composition in crustal granitoid genesis. The example of two granitic suites of northern Portugal. *Lithos* **24**, 21-35.

HOY, L.D. (1993): Regional evolution of hydrothermal fluids in the Noranda district, Quebec: evidence from $\delta^{18}O$ values from volcanogenic massive sulfide deposits. *Econ. Geol.* **88**, 1526-1541.

LINNEN, R. & WILLIAMS-JONES, A.E. (1994): The evolution of pegmatite-hosted Sn-W mineralization at Nong Sua, Thailand: evidence from fluid inclusions and stable isotopes. *Geochim. Cosmochim. Acta* **58**, 735-747.

LONDON, D. (1986): Magmatic-hydrothermal evolution in the Tanco rare element pegmatite: evidence from fluid inclusions and phase equilibrium experiments. *Am. Mineral.* **71**, 376-395.

_____ (1987): Internal differentiation of rare-element pegmatites: effects of boron, phosphorus and fluorine. *Geochim. Cosmochim. Acta* **51**, 403-420.

MAHOOD, G. & HILDRETH, W. (1983): Large partition coefficients for trace elements in high-silica rhyolites. *Geochim. Cosmochim. Acta* **47**, 11-30.

MANNING, D.A.C. & PICHAVANT, M. (1988): Volatiles and their bearing on the behavior of metals in granitic systems. *In* Recent Advances in the Geology of Granite-Related Mineral Deposits (R.P Taylor & D.F. Strong, eds.). *Can. Inst. Mining Metall., Spec. Pap.* **39**, 13-24.

MCBIRNEY, A.R., BAKER, B.H. & NILSON, R.H. (1985): Liquid fractionation. I. Basic principles and experimental simulation. *J. Volcanol. Geotherm. Res.* **24**, 1-24.

MCCARTHY, T.S. & HASTY, R.A. (1976): Trace element distribution patterns and their

relationship to the crystallization of granitic melts. *Geochim. Cosmochim. Acta* **0** 1351-1358.

MITTLEFEHLDT, D.W. & MILLER, C.F. (1983): Geochemistry of the Sweetwater Wash pluton, California: implications for anomalous trace element behaviour during differentiation of felsic magmas. *Geochim. Cosmochim. Acta* **47**, 109-124.

MULJA, T., WILLIAMS-JONES, A.E., MARTIN, R.F. & WOOD, S.A. (1995a): Compositional variation and structural state of Nb-Ta oxide minerals in rare-element granitic pegmatites from the Preissac-Lacorne batholith, Quebec. *Am. Mineral* (in review).

_____,_____, WOOD,S.A. & BOILY, M. (1995b): Geology and mineralogical evolution of rare-element monzogranites and pegmatites in the Preissac-Lacorne batholith, Québec. *Can. Mineral.* **33**, 000-000.

NABELEK, P.I., RUSS-NABELEK, C. & HAEUSSLER, G.T. (1992): Stable isotope evidence for the petrogenesis and fluid evolution in the Proterozoic Harney Peak leucogranite, Black Hills, South Dakota. *Geochim. Cosmochim. Acta* **56**, 403-417.

NASH, W.P. & CRECRAFT, H.R. (1985): Partition coefficients for trace elements in silicic magmas. *Geochim. Cosmochim. Acta* **49**, 2309-2322.

SAWKA, W.N., CHAPPELL, B.W. & KISTLER, R.W. (1990): Granitoid compositional zoning by side-wall boundary layer differentiation: evidence from the Palisade Crest Intrusive Suite, central Sierra Nevada, California. *J. Petrol.* **31**, 519-553.

SHEARER, C.K., PAPIKE, J.J. & JOLLIFF, B.L. (1992): Petrogenetic links among granites and pegmatites in the Harney Peak rare-element granite-pegmatite system, Black Hills, South Dakota. *Can. Mineral.* **30**, 785-809.

SVERJENSKY, D.A. (1984): Europium redox equilibria in aqueous solution. *Earth Planet. Sci. Lett.* **67**, 70-78.

TAYLOR, H.P., JR. (1978): Oxygen and hydrogen isotope studies of plutonic granitic rocks. *Earth Planet. Sci. Lett.* **38**, 177-210.

TINDLE, A.G. & PEARCE, J.A. (1981): Petrogenetic modelling of in situ fractional

crystallization in the zoned Loch Doon Pluton, Scotland. *Contrib. Mineral. Petrol.* **78**, 196-207.

TRUMBULL, R.B. (1993): A petrological and Rb-Sr isotopic study of an early Archean fertile granite-pegmatite system: the Sinceni pluton in Swaziland. *Precamb. Res.* **61**, 89-116.

WOOD, S.A. & WILLIAMS-JONES, A.E. (1993): Theoretical studies of the alteration of spodumene, petalite, eucryptite and pollucite in granitic pegmatites: exchange reactions with alkali feldspars. *Contrib. Mineral. Petrol.* **114**, 255-263.

CHAPTER 4

COMPOSITIONAL VARIATION AND STRUCTURAL STATE OF COLUMBITE-TANTALITE IN RARE-ELEMENT GRANITIC PEGMATITES OF THE PREISSAC-LACORNE BATHOLITH, QUEBEC, CANADA

THOMAS MULJA, ANTHONY E. WILLIAMS-JONES,
ROBERT F. MARTIN
Department of Earth and Planetary Sciences, McGill University,
3450 University St., Montreal, Quebec, Canada H3A 2A7
SCOTT A. WOOD
Department of Geology and Geological Engineering, University of Idaho,
University of Idaho, Moscow, Idaho 83843, U.S.A

ABSTRACT

Rare-element-enriched (Be, Li, Nb, Ta) granitic pegmatites in the Lamotte and Lacorne plutons of the Archean Preissac-Lacorne batholith (Quebec) are zoned from a least fractionated beryl type in the parental pluton through a transitional spodumene-beryl type at the edge of the plutons to a most fractionated spodumene type in the country rocks. Columbite-tantalite is the only primary Nb-Ta oxide mineral; it composition is dominated compositionally by Nb, Ta, Fe and Mn. Ti is present in minor quantities (≤ 0.1 atoms per formula unit). In both plutons, the Ta/(Ta+Nb) and Mn/(Mn+Fe) of columbite-tantalite correlate positively with the degree of pegmatite evolution. These correlations are interpreted to reflect the greater solubility of Mn- relative to Fe- and of Ta- relative to Nb-columbite-tantalite end-members in the magma. In the Lacorne suite, there is a much greater increase in Mn/(Mn + Fe) over Ta/(Ta + Nb) of columbite-tantalite with pegmatite evolution. In pegmatite bodies in the Lacorne suite, where columbite-tantalite crystallization was accompanied by garnet, the Ta/(Ta + Nb) of columbite-tantalite increases at constant Mn/(Mn + Fe) values. We interpret this to indicate that garnet saturation buffered the activities of Fe and Mn in the liquid. The degree of order of columbite-tantalite decreases with the evolution of the pegmatite suites, and reflects increased cooling rates of the more evolved, and more distal, bodies of pegmatite.

INTRODUCTION

Minerals of the columbite-tantalite group [$(Fe,Mn)(Nb,Ta)_2O_6$] are potentially important in deciphering the internal evolution of rare-element-enriched granitic pegmatites (Lahti, 1987; Ercit, 1994a) and hence understanding their petrogenesis (Ercit, 1994b). Trueman and Černý (1982) have proposed a model in which a rare-element-enriched felsic magma, with increasing distance from the parental pluton, becomes saturated first in beryl, then spodumene; as it crystallizes, Nb and Fe are expected to become depleted, whereas Ta and Mn are progressively enriched in the residual liquid. With more rapid crystallization of the successive melt fractions at an increasingly greater distance from the source, Černý et al. (1986) anticipated that the columbite-tantalite would tend to be "stranded" in a more disordered state. However, these propositions have not been adequately tested, because most published studies of columbite-tantalite have been restricted to single bodies of granitic pegmatite (Černý and Turnock, 1971; Grice et al., 1972; Wenger and Armbruster, 1991; Spilde and Shearer, 1992), to suites of granitic pegmatite in which the magmas underwent limited fractionation (Černý et al., 1986; Lahti, 1987; Ercit, 1994a, b), or to groups of pegmatite bodies where petrogenetic links among these pegmatites have not been established (Wise, 1987).

In this contribution, we report the results of a detailed study of the paragenesis, composition and structural state of columbite-tantalite in two suites of comagmatic rare-element granitic pegmatite from the Preissac-Lacorne batholith, northwestern Quebec (Fig. 1). The pegmatite bodies are not deformed or metamorphosed, are well described in terms of their geology and petrochemistry (Dawson 1966; Mulja et al., 1995a, b), and are zoned regionally from a least evolved *beryl type* emplaced in the parental pluton to a most evolved *spodumene type* emplaced away (~2-3 km) from the respective pluton, in the country rocks. Such a regional zonation, although an essential feature of the evolutionary model proposed for rare-element granitic pegmatites, is seldom encountered. The pegmatite suites of the Preissac-Lacorne batholith thus offer a rare opportunity to elucidate the factors that control the relationship between the crystal-chemical properties

Fig. 1. A simplified geological map of the Preissac-Lacorne batholith showing the distribution of intercalated schists and volcanic rocks, basic plutonic rocks, four monzogranitic plutons and structures. The boundaries of the plutons are based on the furthest granitic pegmatite or monzogranite outcrops (Dawson 1966). Recent mapping by Mulja et al. (1995) shows that the Lacorne pluton (Fig. 2B) is most likely smaller than previously outlined. Only the boxed area in the Lacorne pluton, where most outcrops exit, is enlarged in Fig. 2B.

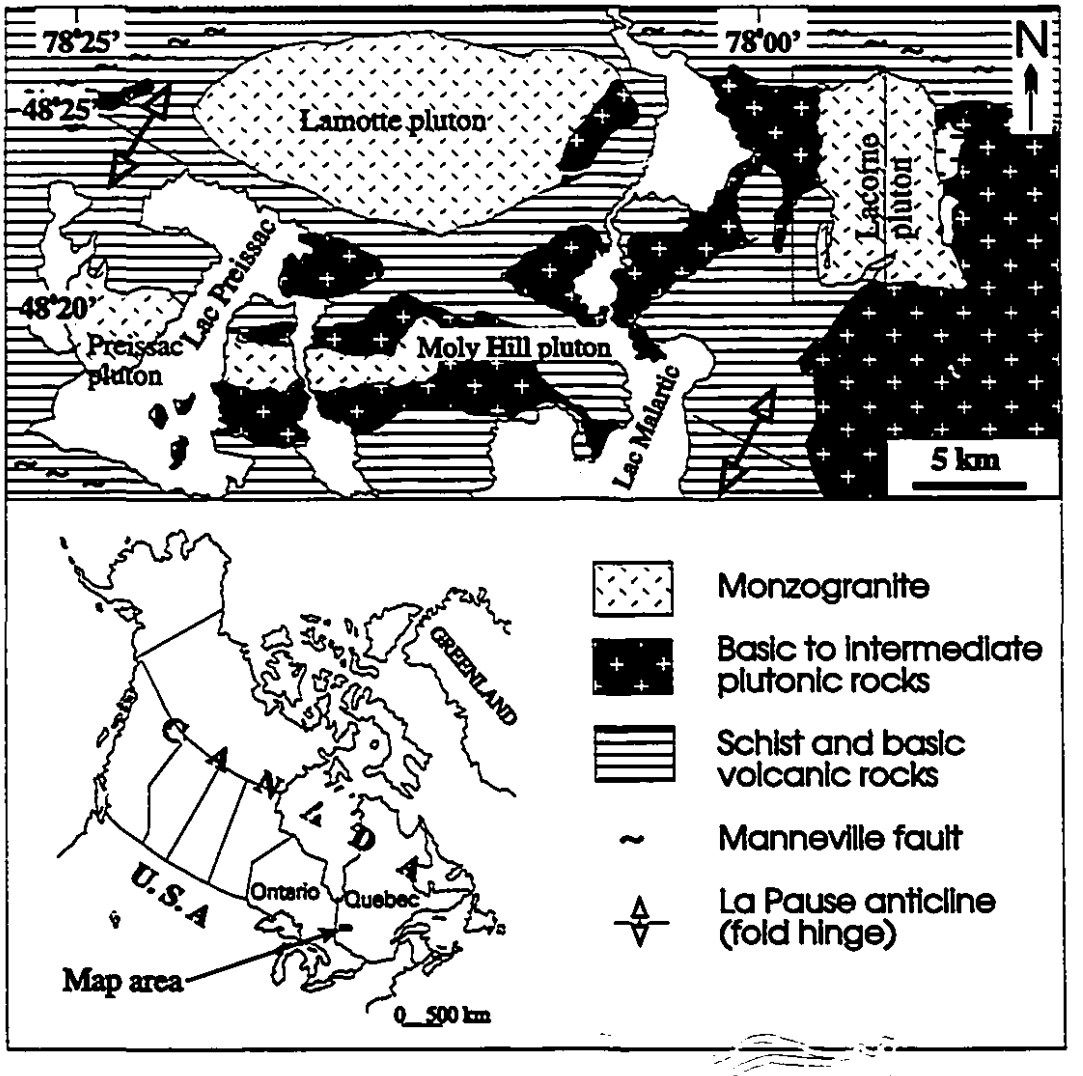
78°25'
78°00'
N
48°25'
48°20'
Lamotte pluton
Lacorne pluton
Lac Preissac
Preissac pluton
Moly Hill pluton
Lac Malartic
5 km
GREENLAND
CANADA
U.S.A
Ontario
Quebec
Map area
0 500 km
Monzogranite
Basic to intermediate plutonic rocks
Schist and basic volcanic rocks
Manneville fault
La Pause anticline (fold hinge)

Figure 1

of columbite-tantalite and the evolution of fractionated granitic liquids in a model rare-element pegmatite system.

GEOLOGY AND PETROGRAPHY OF THE PEGMATITES

The columbite-tantalite-bearing granitic pegmatites are part of the Archean Preissac-Lacorne batholith (~2.64-2.7 Ga: Gariépy and Allègre, 1985; Feng and Kerrich, 1991), which hosts the largest swarm of spodumene-bearing pegmatites in eastern Canada (formerly exploited by the Quebec Lithium mine; Fig. 2B), and many other beryl and spodumene types of pegmatite of subeconomic grade. The batholith, which intruded mafic lavas and biotite schists of the Kinojevis and Malartic Groups in the Abitibi Greenstone Belt of the Superior Province, is made up of an older suite of gabbro, monzodiorite and granodiorite, and four younger plutons of peraluminous monzogranite. Each of these plutons (Preissac, Moly Hill, Lamotte, Lacorne) is zoned compositionally from biotite through two-mica to muscovite monzogranite (Mulja et al., 1995b). The mineralized (Be, Li, Nb, Ta, Mo) pegmatites, which are the focus of this study, are associated with the Lamotte and Lacorne plutons.

The pegmatites occur as tabular dikes ranging from tens of centimeters to eight meters in width and up to hundreds of meters in length, as lenticular bodies up to 5 x 24 meters in plan, and as dike swarms, particularly along the margin of the plutons. They filled zones of dilation (pinch and swell) in the monzogranite and existing fractures in the country rocks that were possibly reactivated during the emplacement of the batholith. Most pegmatite bodies in the Lacorne pluton strike east-west and northwest-southeast, whereas those in the Lamotte pluton show no preferred orientation. In both plutons, the pegmatite bodies dip vertically to subhorizontally. Their intrusive contact with the monzogranite varies from gradational to sharp (planar to convoluted), and shows no evidence of metasomatism. Contacts between spodumene pegmatites and amphibolite are marked by a narrow halo in the amphibolite in which holmquistite replaced hornblende.

On the basis of the predominant rare-element-bearing minerals, the mineralized

Fig. 2. Geological maps of the Lamotte (A) and Lacorne (B) plutons depicting the field relationships among the various subtypes of monzogranite, the zonal distribution of the three main types of pegmatites; beryl (Brl), spodumene-beryl (Spd-Brl) and spodumene (Spd), and the number and location of samples used in this study. In the Lacorne pluton, spodumene pegmatite from the former Quebec Lithium mine (QL) is about 3 km east from the margin of the map. Columbite-tantalite- and molybdenite-bearing albitite dikes (Mo-Ab) occur only in the northernmost part of the Lacorne pluton.

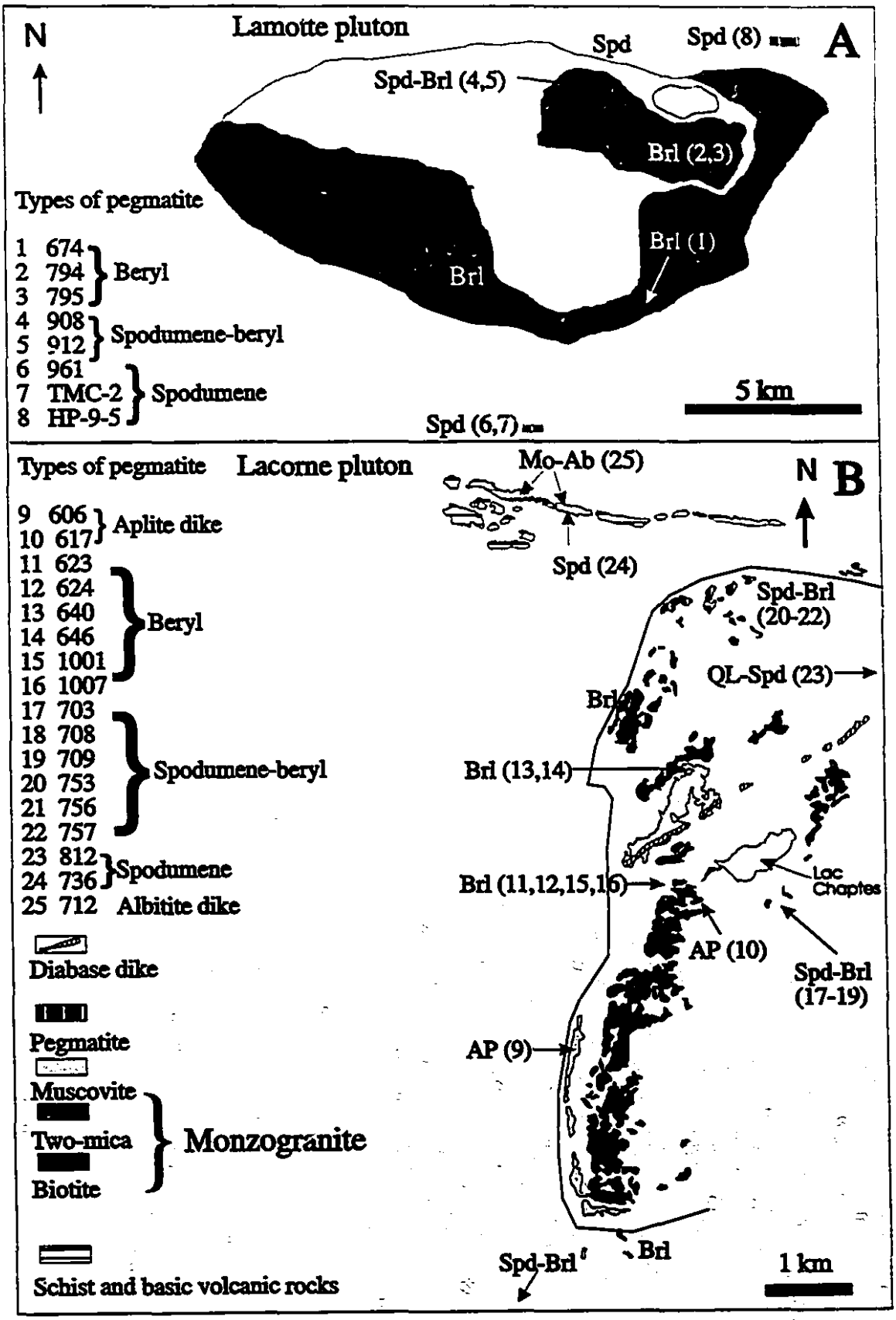
N
Lamotte pluton
Spd
Spd (8)
A
Spd-Brl (4,5)
Brl (2,3)
Brl (1)
Brl
Types of pegmatite
1 674
2 794
3 795
Beryl
4 908
5 912
Spodumene-beryl
6 961
7 TMC-2
8 HP-9-5
Spodumene
5 km
Spd (6,7)
Types of pegmatite
Lacorne pluton
Mo-Ab (25)
N
B
Spd (24)
9 606
10 617
Aplite dike
11 623
12 624
13 640
14 646
15 1001
16 1007
Beryl
17 703
18 708
19 709
20 753
21 756
22 757
Spodumene-beryl
23 812
24 736
Spodumene
25 712 Albitite dike
Spd-Brl
(20-22)
QL-Spd (23)
Brl
Brl (13,14)
Brl (11,12,15,16)
Lac
Chaptes
AP (10)
Spd-Brl
(17-19)
AP (9)
Diabase dike
Pegmatite
Muscovite
Two-mica
Biotite
Monzogranite
Schist and basic volcanic rocks
Spd-Brl
Brl
1 km

Figure 2

pegmatites are subdivided into beryl-, spodumene-beryl-, and spodumene-bearing types. In the text that follows, these types of pegmatite are referred to as beryl, spodumene-beryl and spodumene pegmatite. The pegmatite bodies are zonally distributed from beryl type in and at the margin of the parental plutons, spodumene-beryl type at the margins of the plutons, to spodumene type in the country rocks (Figs. 2A-B). Mineral-chemical and whole-rock geochemical data indicate that they are comagmatic: beryl pegmatite represents the geochemically least evolved type, and spodumene pegmatite the most evolved type (Mulja et al. 1995a, b). Adjacent to the spodumene pegmatite in the northern part of the Lacorne pluton (Fig. 2B), dikes of molybdenite- and columbite-tantalite-bearing albitite occur in the intercalated biotite schist and basalt.

Beryl pegmatite

Small bodies of beryl pegmatite (< one meter wide) are, in general, symmetrically zoned from a narrow marginal sodic aplite (1) through an assemblage of coarse-grained quartz, K-feldspar, albite and muscovite (2), to a central zone of beryl, K-feldspar, and quartz megacrysts (3). Small pockets consisting of quartz and muscovite occur sporadically in the aplite. The transition between zones (1) and (2) is sharp, and is marked locally by books of muscovite, whereas that between zones (2) and (3) is gradational. Columbite-tantalite is concentrated mainly in fine layers of garnet, which occur mostly in the aplite. Larger, subvertical bodies of beryl pegmatite (up to eight meters wide) typically display an asymmetrical zonation as follows: (1) a marginal sodic aplite that is texturally and mineralogically similar to the aplite in the small dikes, (2) muscovite + albite + quartz + locally perthite, (3) beryl + albite + perthite + quartz ± muscovite, (4) quartz + perthite ± beryl, (5) large irregular lenses of quartz intergrown with perthite megacrysts (up to one meter long), or monotonous masses of quartz up to three meters wide, and (6) a marginal facies consisting of muscovite, albite, quartz, and locally perthite. The muscovite occurs mostly as books along the contact with the host monzogranite. Columbite-tantalite occurs in zones 1, 2, 3 and 6.

Spodumene-beryl pegmatite

Spodumene-beryl pegmatite is found only in the northern part of the Lamotte pluton (nos. 4-5, Fig. 2). There, the bodies are asymmetrically zoned, with sodic aplite at one margin and an assemblage of coarse crystals (up to 5 cm across) of albite + K-feldspar + muscovite at the other margin. Like that in beryl pegmatite, the aplite contains fine layers of spessartine. The intermediate zone is simple, comprising albite, K-feldspar and quartz, and the central zone consists of quartz, K-feldspar and spodumene (up to 4 x 10 cm in size). Disseminated columbite-tantalite occurs mainly in the aplite and has not been found in any other zone. From these observations, it is clear that, in the Lamotte suite, the spodumene-beryl pegmatite differs subtly from the beryl-bearing pegmatite, i.e., the former is distinguished from the latter by the presence of spodumene in the core.

In the Lacorne suite, there are three variants of spodumene-beryl pegmatite. The first one is represented by that at the Valor prospect (nos. 17-19, Fig. 2B), which is hosted by the two-mica monzogranite. The pegmatite exhibits a crude symmetrical zonation from a border zone of aplite, which is crenulated, extremely rich in spessartine (concentrations are an order of magnitude higher than in the aplite zone of the Lamotte spodumene-beryl pegmatite) and contains appreciable amounts (~1 %) of columbite-tantalite and traces of schorl and pyrophanite. This zone grades inward into an intermediate zone through a thin transitional zone marked by books of muscovite and crystals of beryl (beryl also occurs as euhedral crystals, > 3 cm across, at the contact between the pegmatite and the host monzogranite, where aplite is locally absent). Spodumene (up to 20 cm x 2 m in size) occurs in the inner part of the intermediate zone and along the aplite-free contact with the monzogranite. Albite is present in rosettes of blades, up to 3-4 cm across. In this intermediate zone, small flakes of lepidolite partially replaced spodumene. The core of the pegmatite consists mainly of quartz, spodumene and lepidolite. The lepidolite occurs as large crystals (~2-3 cm across) intergrown with quartz and albite. Unlike the lepidolite that replaced spodumene in the intermediate zone, it here seems primary.

The second subtype of spodumene-beryl pegmatite, exemplified by a dike near the northern edge of the Lacorne pluton (no. 21, Fig. 2B), is zoned. The border zone aplite contains some accessory garnet. This zone grades sharply into a spodumene-bearing zone that contains small amounts of beryl along the contact. The crystals of spodumene are relatively equigranular (up to 5 cm long) and are intergrown with quartz, albite and minor muscovite. The next zone is dominated by massive lepidolite, albite and quartz, and contains no spodumene. Columbite-tantalite is disseminated throughout the spodumene and lepidolite zones. Although additional zones are not exposed, we believe, on the basis of the internal zonation of the other bodies of spodumene-beryl pegmatite, that there is a core that consists mainly of quartz, and that the pegmatite is symmetrically zoned.

The third subtype of spodumene-beryl pegmatite is a lepidolite-free variety that occurs in contact with biotite schist and basalt of the country rocks (nos. 19 and 22). It has a narrow zone of sodic aplite, which hosts thin layers of garnet and scattered crystals of columbite-tantalite. Beryl crystals are small and occur sporadically along the contact between the aplite and an intermediate zone of spodumene + albite + quartz + muscovite. The interior part of this pegmatite is massive, comprising megacrysts of quartz and K-feldspar.

From the above description, it is clear that in the transition from the main Lacorne intrusion into the country rocks, the variants of spodumene-beryl pegmatite show a systematic decrease in beryl and garnet contents, develop separate zones of spodumene and lepidolite, and eventually become lepidolite-free. These observations indicate that the spodumene-beryl pegmatite at the Valor prospect is the least evolved subtype, the one near the northern margin of the pluton (no. 21), an intermediate subtype, and those at the contact, the most evolved.

Spodumene pegmatite

Spodumene pegmatite also can be subdivided. Less-fractionated examples are located south of the Lamotte pluton (nos. 6 and 7, Fig. 2A) and east of the Lacorne pluton (no. 23, Fig. 2B). The former pegmatite shows subhorizontal layered bodies,

which are characterized by alternating zones, from 20 to 60 cm thick, of massive aplite and pegmatite. The contacts between the two zones are sharp, marked by vertical, acicular crystals of spodumene (up to 1 x 20 cm in size) in the pegmatite. In the upper level of the intrusion, spodumene forms short, columnar crystals (2 cm across) interlocking with quartz, muscovite, K-feldspar, and albite. The less-evolved spodumene pegmatite at Lacorne is massive, consisting of spodumene laths, quartz, albite and K-feldspar, and traces of fluorite. Muscovite, of variable grain-size, is less abundant than in other types of pegmatite. In these bodies of spodumene pegmatite, the minor minerals are, in an order of decreasing abundance, columbite-tantalite (up to 0.5 cm across), molybdenite, beryl and cerianite. Unlike the beryl and spodumene-beryl pegmatites, the aplite in the spodumene pegmatites lacks garnet.

The more evolved type of spodumene pegmatite is represented by bodies in the country rocks north of the Lamotte (no. 8) and Lacorne (no. 24) plutons. The texture and major mineralogy of the Lamotte pegmatites are similar to those of the less evolved Lacorne spodumene pegmatite. In contrast, the more evolved bodies of spodumene pegmatite associated with the Lacorne pluton are zoned from a marginal aplite to a core of coarse-grained perthite + spodumene + quartz. In this subtype of pegmatite from both suites, columbite-tantalite crystals (up to 1 cm across) occur throughout, but garnet is present only in the Locorne suite. Beryl and molybdenite (both of which also are present in the less evolved subtype) are absent in this more evolved subtype.

Albitite dikes

Albitite dikes occur along joints in the metavolcanic rocks and schists (no. 25, Fig. 2B). The dikes, which consist almost entirely of euhedral albite, locally host spectacular molybdenite-rich layers. Columbite-tantalite and Ta-bearing ilmenite are minor interstitial phases, whereas garnet, secondary muscovite, and zircon are accessory phases.

SAMPLES AND ANALYTICAL METHODS

Locations of representative examples of the three types of pegmatite from the Lamotte and Lacorne plutons are shown in Figs. 2A-B. Although both plutons host a complete series of rare-element pegmatites, there are more bodies of pegmatite in and around the Lacorne pluton than in and adjacent to the Lamotte pluton. This difference is reflected in the larger number of samples examined from the Lacorne pluton. We also analyzed columbite-tantalite from discrete dikes of aplite from the Lacorne and Moly Hill plutons, and from a dike of muscovite-garnet monzogranite in the Preissac pluton.

The major-element compositions of columbite-tantalite and related Nb-Ta minerals were determined with an automated CAMECA electron microprobe at McGill University; the operating conditions were: acceleration voltage 20 kV, beam current (measured on MgO) 20 nA, a 2-μm spot size, and a 25-second counting time. Synthetic $MnNb_2O_6$ and Ta_2O_5 were used as standards for Mn and Nb, and Ta, respectively, pure metal for U, and various minerals for other elements. Data reduction was accomplished with the full PAP correction procedures of Pouchou and Pichoir (1985).

Unit-cell dimensions of columbite-tantalite were determined using X-ray diffraction (powder method). Unlike the electron microprobe, which provides compositional information for specific locations (spots) in a single crystal, the powder method provides information on the average composition and average degree of structural order in a volume of material of approximately 0.5 mm^3. In some cases, two sets of diffraction maxima were observed, indicating two dominant columbite-tantalite phases in the material analyzed by XRD. The pulverized material was mixed with synthetic $MgAl_2O_4$ spinel (a = 8.0833 Å at room temperature). The powder pattern, obtained with a Guinier-Hägg focusing camera ($CuK\alpha_1$ radiation), was corrected and then indexed by referring to PDF 16-337 and to the indexed pattern of Wise et al. (1985). Cell parameters were calculated with the program of Appleman and Evans (1973), as modified by Garvey (1986).

COLUMBITE-TANTALITE

Nomenclature

Minerals of the columbite-tantalite group have the general formula of AB_2O_6, in which the *A* position is occupied mostly by Fe^{2+} and Mn^{2+} and, to a lesser extent, by Mg^{2+}, or trivalent cations; the *B* position is occupied mainly by Nb^{5+} and Ta^{5+} and, subordinately, by Ti^{4+} and Sn^{4+}. These orthorhombic minerals include the end-members ferrocolumbite ($FeNb_2O_6$), manganocolumbite ($MnNb_2O_6$), manganotantalite ($MnTa_2O_6$) and magnocolumbite ($MgNb_2O_6$). Although ferrotantalite [$(Fe > Mn)(Ta > Nb)_2O_6$] is a member of the columbite-tantalite group in the classification of Nb-Ta oxides, the end-member $FeTa_2O_6$ is tetragonal and belongs to the tapiolite series (Černý and Ercit, 1989). Magnocolumbite and ferrotantalite were not observed in this suite.

In order to describe the compositional variation of columbite-tantalite within and between bodies of pegmatite, the names ferrocolumbite, manganocolumbite and manganotantalite are restricted to the compositions [Ta/(Ta + Nb) and Mn/(Mn + Fe) < 0.5], [Ta/(Ta + Nb) < 0.5 and Mn/(Mn + Fe) > 0.5] and [Ta/(Ta + Nb) and Mn/(Mn + Fe) > 0.5], respectively. The presence of manganotantalite, which has a similar bulk chemistry to ixiolite $(Mn,Fe,Ti,Ta,Nb)_4O_8$, was confirmed by retention of the orthorhombic structure after heat treatment at 1,000°C for 16 hours. Ixiolite would convert to a monoclinic structure (wodginite) upon such heat treatment (Černý and Ercit, 1985). Columbite-tantalite occurs in a wide range of structural states in granitic pegmatites, as can be appreciated from the continuum of data points in a quadrilateral plot of cell parameters a versus c (Černý and Ercit, 1985, Fig. 1A).

Petrography

Columbite-tantalite (CT) forms finely disseminated crystals, particularly in the garnet-rich aplite, irrespective of whether the aplite is a discrete dike (nos. 9-10) or part of a composite aplite-pegmatite dike. In the aplite zone of beryl and spodumene-beryl pegmatites from both suites, CT crystals are generally small and euhedral (up to 2 x 3

mm) and occur as inclusions, mostly in garnet and albite, and rarely, in perthite, muscovite and quartz (Fig. 3A). In almost all cases, coarser grains of this oxide are interstitial (Fig. 3B). Some euhedral crystals of CT occur between garnet and albite (Fig. 3C). In the intermediate zone of these types of pegmatite, CT crystals are generally interstitial to the silicate minerals mentioned above and spodumene in the spodumene-beryl pegmatite. They were not observed in the core of either subtypes of pegmatite, where large crystals of quartz and beryl, and of quartz, spodumene and lepidolite occur, respectively. These textural relationships indicate that most crystals of CT are earlier than the silicate phases in the aplite zone, and almost all of them in the intermediate zone are late. This interpretation suggests that the columbite-tantalite in the aplite zone is generally earlier than beryl and spodumene. In contrast, columbite-tantalite in spodumene pegmatite is mostly either intergrown with, or interstitial to, spodumene, quartz and albite, pointing to crystallization contemporaneous with and later than these silicate minerals.

Alteration in columbite-tantalite is minimal. Some paragenetically late CT grains in beryl pegmatite are rimmed by masses of U-Th-bearing Nb-Ta oxide (Fig. 3B). In spodumene pegmatites, veinlets and patches of microlite occur in manganotantalite (Fig. 3D), suggesting that the microlite was precipitated at a subsolidus stage that filled fractures in, and partially replaced, the manganotantalite. A less common type of alteration involved the partial replacement of opaque ferrocolumbite by translucent manganocolumbite in an evolved spodumene-beryl pegmatite in the Lamotte pluton (Fig. 3E). Some CT crystals in dikes of aplite and albitite are intergrown with fersmite (Fig. 3F). The nature of this intergrowth cannot be ascertained owing to the rarity of the occurrence and the small size of the crystals.

Compositional variations

The composition of columbite-tantalite from the Lamotte and Lacorne pegmatites is dominated by Fe (total as Fe^{2+}), Mn, Nb and Ta (Tables 1-2). There is a minor proportion of Ti (up to 0.1 atoms per formula unit, apfu) and, in some cases, trace amounts of Mg and Ca. The fersmite noted in the albitite has a composition as follows:

Fig. 3. Photomicrographs exemplifying various modes of occurrence of columbite-tantalite (Ct) and related Nb-Ta minerals from the Preissac-Lacorne pegmatites and albitite. A). A euhedral inclusion of ferrocolumbite (Fcl) in albite (Ab) from a discrete aplite dike. B). An anhedral grain of interstitial ferrocolumbite in a beryl pegmatite, intergrown partially with metamict (Th-U) columbite-tantalite (U-Th Ct). C). A ferrocolumbite prism enclosed mostly in euhedral garnet (Grt) and partly in albite in a beryl pegmatite. Secondary muscovite (Ms) fringes the garnet and ferrocolumbite. D). Manganotantalite (Mtt) replaced by patchy microlite (Mic) and cut by albite veinlets in a spodumene pegmatite. E). A subhedral ferrocolumbite in spodumene (Spd) from spodumene+beryl pegmatite is partially altered by translucent manganocolumbite (Mcl) along the fracture and around the spodumene inclusion. F). Subhedral, interstitial columbite-tantalite crystals (white) in an albitite dike. The elongated grain is altered partially to fersmite (light grey). All scale bars are 100 μm.

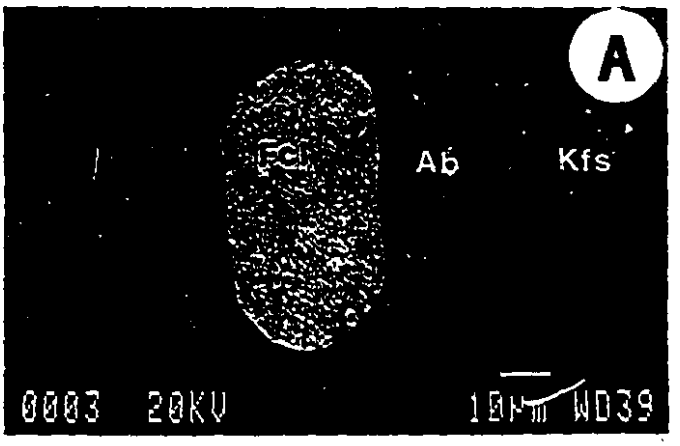
A
Fcl
Ab
Kfs
0003 20KV
10μm WD39

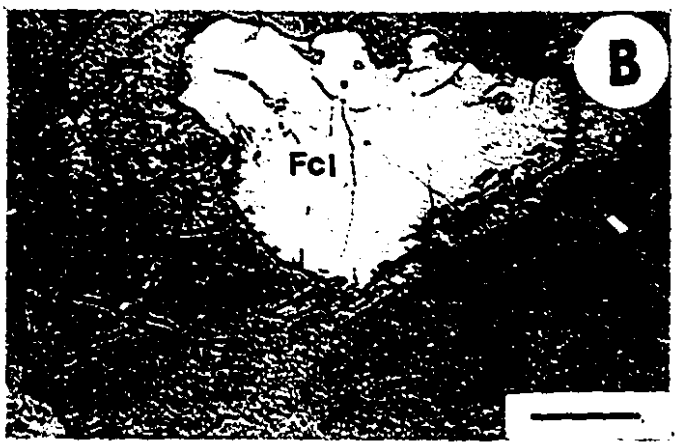
B
Fcl

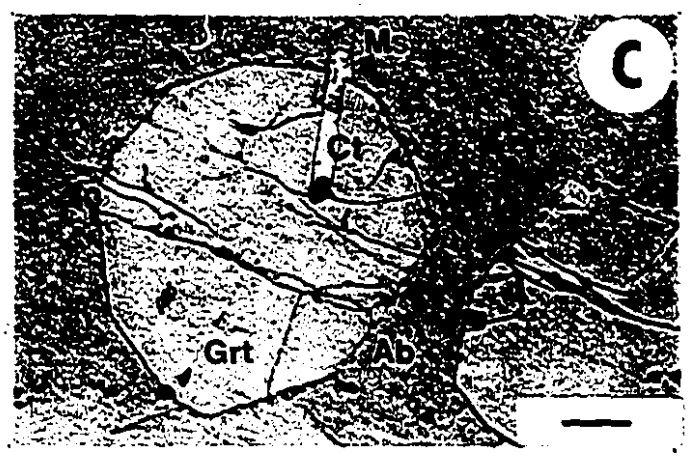
C
Ms
Grt
Ab

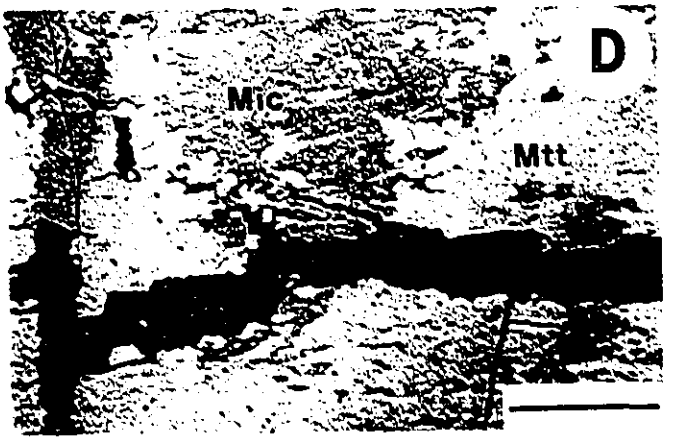
D
Mic
Mtt

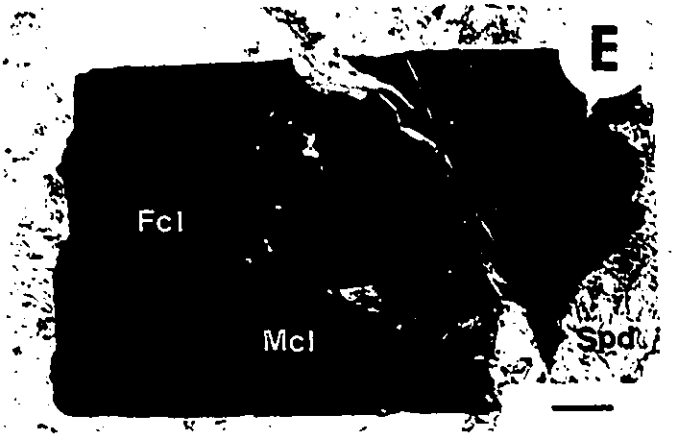
E
Fcl
Mcl
Spd


F
ct

Table 1 Representative compositions of columbite-tantalite from the Preissac, Moly Hill and Lamotte plutons

Pluton	Preissac	Moly Hill			Lamotte					
Lithology*	MGG	AP	Brl		Spd+Brl		Spd			
Sample	471	30	764	795	912	912	C.2	C.2	HP9-5	HP9-5
Nb_2O_5(wt%)	71.57	68.31	72.48	71.28	71.22	67.77	52.73	34.04	23.72	8.33
MgO	0.02	0.11	0.09	0.17	0.06	0.06	0	0.02	0.02	0
CaO	0.01	0.01	0	0	0.02	0.05	0.02	0.02	0	0.02
TiO_2	1.08	1.02	0.58	0.45	0.60	0.40	0.09	0.18	0.15	0.2
FeO	10.69	13.9	13.15	15.42	13.28	12.79	5.39	5.66	3.77	0.45
MnO	9.98	6.00	6.73	4.22	7.68	6.42	12.47	10.71	11.62	14.12
Ta_2O_5	5.34	9.70	6.81	7.14	5.63	11.62	29.01	48.42	61.42	77.4
Total	98.69	99.05	99.84	98.68	98.49	99.11	99.71	99.05	100.7	100.5
				Structural formula based on six oxygen atoms						
Nb	1.873	1.813	1.886	1.881	1.874	1.813	1.513	1.078	0.786	0.303
Mg	0.002	0.010	0.007	0.014	0.005	0.005	0	0.010	0.002	0
Ca	0.001	0.001	0	0	0.001	0.003	0.001	0.001	0	0.002
Ti	0.047	0.045	0.025	0.019	0.026	0.018	0.004	0.009	0.008	0.012
Fe	0.517	0.682	0.633	0.753	0.644	0.633	0.286	0.332	0.231	0.03
Mn	0.489	0.298	0.328	0.209	0.375	0.322	0.670	0.635	0.722	0.961
Ta	0.084	0.155	0.107	0.113	0.089	0.187	0.501	0.922	1.225	1.691
A site	1.009	0.991	0.994	0.996	1.024	0.963	0.957	0.978	0.955	0.993
B site	2.005	2.012	2.018	2.013	1.990	2.018	2.018	2.010	2.019	2.005
Ta/(Ta+Nb)	0.043	0.079	0.054	0.057	0.045	0.094	0.249	0.461	0.609	0.848
Mn/(Mn+Fe)	0.486	0.304	0.341	0.217	0.368	0.337	0.701	0.657	0.757	0.97

*MGG: Muscovite + garnet monzogranite; AP: aplite dike; for pegmatite types, Brl: beryl; Spd: spodumene

A site: Fe, Mn, Mg, Ca; B site: Nb, Ta, Ti

Table 2 Representative compositions of columbite-tantalite in various rock types from the Lacorne pluton

Lithology*	AP	Brl		Spd + Brl			Spd		Ab
Sample	606	1001E	1001L	708	756.S	756.L	812	736	721
Nb_2O_5(wt%)	69.12	69.63	43.42	62.29	62.65	36.43	62.16	1.73	35.85
MgO	0.08	0.07	0.06	0.05	0.02	0	0.09	0	0.52
CaO	0.01	0.02	0.03	0.02	0.01	0.04	0.19	0.05	0.06
TiO_2	0.52	0.67	1.23	0.8	0.45	0.44	1.07	0.63	0.41
FeO	11.05	12.78	11.25	10.45	4.96	0.31	2.44	2.87	9.15
MnO	9.11	7.5	6.29	8.84	14.57	16.57	16.29	10.65	6.78
Ta_2O_5	9.23	8.79	36.86	17.74	17.14	46.7	18.13	82.39	47.93
Total	99.12	99.46	99.14	100.2	99.80	100.5	100.4	98.32	100.7
				Structural formula based on six oxygen atoms					
Nb	1.833	1.830	1.296	1.690	1.705	1.124	1.680	0.067	1.105
Mg	0.007	0.006	0.006	0.005	0.002	0	0.008	0	0.053
Ca	0.001	0.001	0.002	0.001	0.001	0.003	0.012	0.005	0.004
Ti	0.023	0.029	0.061	0.036	0.021	0.022	0.048	0.041	0.021
Fe	0.542	0.621	0.622	0.524	0.250	0.018	0.122	0.205	0.522
Mn	0.453	0.369	0.352	0.449	0.743	0.958	0.825	0.768	0.392
Ta	0.147	0.139	0.662	0.289	0.281	0.867	0.295	1.908	0.889
A site	1.003	0.998	0.981	0.980	0.995	0.979	0.967	0.978	0.971
B site	2.004	1.998	2.019	2.015	2.006	2.013	2.023	2.016	2.015
Ta/(Ta+Nb)	0.074	0.071	0.338	0.146	0.141	0.435	0.149	0.966	0.446
Mn/(Mn+Fe)	0.455	0.373	0.361	0.461	0.749	0.982	0.871	0.790	0.429

*Similar to those in Table 1; Ab: albitite dike

E: early; L: late; S and L: from spodumene and lepidolite zones, respectively

35 wt% Nb_2O_5, 11.5 wt% CaO, 1.45 wt% FeO, 3.44 wt% MnO; 48.2 wt% Ta_2O_5, and 0.56 wt% TiO_2.

For all crystals of CT, the sum of cations ranges from 2.96 to 3.02 apfu; only four out of one hundred and seventy-six analyses gave a cation sum between 3.03 and 3.05 apfu. High totals, i.e., greater than 1% above the ideal value of 3, indicate the presence of trivalent cations (Ercit, 1994a). The closeness of the majority of compositions to the ideal stoichiometry and the small number having slightly higher total cations, suggest that the columbite-tantalite in both suites of pegmatite contains a negligible quantity of trivalent cations. This inference is supported by the linear relationship between Nb and Ta/(Ta + Nb) and between Fe and Mn/(Mn + Fe) in crystals of CT (Fig. 4). The TiO_2 content of columbite-tantalite varies from less than 0.1 to 1.3 wt%, with most crystals containing between 0.1 and 0.4 wt% (Lamotte suite) and between 0.4 and 0.8 wt% (Lacorne suite). The presence of minor Ti in the structure is made possible by a coupled substitution involving $Ti^{4+}_3(Nb,Ta)^{5+}_{-2}(Fe,Mn)^{2+}_{-1}$. This exchange mechanism is confirmed by the sum Nb + Ta + Ti slightly above 2.0 apfu in almost all analyzed crystals. The wide range of compositions of columbite-tantalite therefore mainly reflects the homovalent exchanges $TaNb_{-1}$ and $MnFe_{-1}$ (Fig. 4).

Back-scattered electron images of all crystals of columbite-tantalite do not show compositional zoning. These images are consistent with compositional homogeneity in the small, included crystals, and with subtle chemical variations across the large, mostly interstitial crystals. In the case of the latter, the composition varies subtle; in one example, the core is $Fe_{(0.49}Mn_{0.48}Ti_{0.02})_{0.99}(Nb_{1.49}Ta_{0.5})_{1.99}O_6$ and the rim, $(Fe_{0.51}Mn_{0.45}Ti_{0.03})_{0.99}(Nb_{1.37}Ta_{0.6})_{1.97}O_6$.

Columbite-tantalite in both suites shows compositional variations in Mn/(Mn + Fe) and Ta/(Ta + Nb) from one type of pegmatite to another (Fig. 5), but is invariant in terms of Ti versus either Ta/(Ta + Nb) (Fig. 6) or Mn/(Mn + Ta) (not shown). In the Lamotte pluton, the columbite-tantalite shows a broad linear trend from ferrocolumbite in beryl and spodumene-beryl pegmatites to an intermediate composition in the less evolved spodumene pegmatite to manganotantalite in the more evolved spodumene pegmatite (Fig.

Fig. 4. Plots showing a linear correlation between Nb and Ta/(Ta + Nb), and between Fe and Mn/(Mn + Fe) in columbite-tantalite from the various types of pegmatite discussed in the text and from albitite. These trends indicate homovalent $NbTa_{-1}$ and $FeMn_{-1}$ exchanges. The symbols used here and in subsequent diagrams are: X, discrete aplite dike; solid and open squares (early and late ferrocolumbite, respectively, in the Lacorne suite only), beryl pegmatite; open triangle, spodumene-beryl pegmatite; open circle, less evolved spodumene pegmatite; solid circle, more evolved spodumene pegmatite; cross, albitite dike. In the Lacorne suite we distinguished more evolved (shaded triangle) and most evolved (solid triangle) spodumene-beryl pegmatites. No such distinction has been made for the Lamotte spodumene-beryl pegmatite. Apfu: atoms per formula unit.

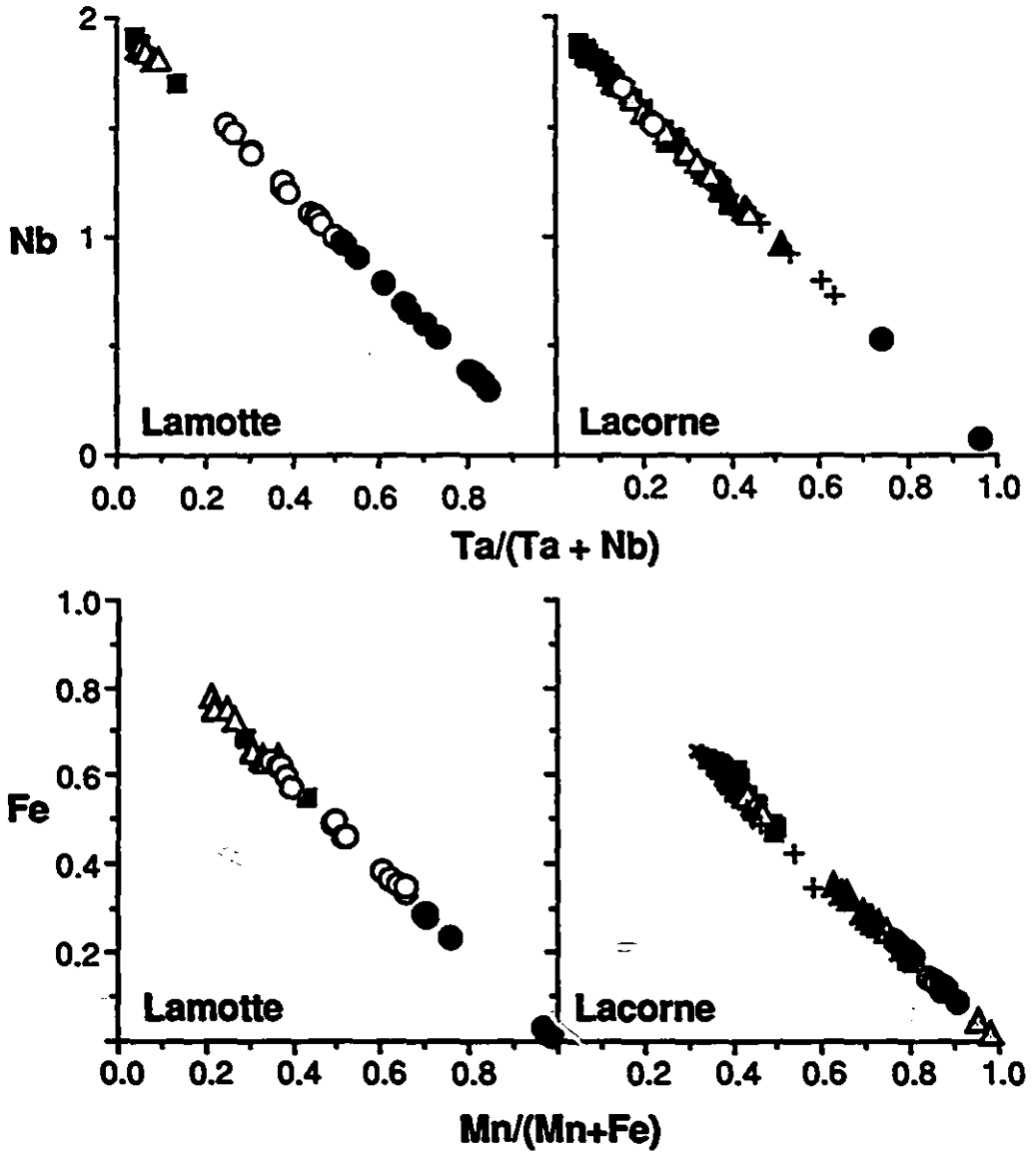

Figure 4

Fig. 5. Compositions of columbite-tantalite from the Lamotte (A) and Lacorne (B) pegmatite suites plotted in quadrilateral diagrams of ferrocolumbite ($FeNb_2O_6$)-manganocolumbite ($MnNb_2O_6$)-manganotantalite ($MnTa_2O_6$)-ferrotapiolite ($FeTa_2O_6$). Although ferrotapiolite occupies one of the end-member compositions in the diagram, it belongs to a framework subclass as opposed to the sheet subclass of columbite-tantalite (Černý and Ercit, 1989). Refer to Fig. 4 for an explanation of the symbols. Compositional trends in different internal zones of pegmatite are indicated by arrows (see text for further discussion): the terms BZ and IZ in the least evolved spodumene-beryl pegmatite (open triangle) refer to columbite-tantalite from the aplite border zone and the intermediate zone, respectively. Similarly, the terms SZ and LZ in the more evolved spodumene-beryl pegmatite refer to the spodumene zone and lepidolite zone, respectively.

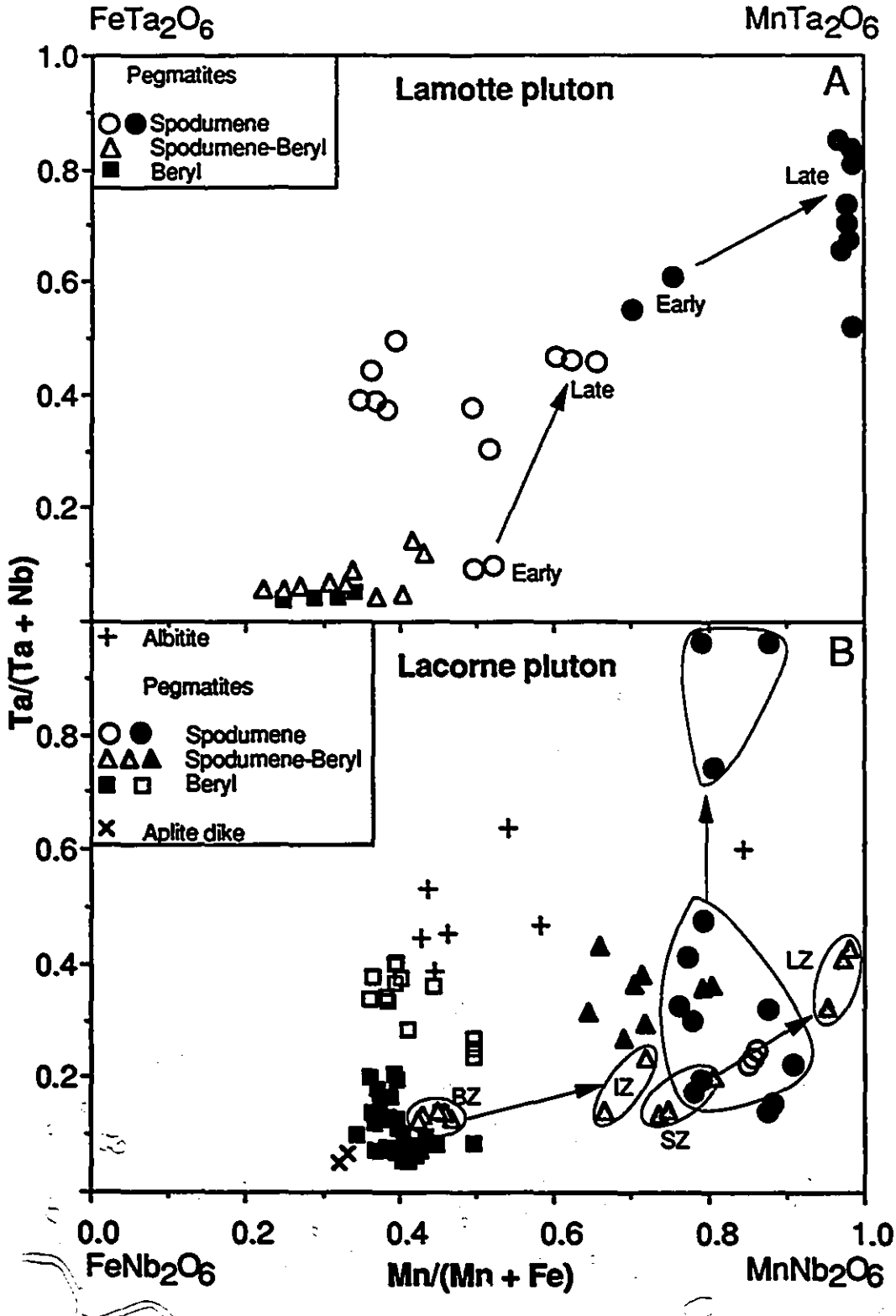
FeTa2O6
MnTa2O6
Pegmatites
Spodumene
Spodumene-Beryl
Beryl
Lamotte pluton
A
Late
Early
Late
Early
Albitite
Pegmatites
Spodumene
Spodumene-Beryl
Beryl
Aplite dike
Lacorne pluton
B
LZ
BZ
IZ
SZ
Ta/(Ta + Nb)
0.0
0.2
0.4
0.6
0.8
1.0
FeNb2O6
Mn/(Mn + Fe)
MnNb2O6

Figure 5

Fig. 6. Plots of Ti versus Ta/(Ta + Nb) in columbite-tantalite from the Lamotte (A) and Lacorne (B) suites of pegmatite. Symbols are the same as in Fig. 4.

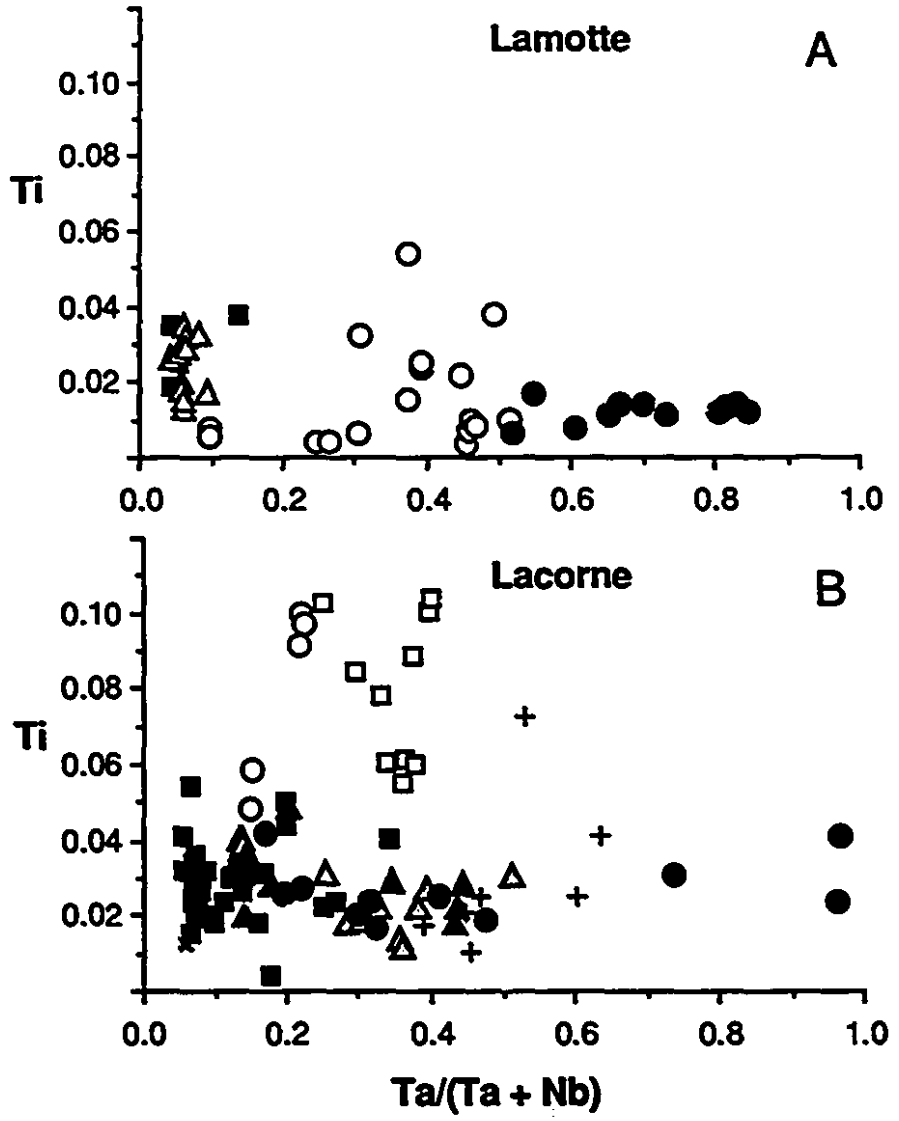
Lamotte
A
Ti
0.10
0.08
0.06
0.04
0.02
0.0
0.2
0.4
0.6
0.8
1.0
Lacorne
B
Ti
0.10
0.08
0.06
0.04
0.02
0.0
0.2
0.4
0.6
0.8
1.0
Ta/(Ta + Nb)

Figure 6

5). This trend is similar to that shown by columbite-tantalite within single bodies of pegmatite (indicated by arrows), in which the paragenetically early crystals are richer in Fe and Nb than the later ones. There is a large overlap in composition between columbite-tantalite in beryl pegmatite and that in spodumene-beryl pegmatite (aplite zone in both cases).

In contrast to the Lamotte suite, the overall compositional variation of columbite-tantalite in the Lacorne suite is from ferrocolumbite in beryl pegmatite to manganocolumbite in spodumene pegmatite, i.e., there is buildup in Mn followed by buildup in Ta. Examples of manganotantalite are scarcer here, as it is present only in the pegmatite portion of the most evolved spodumene composite pegmatite. This chemical trend also is shown by the ferrocolumbite in the beryl pegmatites, in which the interstitial (late) crystals invariably have higher values of Ta/(Ta + Nb) than, but similar values of Mn/(Mn + Fe) to, the included (early) grains (Fig. 5). On the other hand, columbite-tantalite in the least evolved spodumene-beryl pegmatite varies from ferrocolumbite in the aplite zone to manganocolumbite in the intermediate zone, with a very small corresponding increase in Ta/(Ta + Nb) values. The most extreme Mn enrichment in manganocolumbite is shown by the intermediate spodumene-beryl pegmatite, in which the value of Mn/(Mn + Fe) of columbite-tantalite reaches a high of 0.98 in the lepidolite zone from a value of 0.75 in the spodumene zone. Unlike columbite-tantalite compositions in the least evolved spodumene-beryl pegmatite, these attain a substantially higher Ta/(Ta + Nb) value.

In summary, the composition of columbite-tantalite in the Lamotte suite ranges from ferrocolumbite in beryl pegmatite to manganotantalite in spodumene pegmatite and shows a concomitant increase in Mn/(Mn + Fe) and Ta/(Ta + Nb) with pegmatite evolution (Fig. 7). In contrast, the columbite-tantalite in the Lacorne suite varies from ferrocolumbite to manganocolumbite. Within single bodies of beryl and most evolved spodumene pegmatite at Lacorne, the Ta/(Ta + Nb) value of columbite-tantalite increases at a constant Mn/(Mn + Fe) value.

Crystals of ferrocolumbite in discrete aplite dikes in the Lacorne and Moly Hill

Fig. 7. Compositional trends of columbite-tantalite from the various Lamotte and Lacorne pegmatites. Data are from Fig. 5.

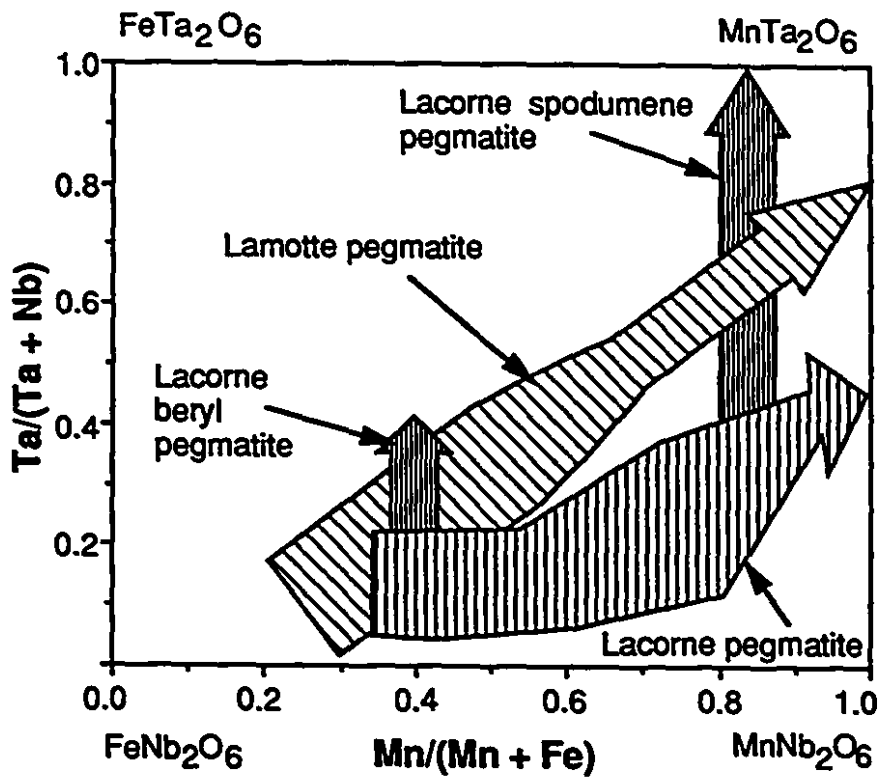
FeTa2O6
MnTa2O6
1.0
0.8
0.6
0.4
0.2
Ta/(Ta + Nb)
Lacorne spodumene pegmatite
Lamotte pegmatite
Lacorne beryl pegmatite
Lacorne pegmatite
0.0
0.2
0.4
0.6
0.8
1.0
FeNb2O6
Mn/(Mn + Fe)
MnNb2O6

Figure 7

plutons are similar compositionally, and have lower values of Mn/(Mn + Fe) (i.e., are less evolved) than their equivalents in the Lacorne beryl pegmatite. Columbite-tantalite from the Preissac muscovite + garnet monzogranite has a very low value of Ta/(Ta + Nb), < 0.04, and the Mn/(Mn + Fe) values range from 0.47 to 0.52. In the albitite dikes, the columbite-tantalite ranges widely, from a Ta/(Ta + Nb) of 0.4 and a Mn/(Mn + Fe) of 0.45 to a Ta/(Ta + Nb) of 0.6 and a Mn/(Mn + Fe) of 0.85. Most of the columbite-tantalite in these dikes thus have a composition between ferrocolumbite and manganotantalite, along a vector that does not lie close to the compositional trend defined for crystals formed from the melt phase.

Structural states

Unit-cell dimensions were refined on columbite-tantalite from representative types of pegmatite; the nature of the host rocks is indicated in the footnotes to Table 3. At Lamotte (Fig. 8), the columbite-tantalite in the aplite zone of both beryl and spodumene-beryl pegmatites has an intermediate degree of order (52-64%: Table 3) and Mn/(Mn + Fe) value, whereas that in the most evolved spodumene pegmatite is relatively disordered (in the range 0-25% order) and relatively Mn-enriched. Note that in one sample of manganotantalite, there are two sets of diffraction maxima, one set being dominant and pertaining to a zone richer in Mn (higher value of $\underline{a}$) than the other. The volume relationship of the two lattices most likely reflects the presence of a core of manganotantalite that is less evolved than the bulk of the crystal chosen for the X-ray diffraction experiment. The peaks of all other samples are single, i.e., devoid of satellites.

At Lacorne (Fig. 8), the ferrocolumbite from the aplite zone of beryl pegmatite is more ordered (61-75% order: Table 3) than that from the intermediate zone (41% order). All other samples plotted, from spodumene-beryl pegmatite and from spodumene pegmatite, are significantly more disordered (0-32% order) and more Mn-enriched. The most strongly disordered crystals are from the geochemically most evolved bodies of each grouping. The trend of increasing Mn/(Mn + Fe) inferred from the cell dimensions is consistent with the measured value (Fig. 5). As in the Lamotte suite, one sample (only)

Table 3 Unit-cell parameters (Å) for columbite-tantalite from the Lamotte* and Lacorne pegmatites.

Sample	a	b	c	V (Å3)	% Order+
Beryl pegmatite					
794*	14.261(2)	5.736(1)	5.100(1)	417.3	54
795*	14.258(3)	5.735(1)	5.101(1)	417.1	52
623	14.338(3)	5.744(1)	5.096(1)	419.7	75
623.1	14.336(3)	5.745(1)	5.096(1)	419.7	74
623.2	14.280(5)	5.741(1)	5.097(1)	417.9	61
1001	14.251(4)	5.740(1)	5.111(1)	418.1	41
Spodumene-beryl pegmatite					
908*	14.274(3)	5.739(1)	5.092(1)	417.1	64
912*	14.276(6)	5.740(2)	5.095(2)	417.5	62
708	14.236(2)	5.738(1)	5.133(1)	419.3	17
753.1	14.262(4)	5.751(1)	5.150(1)	422.4	7
753.2	14.266(3)	5.753(1)	5.147(1)	422.4	11
756.S (D)	14.271(3)	5.749(1)	5.143(1)	421.9	16
LD	14.285(5)	5.750(2)	5.130(1)	421.3	31
756.S (H)	14.386(3)	5.746(1)	5.080(1)	419.9	100
Spodumene pegmatite					
9-5* (D)	14.288(3)	5.753(1)	5.167(1)	424.7	0
LD	14.243(4)	5.744(1)	5.146(1)	421.0	7
9-5*	14.306(7)	5.753(2)	5.141(3)	423.2	25
9-5*	14.270(3)	5.747(1)	5.149(1)	422.3	10
9-5* (H)	14.420(3)	5.760(1)	5.093(1)	423.1	95
812	14.306(5)	5.745(2)	5.134(2)	421.9	32
812.2	14.287(5)	5.752(2)	5.145(1)	422.8	17
736	14.231(17)	5.776(6)	5.153(6)	423.6	0

S: from spodumene zone; D: Dominant; LD: Less dominant
H: heated at 1000ºC for 16 hours
+ % of order calculated according to Cerny and Ercit (1989)
All samples came from the aplite zone of composite aplite-pegmatite bodies, except for samples 1001, 753, 756.S and 812, which came from the pegmatite (intermediate) zone.

Fig. 8. A plot of unit-cell parameters $\underline{a}$ versus $\underline{c}$ showing an increasingly disordered structure of columbite-tantalite from beryl to spodumene pegmatite. Heated (1000°C, 16 hours) manganotantalite from the most evolved Lacorne spodumene pegmatite and a similar sample from the Lamotte pluton are completely ordered. The unit-cell values of the ordered end-members are from Wise et al. (1985). Symbols are the same as those in Fig. 4. A.S.E.: Average standard error, i.e., less than the size of the symbols.

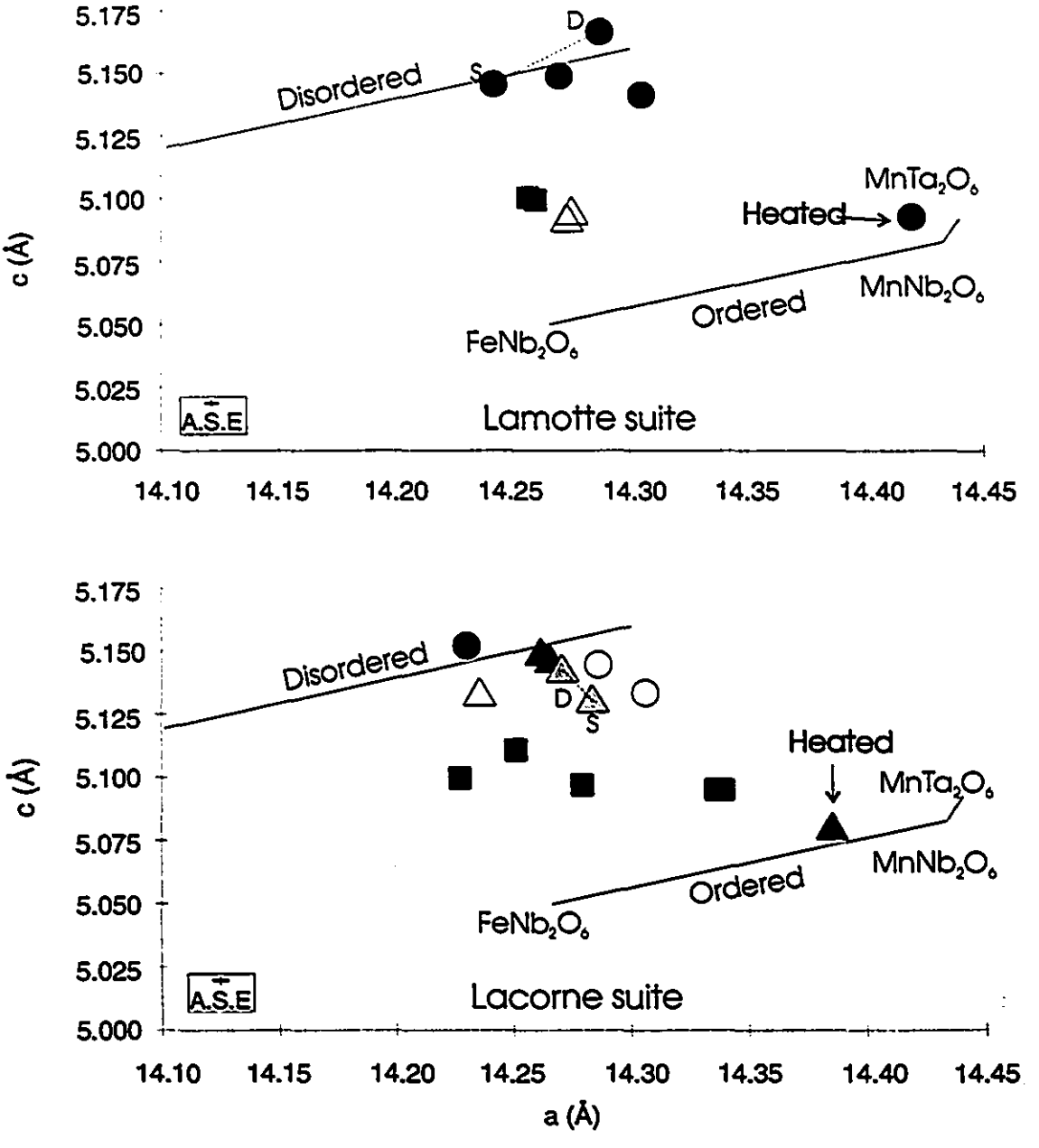
5.175
5.150
5.125
5.100
5.075
5.050
5.025
5.000
c (Å)
D
S
Disordered
MnTa2O6
Heated
MnNb2O6
Ordered
FeNb2O6
A.S.E
Lamotte suite
14.10
14.15
14.20
14.25
14.30
14.35
14.40
14.45
Disordered
Heated
MnTa2O6
MnNb2O6
Ordered
FeNb2O6
Lacorne suite
a (Å)

Figure 8

displays two sets of diffraction maxima. In this case, the two lattices belong to zones of similar degree of Mn enrichment, but differ slightly in degree of cation order, the dominant member of the pair being mode strongly disordered (0 vs. 7% order).

To test that the disordered members of the suite do indeed have the columbite-tantalite structure (and not that of ixiolite), one sample from each locality was heated to 1000°C for 16 hours. In both cases, the highly disordered starting material became highly ordered manganotantalite as a result of the heat treatment (Fig. 8, Table 3), as would be expected in light of the findings of Černý and Ercit (1985). The rapid increase in degree of cation order at 1000°C indicates that the ordered structure is strongly favored over one showing a disordered distribution of divalent and pentavalent cations and the resultant local departure from ideal bond-valence sums that are anticipated.

MICROLITE

As described earlier, microlite [$A_{2-m}B_2O_6(O,OH,F)_{1-n}$ pH_2O (m,n=0-1; p=0-?)] occurs as a secondary phase replacing columbite-tantalite, mostly in spodumene pegmatites and, very rarely, in beryl pegmatites (Fig. 3D). Electron-microprobe data show that the sum of oxides ranges from 91 to 97.5 wt% (Table 4). Low totals are common in microlite (e.g., Splide and Shearer, 1992; Wise and Černý, 1990), and have been attributed by Wise and Černý to the presence of H_2O or F, or both. Examination of the microlite with an energy-dispersion spectrometer attached to the electron microprobe did not indicate the presence of F; H_2O is therefore the most likely dominant volatile species in this case.

The composition of microlite is highly variable; different samples contain uranian microlite (Table 4, anal. 1-3 and 7), sodium-rich microlite (anal. 5 and 6), and U- and Na-free microlite (anal. 4). Na-rich microlite is restricted to spodumene pegmatites, whereas uranmicrolite occurs in both spodumene (812) and spodumene-beryl (756.S) pegmatites.The dominant major-element oxide is Ta_2O_5 (54-80 wt%); Nb_2O_5 (2.3-17.6 wt%) and CaO (10.7-15.2 wt%) are subordinate. The Ti content ranges from 0.5 to 6.3

Table 4 Representative compositions of microlite

Sample	756.S	756.S	756.S	721	HP9-5	HP9-5	812	812
Analyses	1	2	3	4	5	6	7	8
Nb_2O_5 (wt%)	9.44	11.24	17.66	16.21	2.30	1.76	9.58	11.60
UO_2	6.95	7.88	3.97			0.50	8.60	6.72
Na_2O					4.82	3.59	1.23	1.00
MgO				0.07				
CaO	14.19	14.48	15.19	13.48	10.7	10.74	13.81	15.15
TiO_2	5.31	8.33	4.90	1.50	0.58	0.51	5.16	5.98
FeO	0.02		0.16	6.80	0.04		0.02	0.09
MnO	0.46	0.63	1.05	3.68	0.09	0.39	0.69	0.71
Ta_2O_5	55.55	51.55	48.33	54.75	78.48	79.98	54.42	50.9
Total	91.92	94.11	91.26	96.49	97.01	97.47	93.51	92.15
Structural formula based on full-B-site occupancy (Nb+Ta+Ti=4)								
Nb	0.730	0.852	1.287	1.256	0.182	0.139	0.752	0.889
Ta	2.586	2.350	2.119	2.551	3.741	3.794	2.573	2.348
Ti	0.684	0.798	0.594	0.193	0.077	0.067	0.675	0.763
U	0.265	0.286	0.142			0.019	0.333	0.254
Na					1.638	1.214	0.415	0.329
Mg				0.018				
Ca	2.603	2.597	2.624	2.475	2.010	2.007	2.572	2.753
Fe	0.003		0.022	0.974	0.059		0.003	0.013
Mn	1.092	0.895	0.143	1.620	0.013	0.058	1.143	1.151

wt% TiO_2. Fe and Mn are minor constituents. The composition of microlite in this study lies within the compositional field of microlite compiled by Wise and Černý (1990) (Fig. 9), and compares well with that of microlite from the Yellowknife pegmatites, Northwest Territories (Wise and Černý, 1990), and the lepidolite pegmatites from South Africa and Namibia (Baldwin, 1989).

DISCUSSION

Compositional trends and pegmatite evolution

Textural evidence presented earlier indicates that columbite-tantalite in the Lamotte and Lacorne pegmatites is magmatic; the crystals are relatively homogeneous, and free of subsolidus alteration except where noted. The composition of columbite-tantalite, like that of any other magmatic mineral, was therefore controlled by the abundances Nb, Ta, Fe and Mn in the evolving magma, the relative solubilities of the end-members, the nature of the coexisting minerals on the liquidus and the corresponding mineral-liquid partition coefficients for the above elements.

In the Lamotte suite as a whole, columbite-tantalite displays a trend of simultaneously increasing Mn/(Mn + Fe) and Ta/(Ta + Nb) values from beryl to spodumene pegmatite, indicating that the residual liquid was progressively depleted in both Fe and Nb, and enriched in both Mn and Ta with evolution of the residual melt (Figs. 5, 7). The same trend is shown by columbite-tantalite within individual bodies of spodumene pegmatite, i.e., from early to late stages of crystallization. These trends can be explained by the relative solubility of the two end members in the liquid. Ferrocolumbite is less soluble and crystallized first, thereby enriching the residual liquid in Mn and Ta, and causing later crystallization of manganotantalite. This simple explanation is partially supported by experiments of Keppler (1993), who has shown that $MnTa_2O_6$ is approximately nine times more soluble than $MnNb_2O_6$ in F-free haplogranite. Although there are no experimental data for ferrocolumbite, it can be argued on theoretical grounds that because the field strengths (Z/r) of Nb and Fe are higher than

Fig. 9. A Nb-Ti-Ta triangular diagram (atomic proportions) showing the B-site occupancy in microlite. The field boundaries of the three pyrochlore-group minerals are after Hogarth (1977). The compositional fields of known microlite are after Černý and Ercit (1989), Baldwin (1989) and Wise and Černý (1990).

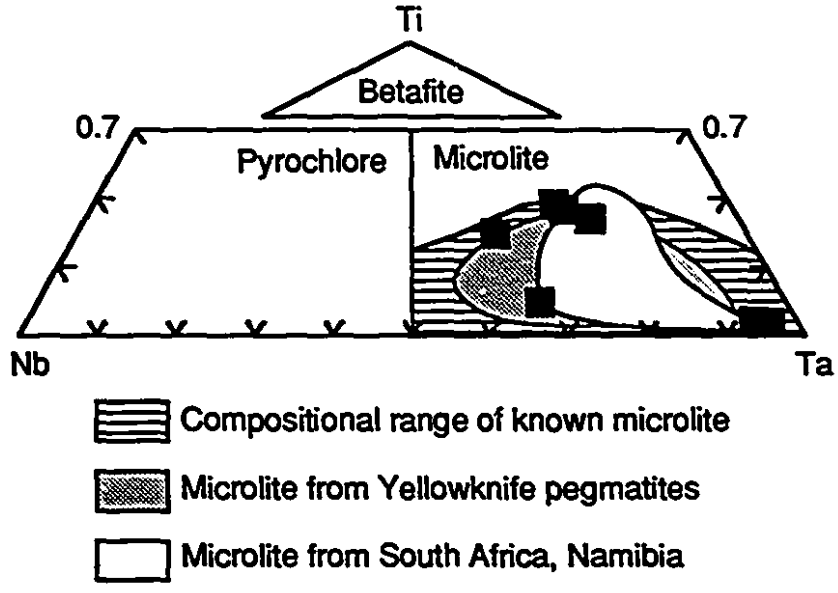
Ti
Betafite
0.7
0.7
Pyrochlore
Microlite
Nb
Ta
Compositional range of known microlite
Microlite from Yellowknife pegmatites
Microlite from South Africa, Namibia

Figure 9

those of Ta and Mn, respectively, ferrocolumbite will be less soluble than either manganocolumbite or manganotantalite.

In the Lacorne suite, the columbite-tantalite also displays an overall trend of increasing Mn/(Mn + Fe) and Ta/(Ta + Nb) from beryl to spodumene pegmatite. However, in contrast to the Lamotte suite, the increase in Ta/(Ta + Nb) is relatively subdued, and the trend is mainly one of Mn enrichment. Similar trends of dominant Mn-enrichment in columbite-tantalite composition have been reported by Černý et al. (1985, 1986) from a number of granitic pegmatite fields and by Spilde and Shearer (1992) for the Black Hills granitic pegmatites (South Dakota). Černý et al. (1985, 1986) attributed such a trend to the presence of F in the melt, and the resultant formation of Mn- and Ta-fluoride complexes, which would increase the partitioning of Mn and Ta (presumably mostly the latter) in favor of the liquid and delay crystallization of manganotantalite until the latest stages of pegmatite evolution. However, in order for this hypothesis to account for a trend toward manganocolumbite in Fig. 7, the partitioning of Ta relative to Nb would have to have become stronger in favor of the liquid than that of Mn relative to Fe.

Although Keppler (1993) has shown that the solubility of manganotantalite in haplogranitic melts does increase sharply with increasing F content, his data provide no evidence of a corresponding preferential increase in the solubility of manganotantalite over that of manganocolumbite. Indeed, the value of $Ks_{MnTa2O6}/Ks_{MnNb2O6}$ (Ks: solubility product) is highest in the F-free system, decreases until the F content of the melt is 2 wt%, and then is essentially constant for higher F contents. These data would appear to rule out fluoride complexing as a viable explanation of the relative suppression of Ta in the crystal. Furthermore, there are no experimental data to test the hypothesis of preferential complexing of Mn relative to Fe by fluoride. However, theoretical considerations do not support this hypothesis. Both Fe and Mn are divalent cations, are intermediate in terms of the hard-soft classification of metals, and are therefore unlikely to form strong complexes with a hard ligand like F^- (Pearson, 1963). Moreover, Al, Na and Li, which are major components of the magma, all associate strongly with fluoride in the melt (e.g., Manning et al., 1980) and thus it seems unlikely that Fe- and Mn-

bearing associations with F would be important.

In the Lacorne suite, with the exception of the beryl pegmatite and the most evolved batches of spodumene pegmatite, the trend defined by columbite-tantalite in Fig. 5 and 7 parallels the overall trend from beryl pegmatite to spodumene pegmatite associated with this pluton, i.e., enrichment in Mn. In contrast, the internal evolution of individual bodies of pegmatite in this swarm follows a distinct vector off the main trend in Fig. 7, along which Ta/(Ta + Nb) increases in columbite-tantalite at a constant Mn/(Mn + Fe) value. The fact that garnet crystallized contemporaneously with columbite-tantalite at all stages of the internal evolution of these bodies probably is responsible for the local decoupling of Fe, Mn from Nb, Ta, the garnet acting as a buffer of Fe and Mn activities. Note that in most bodies, the crystallization of garnet has terminated at the stage of nucleation and growth of columbite-tantalite.

Relationship between degree of cation order in columbite-tantalite and degree of geochemical evolution of the system.

The striking increase in the extent of disorder with increasing Mn enrichment, and the complete absence in these suites of columbite-tantalite plotting close to the "ordered" end-members (Fig. 8) can, in our opinion, be used to extract petrogenetic information. One hypothesis generally mentioned in evaluations of such observations involves the incorporation of "other" cations, such as Ti, leading to a redistribution of the essential cations over the A and B sites, and promoting disorder. Whereas the levels of Ti can reach important levels in minerals of this group, the data reported here on Ti levels of incorporation are all rather low, and do not surpass 0.1 apfu. A plot of degree of order versus Ti content (not shown) does not suggest any dependence on this variable. We tentatively conclude in light of these facts and the close approach of the compositions to stoichiometry (Tables 1, 2; Fig. 4), that coupled substitution involving Ti or other extraneous cations is not of any consequence in this context.

We tentatively conclude, therefore, that the degree of order of the columbite-tantalite in this suite is a function of environmental factors, and specifically, the rate of

cooling and the size of the pegmatite bodies. Using this hypothesis, Černý et al. (1986) proposed, in the case of the Greer pegmatite field, that small bodies of relatively evolved pegmatite emplaced in country rocks cooled much more rapidly than larger, proximal bodies of less evolved pegmatite. The more rapid the rate of cooling, the more likely the preservation of the degree of cation order imposed at the time of growth of the columbite-tantalite. We contend that the observed degree of cation order in both Lamotte and Lacorne suites is close to, if not identical to, the original degree of cation order. There certainly is no evidence of appreciable ordering of CT in any of the bodies sampled. Unfortunately, there is no information in the literature concerning the kinetics of ordering of columbite-tantalite solid solutions as a function of temperature and time of annealing.

An enigmatic aspect of the problem concerns the unlikeliness that a divalent and a pentavalent cation could adopt a disordered distribution in an oxide phase of stoichiometry AB_2O_6. One would predict such serious departures from local charge-balance that "on paper", one would not expect disorder to be possible. Yet, the consensus of structural crystallographers is that such crystals really are disordered. The fact that such disorder is strongly metastable is proven by the efficient conversion of disordered manganotantalite to the ordered equivalent at a temperature far above (~450°C) the inferred temperature of crystallization of the evolved felsic liquids. We can conclude that crystallization of these batches of melt was very rapid, and that the oxide phase crystallized with a pattern of cation distribution resembling that in the melt.

CONCLUSIONS

1. The crystal chemistry of columbite-tantalite in the Lamotte and Lacorne suites of pegmatite is controlled mainly by homovalent $TaNb_{-1}$ and $MnFe_{-1}$ exchanges. The coupled substitution involving $Ti_3(Nb,Ta)_{-2}(Fe,Mn)_{-1}$ is of minor importance.

2. The increases in Mn/(Mn + Fe) and Ta/(Ta + Nb) of columbite-tantalite from the least evolved beryl pegmatite to the most evolved spodumene pegmatite and with progressive crystallization of individual pegmatites, can be explained by the higher

solubility of Ta- relative to of Nb end-members and Mn- relative to Fe end-members. The much larger increases in Mn/(Mn + Fe) relative to Ta/(Ta + Nb) in columbite-tantalite in the Lacorne suite compared to the Lamotte suite may reflect the role and order of crystallization of garnet.

3. In pegmatite bodies where columbite-tantalite and garnet are coeval, the garnet buffered the activity of Mn and Fe in the liquid, and as a result, the evolution of columbite-tantalite composition was marked by increases in Ta/(Ta + Nb) at constant Mn/(Mn + Fe).

4. The degree of disorder of columbite-tantalite increases progressively from beryl- to spodumene pegmatite as a result of the higher cooling rate of pegmatite bodies emplaced in the country rocks as opposed to those in and near the parental plutons. Samples closest to the manganotantalite end-member are completely disordered.

ACKNOWLEDGEMENTS

We are grateful to T. Scott Ercit of the Canadian Museum of Nature for kindly supplying synthetic $MnNb_2O_6$ and Ta_2O_5 mineral standards. His advice is sincerely appreciated. We also thank Petr Černý and Mike Wise for clarifying many aspects of the crystal chemistry of columbite-tantalite. Financial support was provided by an NSERC research grant to AEW-J and RFM, an NSERC strategic grant to AEW-J, an FCAR team grant and a NATO travel grant to SAW.

REFERENCES CITED

Appleman, D.E., and Evans, H.T., Jr. (1973) Job 9214: indexing and least-squares refinement of powder diffraction data. United States Geological Survey, Computer Contributions 20 (NTIS document PB2-16188).

Baldwin, J.R. (1989) Replacement phenomena in tantalum minerals from rare-metal pegmatites in South Africa and Namibia. Mineralogical Magazine, 53, 571-581.

Černy, P., and Ercit, T.S. (1985) Some recent advances in the mineralogy and geochemistry of Nb and Ta in rare-element granitic pegmatites. Bulletin de Minéralogie, 108, 499-532.

— & — (1989) Mineralogy of niobium and tantalum: Crystal chemical relationships, paragenetic aspects and their economic implications. In P. Möller, P. Černý and F. Saupé, Eds., Lanthanides, Tantalum and Niobium. Springer, New York, 28-79.

Černý, P., Goad, B.E., Hawthorne, F.C., and Chapman, R. (1986) Fractionation trends in the Nb- and Ta- bearing oxide minerals in the Greer Lake pegmatitic granite and its pegmatite aureole, southeastern Manitoba. American Mineralogist, 71, 501-517.

Černý, P., Meintzer, R.E., and Anderson, A.J. (1985) Extreme fractionation in rare-element granitic pegmatites: selected examples of data and mechanisms. Canadian Mineralogist, 23, 381-421.

Černý, P., and Turnock, A.C. (1971) Niobium-tantalum minerals from granitic pegmatites at Greer Lake, southeastern Manitoba. Canadian Mineralogist, 10, 755-772.

Dawson, K.R. (1966) A comprehensive study of the Preissac-Lacorne batholith, Abitibi county, Quebec. Geological Survey of Canada Bulletin 142.

Ercit, T.S. (1994a) The geochemistry and crystal chemistry of columbite-group granitic pegmatites, southwest Grenville Province, Canadian Shield. Canadian Mineralogist, 32, 421-438.

— (1994b) Regional chemistry and crystal chemistry of oxide minerals from the Mattawa pegmatite district, Grenville Province, Ontario. Extreme Nb/Ta fractionation for muscovite-class pegmatites. Canadian Mineralogist, 33, 000-000.

Feng, R., and Kerrich, R. (1991) Single zircon age constraints on the tectonic juxtaposition of the Archean Abitibi Greenstone belt and Pontiac subprovince, Quebec, Canada. Geochimica et Cosmochimica Acta, 55, 3437-3441.

Gariépy, C., and Allègre, C.J. (1985) The lead isotope geochemistry and geochronology of late kinematic intrusives from the Abitibi Greenstone belt and the implications for late Archean crustal evolution. Geochimica et Cosmochimica Acta, 49, 2371-2383.

Garvey, R. (1986) LSUCRIPC, least squares unit-cell refinement with indexing on the personal computer. Powder Diffraction, 1 (1), 114.

Grice, J.D., Černý, P., and Ferguson, R.B. (1972) The Tanco pegmatite at Bernic Lake, Manitoba. II. Wodginite, tantalite, pseudoixiolite and related minerals. Canadian Mineralogist, 11, 609-642.

Hogarth, D.D. (1977) Classification and nomenclature of the pyrochlore group. American Mineralogist, 62, 403-410.

Keppler, H. (1993) Influence of fluorine on the enrichment of high field strength trace elements in granitic rocks. Contributions to Mineralogy and Petrology, 114, 479-488.

Lahti, S.I. (1987) Zoning in columbite-tantalite crystals from the granitic pegmatites at Erajarvi area, southern Finland. Geochimica Cosmochimica Acta, 51, 509-517.

Manning, D.A.C., Hamilton, D.L., Henderson, C.M.B., and Dempsey, M.J. (1980) The probable occurrence of interstitial Al in hydrous, F-bearing and F-free aluminosilicate melts. Contributions to Mineralogy and Petrology, 75, 206-215.

Mulja, T., Williams-Jones, A.E., Wood, S.A., and Boily, M. (1995a) Geology and mineralogical evolution of rare-element monzogranite systems in the Preissac-Lacorne batholith, Quebec, Canada. Canadian Mineralogist, 33, 000-000.

Mulja, T., Williams-Jones, A.E., Wood, S.A., and Boily, M. (1995b) Petrogenesis of zoned monzogranites and associated rare-element pegmatites and quartz veins: the Preissac-Lacorne batholith, Quebec, Canada. Canadian Mineralogist, 33, 000-000.

Pearson, R.G. (1963) Hard and soft acids and bases. Journal of the American Chemical Society, 85, 3533-3539.

Pouchou, J.L., and Pichoir, F. (1985) "PAP" (phi-rho-z) procedure for improved quantitative microanalyses. In J.T Armstrong, Ed., Microbeam analyses. San Francisco Press, San Francisco, 104-105.

Spilde, M.N., and Shearer, Jr. C.K (1992) A comparison of tantalum-niobium oxide assemblages in two mineralogically distinct rare-element granitic pegmatites, Black Hills, South Dakota. Canadian Mineralogist 30, 719-747.

Trueman, D.L., and Černý, P. (1982) Exploration for rare-element granitic pegmatites. In P. Černý, Ed., Granitic pegmatites in science and industry. Mineralogical Association of Canada Short Course Handbook, 8, 463-491.

Wenger, M., and Armbruster, T. (1991) Columbite $(Fe,Mn)(Nb,Ta)_2O_6$ in the pegmatites of the calc-alkaline Bergell intrusion (southeast Central Alps). Schweizerische Mineralogische und Petrogrographische Mitteilungen, 71, 349-369.

Wise, M.A (1987) Geochemistry and crystal chemistry of Nb, Ta and Sn minerals from the Yellowknife pegmatite field, N.W.T. Unpublished Ph.D thesis, University of Manitoba, Winnipeg, Manitoba.

Wise, M.A., and Černý, P. (1990) Primary compositional range and alteration trends of microlite from the Yellowknife pegmatite field, Northwest Territories, Canada. Mineralogy and Petrology, 43, 83-98.

Wise, M.A., Turnock, A.C., and Černý, P. (1985) Improved unit cell dimensions for ordered columbite-tantalite end members. Neues Jahrbuch Mineralogische Monatshefte, 372-378.

CHAPTER 5

PHYSICAL AND CHEMICAL EVOLUTION OF FLUIDS IN RARE-ELEMENT PEGMATITES ASSOCIATED WITH THE LACORNE PLUTON, QUEBEC, CANADA

Thomas MULJA[1], Anthony E. WILLIAMS-JONES[1],
Scott A. WOOD[2], and Anne PRÉFONTAINE[3]
[1]Department of Earth and Planetary Sciences, McGill University,
3450 University St., Montréal, Quebec, H3A 2A7.
[2]Department of Geology and Geological Engineering,
University of Idaho, Moscow, ID 83843, U.S.A
[3]1750 Beauchemin, La Plaine, Quebec, J0N 1B0

ABSTRACT

Comagmatic rare-element (Li, Be, Nb, Ta) granitic pegmatites associated with the Archean Lacorne pluton of the Preissac-Lacorne batholith (Quebec), and ranging from a least evolved beryl-bearing type to a most evolved spodumene-bearing type, contain primary fluid inclusions which establish that the magma saturated with vapor peneconteporaneously with emplacement. The earliest orthomagmatic fluid is represented by aqueous liquid-vapor (type 1a) and aqueous liquid-vapor-solid (type 2) inclusions in beryl, which are estimated to have been trapped at temperatures between 500 and 550°C and 3.5 Kb. Based on microthermometric measurements, analyses of the compositions of the residues of decrepitated inclusions and the nature of the solids, the fluid is interpreted to have been NaCl-dominated, to have had low salinity (<15 wt% NaCl eq.), and contained appreciable Fe and dissolved CO_2. In spodumene, the equivalent fluid, which is estimated to have been trapped at somewhat lower temperature (450 to 500°C), contained significant Mn, Li and Cs in place of Fe, reflecting corresponding trends in the chemical evolution of the host rocks.

Vapor-rich, mainly secondary, aqueous inclusions (type 1b) trapped in beryl, are interpreted to reflect temporary sharp drops in pressure later in the crystallization history of the beryl-bearing pegmatites due to local fluid overpressures which led to brecciation and consequent pressure release. These inclusions have high salinity, are $CaCl_2$-rich, and are considered to represent the first incursion of external metamorphic fluids into the pegmatites. In spodumene pegmatite, incursion of these inclusions is interpreted to have occurred earlier and been more important because a high proportion of primary inclusions contain significant Ca, and Ca abundances are generally higher in inclusions hosted by spodumene than by beryl. This interpretation is consistent with the location of spodumene pegmatites in basaltic country rocks and beryl-bearing pegmatites in the pluton.

The crystallization history of the pegmatites coincided with the entrapment of low salinity aqueous-carbonic (type 3 inclusions) in quartz, which is thought to have occurred as a result of unmixing of the orthomagmatic fluid on cooling, probably at temperatures between 250 and 350°C. The history of fluid entrapment and evolution documented in this

study demonstrate the validity of the Jahns-Burnham model for the formation of zoned rare element pegmatites, at least for the case of boron-poor magmatic systems.

INTRODUCTION

The widely accepted Jahns and Burnham (1969) model for the petrogenesis of granitic pegmatites involves the assumption that the corresponding magma is saturated with an aqueous phase, and that this condition is needed in order to produce the large crystals and internal zonation that characterize these rocks. This model has been challenged for the case of boron-rich systems by London (1986) who, on the basis of fluid inclusion data, argued that the Tanco Li-Ta pegmatite did not become saturated with an aqueous phase until relatively late in its crystallization history. Instead, he interpreted his data to indicate the presence of dense, hydrous, alkali borosilicate fluids in the Tanco pegmatite-forming magma. London's interpretation of fluid evolution in the Tanco pegmatite is in conflict with Thomas et al. (1988), who, from the presence of aqueous liquid-vapor inclusions (coexisting with crystal-rich (melt) inclusions) in wall zone schorl, proposed that the magma was saturated with an aqueous phase at the start of its crystallization: London (1986) considered the schorl to be paragenetically late.

There are few other modern studies of fluid evolution in rare-element pegmatites. In one of these, Whitworth and Rankin (1989), using fluid inclusion data in quartz from barren and spodumene pegmatites and parental granite at Leinster (Ireland), proposed that aqueous fluids started to exsolve during the late stage evolution of the parental granite and continued to exsolve during the crystallization of the pegmatites. However, they did not provide evidence of primary entrapment of the fluids, and quartz is well known to trap secondary fluid inclusions (cf. Roedder, 1984). In another study, Ruggieri and Lattanzi (1992) presented fluid inclusion evidence that tourmaline, beryl and quartz in miarolitic cavities, and massive quartz in the Mt. Capanne pegmatites (Italy) crystallized in the presence of aqueous fluids. Although the authors did not discuss the timing of entrapment of these fluids, it is likely to have been late given the location of the host minerals, and thus the study does not indicate whether or not the magma was saturated with an aqueous phase early in its history of crystallization. Finally, Chakoumakos and Lumkin (1990) reported the occurrence of aqueous-CO_2 inclusions in beryl and quartz from the Harding pegmatite, New Mexico, but failed to indicate whether the inclusions

were primary or secondary.

The purpose of this paper is to shed more light on this fundamental issue of pegmatite genesis by reporting results of a study of fluid inclusions in beryl, spodumene and quartz from a suite of variably evolved, boron-poor rare-element granitic pegmatites in the Lacorne pluton of the Preissac-Lacorne batholith (Québec). These pegmatites are comagmatic and comprise a least fractionated beryl-type which intruded the pluton, a transitional spodumene-beryl-type, and a highly fractionated spodumene-type, which was emplaced in the country rocks. Our study shows that in all three types of pegmatite the magma was saturated with an aqueous phase near the onset of crystallization and later exsolved a carbonic phase. We therefore conclude that, at least in the case of boron-poor systems, there is no need to reject the Jahns and Burnham model of pegmatite genesis.

GEOLOGY AND PETROLOGY

The rare-element pegmatites investigated in this study belong to the Lacorne monzogranite pluton of the Archean Preissac-Lacorne batholith (~2.76 Ga, Steiger and Wasserburg, 1985; Feng and Kerrich, 1991), which is composed of older syn-tectonic basic intrusions (gabbro-monzonite-granodiorite) and younger post-tectonic peraluminous monzogranite plutons (Fig. 1). Rocks surrounding the batholith comprise mainly basalt, plus smaller volumes of basic tuffs and komatiite, which regionally have been metamorphosed to upper greenschist facies and locally (within 7 kilometers of the batholith) display evidence of contact metamorphism (cf. Dawson, 1966; Powell, 1994). Mulja et al. (1995b, c) have shown that the Lacorne monzogranite pluton is quasi-concentrically zoned into biotite, two-mica and muscovite monzogranites, and proposed that this occurred as a result of side-wall crystallization. According to their model, the rare-element pegmatites, which occur throughout the pluton and environs, represent fractionation of the residual liquids from monzogranite crystallization. The pegmatite bodies occur as dikes, ranging in width from tens of centimeters to eight meters and up to hundreds of meters in length, and as lenticular bodies up to 5 x 24 m in plan. Most dikes strike east-west and northwest-southeast, and dip vertically to subhorizontally.

Fig. 1. Location and geological map of the Lacorne pluton and associated rare-element pegmatites in the Preissac-Lacorne batholith, Québec. Although Dawson (1966) outlined the limit of the Lacorne pluton depicted in A, recent mapping by Mulja et al. (1995b) has shown that most outcrop is concentrated in the eastern half of the area attributed to the pluton. Abbreviations are as follows: Ab, albitite; Brl, beryl; MG, muscovite monzogranite; Mo, molybdenite, Spd, spodumene. The three sample locations are MBP (Mass beryl prospect), Valor, and QL (former Québec lithium mine), which is about 7 km east of the map.

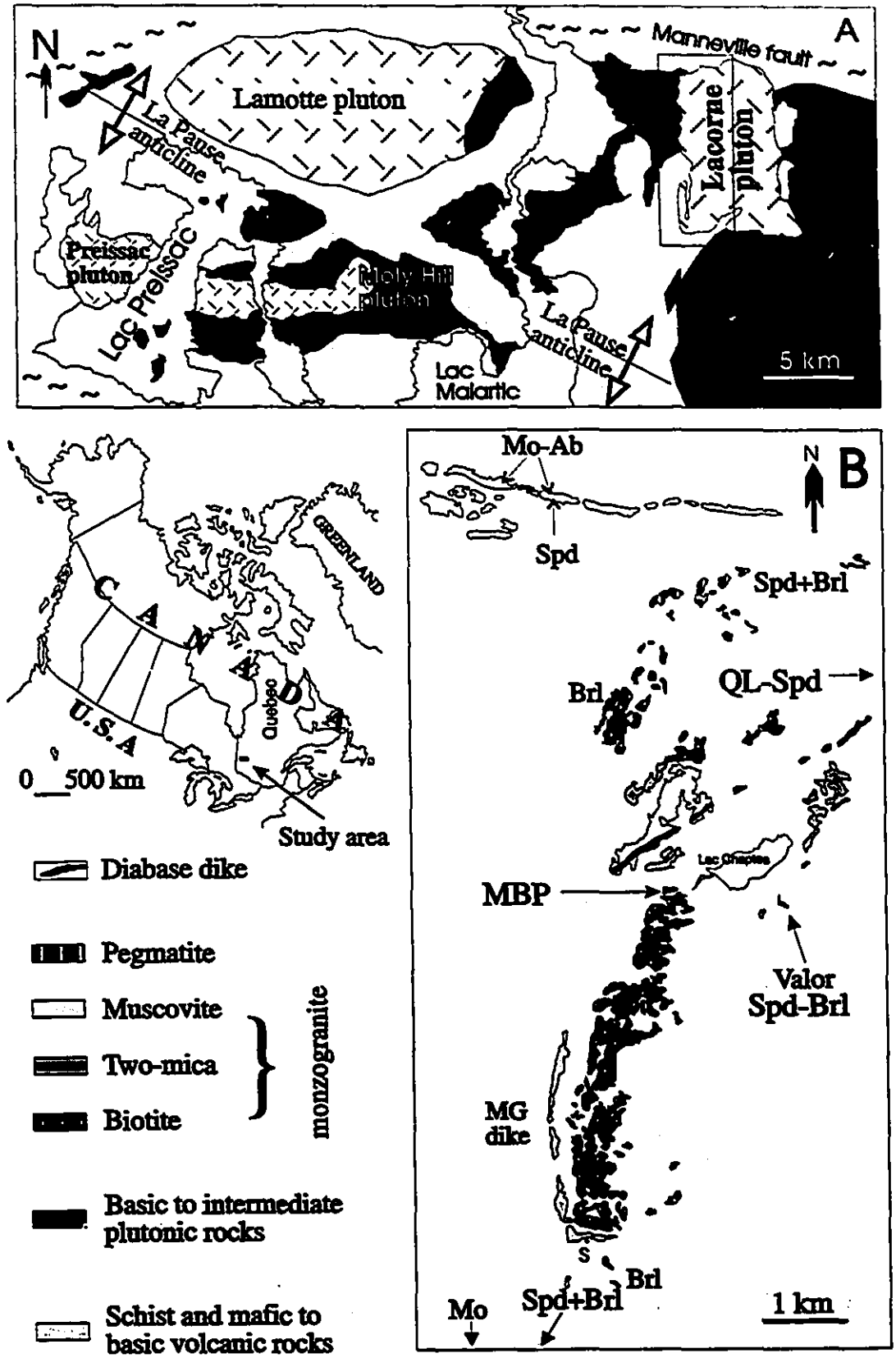
A
N
Manneville fault
Lamotte pluton
La Pause anticline
Lacorne pluton
Preissac pluton
Lac Preissac
Holy Hill pluton
La Pause anticline
Lac Malartic
5 km
CANADA
U.S.A
Quebec
GREENLAND
0 500 km
Study area
B
Mo-Ab
Spd
Spd+Brl
Brl
QL-Spd
MBP
Valor
Spd-Brl
MG dike
S
Brl
Mo
Spd+Brl
1 km
Diabase dike
Pegmatite
Muscovite
Two-mica
Biotite
monzogranite
Basic to intermediate plutonic rocks
Schist and mafic to basic volcanic rocks

Figure 1

Within the Lacorne pluton, local faults cut many pegmatites, but did not significantly deform the major mineral constituents, e.g., beryl and spodumene remain euhedral. In some pegmatites, however, the internal structure has been locally disrupted by brecciation, which has juxtaposed irregularly shaped fragments from different parts of the pegmatite and cemented them with coarse-grained K-feldspar, quartz and muscovite. This brecciation is interpreted to have occurred as a result of excessive fluid pressures (hydrofracturing) prior to complete crystallization of the pegmatite.

On the basis of the predominant rare-element-bearing minerals, the pegmatites have been subdivided into proximal (with respect to the Lacorne pluton) beryl-, intermediate spodumene-beryl- and distal spodumene-types (Fig. 1B). Throughout this paper, they are referred to as beryl, spodumene-beryl and spodumene pegmatites. Molybdenite- and columbite-tantalite-bearing albitite dikes and Mo-bearing quartz veins occur beyond the spodumene pegmatite zone to the north and south of the pluton, respectively (Fig. 1B).

The most important rare-element pegmatites are at the Mass Beryl Prospect (beryl-type), the Valor Prospect (spodumene-beryl-type) and the former Québec Lithium mine (spodumene-type), and have furnished the samples used in this study. These pegmatites vary in size (up to 8 x 120 m in plan) and internal texture (zoned and unzoned). The beryl pegmatites (< 1-m wide), which were studied, are symmetrically zoned, consisting of a sodic aplite wall zone, an intermediate zone of quartz, K-feldspar, coarse-grained muscovite, albite, and beryl, and a central zone of quartz and K-feldspar. Layers of fine-grained garnet and small pockets of quartz + muscovite are common in the aplite. Ferrocolumbite, monazite, gahnite, molybdenite and magnetite are minor phases.

The spodumene-beryl pegmatite has a sodic aplite wall-zone, which contains layers of garnet, ferrocolumbite, and minor disseminated fine-grained schorl. This zone grades inward through beryl and books of muscovite into an intermediate zone comprising mainly albite (as rosettes of cleavelandite), quartz, K-feldspar, and spodumene, and minor pollucite [$(Cs,Na)_2Al_2Si_4O_{22}$ H_2O], and manganocolumbite. Pyrophanite ($MnTiO_3$) and schorl are accessory phases. Beryl also occurs as euhedral crystals (up to 4 cm across) at the contact with the monzogranite where aplite is locally absent, indicating that it was

one of the earliest minerals to have crystallized from the felsic liquid. Spodumene occurs as laths (up to 20 cm wide and 2 m long) throughout the pegmatite. Some crystals of spodumene are intergrown with quartz, a texture which is common in pegmatites elsewhere (Černý and Ferguson, 1972), and has been interpreted to have formed through the breakdown of petalite to spodumene + quartz. The central zone of this pegmatite consists mainly of quartz, spodumene and lepidolite. This lepidolite, which is euhedral and occurs as books (2-3 cm across), is interpreted to be of magmatic origin. In contrast, small flakes of lepidolite which partially replaced spodumene along fractures, are considered to have formed at subsolidus conditions.

The spodumene pegmatite is massive, composed of anhedral quartz, euhedral spodumene and subhedral albite. Spodumene occurs as randomly distributed prismatic crystals (up to 1-cm wide and 3-cm long) oriented at an oblique angle (45-60 degrees) to the pegmatite contact. As is the case in spodumene-beryl pegmatite, some spodumene crystals are intergrown with quartz, and are interpreted to have replaced petalite. Discrete, coarser grains of quartz occur in the inner parts of the pegmatite. Albite is typically subhedral and compositionally homogeneous, with the exception of some grains along the contacts with biotite schist, which have rims of oligoclase or andesine. The transition from the sodic core to the calcic rim varies from sharp to diffused, suggesting that the rim is a subsolidus overgrowth. Manganocolumbite and pollucite are minor phases, and beryl is a trace mineral. The spodumene pegmatite induced biotitization of the surrounding mafic rock and local development of holmquistite $[Li_2(Mg,Fe^{+2})(Al,Fe^{+3})_2(Si_8O_{22})(OH)_2]$. The effect of this metasomatism on the pegmatite was the formation of small anhedral grains of apatite at the contact with the country rocks, and calcic overgrowths on some crystals of albite (above).

FLUID INCLUSIONS

Fluid inclusions were analyzed in beryl and adjacent quartz from beryl and spodumene-beryl pegmatites, and in spodumene and discrete quartz crystals from spodumene pegmatite; quartz intergrown with spodumene lacks fluid inclusions large

enough to be examined petrographically or microthermometrically. Spodumene in spodumene-beryl pegmatite is cloudy and also not suitable for fluid inclusion study. Fortunately, spodumene from spodumene pegmatites, which is finer-grained (averaging 0.5 x 2 cm in section), contains many large fluid inclusions. Because all petalite has been converted to spodumene, and it was not possible to distinguish petrographically between inclusions from primary spodumene and those in spodumene after petalite, the microthermometric data from these two generations of spodumene were treated together.

Petrography

Four main types of fluid inclusion have been recognized: 1) aqueous liquid-vapor (L-V); 2) aqueous liquid-vapor-solid (L-V-S); 3) aqueous liquid-carbonic (L-V, L-L-V and L-L-V-S); and 4) carbonic (L and L-V). Type 1 inclusions occur in all minerals examined and form the bulk of the fluid inclusion population. In beryl from both beryl and spodumene-beryl pegmatites, these inclusions are subdivided into type 1a, which homogenize to liquid (~70% of the type 1 population) and type 1b, which homogenize to vapor. Type 1a inclusions, which are mostly liquid-rich (liquid/vapor values between 4 and 2), range in diameter from < 5 to 12 μm. Approximately a quarter of these inclusions are isolated or occur in clusters, typically have negative crystal shapes (Fig. 2A), are > 5 μm in diameter, and are thus interpreted to be of primary origin (cf. Roedder, 1984). The majority of type 1a inclusions are small (< 5 μm in diameter) and occur along healed fracture planes, indicating that they are secondary, i.e. that they formed after crystallization of the host beryl. Type 1b inclusions normally do not coexist with type 1a inclusions and differ from primary type 1a inclusions in that they are generally larger (15-20 μm in diameter, although some are < 12 μm in diameter) and are mostly vapor-rich (from 55 to 75 vol% of the inclusion, based on visual estimates). Type 1b inclusions are generally aligned along healed fracture planes and are therefore mainly secondary. However, a small proportion are isolated, and could therefore be primary.

In contrast to type 1 inclusions in beryl, those in quartz from the three types of pegmatite, and in spodumene (from spodumene pegmatite), all homogenize to liquid (Type 1a). These inclusions in quartz have petrographic characteristics similar to type

Fig. 2. Examples of types of fluid ± solid inclusions in beryl and spodumene from beryl, spodumene and spodumene-beryl pegmatites. A) An isolated type 1a inclusion in beryl (beryl pegmatite) consisting of liquid (L) and vapor (V). B) A tubular type 2 (solid-bearing) inclusion oriented parallel to the c-axis of the host spodumene (spodumene pegmatite) C) A multi-solid-bearing type 2 inclusion in beryl (spodumene-beryl pegmatite) containing three larger solids (1-3) and two smaller ones (between the vapor (V) and solid 2, and between solids 2 and 3), a liquid (L) and vapor (V). Solid number 2 is interpreted, on the basis of its Raman spectrum (see Fig. 13) to be zabuyelite (Li_2CO_3); the other solids have not been identified. The halo of tiny fluid inclusions surrounding the inclusion is thought to reflect natural decrepitation.

Figure 2

1a inclusions in beryl, whereas in spodumene they occur mostly as negative rectangular crystals (up to 30 μm long; but most are ± 10 μm long). These inclusions are typically oriented parallel to the c-axis of the spodumene. Secondary inclusions in spodumene are very small (< 3 μm) and occur as trails at various angles to the c-axis of the crystal.

Type 2 (L-V-S) inclusions are hosted almost exclusively by beryl in beryl and spodumene-beryl pegmatites, and spodumene in spodumene pegmatites. Halite was not observed in type 2 inclusions in either beryl or spodumene, and only two halite-bearing type 2 inclusions, both of secondary origin, were observed in quartz from a spodumene-beryl pegmatite. In beryl, type 2 inclusions are considerably less common than type 1 inclusions (1:10), whereas in spodumene they are only slightly less abundant than type 1 inclusions. Type 2 inclusions in beryl and spodumene have euhedral (the norm in spodumene) to subhedral negative crystal shapes (Fig. 2B), and are isolated or coexist with primary type 1a inclusions. These relationships suggest that the inclusions are primary. A small number of type 2 inclusions, particularly in beryl, are accompanied by tails of tiny fluid inclusions or are surrounded by them (Fig. 2C). These features indicate that the inclusions are necked down or had decrepitated naturally, respectively. No secondary type 2 inclusions have been observed in beryl or spodumene.

Type 2 inclusions in beryl and spodumene contain from one to five solids. Most commonly they contain one or two solids in beryl and one solid in spodumene. Inclusions containing one or two solids comprise over 80 vol.% liquid plus vapor, while those with more than two solids typically comprise about 70 vol.% liquid plus vapor and rarely as little as 40 vol.% of these phases. In those cases where the inclusions are dominated by solids there is evidence of natural decrepitation (Fig. 2C), suggesting that fluid originally trapped in the inclusions has been lost. The most commonly occurring solid has a rectangular shape (up to 15 μm long), is white and anisotropic (e.g., Fig. 2C). It is present in over 80% of type 2 inclusions in beryl, and in about 25% of these inclusions in spodumene. The next most common mineral has a rhombic shape (~3 μm across) and is weakly to moderately birefringent. This mineral is slightly more common in spodumene than in beryl. Irregularly shaped solids are less abundant and generally small (typically 2 μm across), but in some cases, occur in pairs. Like the above solids,

these solids are white and anisotropic. They are more common in beryl than in spodumene. The least common solid, found only in three type 2 inclusions, is reddish brown and roughly equidimensional. This solid, probably hematite, was observed only in beryl and invariably was accompanied by one or two other minerals among those described above.

Type 3 carbonic inclusions are present mainly in quartz, rarely in beryl, and are absent from spodumene. At room temperature, these inclusions consist of two phases (liquid H_2O and liquid or vapor CO_2) or three phases (liquid H_2O, liquid CO_2 and vapor CO_2). Phase ratios are quite variable, even among adjacent inclusions, suggesting that the H_2O and CO_2 were immiscible at the time of entrapment. A small number of type 3 inclusions in quartz from the spodumene-beryl pegmatite contain the white, rectangular solid (< 2 μm) described above. Most type 3 inclusions have negative to subhedral crystal forms and are isolated, suggesting that they are primary. At room temperature, the CO_2 phase(s) of the inclusion generally comprises a volume fraction of between 0.15 and 0.2. These inclusions also coexist with primary type 1a inclusions; both types of inclusion have similar abundances in quartz from beryl and spodumene-beryl pegmatites, but type 3 inclusions are less common than type 1 inclusions in quartz from spodumene pegmatite. A small proportion of solid-free, type 3 inclusions occur along fracture planes, indicating that they are of secondary origin.

Type 4 inclusions are present only in quartz from beryl and spodumene-beryl pegmatites. The majority of these inclusions are irregularly shaped and occur along healed fracture planes, indicating their secondary origin. At room temperature (23°C), the inclusions consist of a liquid or liquid and vapor. The liquid inclusions nucleate a vapor bubble upon cooling.

Analytical methods

Microthermometric measurements of phase changes in fluid inclusions were conducted on a Fluid Inc. USGS-adapted gas-flow heating and freezing stage (Werre et al., 1979). This instrument was calibrated with synthetic fluid inclusions for temperatures between -56.6°C and 374.1°C, and with a quartz disk for higher temperature (the α-β

transition is at 573°C). The accuracy was ± 0.2 and ± 3°C for the low and high temperature measurements, respectively.

The chemical compositions of precipitates or residues from decrepitated inclusions and of solids in opened inclusions were determined with an energy dispersive X-ray spectrometer attached to a JEOL 840 scanning electron microscope. Cleaned, doubly-polished wafers were heated in the fluid inclusion stage until the inclusions decrepitated (at temperatures less than 450°C). Residues on the wafer were analyzed in raster mode using 25-30 second counting times. Mineral chips opened for analyses of the included solids were frozen with liquid nitrogen, broken, and glued onto silica glass slides. The slides were coated with carbon on a rotating stage to ensure uniform coating. Solids in unopened fluid inclusions were identified with a Bruker IFS-88 FT Raman spectrometer equipped with microscope. Typically, 200 scans were co-added at a resolution of 4 cm^{-1}, using a Nd-YAG laser (1064 nm) at 300 mW. Most of these analyses were carried out at McGill University. Additional Raman analyses were performed by Dr. Iain Samson of the University of Windsor, Windsor (Ontario); details of the analytical method can be found in Samson and Sinclair (1992).

MICROTHERMOMETRY

Results of microthermometric measurements of fluid inclusions are summarized in Table 1 and are presented graphically in Figures 3-8. Initial, or quasi-eutectic, ice-melting temperatures (Te) were difficult to observe in many inclusions, and as a result, only a small number of measurements were made. Fluid salinities (in weight percent NaCl equivalent) were calculated from final ice melting temperatures (Tm) using the equation of Potter et al. (1978) for type 1 inclusions and non-halite-bearing type 2 inclusions, and from final melting temperatures of clathrate (Tm clath) using the equation of Darling (1991) for type 3 inclusions.

Type 1 inclusions (L-V)

Initial ice-melting temperatures (Te) for primary type 1a inclusions in beryl from

Table 1. Summary of microthermometric measurements of fluid inclusions in beryl, quartz and spodumene (Spd) from the various types of pegmatite. The values are the mean, the standard deviation, and the number of analyses.

Host Mineral	Type	Te (°C)	Tm (°C)	Th (°C)	Tm CO_2(°C)	Tds (L-V-S) or Tm Clath (°C)	Th CO_2 (°C)	Wt.% NaCl eq.	XCO_2
				Beryl pegmatite					
Beryl	L-V 1a	- 35.5 (10) [6]	- 7.7 (6.6) [25]	343 (86) [27]				10.4 (6.8) [25]	
	L-V 1b	- 50.3 (5) [17]	- 22.7 (5) [24]	550 (63) [16]				25 (2.4) [24]	
	L-V Sec.	- 28 (15) [3]	- 17.7 (7) [10]	455 (119) [9]				20.3 (6.4) [10]	
	L-V-S	- 15.2 (0.8) [4]	- 5.08 (0.85) [6]	284 (41) [6]		> 500		8.15 (1.1) [6]	
Quartz	L-V 1a	- 39.7 (4) [3]	- 6 (8) [22]	242 (96) [20]				7.6 (9) [22]	
	L-V Sec.	- 47.4 (4) [5]	- 14.9 (4.9) [10]	188 (109) [13]				18.4 (4) [10]	
	L-L-V CO_2	- 33.3 (5.4) [8]	- 14 (6) [18]	260 (52) [18]	57.3 (1.21) [18] 57 (0.39) [45]	5.67 (1.87) [18]	20 (7.41) [18] 20 (7.4) [45]	7.81 (2.84) [18]	0.13 (0.09) [16]
				Spodumene-beryl pegmatite					
Beryl	L-V 1a	- 294 (8.6) [7]	- 7.23 960 [18]	297 (69) [18]				10.1 (6.1) [18]	
	L-V 1b	-32	- 13.2 (7) [10]	446 (54) [10]				15.5 (6.6) [10]	
	L-V Sec.	- 28.6 (1.8) [9]	- 16.5 (5.4) [14]	452 (100) [14]				19.6 (5.45) [14]	
	L-V-S	n.a	- 4.45 (0.5) [8]	281 (39) [8]		> 500		7.29 (0.71) [8]	
Quartz	L-V 1a	-33	- 5.57 (2.7) [16]	218 (39) [16]				8.61 (3.47) [16]	
	L-V Sec.	- 52 (6.65) [3]	- 23.5 (0.16) [5]	284 (68) [5]				25.1 (0.1) [5]	
	L-L-V CO_2	- 34 (5) [5]	- 11.8 (4) [18]	286 (39) [17]	56.9 (0.17) [18] 56.8 (0.16) [6]	5.24 (1.27) [18]	21 (6.14) [18] 20.1 (2.51) [6]	8.58 (1.94) [18]	0.14 (.08) [18]
				Spodumene pegmatite					
Spd	L-V 1a	- 26.4 (10) [12]	- 3.7 (3) [34]	219 (39) [39]				5.9 (3.89) [34]	
	L-V 1a*	- 65.2 (2.86) [4]	- 35 (1.4) [4]	212 (37) [4]				32.8 (1.06) [4]	
	L-V-S	- 27.7 (8.2) [12]	- 3.16 (1.5) [19]	242 (50) [23]				5.32 (2.24) [19]	
Quartz	L-V	- 37.8 (14.5) [27	- 7.8 (9.1) [38]	250 (75) [41]				10.1 (8.05) [38]	
	L-L-V	- 35.7 (2.22) [8]	- 12.3 (2.9) [11]	260 (29) [11]	57.9 (1.67) [11]	6.26 (0.78) [11]	16 (6.67) [11]	7 (1.31 0 [11]	0.08 (0.03) [10]

* These four analyses are separated from the others because of their very low eutectic temperature.

beryl and spodumene-beryl pegmatites vary from -40 to -10°C, with the majority being between -40 and -35°C, and between -35 and -30°C, respectively (Fig. 3). By contrast, the Te values of these inclusions from spodumene pegmatite have a bimodal distribution with peaks at -70 to -60°C and -25 to -20°C in spodumene, and at -70 to -60°C and -40 to -35°C in quartz. Primary type 1a inclusions in quartz from beryl and spodumene-beryl pegmatites also show a bimodal distribution of Te, from -40 to -30°C and from -20 to -15°C, and from -40 to -30 and from -25 to -20°C, respectively. Type 1b inclusions in beryl from beryl pegmatite show a wide range of Te values from -60 to -35°C, with a peak between -50 and -45°C. The Te values of secondary inclusions are scattered from as low as -60°C in quartz from spodumene-beryl pegmatite to as high as -5°C in beryl from beryl pegmatite; secondary inclusions hosted by beryl from spodumene-beryl pegmatite have a Te mode at -30 to -25°C. These data indicate that many of the inclusions, i.e. those which have a Te value lower than -20.8°C (Te of H_2O-NaCl; Crawford, 1981), contain, in addition to NaCl, salts such as $FeCl_2$, $CaCl_2$ and perhaps LiCl, which depress the eutectic temperature of the system NaCl-H_2O to -55°C, -52°C and -78 to -75°C (Roedder, 1984), respectively. A number of residues from decrepitated fluid inclusions contain significant Ca and Fe, in addition to Na and Cl, confirming the interpretation that salts such as $CaCl_2$ and $FeCl_2$ were partly or wholly responsible for the low Te of some of these inclusions. It is also likely that LiCl contributed to the low Te (see below). However, this cannot be confirmed as Li is undetectable with the EDS.

The majority of final ice-melting temperature measurements (Tm) of primary type 1a inclusions are between -10 and -0.3°C for all inclusions from the three types of pegmatite, corresponding to salinities between 10 and 2.5 wt% NaCl eq. (Fig. 4); the few primary inclusions in spodumene and quartz from spodumene pegmatite, which have very low Te, have Tm values from -35 to -40°C, corresponding to salinities of 30 wt.% NaCl eq. If the compositions of these fluid inclusions are modelled in the system NaCl-$CaCl_2$-H_2O, the minimum weight fractions $CaCl_2$/($CaCl_2$+NaCl) are 0.8 and 0.9, respectively (Oakes et al., 1992). Type 1b inclusions in beryl from beryl and spodumene-beryl pegmatites show a modal Tm value between -30 and -20°C, corresponding to salinities between 27.5 and 22.5 wt% NaCl eq. If the lower Tm value reflects the presence of

Fig. 3. Histograms of the initial melting temperatures of ice (Te) in the different types of fluid inclusion in beryl, spodumene-beryl and spodumene pegmatite. In this and subsequent diagrams (to Fig. 5), the various types of fluid inclusions are distinguished as follows: black, type 1a; vertical hatching, type 1b; diagonal hatching, type 2; horizontal hatching, type 3 (in quartz only); and blank, secondary (types 1a and b).

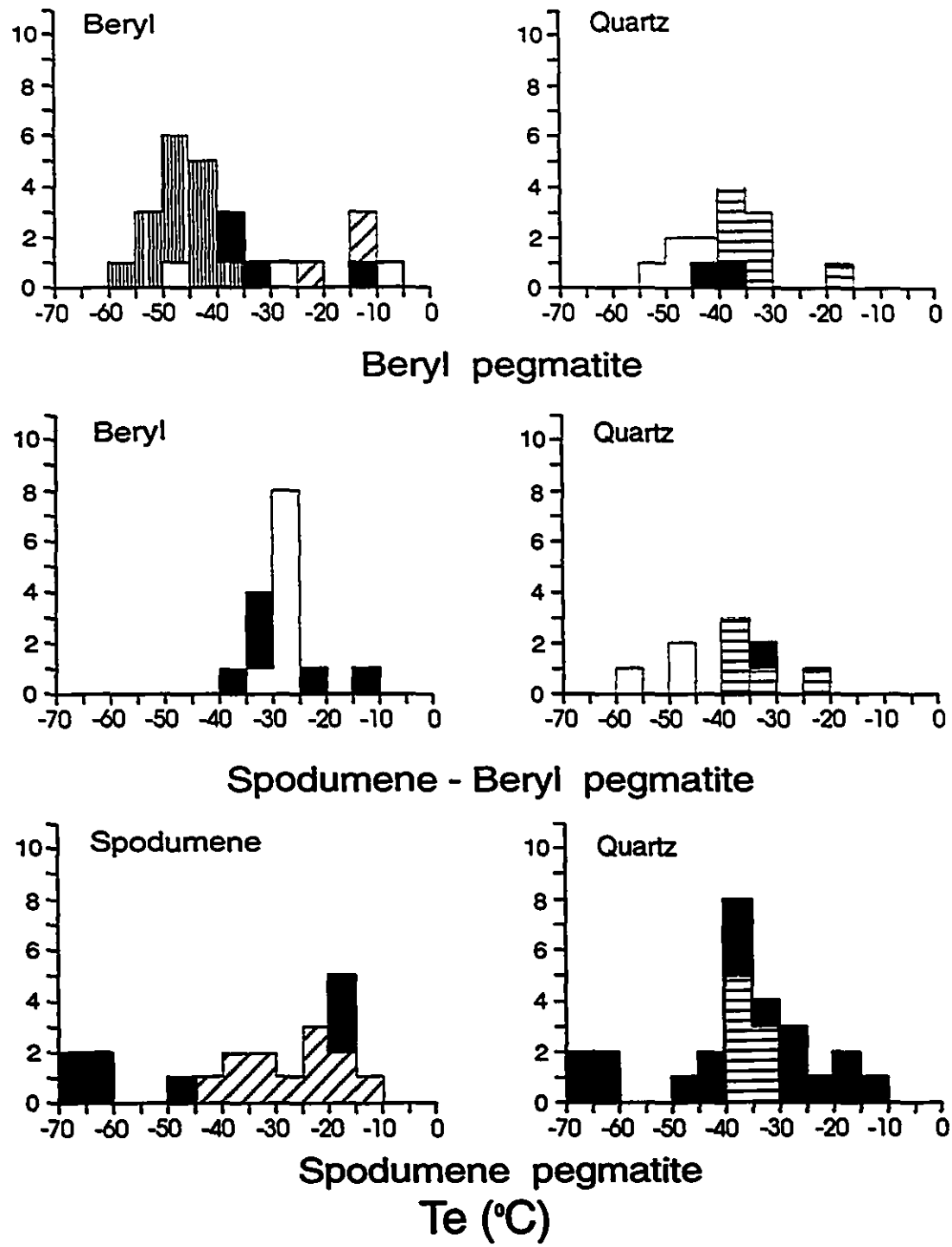
Beryl
Quartz
Beryl pegmatite
Beryl
Quartz
Spodumene - Beryl pegmatite
Spodumene
Quartz
Spodumene pegmatite
Te (°C)

Figure 3

Fig. 4. Histograms showing temperatures of final melting of ice (Tm) in various types of fluid inclusions and the corresponding salinity. See the caption of Fig. 3 to identify the types of inclusion.

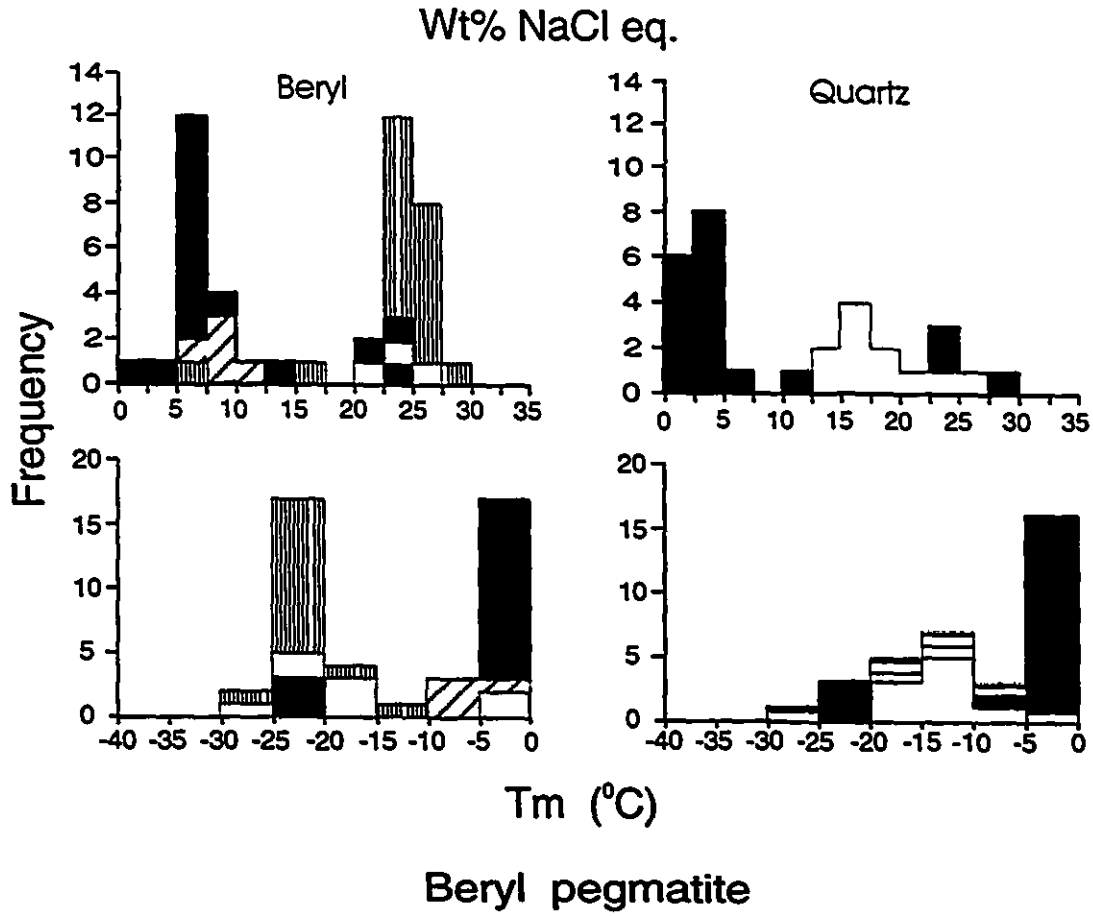

Beryl pegmatite

Figure 4a

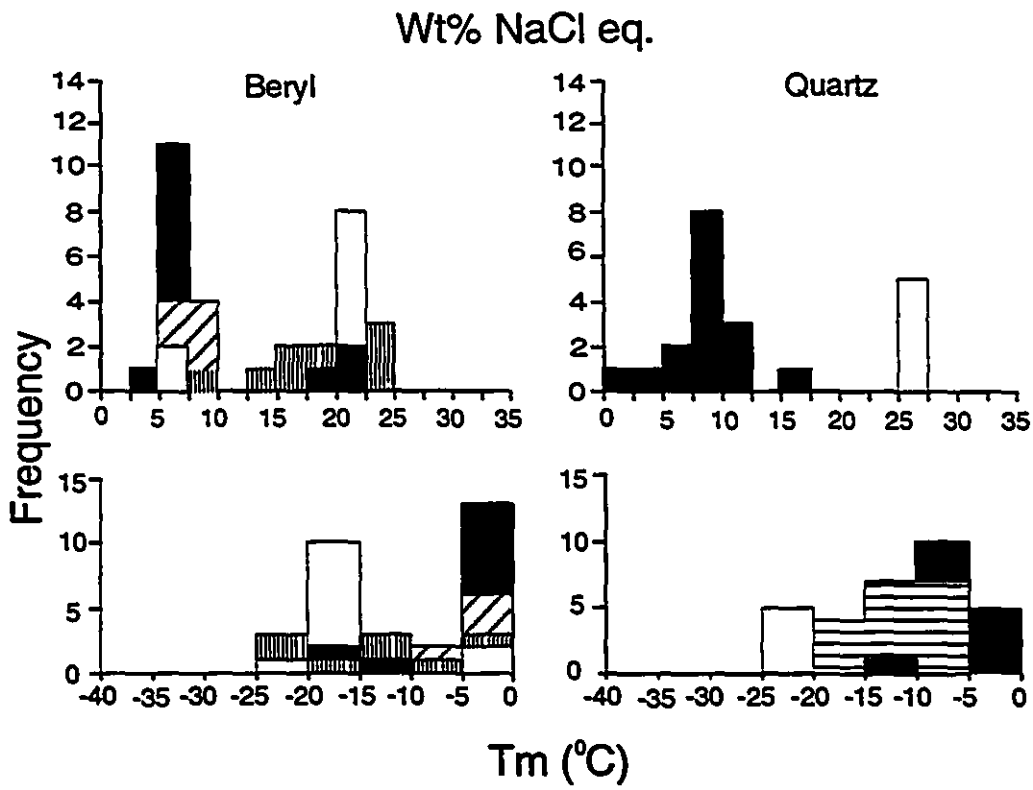

Spodumene - Beryl pegmatite

Figure 4b

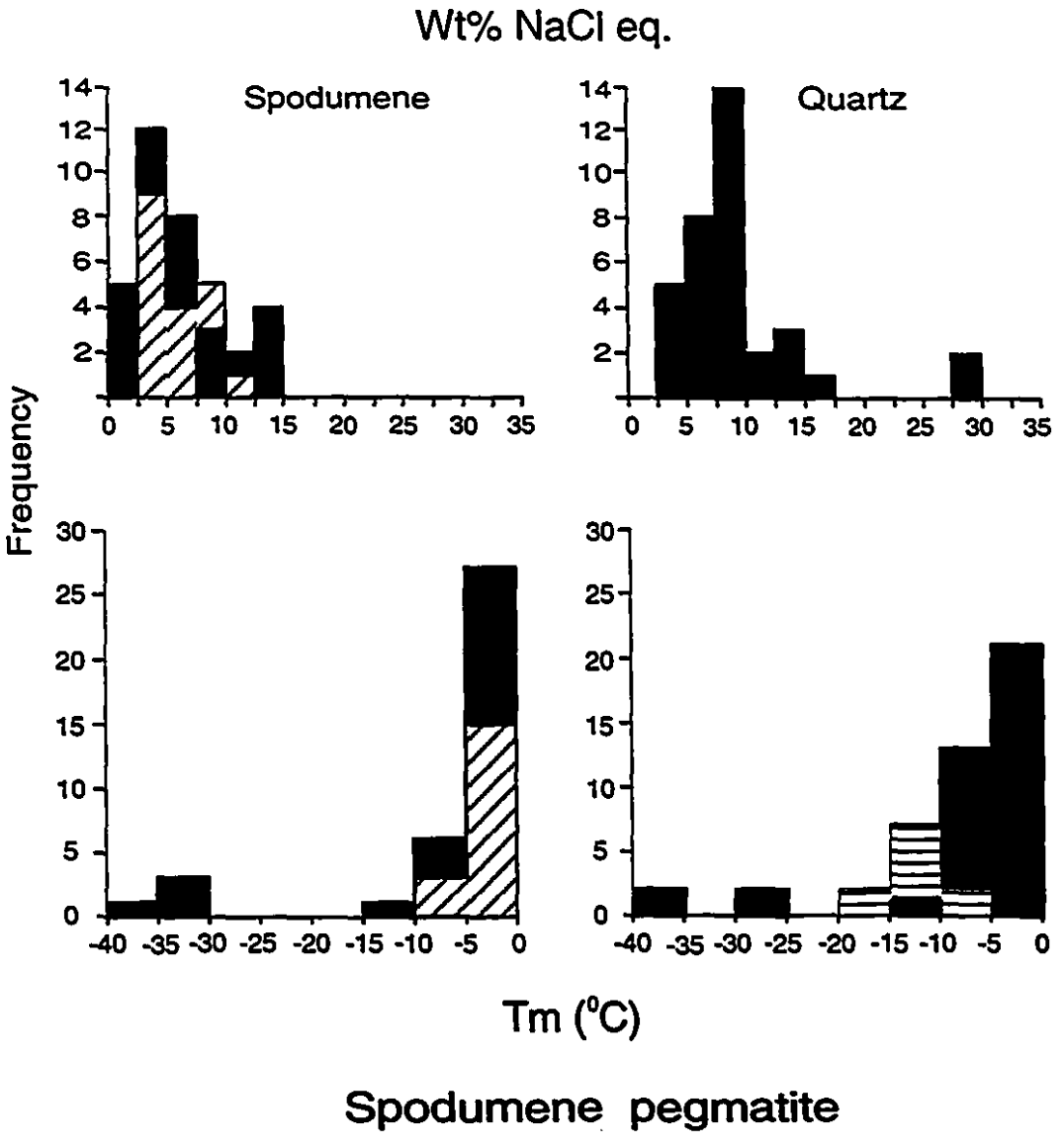
Wt% NaCl eq.
Spodumene
Quartz
Frequency
Tm (°C)
Spodumene pegmatite

Figure 4c

$CaCl_2$, the corresponding minimum weight fraction of $CaCl_2/(CaCl_2+NaCl)$ is 0.7. Secondary type 1 inclusions in beryl from beryl pegmatite have highly variable Tm values and therefore salinities, whereas those from spodumene-beryl pegmatite display a Tm mode between -20 and -15°C, and salinities from 22.5 to 20 wt% NaCl eq. Secondary type 1 inclusions in quartz from beryl pegmatite generally have Tm values in the range from -20 to -10°C, corresponding to salinities between 20 and 12.5 wt% NaCl eq. In spodumene-beryl pegmatite, these inclusions have a narrower range of Tm from -25 to -20 °C, corresponding to salinities of 27.5 to 25 wt% NaCl eq.

Although type 1a inclusions show a wide range of homogenization temperature from 125 to > 500°C in beryl, and from 150 to < 400°C in spodumene and quartz (Fig. 5), the majority of type 1a inclusions in the three types of pegmatite have Th modes between 200 and 350°C. By contrast, type 1b inclusions in beryl from both beryl and spodumene-beryl pegmatites homogenize at higher temperature, from 300 to > 550°C, and those from beryl pegmatite have a modal Th value between 500 and > 550°C. The secondary inclusions in beryl show a wide range of Th values from 200 to 550°C, and like type 1b inclusions, a large population homogenizes at high temperature, > 450°C. The majority of secondary inclusions in quartz homogenize between < 150 and 400°C, with a mode from 150 to 175°C in beryl pegmatite and from 300 to 350°C in spodumene-beryl pegmatite.

Type 2 inclusions (L-V-S)

Initial ice-melting temperatures of type 2 inclusions range from -25 to -10 °C in beryl from beryl pegmatite (Fig. 3), indicating that the fluid was dominated by NaCl ± KCl. In contrast, Te for inclusions in spodumene from spodumene pegmatite varies from -45 to -10°C, suggesting, as in the case for type 1 inclusions, that the fluids contain appreciable concentrations of $CaCl_2$ ± $FeCl_2$ or LiCl. Final ice-melting temperatures in the three types of pegmatite range from -10 to -3°C, corresponding to salinities between 5 and 12.5 wt% NaCl eq (Fig. 4). Significantly, these values are similar to those of type 1a inclusions.

The liquid and vapor in type 2 inclusions homogenize to liquid at a modal

Fig. 5. Histograms showing the temperature of homogenization (Th) of the various types of fluid inclusion. See the caption of Fig. 3 to identify the types of inclusion.

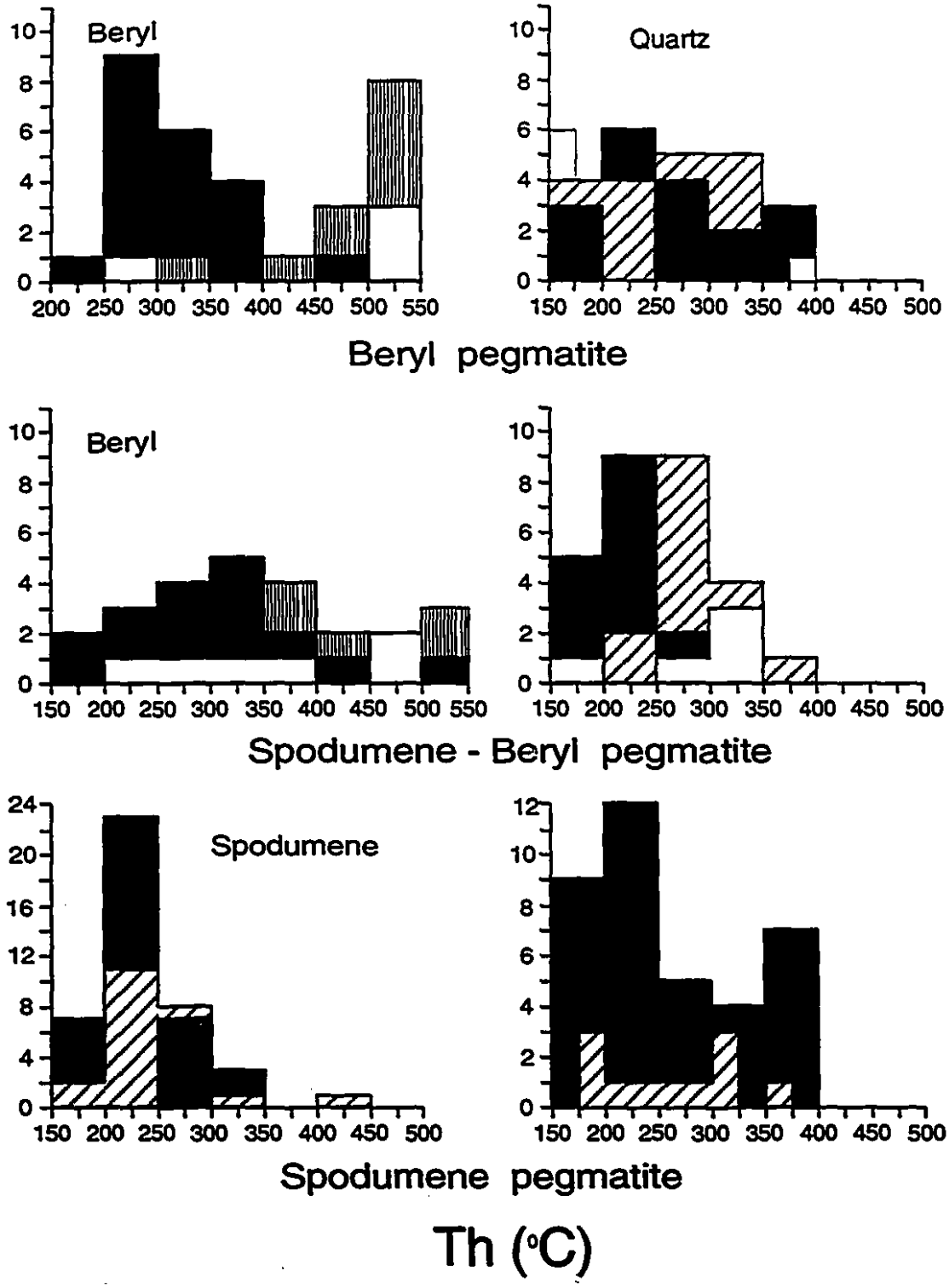
Beryl
Quartz
Beryl pegmatite
Beryl
Spodumene - Beryl pegmatite
Spodumene
Spodumene pegmatite
Th (°C)

Figure 5

temperature between 250 and 300°C in beryl pegmatite, between 250 and 300°C in spodumene-beryl pegmatite, and between 200 and 300°C in spodumene pegmatite (Fig. 5). The only solid to dissolve was the rhombic mineral in inclusions hosted by spodumene, which did so at a mean temperature of 456 ± 74°C (Table 1). However, this mineral dissolved only in a small proportion of the inclusions. Its dissolution also showed no correlation with the temperature of liquid-vapor homogenization. In beryl, there was no change in the solids, including the rhombic phase, to the maximum temperature of heating. Many type 2 inclusions in both spodumene and beryl decrepitated, commonly at temperatures below 400°C.

Type 3 inclusions (aqueous carbonic)

As stated earlier, type 3 inclusions are common in quartz from all types of pegmatite, rarely present in beryl and never in spodumene. These inclusions generally show negative crystal forms and coexist with type 1 inclusions. The XCO_2, calculated using the method of Bodnar (1983), ranges from 0.02 to 0.3 (the majority of inclusions have XCO_2 between 0.06 and 0.1; Table 1). The initial melting temperature (Te) of the aqueous phase ranges from -40 to -15°C, but is mainly between -40 and -35°C (Fig. 3). Final ice-melting temperatures range from -26 to -2°C, from -20 to -8°C and from -16 to -6°C in quartz from beryl, spodumene-beryl and spodumene pegmatite, respectively (Fig. 5). The mode of the final melting temperature of clathrate and the corresponding salinity of the fluid in type 3 inclusions are as follows: beryl pegmatite (6-7°C, 5-7.5 wt% NaCl eq.); spodumene-beryl pegmatite (6-7°C, 5-12.5 wt% NaCl eq.); spodumene pegmatite (5-7°C, 5-7.5 wt% NaCl eq.) (Fig. 6).

Final melting temperatures of CO_2 solid range from -57.6 to -56.6°C, with a well-defined peak between -57.1 and -56.6°C, in quartz from both beryl and spodumene-beryl pegmatites, and from -61.7 to -56.6°C, but mostly between -58.1 and -56.6°C, in quartz from spodumene pegmatite (Fig. 7). These temperatures indicate that the carbonic fluid is dominated by CO_2, which has a melting point of -56.6°C (Angus et al., 1976). However, the low $TmCO_2$ values of some inclusions in spodumene pegmatite indicate that

Fig. 6. Histograms of the final melting temperatures of clathrate in aqueous carbonic L-L-V, L-L and L-V (type 3) inclusions hosted by quartz and the corresponding salinities. The host pegmatites are depicted as follows: black, beryl pegmatite; vertical hatching, spodumene-beryl pegmatite; blank, spodumene pegmatite.

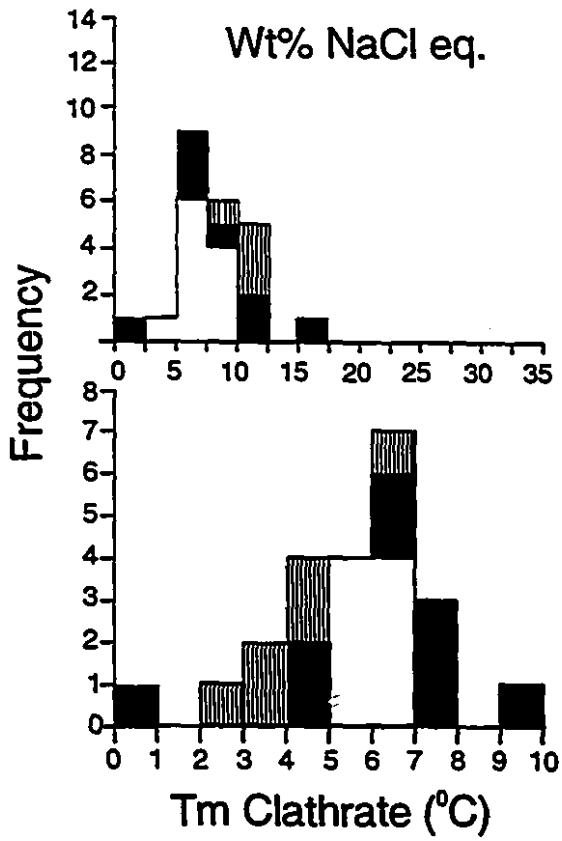

Figure 6

Fig. 7. Histograms showing the initial melting temperature of the frozen carbonic solid (Tm CO_2) of aqueous carbonic (type 3) and carbonic (type 4) inclusions in quartz from the three types of pegmatite. Type 3 inclusions are shown in white, and type 4 inclusions in black. The data indicate that the majority of inclusions consist mainly of CO_2, i.e., the temperatures are close to that of the triple point of the system CO_2 (-56.6°C).

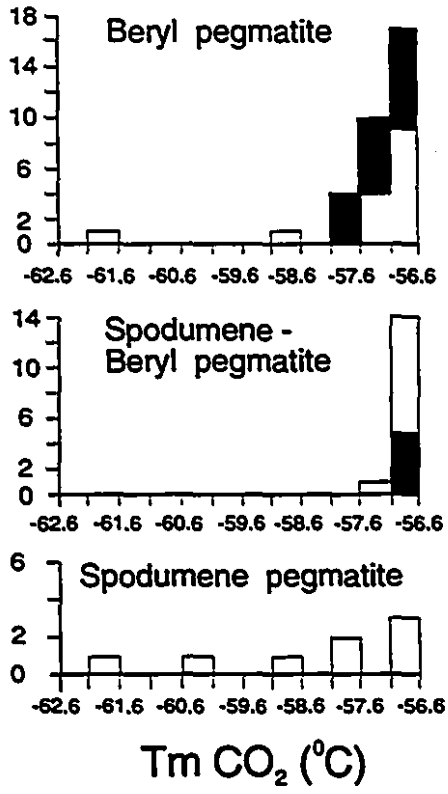
Beryl pegmatite
18
14
10
6
2
0
-62.6 -61.6 -60.6 -59.6 -58.6 -57.6 -56.6
Spodumene -
Beryl pegmatite
14
10
6
2
0
-62.6 -61.6 -60.6 -59.6 -58.6 -57.6 -56.6
Spodumene pegmatite
6
2
0
-62.6 -61.6 -60.6 -59.6 -58.6 -57.6 -56.6
Tm CO_2 (^{0}C)

Figure 7

they contain appreciable $CH_4 \pm N_2$. The maximum estimated value of XCH_4 eq. calculated following the method of Heyen et al. (1982) is 0.24.

The CO_2 liquid and vapor homogenize to either liquid, or vapor, or rarely, a critical fluid. Homogenization temperatures of the CO_2 phases vary widely from -1 to 31 °C (Fig. 8). Complete homogenization of these inclusions was to either the CO_2 phase or the H_2O phase and occurred at temperatures from 150 to 400°C (Fig. 5), with a modal temperature of 250-300°C for inclusions from spodumene-beryl pegmatite; the homogenization temperature distributions for beryl and spodumene pegmatites show no clearly defined peaks.

Type 4 inclusions (carbonic L-V)

The final melting temperature (Tm) of solid in type 4 inclusions ranges, in most cases, between -58.1 and -56.6°C, with a well-defined peak between -57.1 and -56.6°C (Fig. 7), indicating that the solid consists largely of CO_2. The homogenization temperatures, however, vary widely from -1 to 31.1°C in beryl pegmatite and from 15 to 27°C in spodumene-beryl pegmatite (Fig. 8).

Relationships between temperature of homogenization and salinity

Most primary type 1a inclusions in beryl from beryl and spodumene-beryl pegmatites and in spodumene from spodumene pegmatite, all type 2 inclusions, and all type 3 inclusions in quartz have salinities of < 12.5 wt% NaCl eq. and Th from 150 to 400°C (Fig. 9): the total Th of type 2 inclusions ranges from 325 to 575°C. A few type 1a, all type 1b and secondary inclusions in beryl from beryl and spodumene-beryl pegmatites have high salinity (20-25 wt% NaCl eq.), and homogenize at high temperature, generally greater than 400°C. Some type 2 inclusions in spodumene-beryl pegmatite homogenize at lower temperature. Type 1a inclusions in quartz from all types of pegmatite belong mainly to the low salinity-low temperature population; those from spodumene pegmatite appear to show a subtle positive correlation between salinity and Th.

Fig. 8. Histograms showing the homogenization temperature of the carbonic phases in type 3 inclusions and the total homogenization temperature of type 4 inclusions (inclusions homogenize to either liquid, vapor or a critical fluid). Type 3 inclusions are shown in white, and type 4 inclusions in black.

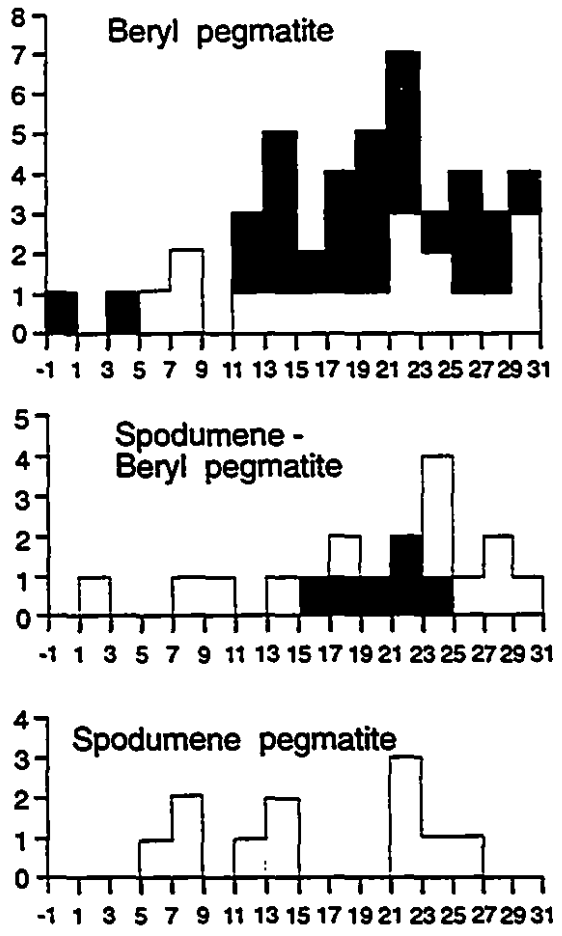
Beryl pegmatite
Spodumene -
Beryl pegmatite
Spodumene pegmatite
-1 1 3 5 7 9 11 13 15 17 19 21 23 25 27 29 31
Th CO_2 (^{0}C)

Figure 8

Fig. 9. Plots of homogenization temperature vs. salinity for fluid inclusion types 1-3. The symbols are: black, type 1a; cross, type 1b; partially filled square, type 2 (total homogenization temperature); diagonal hatching, type 2 (partial (L-V) homogenization temperature); cross hatching, type 3 (in quartz only); and blank, secondary.

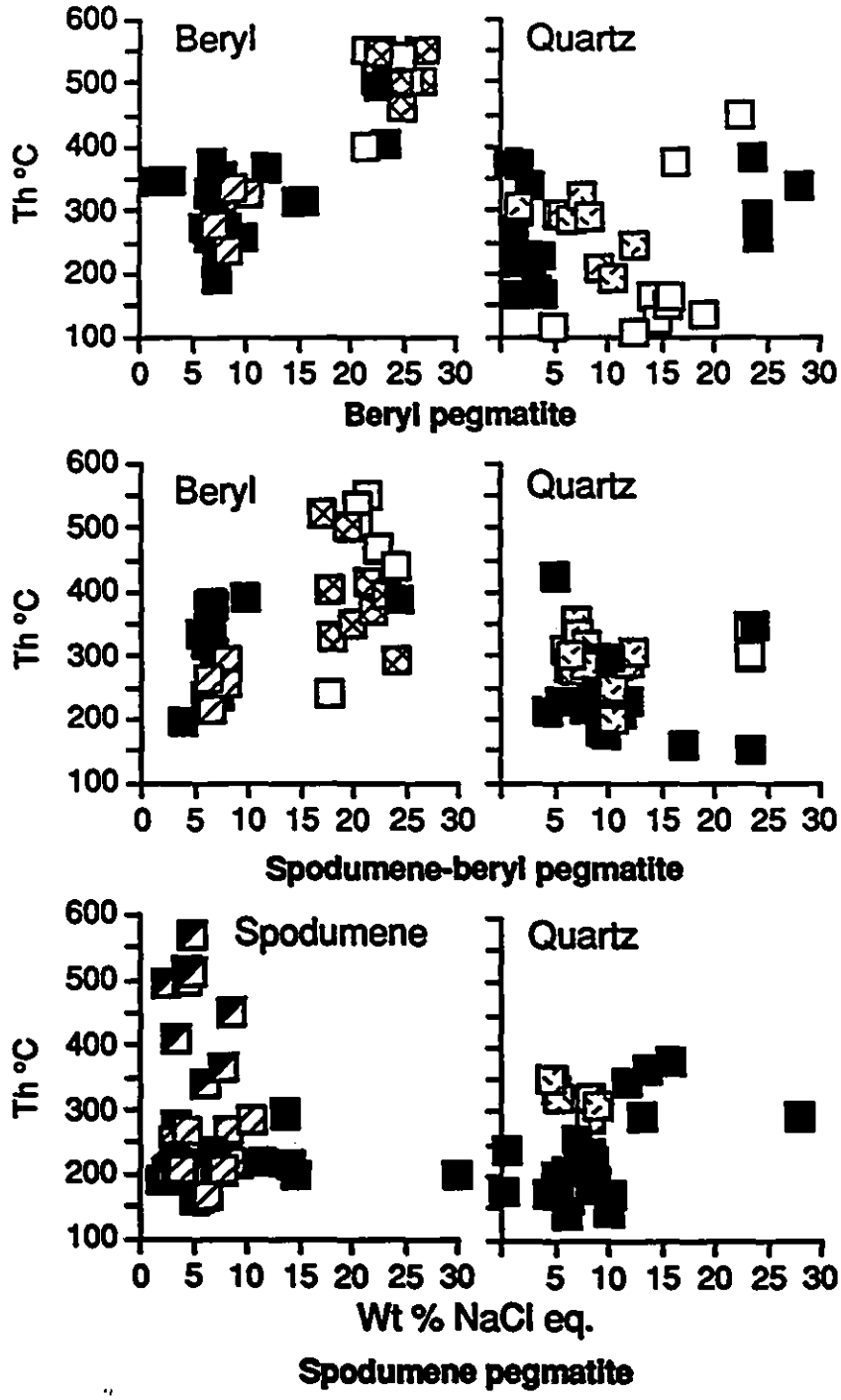
Beryl
Quartz
Th °C
600
500
400
300
200
100
0 5 10 15 20 25 30
5 10 15 20 25 30
Beryl pegmatite
Beryl
Quartz
Spodumene-beryl pegmatite
Spodumene
Quartz
Wt % NaCl eq.
Spodumene pegmatite

Figure 9

EDS-SEM ANALYSES AND RAMAN SPECTROSCOPY

Decrepitate residues

A total of 127 analyses were made of the compositions of the residues of decrepitated fluid inclusions in beryl from beryl and spodumene pegmatite, spodumene from spodumene pegmatite, and quartz from each of the pegmatite types. As discussed earlier, the analyses were carried out using an energy dispersive X-ray spectrometer attached to a scanning electron microscope and, because of the irregular shapes of the residues (Fig. 10) and the potential for compositional heterogeneity, they were conducted in raster mode. The results of these analyses, adjusted to reflect average salinities, are summarized in Table 2.

Cation contents: The data indicate that Na^+ is the dominant cation in all precipitates, that Ca^{2+} and Fe^{2+} are relatively abundant in some inclusions, that K^+ is generally a minor constituent and that measurable quantities of Mn^{2+} are present only in precipitates from spodumene pegmatite (Table 2). In the case of beryl and spodumene-beryl pegmatites, the precipitates form two populations characterized by very low (below the detection limit of the EDS) and moderately high Ca contents (up to 9.6 wt %), respectively. By contrast, most precipitates from spodumene pegmatite have moderately high Ca contents (up to 11.5 wt%). The content of Fe was above detection only in precipitates from beryl in beryl and spodumene-beryl pegmatites, and in these precipitates decreased in abundance from beryl (6.1 wt%) to beryl-spodumene pegmatite (2.1 wt%). Finally, significant K contents were measured only in beryl from beryl-spodumene pegmatite and spodumene from spodumene pegmatite. Precipitates hosted by quartz in all pegmatites only contain Na ± Ca at levels above detection. The occurrence of low- and high-Ca precipitate populations helps explain the wide range of initial ice melting temperatures. The high Ca content of some precipitates may also help explain the high final melting temperature of ice in type 1b inclusions, some primary type 1a inclusions in spodumene and quartz from spodumene pegmatite and many secondary inclusions in all three pegmatite types. However, the precipitate compositions also show that the low initial and high final melting temperatures are partly a reflection of high contents of Fe

Fig. 10. Back-scattered SEM images showing the types of precipitates formed from decrepitated fluid inclusions. A) Cryptocrystalline precipitates in and around an opened negative crystal in beryl. B) Globular precipitates in spodumene.

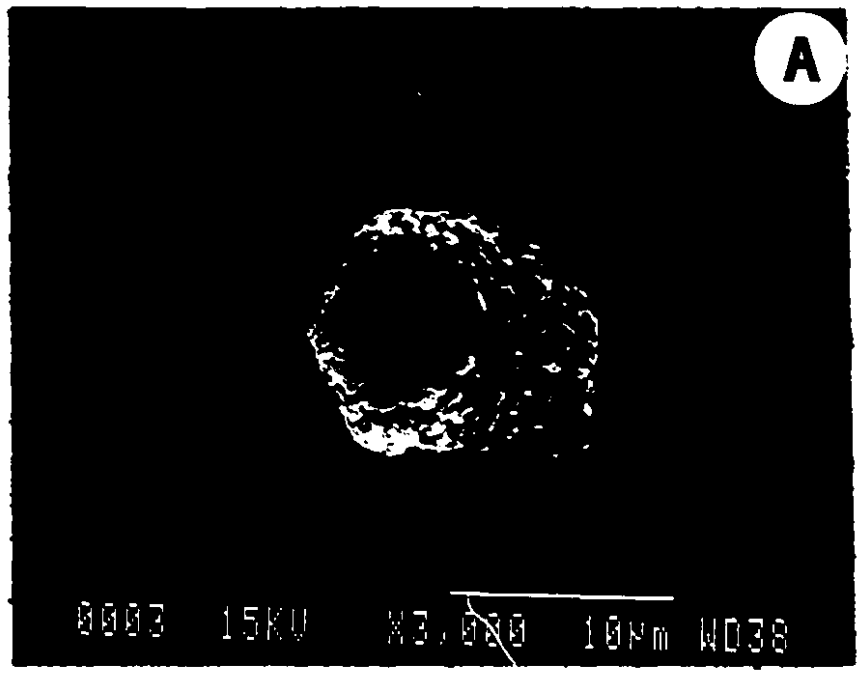

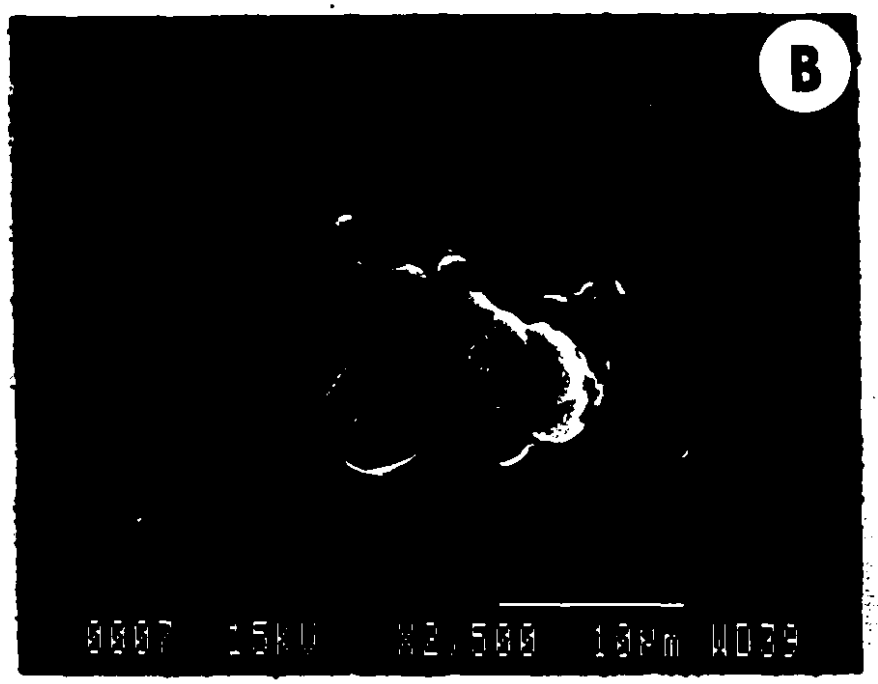

Figure 10

Table 2. Summary of composition of precipitates of decrepitated fluid inclusions

Host	Beryl pegmatite				Spodumene-beryl pegmatite			Spodumene pegmatite	
Mineral	Brl n=14 Low Ca	Brl n=10 High Ca	Qtz n=17 Low Ca	Qtz n=5 High Ca	Brl n=8 Low Ca	Brl n=7 High Ca	Qtz n=25	Spd n=25	Qtz n=26
Na (wt.%)	54	45	47	41	52	48	48.6	38	35
K	0.1	0.1			1.32	3.63		2.6	
Ca		9.6		7.12		7.1		8.5	11.5
Fe	4.9	7.9			0.75	2.91			
Mn								1.4	
S					0.78	0.9		0.4	1.6
Cl	36.4	34	44.4	51	39.2	33	48.2	44	50.3
Molality									
Na	1.141	4.106	0.432	3.242	1.205	3.609	1.637	0.818	1.403
K	0.004	0.025			0.018	0.160		0.034	
Ca		0.507		0.324		0.304		0.105	0.262
Fe	0.042	0.293				0.072			
Mn								0.006	
S					0.012	0.047		0.010	0.049
Cl	0.499	2.338	0.278	2.613	0.593	1.630	1.059	0.764	1.354
HCO_3^-	0.728	3.508	0.130	1.272	0.618	2.845	0.577	0.300	0.525

in the fluids.

Anion contents: The only two elements measured that form anionic components are Cl and S, and in most inclusions Cl was the only one of these elements detected. Sulfur, where present, was generally in concentrations below 1 wt% in the precipitates (Table 2). Fluorine, which occurs in significant concentrations in some minerals in the pegmatites, notably muscovite, was not detected. In the case of Ca-bearing precipitates, this is not surprising, because the presence of even relatively low concentrations of Ca is sufficient to cause precipitation of fluorite, thereby buffering aF to extremely low levels (Holland and Malinin, 1979). Although, Cl and S were the only anionic elements detected, the precipitate compositions reflect a consistent excess positive charge, suggesting that an important anionic component was not analysed. The most likely candidate for this additional anion is HCO_3^- .

Fluid inclusion solids

The solids in type 2 inclusions were identified with the assistance of EDS-SEM analyses and, in a few cases, Raman spectroscopic analyses. The most commonly encountered solid in opened inclusions is calcite. Significantly its composition varies from near end-member calcite (hereafter referred to as calcite) and magnesian calcite in beryl pegmatite to manganoan calcite in spodumene pegmatite (Table 3). Commonly its habit is rhombohedral, which might identify it as the rhombic mineral which dissolved on heating in some inclusions. However, calcite displays retrograde solubility over a very wide range of conditions and fluid compositions (Fein and Walther, 1987, 1989), which suggests that the soluble rhombic mineral is not calcite. This is also supported by the observation that the rhombic phase which dissolved was only observed to do so in spodumene and not in all inclusions hosted by this mineral, i.e. there is more than one rhombic solid.

The second most widely encountered solid is prismatic and apparently has a trigonal cross section (Fig. 11). It occurs mainly alone and, less commonly, is accompanied by one or more solids, of which the most frequently occurring is calcite. EDS analyses of this solid yielded a spectrum with O, Al and Si peaks (Fig. 11). The Al

Table 3. Mineralogy of solids inside opened fluid inclusions in beryl (Brl), spodumene (Spd) and quartz (Qtz) from various types of pegmatite

Pegmatite		Beryl	Spd-brl		Spd	
Mineral	Formula	Brl	Brl	Spd	Spd	Qtz*
Carbonates						
Calcite	$CaCO_3$	C	VR	VR	VR	
Magnesian calcite		C		VR		
Manganoan calcite			C	R	C	R
Zabuyelite ?	Li_2CO_3			VR	VR	VR
Silicates						
Quartz	SiO_2	R	R	R	R	
Albite	$NaAlSi_3O_8$	VR		VR	R	
Pollucite	$CsAlSi_2O_6 H_2O$			C	R	R
Unidentified						
Al or Al+Si		C	VR	VR	VR	C
n/a	LiCl		VR			
Spodumene ?	$LiAlSi_2O_6$					R
Others						
Na-Ta oxide	$(Fe,Mn)(Nb,Ta)_2O_6$			VR		
Cassiterite ?	SnO_2	VR				
Barite	$BaSO_4$	VR				

* discrete crystals

C: common (> 5 obeservation); R: rare (3-5 observations)

VR: very rare (1-2 observations)

Fig. 11. Back-scattered SEM images of an unidentified prismatic crystal (A) with a trigonal cross-section (B) which yields an EDS spectrum with peaks for Al, Si and O (C). See text for further elaboration.

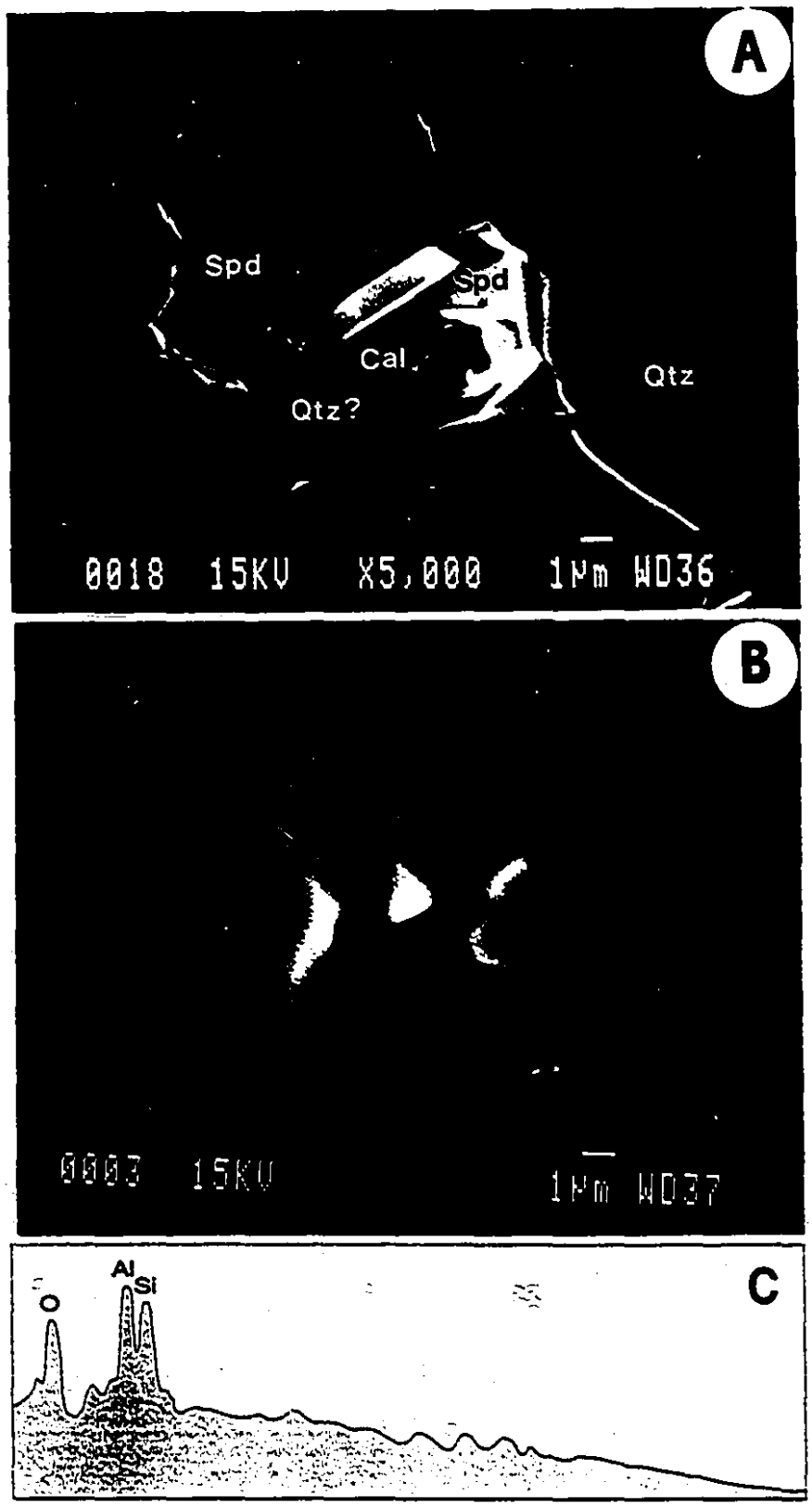
A
Spd
Spd
Cal
Qtz
Qtz?
0018 15KV X5,000 1µm WD36
B
0003 15KV 1µm WD37
C
O
Al
Si
0.00
keV
10.24

Figure 11

peak is significantly higher than the Si peak, which is the reverse of the relative peak heights of these elements in spectra of beryl or spodumene. If the solid is composed of the three elements, then, on the basis of semi-quantitative analyses, it has an Al/Si value of about 1.4 (Table 4). This is close to the Al/Si value of 1.6 for eookeite [$LiAl_4(Si_3Al)O_{10}(OH)_8$], which is a common phase in rare-element pegmatites (London and Burt, 1982). Alternatively, if the Si peak is an interference from the host mineral (beryl, spodumene or quartz), then the solid is an Al oxide or hydroxide mineral.

Quartz and pollucite are the next most common solids; quartz occurs as subhedral prisms in inclusions in beryl and spodumene from the three types of pegmatite, while pollucite forms an anhedral phase in inclusions in spodumene from both spodumene-beryl and spodumene pegmatites and in quartz from spodumene pegmatite. The EDS spectrum of pollucite shows a very small Na peak, indicating that its composition is close to being stoichiometric ($CsAlSi_2O_6 \cdot H_2O$). Albite was found in a few inclusions, and is invariably euhedral and small (3 μm long). In some cases (in spodumene pegmatite), it was accompanied by manganoan calcite (Fig. 12). Other positively identified solids are Nb-Ta oxide, barite and cassiterite, all of which are rare.

Among less commonly observed minerals that cannot be positively identified, is an anhedral to subhedral solid (~2 μm across) in inclusions hosted by spodumene from spodumene-beryl and spodumene pegmatites, which produces a spectrum with strong peaks for C, O, Al and Si (Fig. 13A), and in inclusions hosted by quartz from spodumene pegmatite produces peaks for C, O and Si. The peaks for Al and Si have intensities similar to those of the host minerals, suggesting that the solid is a carbonate of Li or Be; neither element can be detected by EDS. As far as we know, Be-bearing carbonates have not been found in nature. On the other hand, the Li-bearing carbonate, zabuyelite (Li_2CO_3), has been reported to occur in fluid inclusions from a number of spodumene-bearing pegmatites in other localities (Anderson et al., 1994). The interpretation that the above solid is zabuyelite is supported by the Raman spectrum of a solid in an unopened inclusion (Fig 2c, crystal 2), which matches that of the published Raman spectrum for zabuyelite (Fig. 13B). This mineral commonly has a rhombic habit, and decomposes at temperatures >400°C (London, 1986). It is thus the most likely candidate for the rhombic

Table 4 Semi-quantitative analyses of Al-rich included solid

	Wt%		Atomic proportion		
	Al	Si	Al	Si	Al/Si
1	28.2	21.3	1.045	0.758	1.38
2	28.05	19.76	1.039	0.703	1.48
3	27.6	20.6	1.023	0.733	1.40
4	29.1	22.8	1.078	0.812	1.33
				Average	1.39

Fig. 12 A back-scattered SEM image showing albite (Ab) and calcite (Cal) in an opened inclusion in spodumene from a spodumene pegmatite. The calcite is the manganoan variety, which occurs only in the more evolved spodumene-beryl and spodumene pegmatites.

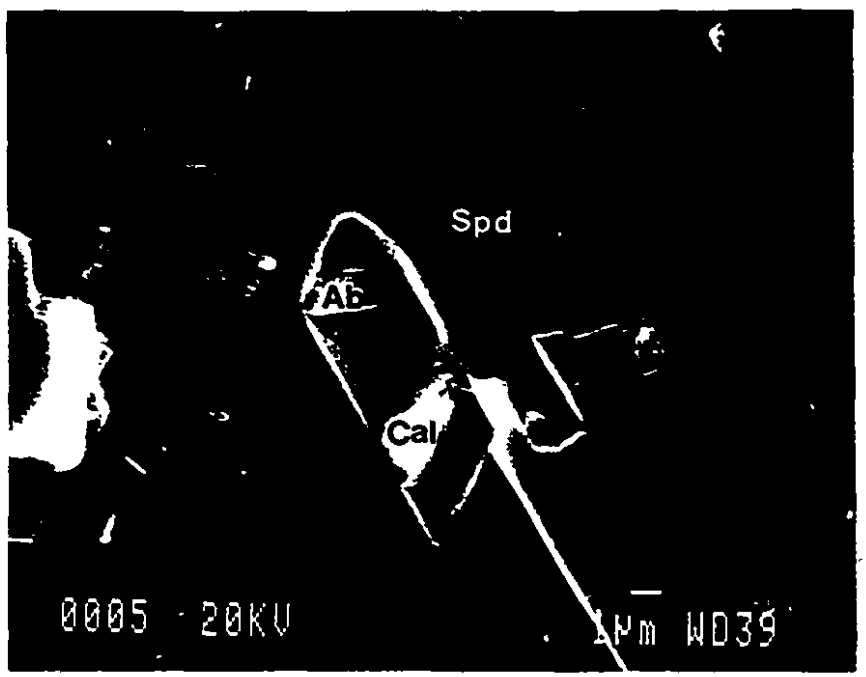

Figure 12

Fig. 13. An EDS-SEM spectrum (A) and a Raman spectrum (B) of a carbonate mineral which may be zabuyelite (Li_2CO_3). The Al and Si peaks in A are from the host spodumene. The value of the Raman shift for the mineral is from Degen and Newman (1993). See text for further discussion.

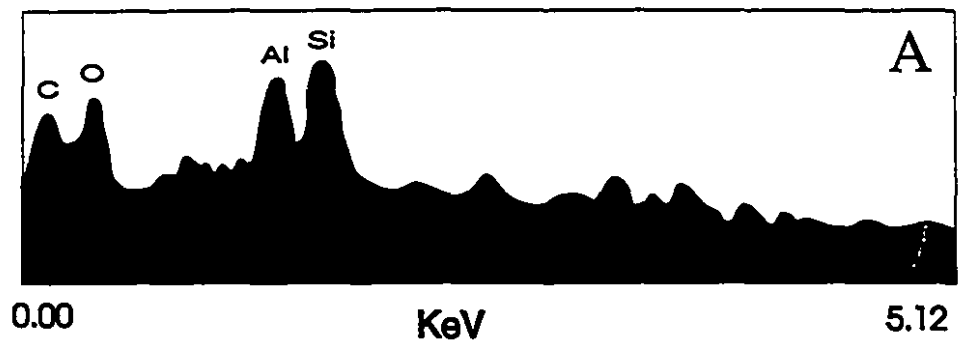
A
C
O
Al
Si
0.00
KeV
5.12

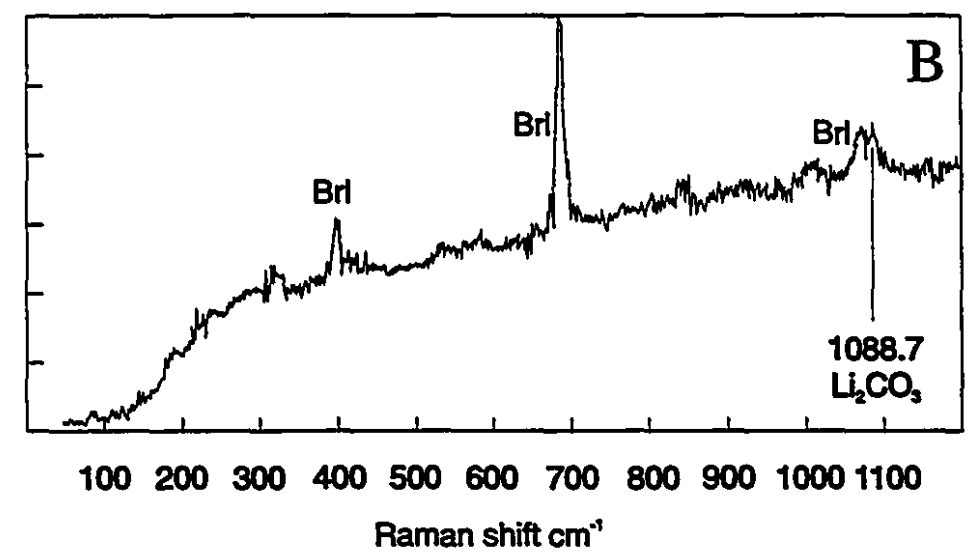
B
BrI
BrI
BrI
1088.7
Li2CO3
100 200 300 400 500 600 700 800 900 1000 1100
Raman shift cm-1

Figure 13

phase that apparently "dissolved" in some inclusions hosted by spodumene.

Another potential lithium mineral is a small cubic solid (2 μm in diameter), which was found in two inclusions hosted by beryl from spodumene-beryl pegmatite and produced an EDS spectrum for O, Al, Si and Cl (Fig. 14). As in the case of zabuyelite, the peaks for Al and Si are interpreted to be from the host mineral, and the cation accompanying Cl^- cation is thus either Be^{2+} or Li^+. Given its cubic habit, we speculate that the mineral has the composition of LiCl; $BeCl_2$ occurs as hexagonal prisms (Everest, 1964).

In a rare type 2 inclusion hosted by quartz from spodumene pegmatite (Fig. 13), one of the solids, which appears to display a short columnar habit, yielded a spectrum with peaks for O, Al and Si. The intensities of these peaks are identical to those of known spodumene, and we therefore speculate that the solid is spodumene. This interpretation implies that spodumene was, at least locally, precipitated by hydrothermal fluids.

OXYGEN ISOTOPE ANALYSES

Oxygen isotope compositions of quartz and garnet in beryl and spodumene-beryl pegmatites were determined (at the University of Saskatchewan) in order to provide estimates of the temperature of equilibration of these minerals in their respective pegmatites. The $\delta^{18}O$ values (referenced to SMOW) of quartz and garnet from the beryl and spodumene-beryl pegmatites are 9.3 and 5.1 ‰, and 9.6 and 5.9 ‰, respectively, corresponding to equilibration temperatures of 470 and 540 ± 50°C using the equations of Clayton et al. (1972) and Bottinga and Javoy (1975). These isotopic data were also be used to estimate the $\delta^{18}O$ values of the coexisting water, which using the equation of Clayton et al. (1972), is calculated to have been 6.6 and 7.76 ‰, respectively. These values are within the range of the $\delta^{18}O$ for magmatic water (Taylor, 1979).

Fig. 14. The EDS-SEM spectrum of a cubic chloride mineral in beryl from spodumene-beryl pegmatite, tentatively interpreted to have the composition of LiCl.

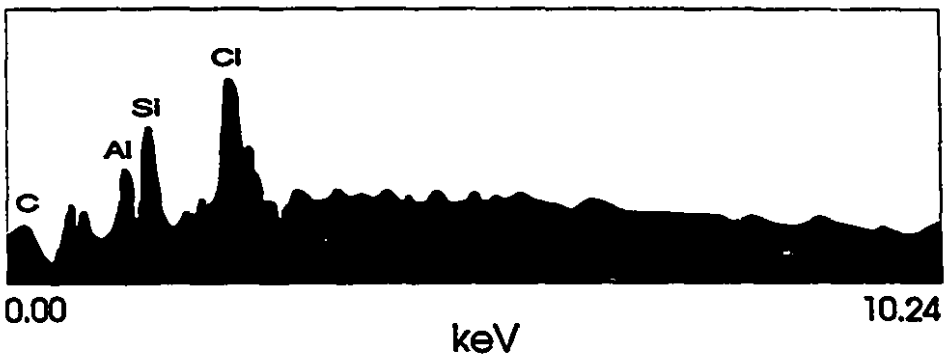

Figure 14

DISCUSSION

Pressure-Temperature conditions during pegmatite evolution.

Estimates of the pressure of emplacement of the Preissac Lacorne batholith have been made by Feng and Kerrich (1990) and Powell (1994) based on applications of the plagioclase-garnet-muscovite-biotite geothermobarometer to the intrusive facies, and multi-equilibrium modeling of contact metamorphic assemblages, respectively. The pressures estimated by Feng and Kerrich (1990) range from 3.6 Kb for the pegmatites to 4.9 Kb for the monzogranites, whereas Powell's estimate of the contact metamorphic pressure is from 2.5 to 4 Kb (most equilibria intersect at 3.5 Kb). We believe, as proposed by Powell (1994) that the most reasonable explanation for the discrepancy between his estimates and those of Feng and Kerrich, is that the actual emplacement pressure was approximately 3.5 Kb, and that the higher pressure obtained by Feng and Kerrich for the monzogranites reflects a deeper seated pre-emplacement condition. This interpretation is consistent with conclusions of both studies that regional metamorphic pressures in this part of the Abitibi greenstone belt never exceeded 4 Kb.

Minimum estimates of the temperature of crystallization of the pegmatites are provided by the oxygen isotopic compositions of quartz and garnet. As mentioned above, analyses of two pairs of these minerals gave temperatures of 470 and 540°C. It should be cautioned that these temperatures may not necessarily represent those of crystallization, but lower temperature subsolidus equilibration.

We have made other estimates of temperature by projecting isochores from the homogenization temperatures of type 1a and b inclusions using the program FLINCOR in conjunction with the equation of state of Brown and Lamb (1989). Limiting isochores, representing the mean isochore plus or minus one standard deviation, are shown in Figure 15 for primary type 1a inclusions and 1b inclusions (mainly secondary) in beryl from beryl pegmatite and primary type 1a inclusions in beryl from spodumene-beryl pegmatites, and spodumene from spodumene pegmatites. The standard deviation for isochores of type 1a inclusions hosted by quartz are very much larger. For this reason and for purposes of clarity, only mean isochores are plotted for inclusions hosted by this mineral. Also

Fig. 15. P-T conditions in beryl pegmatite (A), spodumene-beryl pegmatite (B), and spodumene pegmatite (C), deduced from limiting isochores representing one standard deviation above and below the mean isochores of type 1a and b inclusions in beryl, type 1a inclusions in spodumene (solid lines), and mean isochores of type 1a and 1b inclusions in quartz (dashed lines). Superimposed are the quartz-garnet oxygen isotope geothermometer (vertical broken lines) and the experimentally determined phase boundary separating the stability fields of petalite and spodumene plus quartz (London, 1984). The double ended arrows indicate estimated ranges of temperature of early orthomagatic fluid entrapment. The pressure, 3.5 kbar, is that estimated for emplacement of the pegmatites (see text).

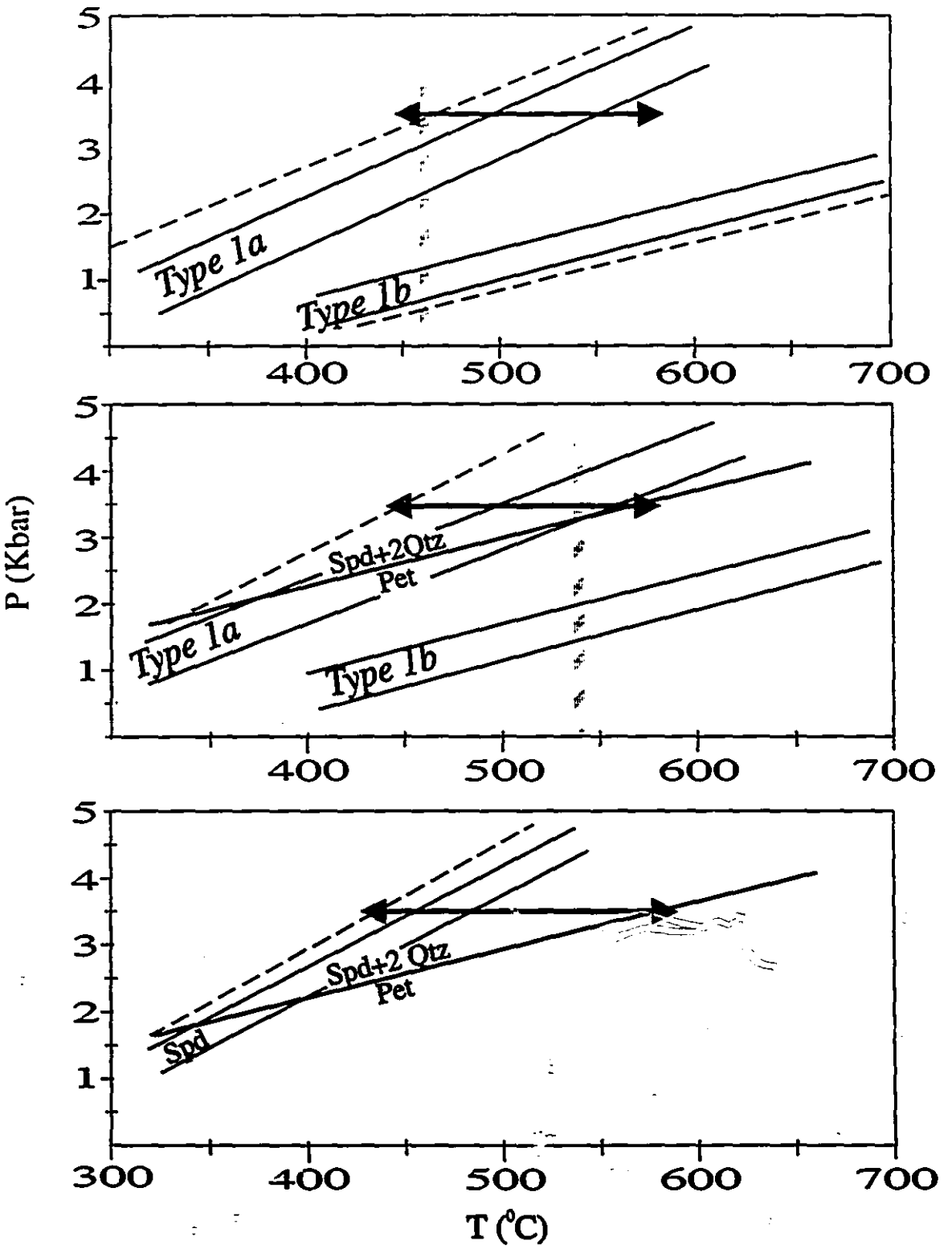

Figure 15

plotted are the temperatures estimated from oxygen isotopic fractionation between quartz and garnet from beryl and spodumene-beryl pegmatites, the phase boundary for the reaction petalite = spodumene + quartz (London, 1984), and the 3.5 Kb isobar estimated by Powell (1994) for the emplacement of the Preissac-Lacorne batholith.

Assuming an emplacement pressure of 3.5 Kb, the trapping temperatures of primary type 1a inclusions in beryl from beryl pegmatite are estimated to have been between 500°C (30°C above the oxygen isotopic temperature reported earlier) and 560°C. The corresponding temperatures for type 1b inclusions are considerably higher, i.e., 790 to 860°C, and much higher even than the solidus temperature (675°C) estimated for the co-magmatic muscovite monzogranite (Mulja, 1995a). Moreover, as noted above, these inclusions are mainly secondary. It therefore seems more likely that the trapping pressures for type 1b inclusions were much lower than those of type 1a inclusions, and the simplest explanation for this is that conditions changed from lithostatic to near hydrostatic during trapping of the type 1b inclusions. This explanation is supported by observations of strong local brecciation, which we interpreted earlier, to reflect hydrofracturing prior to complete crystallization of the pegmatite-forming magma. We thus suggest that, locally, fluid pressure built up until it exceeded the strength of the pegmatite, which then failed, leading to a period during which pressure fell to near hydrostatic levels.

Trapping temperatures of primary type 1a inclusions in beryl in spodumene-beryl pegmatite are predicted by the limiting isochores to have been between 500 and 570°C, which, in turn brackets the oxygen isotopic temperature estimate of 540°C. Significantly, the upper limit of the range is almost coincident with that of the stability of the assemblage, spodumene-quartz, which further helps to constrain crystallization temperatures for this pegmatite type. As for the beryl pegmatites, the isochores for the type 1b inclusions imply trapping of fluid at pressures considerably below lithostatic pressure.

The limiting isochores for primary type 1a inclusions in spodumene from spodumene pegmatites inclusions predict much lower trapping temperatures than those for beryl in the other two pegmatites, i.e., they intersect the 3.5 Kb isobar at temperatures

between 450 and 480°C. No type 1b inclusions were observed in spodumene pegmatites.

As mentioned above, the standard deviation for isochores defined by type 1a inclusions in quartz is very much wider than those for type 1a inclusions in beryl and spodumene (probably because of the higher frequency of secondary inclusions in quartz and the difficulty of distinguishing them from primary inclusions). Consequently these inclusions are less useful in estimating trapping temperatures. Nevertheless, it is probably significant that the mean trapping temperature predicted by these inclusions for all three pegmatite types is greater than one standard deviation below the mean temperatures predicted by isochores for type 1a inclusions in beryl and spodumene. The mean trapping temperatures for quartz in beryl pegmatite, spodumene-beryl pegmatite and spodumene pegmatite are, 480, 450, and 430°C, respectively.

In summary, various lines of evidence suggest that the Lacorne rare element pegmatites were emplaced at a pressure of approximately 3.5 Kb, that beryl was crystallizing at temperatures between 500 and 570°C , that spodumene crystallization extended to temperatures possibly as low as 450°C and that quartz continued to crystallize at somewhat lower temperatures.

Nature of the fluids

From the types of fluid inclusions recognized petrographically in each host mineral, the microthermometric data obtained for them, and analytical data on trapped solids, daughter minerals and residues from decrepitated fluid inclusions, it is evident that the fluids which circulated in the pegmatites were dominantly aqueous, that they varied considerably in composition, and that they coexisted during later stages of fluid evolution with an immiscible CO_2-rich carbonic fluid. In respect to the type 2 inclusions, it should be pointed out that London (1986) has described crystal-rich fluid inclusions in the Tanco pegmatite, Manitoba, which he demonstrated represent a hydrous melt phase or gel that was immiscible with the main silicate liquid. However, we do not believe that this interpretation is applicable to the type 2 inclusions, primarily because of the generally high proportion of fluid and inconsistent phase ratios (variable numbers of solids and variable fluid to solid ratios). The aqueous fluid inclusions can be classified into a low

salinity population (< 15 wt% NaCl eq.) comprising primary type 1a inclusions, some secondary type 1a inclusions and all type 2 inclusions, and a high salinity population (> 20 wt% NaCl eq.) consisting of type 1b (largely secondary) and secondary type 1a inclusions. In both cases the principal salt in solution is NaCl. Nevertheless, these inclusions can be further classified into a population characterised by calcium contents below detection, and another population in which the calcium content is moderately high (up to 12 wt% of the dissolved salts).

As discussed earlier, the type 1b inclusions and high salinity secondary type 1a inclusions have eutectic and final ice melting temperatures which indicate substantial quantities of a dissolved salt in addition to NaCl. It thus seems likely that these inclusions represent part of the high calcium population. The rarity of low Ca residues among fluid inclusions decrepitated in spodumene pegmatite (four among 25 residues analysed have Ca contents from 0 to 1.9 wt%) and the low eutectic temperatures of primary type 1a inclusions in this type of pegmatite, suggest that these latter inclusions also belong mainly to the high Ca population.

Establishing the affinity of the essentially Ca-free population is more difficult. Type 1a (primary and some secondary) and type 2 inclusions from beryl pegmatite and spodumene-beryl pegmatite might be candidates because of their higher eutectic temperatures (many of the Te values are below the eutectic temperature for the system $NaCl-H_2O$, but this could reflect the presence of $FeCl_2$ which is commonly a significant component of both high and low Ca inclusions in beryl). However, calcite occurs in almost all type 2 inclusions and could possibly be a daughter mineral, although this seems unlikely given that it has retrograde solubility (see earlier discussion). If it were a daughter mineral, this would imply a high concentration of Ca in the fluid. On the other hand, as a trapped mineral it could represent a fluid with a high bicarbonate ion activity (see below) and a relatively low content of Ca. We conclude that the low Ca population is represented largely by primary and some secondary type 1a inclusions from beryl and beryl-spodumene pegmatite, and also probably by type 2 inclusions. At least some low Ca fluid was also trapped in spodumene pegmatite (reflected by the small proportion of Ca-free decrepitate residues referred to above) presumably as primary type 1a and/or type

2 inclusions. It is also possible, given the low salinity and low eutectic temperatures of the aqueous phase in type 3 inclusions, particularly in beryl and spodumene-beryl pegmatites that these too, had low calcium contents.

In addition to Na, Cl, and Ca, as mentioned above, Fe is also a significant component of some fluid inclusions, but apparently only those hosted by beryl (it is highest in beryl from beryl pegmatite, which yielded decrepitate residues containing on average 6.2 wt% Fe versus 1.8% Fe in beryl from spodumene-beryl pegmatite). The only other significant cationic elements are K which is found in inclusions in all three pegmatite types, but only in beryl and spodumene, and Mn which is restricted to inclusions in spodumene from spodumene pegmatite. Sulphur was the only anionic element detected in decrepitate residues, and is present in minor quantities without any obvious pattern of distribution in terms of host mineral or pegmatite type. However, as discussed previously, the decrepitate residue compositions indicate an appreciable anion deficiency which could reflect significant concentrations of bicarbonate ions

The carbonic phases of type 3 inclusions, and type 4 inclusions consist almost entirely of CO_2, except in some inclusions in spodumene pegmatite, which on the basis of low melting temperatures of carbonic solid, are interpreted to contain CH_4 and/or N_2

Fluid Evolution

From the above discussion, it is reasonable to assume that aqueous fluids were present at an early stage of pegmatite crystallization, and that these fluids are represented by primary type 1a and/or type 2 inclusions. It is also reasonable to assume that the early fluids would have been dominantly orthomagmatic. Given the composition of the magma, such fluids can be predicted to have been dominated by NaCl, and to have contained minor concentrations of KCl. At the conditions interpreted for entrapment of primary type 1a inclusions (530°C in beryl and 470°C in spodumene), a fluid in equilibrium with albite and K-feldspar (major constituents of the pegmatites), is predicted to have a Na/(Na+K) atomic ratio of 0.86±0.1 (calculated using SUPCRT92; Johnson et al., 1992) which is actually somewhat lower than estimated by analyses of decrepitate residues (Table 2). It is extremely unlikely that the orthomagmatic fluids would have contained

any significant $CaCl_2$. However, appreciable concentrations of Fe would not be unexpected, and in fact are known to occur in orthomagmatic fluids from porphyry copper systems (e.g., Eastoe, 1978; Wilson et al., 1980). In view of the above and the preceding discussion of fluid inclusion compositions, we propose that the orthomagmatic fluid is represented by the low Ca primary type 1a inclusions which occur mainly in beryl and rarely in spodumene.

In view of the intimate association of type 2 inclusions with primary type 1a inclusions and the similar microthermometric behavior of the two inclusion types, we consider it likely that type 2 inclusions also trapped the orthomagmatic fluid, i.e., this fluid was saturated with solids, including calcite, prior to entrapment of either primary type 1a or type 2 inclusions, and that type 2 fluid inclusions are only different from type 1a inclusions to the extent that they accidentally trapped some of these solids. If this interpretation is correct it implies that the fluid had a high bicarbonate content, which is supported by the anion deficiency in decrepitate residues.

The early aqueous fluid chemistry of beryl pegmatite appears to have been somewhat different from that of spodumene pegmatite, in that the former fluids had relatively high Fe contents, whereas the latter fluids were enriched in Mn, Li, and Cs. The high content of Fe is indicated by the composition of decrepitate residues from beryl-hosted inclusions, and the enrichment in Mn by the composition of decrepitate residues and the composition calcite in the type 2 inclusions from spodumene. Occurrences of pollucite and probable lithium chloride and carbonate minerals in these type 2 inclusions provide the evidence for enrichment of the fluid in Cs and Li. Additional evidence of the enrichment in Li is provided by the formation of holmquistite $[Li_2(Mg,Fe^{+2})(Al,Fe^{+3})_2(Si_8O_{22})(OH)_2]$ in the adjacent mafic country rocks; high Li contents in the fluid are also predicted by calculations of Wood and Williams-Jones (1993) for fluid-mineral equilibria involving spodumene and feldspars. These compositional variations in the fluid from beryl to spodumene pegmatite are matched by corresponding changes in the mineral chemistry of the pegmatites (Mulja et al., 1995b), and whole-rock chemical trends among the various intrusive facies of the Lacorne pluton (Mulja, 1995c), supporting a conclusion that they reflect evolution of an exsolving orthomagmatic fluid.

Late in the crystallization history of beryl and spodumene-beryl pegmatites, as discussed earlier, there was a sharp drop in pressure, recorded by the entrapment of type 1b inclusions in beryl and brecciation of the incompletely crystallized pegmatite. The type 1b inclusions, as has also been discussed, were enriched in calcium and had relatively high salinity. We propose that this event in these two pegmatite types marked the incursion of an external high salinity Ca-bearing fluid from the country rocks, which are predominantly metamorphosed basalts and mafic tuffs, and therefore rich in Ca. Although the nature of this fluid is unknown, given the depth of emplacement, and the width of the contact metamorphic aureole surrounding the Preissac Lacorne batholith (up to 7 Km; Powell, 1994) it is likely to have been metamorphic. There is also no need to invoke a special source to explain the high salinity as there is increasing evidence that metamorphic fluids are considerably more saline than previously believed (cf. Roedder, 1984). Moreover, in environments dominated by basalt, they are commonly Ca-rich brines.

In the spodumene pegmatites, influx of calcium-bearing fluids probably occurred earlier, as indicated by the fact that, unlike inclusions in beryl and beryl-spodumene pegmatites, most inclusions are relatively rich in calcium. This is not unexpected given that these pegmatites are small bodies intruded into the country rocks, whereas beryl and beryl-pegmatites are hosted by the monzogranites, and therefore better shielded from external basalt-sourced fluid. There is also good mineralogical evidence of the greater importance of Ca-bearing fluids in the spodumene pegmatites, namely the development of rims of oligoclase or andesine around albite and the presence of microlite that partially replaced manganocolumbite (Mulja et al., 1995a). These features are not observed in the beryl and spodumene-beryl pegmatites.

After the initial influx of a Ca-brine into the pegmatites the next and final event in the crystallization history of the pegmatites was the appearance of an immiscible CO_2-dominated fluid (type 3 inclusions) coincident with crystallization of late quartz (CO_2-bearing fluid inclusions are restricted to quartz, i.e. they are not observed in beryl or spodumene). Possible explanations for the origin of the carbonic phase are that it was introduced from the country rocks, or that the orthomagmatic fluid contained dissolved

CO_2 which started to exsolve when the pegmatite system cooled to a temperature sufficient to enter the two phase field of the system H_2O-CO_2. We favor the second alternative mainly because, if the CO_2 came from the country rocks, it is reasonable to expect that it would have accompanied introduction of the Ca-brine and therefore have been trapped not only in quartz but also in beryl and particularly spodumene. The presence of calcite (and probable zabuyelite (Li_2CO_3)), in the type 2 fluid inclusions, and the very low Ca content of the orthomagmatic fluid implies that the latter contained appreciable dissolved CO_2. This is consistent with the anion deficiency of the decrepitate residues, which we have interpreted to represent bicarbonate ions. At the temperatures and pressures proposed for the entrapment of these inclusions, i.e. between 450 and 550°C and 3.5 Kb, the CO_2 would probably have been dissolved mainly as the neutral species $H_2CO_3^0$ rather than $HCO3^-$; predominance of $HCO3^-$ at these conditions would have required a pH between 8.6 and 9.7 (calculated using SUPCRT92; Johnson et al., 1992) which is probably much higher than the pH which is likely to have prevailed, given the presence of muscovite in the pegmatites. On cooling to temperatures below about 400°C, approximately the consolute point of the system H_2O-CO_2 -6 wt% NaCl (cf. Bowers and Helgeson, 1983), the orthomagmatic fluid would have begun to unmix, with the temperature of unmixing depending on XCO_2. Based on the homogenization temperatures of type 3 inclusions (Fig. 5) this would probably have been between 250 and 350°C. We therefore propose that pegmatite formation terminated with the crystallization of quartz at temperatures between 250 and 350°C, and that this was associated with unmixing of the orthomagmatic fluid and heterogenous entrapment of these fluids as type 3 inclusions. The lack of evidence of post-entrapment unmixing of the orthomagmatic fluids trapped at higher temperature can be explained by the fact that the pH of the H_2CO_3-HCO_3^- predominance boundary decreased sharply on cooling and stabilized HCO_3^- at the expense of $H_2CO_3^0$ (this assumes that the high temperature pH was at least partly preserved, which seems reasonable given that the H_2CO_3-HCO_3^- predominance boundary is close to neutrality, whereas at room temperature and pressure it is significantly lower, 6.3 versus 7 (calculated using SUPCRT92; Johnson et al., 1992)). The above notwithstanding, we cannot exclude the possibility, particularly for the spodumene pegmatites, which contain

a small proportion of inclusions with significant $CH_4 \pm N_2$ that there might have been some contribution of carbonic fluid from the country rocks.

After crystallization, aqueous and carbonic fluids continued to circulate in the pegmatites until relatively low temperatures and are now represented by secondary type 1, type 3 and type 4 (CO_2-only) inclusions.

The fluid evolution that has been proposed in the preceding paragraphs is illustrated schematically in Figure 16 and starts with the emplacement of a vapour- or near vapour-saturated pegmatite-forming magma at a temperature of perhaps 550°C or somewhat higher temperature and a pressure of 3.5 Kb. The exsolving vapor is a low salinity, CO_2-bearing, Na-dominated fluid containing significant Fe in the beryl pegmatites, and enriched in Mn, Li and Cs in the spodumene pegmatites. In the latter pegmatites the fluid is initially in equilibrium with petalite, but soon evolves along a cooling path into the spodumene field. Relatively late in the crystallization history of the beryl-bearing pegmatites there are local fluid overpressures which cause the pegmatites to fail, leading to brecciation and subsequent temporary drops in pressure. This marks the onset of incursions of Ca-brines of metamorphic origin into the pegmatites. In the spodumene pegmatites, which were intruded into the mafic rocks surrounding the Lacorne pluton, and are thus directly in contact with the metamorphic fluids rather than being shielded from them, as was the case for the beryl-bearing pegmatites (which are intruded into the pluton), incursions of Ca brines start earlier and are more important. The final event in the fluid history of the crystallizing pegmatite is the unmixing of the orthomagmatic fluid into separate aqueous and CO_2 phases and their heterogeneous entrapment in late quartz at temperatures between 250 and 350°C.

SUMMARY AND CONCLUSIONS

The observations and data presented in this paper show that the Lacorne rare element pegmatite-forming liquid was saturated by an aqueous fluid penecontemporaneously with emplacement, and that this fluid contained significant concentrations of dissolved CO_2, which exsolved in response to cooling during the late

Fig. 16. The interpreted P-T path of fluid evolution in the Lacorne rare-element pegmatite system. 1) emplacment of the vapor-saturated pegmatite-forming liquid, 2) crystallization of petalite and beryl, followed by spodumene as conditions cross the phase boundary for the reaction petalite $\Rightarrow$ spodumene + 2 quartz, 3) local hydrofracturing leading to a temporary drop in fluid pressure, 4) entrapment of high salinity fluid inclusions following brecciation and incursion of external metamorphic brines, 5) termination of beryl crystallization, 6) termination of spodumene crystallization, 7) unmixing of the orthomagmatic fluid into aqueous and CO_2 phases, and their entrapment in late crystallizing quartz.

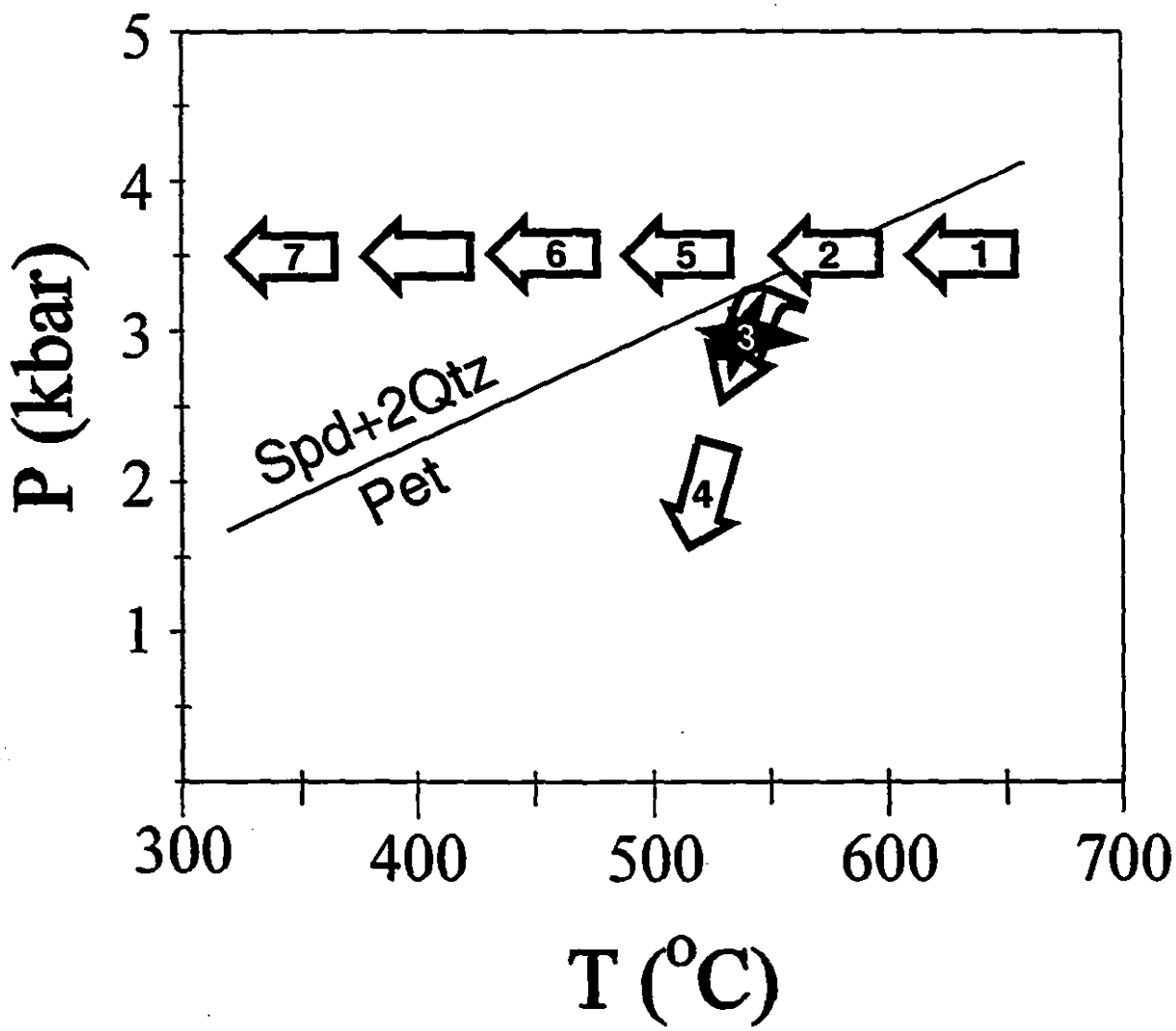

Figure 16

stages of pegmatite crystallization. This evidence of early saturation of the pegmatite-forming magma with vapor is consistent with the Jahns and Burnham (1969) model for the formation of pegmatites, but does not exclude the possibility of pegmatite formation without aqueous phase saturation (cf London et al., 1989).

The only other rare element pegmatite for which the timing of fluid entrapment has been extensively documented is the tourmaline-rich pegmatite at Tanco, Manitoba where London (1986) and Thomas et al. (1988) have presented conflicting evidence over whether aqueous phase saturation was early or late, respectively. In other studies of which we are aware, where the nature of the fluid inclusions in rare element pegmatites has been documented, either the inclusions were in late stage parageneses (e.g. Ruggieri and Lattanzi, 1988), restricted to quartz, in which primary and secondary inclusions are difficult to distinguish (e.g., Whitworth and Rankin, 1989), or the authors failed to indicate whether the inclusions were primary or secondary (e.g., Chakoumakos and Lumpkin, 1990).

Setting aside the question of the timing of aqueous phase saturation, the fluid evolution in the Lacorne pegmatites differs in one important respect from that of the Tanco pegmatite, namely the lack of crystal-rich inclusions that could represent a melt. London (1986) showed that the solids in such inclusions at Tanco dissolve/melt on heating, and when quenched produce a glass or gel, which he interpreted to represent an immiscible hydrous borosilicate liquid. Interestingly, the only other pegmatites known to us where a melt origin has been ascribed to crystal-rich inclusions are those at Mt. Capanne, Italy, which, like Tanco, are boron-rich (Ruggieri and Lattanzi, 1988). In the Lacorne pegmatites, although, as discussed above, early solid-bearing inclusions are common, the proportion of aqueous fluid is sufficiently high as to make it unlikely that they represent melt. It is therefore attractive to propose that boron-rich and -poor rare element pegmatite systems may evolve along somewhat different paths, distinguished by whether or not an immiscible hydrous melt phase is formed, respectively. However, this hypothesis has been undermined recently by the finding of Anderson (1994) that the B-bearing solid identified by London et al. (1987) as diomignite ($Li_2B_4O_7$), and used to support his interpretation of an immiscible melt phase at Tanco, is in fact the mineral

zabuyelite (Li_2CO_3).

An important feature of the fluid evolution of the Lacorne pegmatites, which is shared by many rare element pegmatites, including Tanco, is the formation of an immiscible CO_2 phase, typically at a late stage of pegmatite crystallization. Most authors, including ourselves, attribute the source of the CO_2 to an aqueous orthomagmatic fluid, and explain its occurrence as a separate phase as being due to fluid unmixing as a result of cooling. London (1986), however, from the abundance of zabuyelite in crystal-rich inclusions from late spodumene at Tanco has proposed, instead, that the CO_2 is produced by decomposition of this mineral. Although carbonate minerals, including zabuyelite, are common in the Lacorne pegmatites, we consider it more likely that they are simply a reflection of the activity of dissolved CO_2 in the aqueous phase. Indeed any carbonate that was precipitated at high temperature (mainly calcite) would have tended to dissolve on cooling because of retrograde solubility (Fein and Walther, 1987 & 1989), which may explain why calcite is not part of the pegmatite paragenesis.

In summary the results of this study suggest, at least for the case of boron-poor pegmatites, that aqueous phase saturation can take place at an early stage of rare element pegmatite crystallization, that pegmatite evolution is matched by the evolution of the solute chemistry of the exsolving aqueous fluid, that CO_2 is an important component of this fluid, and that the common occurrence of aqueous-carbonic fluid inclusions in quartz is a natural consequence of the cooling of the system.

ACKNOWLEDGEMENTS

The authors gratefully acknowledge the insightful comments of R.F. Martin and J.B. Fein. We thank Drs. Stephane Brienne (McGill) and Iain Samson (Windsor) for their assistance with the Raman analyses. Funding for the research was provided by NSERC research grants to AEW-J and SAW, and an FCAR team grant to AEW-J.

REFERENCES

ANGUS S., ARMSTRONG, B., DEREUCK K.M., ALTUNIN V.V., GADETSKII O.G., CHAPELA G.A., AND ROWLINSON J.S. (1976) *International thermodynamic tables of the fluid state, vol. 3 Cabon dioxide.* Pergamon Press, Oxford England.

ANDERSON A.J., CLARK A.H., HARRISON F., AND BODNAR R.J. (1994) Zabuyelite (Li_2CO_3) in spodumene-bearing pegmatites. Geol.- Mineral. Assoc. Can. Programs with abstracts, v. 19, p. A3.

BONDAR R.J. (1983) A method of calculating fluid inclusion volumes based on vapor bubble diameters and P-V-T-X properties of fluid inclusions. *Econ. Geol.* **78**, 535-542.

BOTTINGA Y. AND JAVOY M. (1975) Oxygen isotope partitioning among the minerals in igneous and metamorphic rocks. *Rev. Geophysi. Space Phys.* **13**, 401-418.

BOWERS T.S. AND HELGESON H.C. (1983) Calculation of thermodynamic and geochemical consequences of on ideal mixing in the system H_2O-CO_2-NaCl on phase relations in geologic systems: equation state for the H_2O-CO_2-NaCl fluids at high pressures and temperatures. *Geochim. Cosmochim. Acta* **47**, 1247-1275.

BROWN P.E. AND LAMB W.M. (1989) P-V-T properties of fluids in the system $H_2O \pm CO_2 \pm NaCl$: new graphical presentations and implications for fluid inclusion studies. *Geochim. Cosmochim. Acta* **53**, 1209-1221.

ČERNY P. AND FERGUSON R.B. (1972) The Tanco pegmatite at Bernic Lake, Manitoba. 4. Petalite and spodumene reactions. *Can. Mineral.* **11**, 660-678.

CHAKOUMAKOS B.C. AND LUMPKIN G.R. (1990) Pressure-temperature constraints on the crystallization of the Harding pegmatite, Taos County, New Mexico. *Can. Mineral.* **28**, 287-298.

CLAYTON R.N., O'NEIL J.R., AND MAYEDA T.K. (1972) Oxygen isotope exchange between quartz and water. *J. Geophys. Res.* **77**, 3057-3067.

CRAWFORD M.L. (1981) Phase equilibria in aqueous fluid inclusions. In *Short course in fluid inclusions: applications to petrology* (eds. L.S. Hollister and M.L. Crawford), Mineral. Assoc. Can., **6**, 157-181.

DARLING R.S. (1991) An extended equation to calculate NaCl contents from final clathrate melting temperatures in H_2O-CO_2-NaCl fluid inclusions: implications for P-T isochore location. *Geochim. Cosmochim. Acta*, **55**, 3869-3871.

DAWSON K.R. (1966) *A comprehensive study of the Preissac-Lacorne batholith, Abitibi county, Québec*. Geol. Surv. Can. Bull. 142.

DEGEN I.A. AND NEWMAN G.A. (1993) Raman spectra of inorganic ions. *Spectrochimica Acta*, 49A, 859-887.

EASTOE, C.J. (1978) A fluid inclusion study of the Panguna porphyry copper deposit, Bougainville, Papua New Guinea. *Econ. Geol.* **73**, 721-748.

EVEREST, D.A. (1964) *The chemistry of beryllium*. Elsevier.

FEIN, J.B AND WALTHER J.V. (1987) Calcite solubility in supercritical CO_2-H_2O fluids. *Geochim. Cosmochim. Acta* **51**, 1665-1673.

FEIN, J.B AND WALTHER J.V. (1989) Calcite solubility and speciation in supercritical NaCl-HCl aqueous fluids. *Contrib. Mineral. Petrol.* **103**, 317-324.

FENG R. AND KERRICH R. (1990) Geobarometry, differential block movements, and crustal structure of the southwestern Abitibi greenstone belt, Canada. *Geology* **18**, 870-873.

FENG R. AND KERRICH R. (1991) Single zircon age constraints on the tectonic juxtaposition of the Archean Abitibi greenstone belt and Pontiac subprovince, Quebec, Canada. *Geochim. Cosmochim. Acta*, **55**, 3437-3441.

HEYEN G., RAMOZ C., AND DUBESSY A. (1982) Simulation des equilibres de phases dans le systeme CO_2-CH_4 en dessous de 50°C et de 100 bar. Application aux inclusions fluides. *C. R. Acad. Sci. Paris*, **294**, 203-206.

HOLLAND H.H. AND MALININ S.D. (1979) The solubility and occurrence of non-ore minerals. In H.L. Barnes (ed.) Geochemistry of hydrothermal ore deposits. *Wiley Interscience, New York*, 798 p.

JAHNS R. AND BURNHAM C.W. (1969) Experimental studies of pegmatite genesis: I. A model for the derivation and crystallization of granitic pegmatites. *Econ. Geol.* **64**, 843-864.

JOHNSON J.W., OELKERS E.H., AND HELGESON H.C. (1992) SUPCRT92: A software package for calculating the standard molal thermodynamic properties of minerals, gases, aqueous species and reactions from 1 to 5000 bars and 0° to 1000 °C. *Comput. Geosci.* **18**, 899-920.

LONDON D. (1984) Experimental phase equilibria in the system $LiAlSiO_4$-SiO_2-H_2O: a petrogenetic grid for lithium-rich pegmatites. *Am. Mineral.* **69**, 995-1004.

LONDON D. (1985) Origin and significance of inclusions in quartz: a cautionary example from the Tanco pegmatite, Manitoba. *Econ. Geol.* **80**, 1988-1995.

LONDON D. (1986) Magmatic-hydrothermal evolution in the Tanco rare element pegmatite: evidence from fluid inclusions and phase equilibrium experiments. *Am. Mineral.* **71**, 376-395.

LONDON D. AND BURT D. (1982) Lithium minerals in pegmatites. *In* P. Černy (ed.) *Granitic pegmatites in science and industry*, MAC short cource **8**, 405-461.

LONDON D., ZALENSKI M.E., AND ROEDDER E. (1987) Diomignite: natural $Li_2B_4O_7$ from the Tanco pegmatite, Bernic Lake, Manitoba. *Can. Mineral.* **25**, 173-180.

MULJA T., WILLIAMS-JONES A.E., MARTIN R.F., AND WOOD S.A. (1995a) Compositional variation and structural state of Nb-Ta oxide minerals in rare-element granitic pegmatites from the Preissac-Lacorne batholith, Quebec. *Am. Mineral.* (in review)

MULJA T., WILLIAMS-JONES A.E., WOOD S.A., AND BOILY M. (1995b) Geology and mineralogical evolution of rare-element monzogranites and pegmatites in the Preissac-Lacorne batholith, Québec: *Can. Mineral.* **33**, 000-000.

MULJA T., WILLIAMS-JONES A.E., WOOD S.A., AND BOILY M. (1995c) Petrogensis of zoned rare-element monzogranites and associated rare-element pegmatites and quartz veins: the Preissac-Lacorne batholith, Québec, Canada. *Can. Mineral.* **33**, 000-000.

OAKES C.S., BODNAR R.J., AND SIMONSON J.M. (1990) The system NaCl-$CaCl_2$-H_2O: I. The ice liquidus at 1 atm total pressure. *Geochim. Cosmochim. Acta* **54**, 603-610.

O'NEIL J.R. AND TAYLOR H.P. JR (1969) Oxygen isotope fractionation between muscovite and water. *J. Geophys. Res.* **74**, 6012-6022.

POTTER R.W. II., CLYNNE M.A., AND BROWN D.L. (1978) Freezing point depression of aqueous sodium chlorite solutions. *Econ. Geol.* **73**, 284-285.

POWELL W.G (1994) *A petrological and geochronological study of the metamorphic history of the Rouyn-Noranda area, Quebec.* Unpublished Ph.D thesis, Queen's University, Kinston, Ontario.

ROEDDER E. (1984) Fluid inclusions: *Rev. Mineral.* **12**, MSA.

RUGGIERI G. AND LATTANZI R. (1992) Fluid evolution studies on Mt. Capanne pegmatites, Isola d'Elba, Tuscany, Italy. *Eur. J. Mineral.* **4**, 1085-1096.

SAMSON I.M. AND SINCLAIR W.D. (1992) magmatic hydrothermal fluids and the origin of quartz-tourmaline orbicules in the Seagull batholith, Yukon Territory. *Can. Mineral.* **30**, 937-954.

STEIGER R.H. AND WASSERBURG G.J. (1969) Comparative U-Th-Pb systematics in 2.7 x 10^9 yr plutons of different geological histories. *Geochim. Cosmochim. Acta*, **33**, 1213-1232.

THOMAS A.V., BRAY C.J., AND SPOONER E.T.C. (1988) A discussion of the Jahns-Burnham proposal for the formation of zoned granitic pegmatites using solid-liquid-vapour inclusions from the Tanco pegmatite, S.E. Manitoba, Canada. *Trans. R.S. Edin.: Earth Sci.* **79**, 299-315.

TROMMSDORF V., SKIPPEN G., AND ULMER P. (1985) Halite and sylvite as solid inclusions in high grade metamorphic rocks. *Contrib. Mineral. Petrol.* **89**, 24-29.

WERRE R.W.JR., BODNAR R.J., BETHKE P.M., AND BARTON P.B.JR (1979) A novel gas-flow fluid inclusion heating/freezing stage (Abstr.). *Geol. Soc. Ame. Abstrc. Progs.* **11**, 539.

WHITWORTH M.P. AND RANKIN A.H. (1989) Evolution of fluid phases associated with lithium pegmatites from SE Ireland. *Mineral. Mag.* **53**, 271-284.

WILSON J.W.J. KESLER S.E., CLOKE P.L., AND KELLY W.C. (1980) Fluid inclusion geochemistry of the Granisle and Bell porpohyry copper deposits. British

Columbia. *Econ. Geol.* **75**, 45-61.

WOOD, S.A. AND WILLIAMS-JONES, A.E. (1993) Theoretical studies of the alteration of spodumene, petalite, eucryptite and pollucite in granitic pegmatites: exchange reactions with alkali feldspars. *Contrib. Mineral. Petrol.* **114**, 255-263.

CHAPTER 6

EPILOGUE

Conclusions

This study has deciphered the petrogenesis of four monzogranite plutons (Preissac, Moly Hill, Lamotte, Lacorne) and associated rare element pegmatites in the Archean Preissac Lacorne batholith, Québec. The monzogranites comprise biotite, two-mica (biotite-muscovite) and muscovite facies, and have been shown on the basis of geological relationships, mineral chemistry and petrochemistry to have been formed by fractional crystallization of a felsic (biotite-bearing granitic) liquid. The smaller Preissac and Moly Hill plutons are interpreted to have been produced by smaller batches of felsic liquid, each of which was emplaced separately; the intrusion of the Moly Hill liquid appears to have been controlled by faults, whereas control of the emplacement of the Preissac liquid has yet to be determined. The residual melt in these two plutons was prematurely saturated with an aqueous phase, thereby inhibiting the formation of hydrous, highly fractionated liquid, which potentially could have crystallized rare-element-enriched pegmatites. Instead, the early release of aqueous fluid promoted development of a few barren granitic pegmatites, and precipitation of quartz, muscovite and molybdenite as Mo-bearing quartz veins adjacent to the parental monzogranite.

The mechanism of fractionation in the larger Lamotte and Lacorne plutons is believed to have been side-wall crystallization and to have been responsible for the quasi-concentric zonation of monzogranite facies in these plutons. The crystallization created a highly evolved liquid inside the magma chamber, which eventually was emplaced in and around the pluton as rare-element-enriched granitic pegmatites. Evidence for this comagmatic relationship between the monzogranites and pegmatites is: 1) the pegmatites cut all types of monzogranite and are regionally zoned from least

evolved beryl-bearing in the pluton through spodumene-beryl-bearing to a spodumene-bearing type in the country rocks, i.e., farthest from the source rock; 2) there is a compositional continuum in the chemistry of the rock-forming minerals, particularly the trace element chemistry of muscovite, from the most evolved muscovite monzogranite to the pegmatites; and 3) there are coherent whole-rock trace-element trends between the two suites of rock. Various lines of evidence, including a gradual transition from beryl-bearing to spodumene-bearing varieties, indicate that the rare element pegmatites are also comagmatic. The strongest evidence for this comagmatic relationship is provided by the crystal-chemistry of columbite-tantalite, which shows a trend of increasing Mn/(Mn+Fe) and Ta/(Ta+Nb) ratios from beryl- to spodumene-bearing pegmatite types. The increase in these elemental ratios reflects the higher solubility of Fe-relative to Mn-, and Ta- relative to Nb-columbite-tantalite end-members. The structural state of this mineral also correlates well with the degree of fractionation of the host pegmatite and its location with respect to the pluton.

On the basis of microthermometric data and analyses of trapped solids and precipitates of decrepitated fluid inclusions in beryl, spodumene and quartz, the pegmatite-forming liquid for the Lacorne pluton is interpreted to have been saturated with an orthomagmatic fluid during its emplacement at 500-570°C and 3.5 kbar. The fluid, in the less evolved beryl pegmatites had low salinity, was NaCl-dominated and contained appreciable concentrations of Fe and dissolved CO_2. During the late stages of crystallization of these pegmatites, hydraulic fracturing occurred as a result of fluid overpressures. This event was accompanied by the influx of an external Ca-bearing brine of metamorphic origin, which was trapped by beryl and quartz as high salinity inclusions. The fluid evolution associated with spodumene-bearing pegmatite was marked by an earlier incursion of external Ca-brines. Evolution of the orthomagmatic fluid from beryl- to spodumene-type pegmatites was associated with a loss of Fe and an enrichment in Mn, Li, and Cs, and was matched by corresponding changes in the mineral chemistry of the pegmatites and whole-rock chemical trends among the various intrusive facies of the Lacorne pluton. On cooling to about 350°C, the fluid in the pegmatites underwent unmixing to form separate aqueous and CO_2-dominated carbonic

fluids. Demonstration that primary aqueous fluid inclusions were trapped at an early stage of pegmatite crystallization provides important support for the hypothesis of Jahns and Burnham (1969) that an aqueous fluid phase is commonly present at the onset of pegmatite crystallization.

Contributions to original knowledge

1) The thesis provides the first integrated study of the petrogenesis of zoned granitic plutons and associated rare-element-enriched pegmatites; the study demonstrates that the zonation of the plutons was produced by fractional crystallization, that the pegmatites were comagmatic with the monzogranites, and that the zonal distribution of the former, from least evolved beryl-type through spodumene-beryl-type to most evolved spodumene-type is consistent with injection of the evolving residual melt from progressively deeper levels of a downward crystallizing magma chamber.

2) The thesis is the first to compare compositional and structural variations in columbite-tantalite from two contrasting suites of rare-element pegmatites. Results of the study show that the chemical trends of this mineral can be more plausibly explained by differences in the solubility of Fe-, Mn-, Nb- and Ta-end members of columbite-tantalite, than by the widely accepted, yet unproven, hypothesis of F-Mn or F-Ta complexation. The study also demonstrates the important control which the timing of saturation of the Mn buffer, spessartine garnet, can have on the evolution of columbite-tantalite composition. Finally the columbite-tantalite study provides evidence that the structural state of this mineral is governed by the cooling rate of the felsic liquid.

3) The thesis presents the most comprehensive investigation of fluid evolution in a boron-poor rare element pegmatite system undertaken to date. This investigation contributes important evidence about the timing of aqueous phase saturation in rare element pegmatite magmas, and suggests that, at least for boron-free systems, it probably occurs soon after emplacement, rather than at a late stage, as has been proposed by London (1986) and London et al. (1989) for boron-rich systems. The study also provides the first relatively detailed reconstruction of the chemical evolution of the orthomagmatic aqueous fluid, shows how this evolution parallels that of the pegmatite

magma, as documented by trends in mineral and whole-rock chemical compositions, and furnishes a satisfactory explanation for the origin of carbonic fluids commonly trapped by late crystallizing quartz.

REFERENCES

Jahns R.H. and Burnham, C.W. (1969) Experimental studies of pegmatite genesis: I. A model for the derivation and crystallization of granitic pegmatites. *Economic Geology* 64, 843-864.

London D (1986) Magmatic-hydrothermal transition in the Tanco rare-element pegmatite: evidence from fluid inclusions and phase-equilibrium experiments. *American Mineralogist* 71, 376-395.

London D., Morgan G.B. VI. and Hervig, R.L. (1989) Vapor-undersaturated experiments with Macusani glass+H_2O at 200 MPa, and the internal differentiation of granitic pegmatites. *Contributions to Mineralogy and Petrology* 102, 1-17.

Appendix 1

Sample location maps

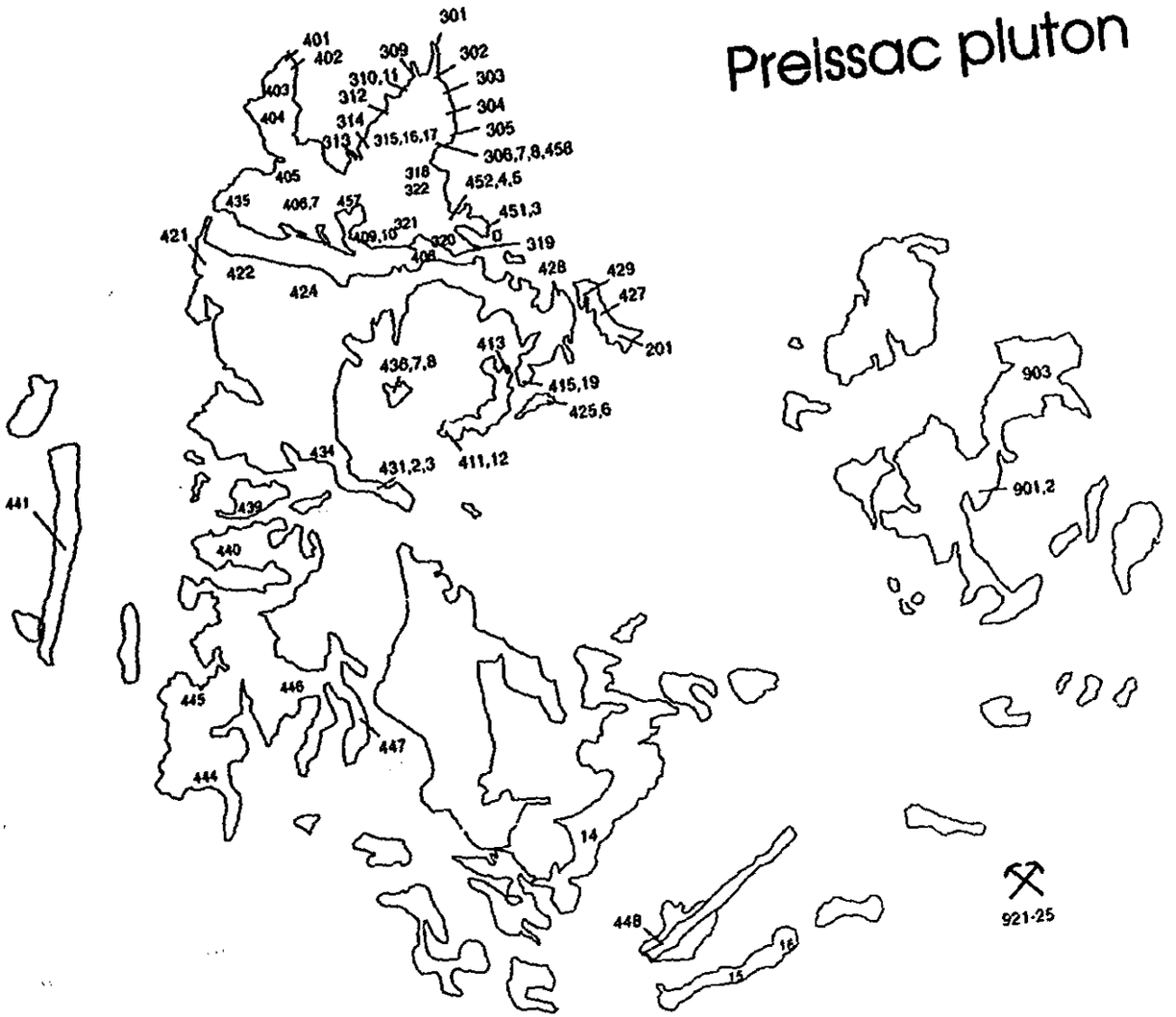
Preissac pluton
301
401
402
309
302
310,11
303
312
304
314
305
313
315,16,17
306,7,8,458
318
322
452,4,5
405
435
406,7
457
451,3
421
409,10
321
320
319
422
408
428
429
424
427
201
436,7,8
413
415,19
425,6
903
434
431,2,3
411,12
901,2
441
439
440
445
446
447
444
14
448
16
15
921-25

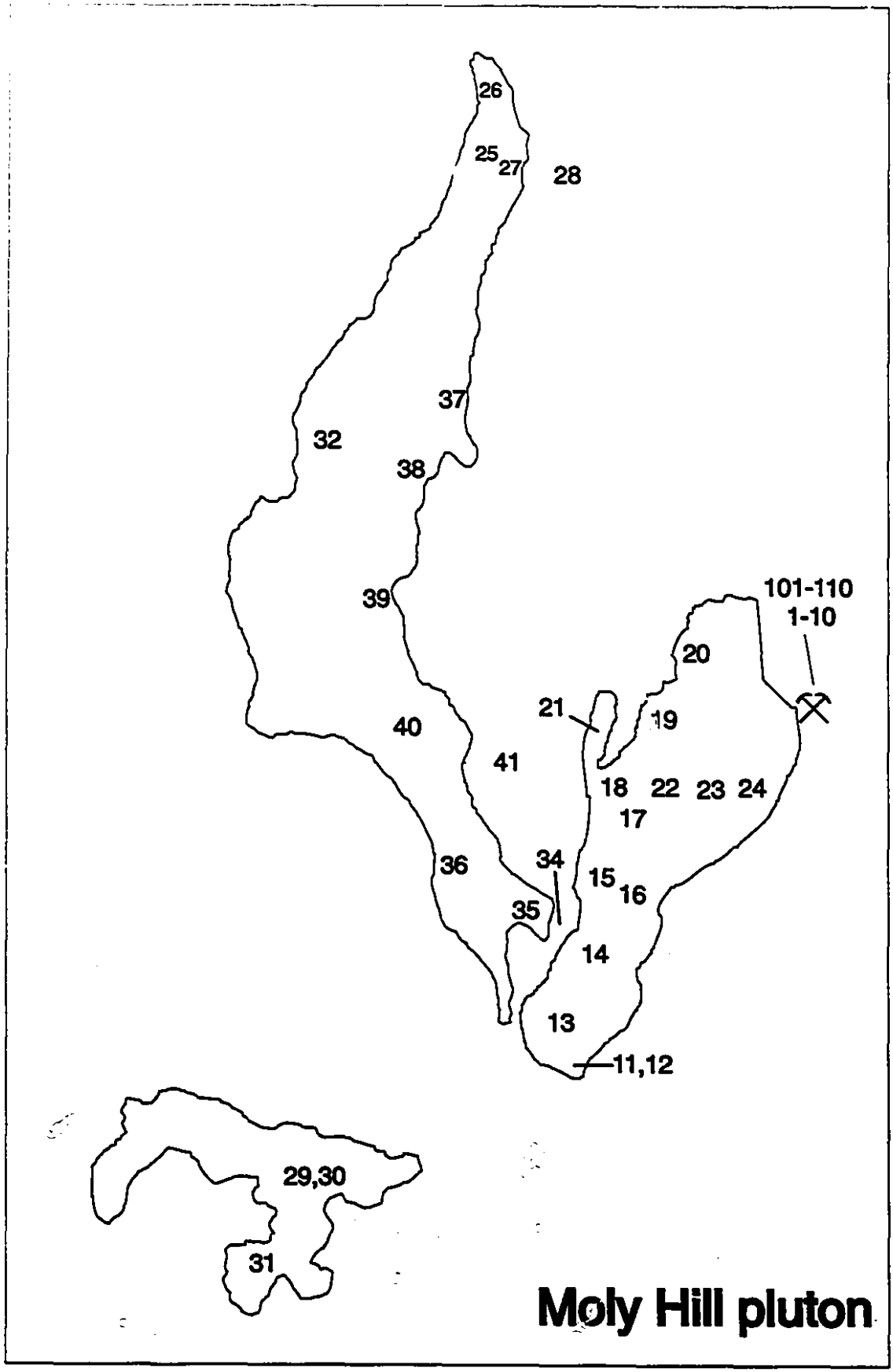
26
25
27
28
37
32
38
39
101-110
1-10
20
21
19
40
41
18
22
23
24
17
36
34
15
16
35
14
13
11,12
29,30
31
Moly Hill pluton

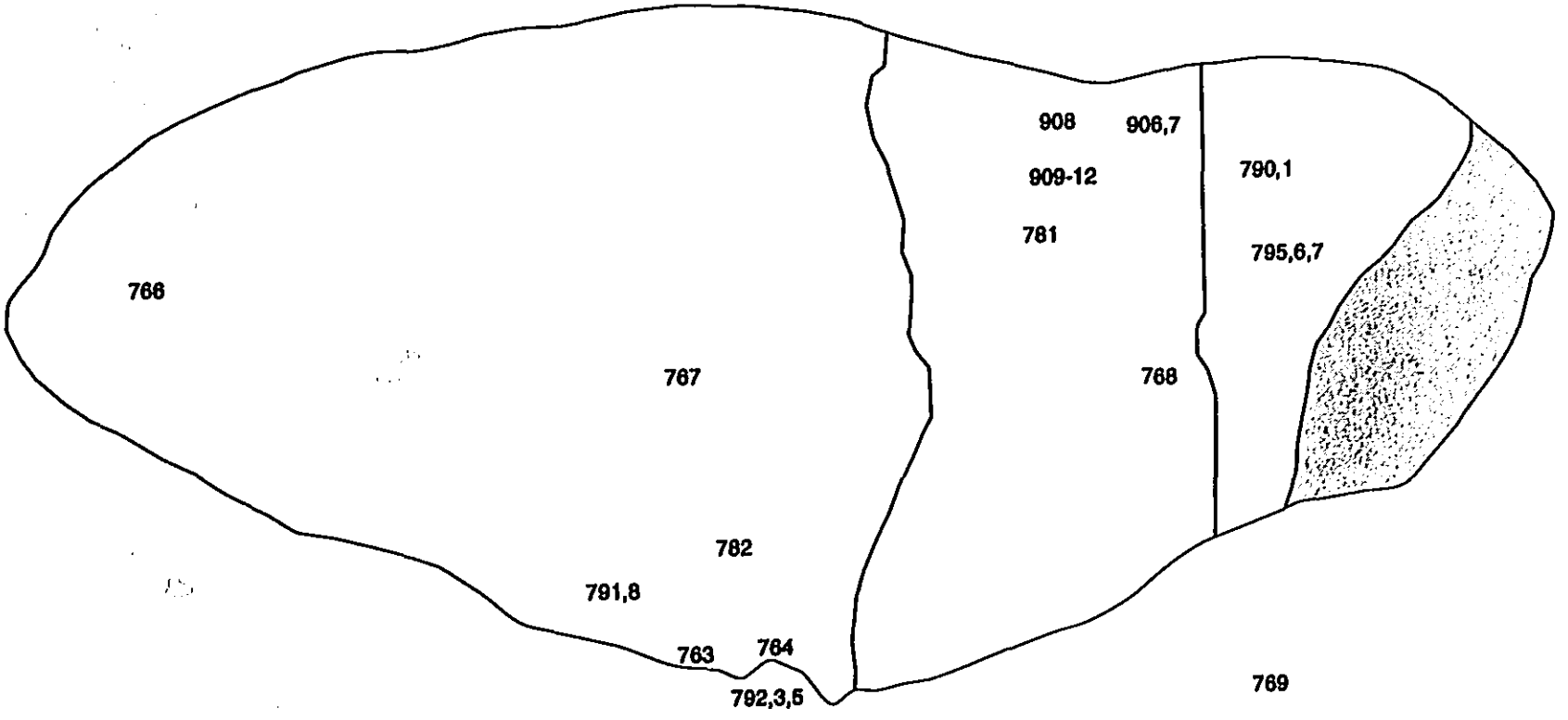

Lamotte pluton

TMC-2,3

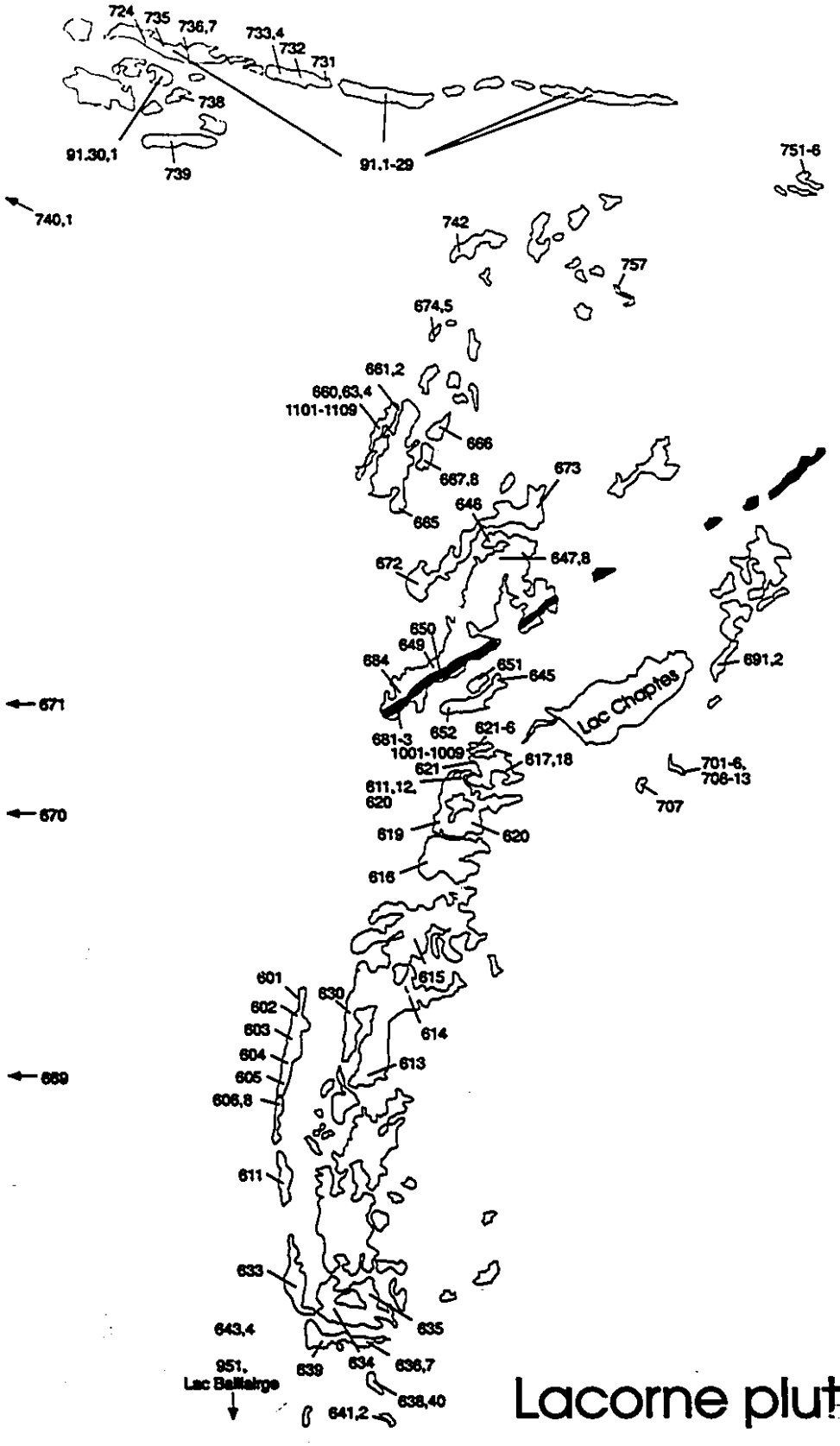

Lacorne pluton

Appendix 2

Mineral Chemistry

Composition of biotite from the Preissac pluton

	Biotite monzogranite							Two-mica monzogranite	
Sample	402	402	402	402	402	402	402	903	903
SiO2	35.89	35.55	34.58	35.78	36.93	36.37	36.27	37.00	37.08
TiO2	2.90	3.22	2.66	2.20	2.56	2.58	2.22	2.80	2.48
Al2O3	16.39	16.11	17.80	17.03	16.78	16.76	17.35	17.07	17.21
FeO	25.92	25.55	24.97	25.93	25.48	25.33	24.52	22.31	21.59
MnO	0.95	0.89	0.75	0.98	0.95	0.89	0.83	0.77	0.70
MgO	3.89	4.06	4.12	4.22	4.12	4.15	4.33	5.40	5.60
Na2O	0.02	0.04	0.08	0.05	0.08	0.14	0.10	0.04	0.01
K2O	10.05	10.06	9.23	9.86	9.85	9.84	9.98	10.24	10.15
F	0.62	0.67			0.59	0.69	0.67	1.34	1.37
	96.63	96.15	94.19	96.05	97.34	96.75	96.27	96.97	96.19
F=O	0.26	0.28	0.00	0.00	0.25	0.29	0.28	0.56	0.58
Total	96.37	95.87	94.19	96.05	97.09	96.46	95.99	96.41	95.61
Si	5.647	5.625	5.496	5.615	5.717	5.680	5.673	5.719	5.666
Ti	0.343	0.383	0.318	0.259	0.298	0.303	0.261	0.325	0.285
ivAl	2.353	2.375	2.504	2.385	2.283	2.320	2.327	2.281	2.281
vlAl	0.687	0.628	0.831	0.766	0.779	0.765	0.870	0.829	0.829
Al(t)	3.040	3.004	3.335	3.151	3.062	3.085	3.197	3.110	3.100
Fe	3.411	3.380	3.320	3.404	3.300	3.308	3.207	2.884	2.759
Mn	0.126	0.119	0.101	0.130	0.124	0.118	0.109	0.101	0.091
Mg	0.912	0.957	0.977	0.987	0.952	0.966	1.008	1.244	1.275
Na	0.007	0.011	0.025	0.014	0.026	0.043	0.030	0.013	0.003
K	2.016	2.031	1.873	1.975	1.946	1.961	1.990	2.020	1.979
F	0.309	0.335			0.287	0.339	0.331	0.653	0.662

Composition of muscovite from the Preissac pluton

	Biotite monzogranite			Two-mica monzogranite			Muscovite monzogranite												
Sample	402	402	402	902	903	903	302	303	303	304	304	319	403	403	406	406	421	424	428
SiO2	46.93	46.88	46.76	47.24	46.72	46.43	46.95	46.50	45.51	47.37	46.83	45.96	46.14	45.77	46.56	46.71	48.08	45.60	46.30
TiO2	0.91	1.09	0.73	0.97	0.81	0.84	0.62	0.23	0.04	0.18	0.20	0.40	0.00	0.31	0.00	0.43	0.26	0.46	0.43
Al2O3	27.82	29.51	29.43	28.87	28.97	28.47	27.14	31.50	35.62	31.96	31.38	30.63	34.03	31.14	36.76	31.09	31.26	30.74	30.54
FeO	6.11	5.31	5.53	5.58	5.39	5.76	6.21	4.27	2.27	4.66	5.09	5.01	2.93	4.85	0.42	4.93	5.26	4.90	4.85
MnO	0.11	0.08	0.13	0.10	0.11	0.11	0.15	0.06	0.04	0.11	0.08	0.06	0.14	0.10	0.01	0.04	0.08	0.03	0.08
MgO	1.45	1.21	1.22	1.42	1.39	1.31	1.73	0.43	0.24	0.36	0.44	0.63	0.10	0.40	0.03	0.60	0.61	0.67	0.73
Na2O	0.15	0.21	0.26	0.23	0.28	0.20	0.20	0.30	0.30	0.20	0.29	0.23	0.27	0.29	0.23	0.24	0.25	0.33	0.23
K2O	11.38	11.34	11.46	11.44	11.36	11.50	11.25	11.58	10.92	11.05	10.82	11.42	11.46	11.68	11.52	11.39	11.11	11.16	11.17
F		0.32	0.45																
Total	94.86	95.63	95.52	95.85	95.03	94.62	94.25	94.87	94.94	96.09	95.13	94.34	95.07	94.54	95.53	95.43	96.91	93.89	94.33
Si	6.484	6.392	6.397	6.439	6.421	6.430	6.534	6.353	6.119	6.375	6.375	6.345	6.237	6.312	6.166	6.358	6.429	6.316	6.374
Ti	0.095	0.112	0.075	0.100	0.083	0.087	0.064	0.024	0.004	0.018	0.021	0.041	0.000	0.032	0.000	0.044	0.026	0.048	0.044
iv Al	1.516	1.608	1.603	1.561	1.579	1.570	1.466	1.647	1.881	1.625	1.625	1.655	1.763	1.688	1.834	1.642	1.571	1.684	1.626
vi Al	3.013	3.135	3.143	3.078	3.114	3.077	2.985	3.426	3.764	3.446	3.410	3.328	3.659	3.373	3.903	3.347	3.356	3.333	3.330
Al	4.529	4.743	4.745	4.639	4.693	4.647	4.451	5.073	5.645	5.071	5.035	4.984	5.422	5.061	5.738	4.988	4.927	5.017	4.955
Fe	0.706	0.605	0.632	0.636	0.619	0.667	0.723	0.488	0.255	0.547	0.580	0.578	0.331	0.559	0.046	0.562	0.558	0.568	0.559
Mn	0.013	0.009	0.015	0.012	0.012	0.013	0.018	0.007	0.005	0.013	0.009	0.007	0.016	0.012	0.001	0.005	0.009	0.003	0.010
Mg	0.298	0.245	0.250	0.288	0.286	0.271	0.359	0.088	0.049	0.072	0.089	0.130	0.021	0.082	0.007	0.121	0.121	0.138	0.149
Na	0.039	0.055	0.068	0.060	0.075	0.055	0.053	0.081	0.077	0.052	0.077	0.063	0.072	0.078	0.060	0.063	0.065	0.090	0.061
K	2.005	1.972	2.000	1.990	1.991	2.031	1.998	2.018	1.872	1.897	1.879	2.011	1.976	2.056	1.947	1.978	1.895	1.971	1.962

Composition of muscovite from the Preissac pluton

	Muscovite monzogranite														Muscovite-garnet monzogranite				
Sample	428	428	428	435A	435B	443	443	445	459B	201A	201A	201A	201A	201A	201	201	201	201	201
SiO2	47.19	46.52	46.52	46.51	45.93	47.20	47.07	44.48	46.36	46.51	44.90	46.56	48.82	46.86	46.17	47.11	46.92	46.17	46.65
TiO2	0.44	0.42	0.34	0.20	0.26	0.02	0.49	0.55	1.05	0.26	0.30	0.53	0.14	0.30	0.27	0.27	0.25	0.28	0.09
Al2O3	30.71	31.03	30.59	31.61	32.18	35.35	29.64	30.28	29.97	31.21	30.59	31.50	32.68	32.23	31.12	30.47	30.90	31.11	30.96
FeO	5.00	4.86	4.82	4.06	3.84	1.08	4.96	5.33	4.56	4.64	4.53	5.17	3.63	4.92	5.93	5.51	5.46	5.70	5.40
MnO	0.10	0.07	0.03	0.15	0.11	0.00	0.13	0.13	0.14	0.11	0.09	0.10	0.50	0.11	0.12	0.18	0.01	0.09	0.14
MgO	0.76	0.55	0.69	0.41	0.39	0.22	1.09	0.69	0.57	0.49	0.47	0.52	0.28	0.41	0.47	0.62	0.55	0.51	0.59
Na2O	0.23	0.19	0.16	0.30	0.32	0.27	0.28	0.26	0.21	0.23	0.37	0.23	0.09	0.26	0.23	0.22	0.23	0.28	0.28
K2O	11.17	11.52	11.35	11.14	10.71	11.62	11.24	10.83	11.21	11.38	10.52	10.57	10.57	11.07	10.98	10.80	11.12	11.22	10.78
F																			
Total	95.60	95.16	94.50	94.38	93.74	95.76	94.90	92.55	94.07	94.83	91.77	95.18	96.71	96.16	95.29	95.18	95.44	95.36	94.89
Si	6.404	6.356	6.392	6.365	6.306	6.261	6.443	6.261	6.397	6.364	6.333	6.332	6.456	6.314	6.318	6.426	6.389	6.317	6.381
Ti	0.045	0.043	0.035	0.020	0.027	0.002	0.051	0.059	0.109	0.027	0.032	0.055	0.014	0.030	0.028	0.028	0.025	0.028	0.009
iv Al	1.596	1.644	1.608	1.635	1.694	1.739	1.557	1.739	1.603	1.636	1.667	1.668	1.544	1.687	1.682	1.575	1.611	1.684	1.619
vi Al	3.315	3.352	3.346	3.464	3.512	3.788	3.226	3.283	3.272	3.397	3.418	3.381	3.550	3.431	3.337	3.324	3.348	3.334	3.371
Al	4.912	4.996	4.954	5.099	5.207	5.527	4.782	5.022	4.875	5.033	5.085	5.049	5.094	5.118	5.019	4.898	4.959	5.017	4.990
Fe	0.568	0.556	0.554	0.465	0.441	0.120	0.568	0.627	0.526	0.532	0.534	0.587	0.401	0.554	0.679	0.628	0.621	0.653	0.618
Mn	0.011	0.008	0.004	0.018	0.013	0.000	0.015	0.015	0.017	0.013	0.011	0.011	0.056	0.012	0.014	0.021	0.002	0.011	0.017
Mg	0.154	0.113	0.141	0.063	0.080	0.044	0.223	0.145	0.117	0.099	0.099	0.105	0.056	0.082	0.097	0.126	0.112	0.103	0.121
Na	0.060	0.051	0.042	0.079	0.084	0.069	0.074	0.071	0.057	0.061	0.103	0.060	0.024	0.068	0.061	0.058	0.061	0.076	0.075
K	1.934	2.007	1.989	1.944	1.876	1.966	1.962	1.945	1.973	1.986	1.893	1.834	1.782	1.903	1.916	1.879	1.932	1.958	1.880

Composition of muscovite from the Preissac pluton

	Muscovite-garnet monzogranite																		
Sample	427	427	427	471	471	473	473	477	477	479	479	2	2	2	2	11	11	11	11
SiO2	45.87	45.89	45.58	45.49	45.89	45.94	44.95	45.76	46.29	46.75	46.33	47.49	47.55	47.00	48.80	47.84	47.22	47.68	47.09
TiO2	0.28	0.21	0.14	0.06	0.24	0.22	0.02	0.19	0.22	0.22	0.18	0.29	0.20	0.29	0.10	0.90	0.39	0.82	0.65
Al2O3	30.66	30.98	30.23	33.34	32.59	32.08	31.57	31.71	31.85	31.47	31.04	31.89	31.72	30.76	30.25	30.12	30.62	27.94	29.04
FeO	5.13	5.38	5.30	4.46	4.88	4.92	7.06	5.17	5.01	5.22	5.60	4.46	4.46	4.70	2.92	3.60	4.01	3.85	3.65
MnO	0.14	0.12	0.17	0.15	0.10	0.13	0.19	0.17	0.12	0.12	0.12	0.02	0.07	0.10		0.05	0.10	0.11	0.12
MgO	0.35	0.33	0.37	0.05	0.52	0.59	0.03	0.61	0.53	0.71	0.50	1.10	1.07	1.28	1.72	1.55	1.35	1.85	1.41
Na2O	0.39	0.42	0.43	0.14	0.39	0.20	0.11	0.35	0.22	0.31	0.20	0.33	0.28	0.41	0.24	0.22	0.14	0.30	1.41
K2O	11.03	10.95	11.09	11.18	11.26	11.54	11.41	11.33	11.14	11.02	11.33	11.21	11.35	10.92	10.99	11.40	11.58	11.25	11.60
F															0.75				
Total	93.85	94.28	93.31	94.89	95.87	95.62	95.34	95.29	95.38	95.82	95.30	96.79	96.70	95.46	95.02	95.68	95.41	93.80	94.97
Si	6.357	6.341	6.369	6.205	6.220	6.253	6.208	6.259	6.298	6.335	6.339	6.345	6.364	6.378	6.567	6.450	6.407	6.576	6.498
Ti	0.029	0.022	0.015	0.006	0.025	0.022	0.002	0.019	0.022	0.022	0.018	0.029	0.021	0.029	0.010	0.092	0.040	0.085	0.068
Iv Al	1.643	1.659	1.631	1.795	1.780	1.747	1.793	1.741	1.702	1.665	1.661	1.655	1.637	1.622	1.433	1.550	1.593	1.424	1.502
vi Al	3.364	3.375	3.347	3.565	3.426	3.399	3.345	3.370	3.405	3.360	3.345	3.367	3.366	3.297	3.364	3.237	3.304	3.117	3.221
Al	5.007	5.034	4.978	5.361	5.207	5.146	5.137	5.112	5.107	5.025	5.006	5.022	5.002	4.919	4.797	4.787	4.896	4.541	4.723
Fe	0.595	0.620	0.619	0.509	0.553	0.560	0.815	0.592	0.570	0.591	0.641	0.498	0.499	0.534	0.329	0.406	0.455	0.444	0.422
Mn	0.016	0.014	0.020	0.018	0.011	0.015	0.022	0.020	0.014	0.014	0.014	0.003	0.008	0.011		0.006	0.012	0.013	0.014
Mg	0.073	0.069	0.077	0.011	0.104	0.120	0.007	0.123	0.107	0.143	0.102	0.219	0.214	0.259	0.344	0.311	0.273	0.380	0.290
Na	0.106	0.112	0.116	0.037	0.101	0.054	0.030	0.092	0.058	0.082	0.053	0.087	0.072	0.107	0.063	0.057	0.037	0.080	0.071
K	1.949	1.926	1.976	1.945	1.948	2.003	2.009	1.977	1.934	1.905	1.978	1.910	1.938	1.890	1.887	1.961	2.004	1.979	2.041

Composition of muscovite from the Preissac pluton

Sample	12T	12B	12B	12B	12B	12B	12B	12B	13	13	13	14	14	15	15	15	15
SiO2	47.23	46.81	46.32	46.84	46.92	47.40	46.84	47.52	46.47	46.64	47.85	46.62	46.23	47.89	47.80	45.47	46.09
TiO2	0.69	0.93	0.34	0.34	0.37	0.35	0.15	0.12	0.36	0.74	0.70	0.40	0.42	0.24	0.29	0.42	0.02
Al2O3	28.58	30.38	30.30	30.85	31.36	30.34	32.49	31.55	31.08	30.98	27.59	30.91	31.93	30.00	30.05	31.62	34.17
FeO	3.75	3.73	3.78	3.65	3.86	3.74	3.03	2.60	4.04	3.93	3.90	4.11	4.12	3.84	3.90	3.92	2.06
MnO	0.09	0.10	0.11	0.06	0.04	0.08	0.11	0.14	0.06	0.03	0.12	0.07	0.06	0.19	0.14	0.06	0.12
MgO	1.49	1.38	1.27	1.23	1.29	1.65	0.83	1.18	1.31	1.08	1.53	1.21	0.83	1.50	1.45	1.13	0.61
Na2O	0.38	0.33	0.33	0.34	0.42	0.45	0.14	0.15	0.31	0.22	0.21	0.18	0.37	0.12	0.24	0.27	0.21
K2O	11.71	11.13	11.17	11.24	11.39	11.32	11.78	11.68	11.40	11.43	11.46	11.52	11.35	11.53	11.49	11.42	11.47
F																	
Total	93.92	94.79	93.62	94.57	95.65	95.33	95.37	94.94	95.03	95.05	93.36	95.02	95.31	95.31	95.36	94.31	94.75
Si	6.523	6.379	6.396	6.392	6.344	6.425	6.327	6.427	6.335	6.349	6.633	6.358	6.283	6.493	6.480	6.251	6.224
Ti	0.072	0.096	0.036	0.035	0.038	0.036	0.015	0.012	0.037	0.076	0.073	0.041	0.043	0.025	0.030	0.044	0.002
iv Al	1.477	1.621	1.605	1.608	1.656	1.575	1.673	1.573	1.665	1.651	1.367	1.642	1.717	1.507	1.520	1.750	1.776
vi Al	3.174	3.259	3.326	3.355	3.342	3.273	3.499	3.456	3.329	3.320	3.142	3.326	3.397	3.287	3.281	3.374	3.661
Al	4.652	4.879	4.930	4.963	4.998	4.848	5.172	5.029	4.994	4.971	4.509	4.968	5.114	4.794	4.801	5.123	5.437
Fe	0.433	0.426	0.437	0.417	0.436	0.424	0.343	0.294	0.460	0.448	0.452	0.469	0.469	0.436	0.442	0.450	0.233
Mn	0.010	0.012	0.013	0.009	0.005	0.009	0.013	0.017	0.006	0.004	0.014	0.008	0.007	0.022	0.016	0.007	0.014
Mg	0.306	0.280	0.262	0.251	0.260	0.334	0.167	0.237	0.266	0.219	0.317	0.245	0.168	0.302	0.294	0.231	0.124
Na	0.102	0.087	0.089	0.090	0.110	0.119	0.036	0.040	0.082	0.059	0.057	0.047	0.096	0.031	0.064	0.073	0.054
K	2.063	1.936	1.968	1.957	1.965	1.958	2.029	2.015	1.982	1.985	2.026	2.005	1.968	1.994	1.986	2.002	1.976

Composition of feldspar from the Preissac pluton

	Biotite monzogranite							Two-mica monzogranite									Muscovite monzogranite		
Sample	402	402	402	402	402	402	402	403	403	902	902	902	902	903	903	903	201A	201A	201A
SiO2	64.11	66.82	67.28	67.67	64.91	68.56	68.35	65.07	69.05	69.58	67.05	66.99	65.60	67.37	66.31	65.09	68.41	69.11	65.83
Al2O3	17.94	20.51	20.35	19.81	18.08	19.27	19.25	18.23	19.30	18.96	20.46	20.47	18.05	19.41	20.87	17.65	19.86	19.30	18.33
Na2O	0.45	10.59	10.71	10.84	0.44	11.51	11.24	0.46	11.61	11.37	10.39	10.20	0.51	10.91	10.05	0.62	11.85	11.67	0.77
K2O	16.67	0.14	0.06	0.09	16.86	0.05	0.22	17.00	0.05	0.03	0.13	0.12	16.16	0.07	0.19	16.66	0.05	0.07	16.30
CaO	0.09	1.70	1.38	0.93	0.10	0.24	0.24	0.00	0.06	0.11	1.55	1.91	0.00	1.25	2.22	0.01	0.32	0.13	
Si	2.997	2.935	2.949	2.974	2.999	3.002	2.999	2.996	3.009	3.027	2.944	2.941	3.017	2.977	2.917	3.015	2.977	3.005	3.005
Al	0.989	1.062	1.052	1.026	0.984	0.995	0.996	0.989	0.991	0.972	1.059	1.059	0.978	1.011	1.083	0.964	1.018	0.989	0.986
Na	0.041	0.902	0.911	0.924	0.039	0.977	0.957	0.041	0.981	0.959	0.885	0.868	0.046	0.935	0.858	0.055	0.999	0.992	0.068
K	0.994	0.008	0.004	0.005	0.994	0.003	0.012	0.998	0.003	0.002	0.008	0.007	0.948	0.004	0.011	0.985	0.003	0.004	0.949
Ca	0.004	0.080	0.065	0.044	0.005	0.011	0.011	0.000	0.003	0.005	0.073	0.090	0.000	0.059	0.105	0.001	0.015	0.006	
Ab	4	91	93	95	4	99	98	4	99	99	92	90	5	94	88	5	98	99	7
Or	96	1	0	1	96	0	1	96		0	1	1	95	0	1	95	0	0	93
An	0	8	7	5	0	1	1		1	1	8	9		6	11	0	1	1	

Composition of feldspar from the Preissac pluton

Muscovite monzogranite

Sample	201A	201A	302	302	303	303	303	304	304	304	309	309	320	320	320	320	406	406	403
SiO2	65.43	65.03	67.44	65.13	68.68	68.95	65.27	64.60	64.68	67.70	68.56	65.33	69.11	67.63	64.43	65.10	64.96	69.14	68.87
Al2O3	18.31	18.17	20.56	17.96	19.40	18.68	17.34	18.13	18.13	19.62	19.44	18.08	19.16	19.57	18.00	18.07	17.97	19.69	19.64
Na2O	0.57	0.35	10.61	0.34	11.09	11.75	0.31	0.32	0.35	11.30	11.58	0.42	11.27	11.03	0.35	0.22	0.44	11.15	11.41
K2O	16.11	17.07	0.14	16.89	0.09	0.05	17.34	17.29	17.33	0.06	0.05	17.15	0.03	0.10	17.03	17.08	16.99	0.09	0.05
CaO	0.01	0.01	1.87	0.00	1.21	0.29	0.01	0.00	0.00	0.68	0.33	0.00	0.21	0.68	0.00		0.02	0.70	0.48
Si	3.006	2.999	2.935	3.009	2.989	3.022	3.025	2.994	2.994	2.979	2.995	3.004	3.016	2.982	2.998	3.005	3.004	2.994	2.992
Al	0.992	0.987	1.055	0.978	0.995	0.960	0.947	0.990	0.989	1.018	1.001	0.980	0.986	1.017	0.987	0.983	0.980	1.005	1.006
Na	0.051	0.031	0.912	0.031	0.936	0.998	0.028	0.029	0.031	0.964	0.980	0.037	0.954	0.943	0.032	0.019	0.039	0.936	0.961
K	0.944	1.004	0.008	0.996	0.005	0.003	1.026	1.022	1.024	0.003	0.003	1.006	0.002	0.006	1.011	1.006	1.002	0.005	0.003
Ca	0.001	0.000	0.087	0.000	0.057	0.014	0.000		0.000	0.032	0.015	0.000	0.010	0.032			0.001	0.033	0.022
Ab	5	3	91	3	94	98	3	3	3	94	97	4	99	96	3	2	4	96	97
Or	95	97	1	97	1	0	97	97	97	3		96	0	1	97	98	96	0	0
An	0	0	9	0	6	1	0		0	0	3	0	1	3			0	3	2

Composition of feldspar from the Preissac pluton

Muscovite monzogranite

Sample	421	421	421	424	424	424	427	427	427	428	428	428	434	434	435A	435A	435A	435B	435B
SiO2	69.30	65.02	64.85	64.50	64.34	68.02	68.32	66.43	64.91	65.11	69.29	68.00	64.84	67.79	64.72	65.13	67.12	67.51	66.98
Al2O3	19.50	18.23	18.26	17.95	18.06	19.69	19.14	18.62	18.11	17.92	19.28	20.29	16.77	19.29	18.00	19.07	20.23	19.92	20.03
Na2O	11.53	0.34	0.33	0.38	0.39	11.07	11.73	11.14	0.44	0.35	11.43	11.19	0.40	11.68	0.55	0.42	10.87	10.88	10.78
K2O	0.04	17.22	17.25	17.00	17.17	0.06	0.07	0.09	16.87	17.01	0.06	0.04	16.75	0.07	16.56	16.80	0.09	0.06	0.10
CaO	0.20	0.00	0.00	0.00	0.06	0.69	0.42	0.56			0.18	1.05	0.00	0.48	0.00	0.01	1.16	0.84	1.19
Si	3.005	2.996	2.993	3.001	2.992	2.984	2.997	2.998	3.001	3.009	3.012	2.957	3.026	2.987	3.004	3.005	2.952	2.971	2.957
Al	0.996	0.990	0.993	0.985	0.990	1.018	0.990	0.990	0.987	0.976	0.988	1.040	0.923	1.002	0.984	0.983	1.049	1.033	1.042
Na	0.969	0.031	0.029	0.034	0.036	0.941	0.998	0.974	0.040	0.031	0.963	0.944	0.036	0.998	0.049	0.037	0.927	0.928	0.923
K	0.002	1.012	1.016	1.008	1.019	0.003	0.004	0.005	0.995	1.003	0.003	0.002	0.997	0.004	0.980	0.989	0.005	0.004	0.005
Ca	0.010	0.000	0.000	0.000	0.003	0.032	0.020	0.027			0.009	0.049	0.000	0.023		0.001	0.055	0.040	0.057
Ab	99	3	3	3	3	96	98	97	4	3	1	95	3	97	5	4	94	96	94
Or	0	97	97	97	96	0	0	1	96	97	0	0	97	0	95	96	0	0	1
An	1				0	3	2	3			1	5		2		0	6	4	6

Composition of feldspar from the Preissac pluton

	Muscovite monzogranite							Muscovite-garnet monzogranite											
Sample	435B	443	443	445	445	459B	459B	201	201	201	201	201	201	201	471	471	471	471	473
SiO2	64.46	64.67	67.39	63.95	68.43	67.67	68.69	67.89	67.46	68.65	68.21	68.06	65.12	65.62	67.97	64.43	64.03	64.50	68.10
Al2O3	17.98	18.24	20.35	17.85	19.34	20.15	19.48	20.20	20.24	19.93	19.97	20.06	17.81	17.93	20.13	18.42	18.47	19.49	20.02
Na2O	0.31	0.51	10.65	0.31	11.19	10.48	10.22	10.88	11.38	11.41	11.32	11.37	0.74	0.30	11.60	0.66	1.34	0.47	11.35
K2O	16.72	16.83	0.09	16.93	0.03	0.06	0.07	0.11	0.12	0.05	0.74	0.06	16.21	16.94	0.05	16.54	15.56	17.12	0.07
CaO	0.00	0.02	1.41	0.06	0.19	1.17	0.73	1.03	1.03	0.84	0.74	1.05			0.69	0.01	0.02		0.66
Si	3.003	2.992	2.951	2.999	3.005	2.968	3.010	2.964	2.950	2.974	2.972	2.962	3.013	3.015	2.961	2.983	2.977	2.980	2.970
Al	0.987	0.994	1.050	0.985	1.001	1.042	1.006	1.039	1.043	1.018	1.026	1.029	0.971	0.971	1.034	1.005	1.012	1.007	1.029
Na	0.028	0.046	0.904	0.028	0.953	0.891	0.868	0.921	0.964	0.959	0.957	0.959	0.066	0.263	0.979	0.060	0.121	0.042	0.960
K	0.994	0.993	0.005	1.013	0.002	0.003	0.004	0.006	0.007	0.003	0.004	0.004	0.957	0.993	0.003	0.977	0.923	1.009	0.004
Ca	0.000	0.001	0.066	0.003	0.009	0.055	0.034	0.048	0.048	0.039	0.035	0.049			0.032	0.000	0.001		0.031
Ab	3	4	97	3	99	94	96	94	95	96	96	95	6	3	97	6	2	4	97
Or	97	95	1	97	0	0	0	1	1	0	0	0	94	97	0	94	88	96	0
An	0	0	7	0	1	6	4	5	5	4	3	5			3	0			3

Composition of feldspar from the Preissac pluton

Muscovite-garnet monzogranite

Sample	473	473	477	477	477	477	477	479	479	479	2	2	2	2	2	2	12	12	12 B
SiO2	67.45	64.30	66.88	67.42	67.44	63.87	64.30	69.17	63.59	67.83	68.42	69.58	69.66	66.32	64.11	65.15	68.59	65.26	66.89
Al2O3	20.27	18.46	19.68	19.91	19.44	17.99	18.15	20.29	17.98	19.92	19.70	19.75	19.66	19.37	18.24	18.54	20.21	18.33	20.16
Na2O	11.18	0.49	11.00	11.16	11.29	0.30	0.28	8.94	0.43	11.60	11.58	11.38	11.57	11.76	0.32	1.00	10.88	0.45	10.86
K2O	0.07	16.77	0.01	0.07	0.06	17.18	16.97	0.07	16.86	0.08	0.15	0.08	0.10	0.10	16.80	16.01	0.06	16.69	0.07
CaO	0.97	0.02	0.66	0.75	0.68			0.69		0.54	0.08	0.22	0.22	0.10			0.84		1.12
Si	2.953	2.981	2.973	2.967	2.980	2.989	2.992	3.011	2.989	2.969	2.989	3.001	3.001	2.994	2.990	2.990	2.975	2.999	2.952
Al	1.046	1.009	1.031	1.033	1.013	0.992	0.996	1.041	0.996	1.028	1.014	1.004	0.998	1.000	1.003	1.003	1.033	0.993	1.049
Na	0.949	0.045	0.948	0.952	0.968	0.028	0.026	0.754	0.039	0.985	0.981	0.952	0.967	0.999	0 029	0.089	0.915	0.040	0.929
K	0.004	0.991	0.001	0.004	0.003	1.026	1.007	0.004	1.011	0.005	0.009	0.004	0.005	0.005	1.000	0.938	0.003	0.979	0.004
Ca	0.045		0.032	0.035	0.032			0.032		0.025	0.004	0.010	0.010	0.005			0.039		0.053
Ab	95	4	97	96	96	3	2	95	4	97	99	98	98	99	3	9	96	4	95
Or	0	96	0	0	0	97	98	0	96	0	1	0	1	1	97	91	0	96	0
An	5		3	4	3			4		2	0	1	1	0			4		5

Composition of feldspar from the Preissac pluton

Muscovite-garnet monzogranite

Sample	13	13	14	14	15	15
SiO2	67.66	64.70	68.22	65.31	66.51	64.30
Al2O3	20.06	17.94	20.11	18.25	20.43	18.23
Na2O	11.39	0.20	11.09	0.37	11.06	0.47
K2O	0.05	17.25	0.13	17.03	0.07	16.65
CaO	0.59		1.02		1.42	0.03
Si	2.965	3.003	2.966	3.001	2.931	2.991
Al	1.036	0.981	1.031	0.988	1.061	0.999
Na	0.968	0.018	0.935	0.033	0.945	0.043
K	0.003	1.021	0.007	0.998	0.004	0.988
Ca	0.028		0.048		0.067	0.002
Ab	97	2	94	3	93	4
Or	0	98	1	97	0	96
An	3		5		7	0

Composition of garnet from the Preissac pluton

Muscovite monzogranite

Sample	201A	201A	201A	302	302	302	302	304	304	305	305	314	314	319	403	403	403	421	434	434
SiO2	36.39	36.09	35.87	36.82	36.72	36.90	36.88	36.12	36.53	36.30	36.29	36.22	36.27	36.59	36.81	36.96	36.95	36.99	35.92	36.36
TiO2	0.11	0.15	0.15	0.03	0.23	0.09	0.10	0.08	0.07	0.07	0.07	0.11	0.05	0.03	0.09	0.09	0.06	0.07	0.17	0.18
Al2O3	20.45	20.20	19.77	19.76	19.51	19.77	19.59	20.36	20.11	20.23	20.32	20.06	19.96	20.35	20.15	20.25	20.24	20.24	20.17	20.30
FeO	20.06	18.76	18.45	18.40	16.53	17.31	18.00	19.58	17.38	17.02	18.17	20.39	20.58	19.10	20.88	20.59	19.27	19.80	16.12	16.33
Fe2O3	0.81	0.71	1.10	1.21	1.21	1.25	1.45	0.48	0.54	0.27	0.41	0.40	0.61	0.49	0.70	0.63	0.65	0.60	0.39	0.15
MnO	22.65	23.45	23.63	22.35	23.61	23.56	22.76	22.52	24.13	24.55	23.87	20.70	20.66	22.90	20.70	20.98	22.42	21.51	25.52	25.15
MgO	0.26	0.22	0.20	0.44	0.47	0.50	0.44	0.16	0.10	0.16	0.17	0.25	0.23	0.24	0.27	0.23	0.17	0.20	0.21	0.21
CaO	0.80	0.72	0.71	0.79	0.69	0.78	0.83	0.82	0.67	0.61	0.64	0.75	0.66	0.89	0.72	0.72	0.66	0.72	0.76	0.72
Total	101.45	100.30	99.89	99.80	98.97	100.16	100.05	100.12	99.53	99.21	99.94	98.88	99.02	100.59	100.32	100.45	100.42	100.13	99.26	99.40
Si	5.947	5.961	5.968	6.060	6.101	6.073	6.083	5.967	6.048	6.025	5.988	6.031	6.040	6.004	6.048	6.058	6.061	6.074	5.975	6.017
Ti	0.014	0.019	0.019	0.004	0.029	0.011	0.012	0.010	0.009	0.009	0.009	0.014	0.006	0.004	0.011	0.011	0.007	0.009	0.021	0.022
IvAl	0.053	0.039	0.032					0.033	0.000	0.000	0.012	0.000	0.000	0.000				0.000	0.025	0.000
vlAl	3.886	3.893	3.844	3.845	3.821	3.835	3.808	3.931	3.924	3.958	3.940	3.937	3.917	3.936	3.902	3.912	3.913	3.917	3.930	3.959
Fe2+	2.744	2.592	2.569	2.540	2.296	2.382	2.483	2.705	2.407	2.362	2.507	2.840	2.866	2.621	2.868	2.822	2.643	2.718	2.242	2.259
Fe3+	0.100	0.088	0.137	0.151	0.151	0.154	0.179	0.059	0.068	0.034	0.051	0.050	0.076	0.061	0.087	0.077	0.080	0.075	0.049	0.019
Mn	3.122	3.281	3.330	3.126	3.323	3.284	3.180	3.151	3.384	3.452	3.337	2.920	2.914	3.183	2.881	2.913	3.115	2.992	3.596	3.525
Mg	0.063	0.054	0.050	0.108	0.116	0.123	0.108	0.039	0.025	0.040	0.042	0.062	0.057	0.059	0.066	0.056	0.042	0.049	0.052	0.052
Ca	0.140	0.127	0.127	0.140	0.123	0.138	0.147	0.145	0.119	0.109	0.141	0.134	0.118	0.157	0.127	0.126	0.116	0.127	0.136	0.128
Alm	45.2	42.8	42.3	43.0	39.2	40.2	42.0	44.8	40.6	39.6	41.6	47.7	48.1	43.5	48.3	47.7	44.7	46.2	37.2	37.9
Prp	1.0	0.9	0.8	1.8	2.0	2.1	1.8	0.7	0.4	0.7	0.7	1.0	1.0	1.0	1.1	1.0	0.7	0.8	0.9	0.9
Grs	0.0	0.0	0.0	0.0	0.0	0.0	0.0	0.7	0.1	0.8	0.9	0.7	0.0	1.0	0.0	0.0	0.0	0.0	0.5	1.1
Sps	51.4	54.2	54.8	52.9	56.7	55.4	53.7	52.2	57.0	57.9	55.4	49.0	48.9	52.9	48.5	49.2	52.7	50.8	59.7	59.1
Adr	2.3	2.1	2.1	2.4	2.1	2.3	2.5	1.7	1.9	1.1	1.5	1.6	2.0	1.6	2.1	2.1	2.0	2.1	1.8	1.0

Composition of garnet from the Preissac pluton

Muscovite-garnet monzogranite

Sample	201	201	201	427	427	427	471	471	471	473	473	473	473	477	477	477	477	477	477	477	477
SiO2	35.84	35.87	36.06	36.04	36.27	35.68	36.00	36.07	35.92	35.83	36.19	36.12	36.19	35.88	35.74	36.01	35.56	35.75	36.19	36.30	36.27
TiO2	0.17	0.12	0.11	0.10	0.11	0.11	0.15	0.14	0.12	0.16	0.12	0.14	0.10	0.13	0.14	0.12	0.08	0.15	0.16	0.10	0.13
Al2O3	19.79	20.15	19.96	19.51	19.49	19.35	19.96	19.92	19.93	20.02	19.99	19.83	19.73	19.60	19.78	19.79	19.66	19.42	19.31	19.34	19.57
FeO	18.69	18.40	18.66	15.43	15.69	16.22	16.43	16.15	16.11	16.37	16.39	16.48	16.07	16.20	16.04	16.40	16.11	15.78	15.73	15.55	15.57
Fe2O3	1.41	0.92	1.24	1.15	1.23	1.10	1.06	1.20	1.03	1.19	0.97	1.34	1.26	0.93	1.07	0.95	1.02	1.22	1.48	1.40	1.25
MnO	23.78	23.86	23.79	26.26	25.71	25.20	25.87	26.24	25.99	26.14	26.02	26.04	26.24	25.39	26.03	25.55	25.89	25.23	24.88	24.90	24.90
MgO	0.21	0.18	0.21	0.10	0.11	0.07	0.22	0.22	0.25	0.16	0.17	0.19	0.16	0.22	0.22	0.22	0.17	0.23	0.25	0.21	0.26
CaO	0.72	0.80	0.81	0.66	0.66	0.68	0.70	0.75	0.72	0.75	0.69	0.76	0.80	0.65	0.69	0.67	0.73	0.74	0.70	0.69	1.13
Total	100.61	100.30	100.84	99.25	99.27	98.41	100.39	100.69	100.07	100.62	100.54	100.90	100.55	99.00	99.91	99.71	99.22	98.52	98.70	98.49	99.08
Si	5.939	5.939	5.951	6.024	6.051	6.018	5.957	5.957	5.959	5.928	5.975	5.960	5.985	6.006	5.974	5.990	5.960	6.024	6.077	6.061	6.046
Ti	0.021	0.015	0.014	0.013	0.014	0.014	0.019	0.017	0.015	0.020	0.015	0.017	0.012	0.016	0.018	0.015	0.010	0.203	0.126	0.016	0.016
ivAl	0.061	0.061	0.049				0.043	0.044	0.041	0.072	0.025	0.040	0.015	0.000	0.026	0.010	0.040				
viAl	3.803	3.871	3.833	3.843	3.832	3.846	3.849	3.833	3.856	3.832	3.865	3.816	3.830	3.866	3.849	3.868	3.843	3.857	3.816	3.855	3.844
Fe2+	2.590	2.547	2.575	2.157	2.189	2.287	2.274	2.230	2.235	2.265	2.263	2.274	2.223	2.268	2.229	2.283	2.230	2.556	2.217	2.220	2.187
Fe3+	0.176	0.114	0.154	0.144	0.154	0.140	0.132	0.149	0.129	0.149	0.121	0.166	0.157	0.117	0.134	0.117	0.147	0.123	0.172	0.129	0.139
Mn	3.338	3.346	3.326	3.718	3.634	3.600	3.626	3.671	3.653	3.663	3.639	3.640	3.676	3.600	3.665	3.600	3.675	3.551	3.531	3.525	3.516
Mg	0.052	0.044	0.052	0.025	0.027	0.018	0.054	0.054	0.062	0.040	0.042	0.047	0.039	0.055	0.055	0.545	0.043	0.063	0.052	0.064	0.065
Ca	0.128	0.142	0.143	0.118	0.118	0.123	0.124	0.133	0.128	0.133	0.122	0.134	0.142	0.117	0.123	0.190	0.131	0.134	0.126	0.124	0.202
Alm	42.4	41.9	42.2	35.8	36.7	38.0	37.4	36.6	36.8	37.1	37.3	37.3	36.6	37.6	36.7	37.7	36.8	37.6	37.4	37.4	36.6
Prp	0.9	0.7	0.9	0.4	0.5	0.3	0.9	0.9	1.0	0.7	0.7	0.8	0.7	0.9	0.9	1.0	0.7	1.1	0.9	1.1	1.1
Grs	0.0	0.0	0.0	0.0	0.0	0.0	0.0	0.0	0.0	0.0	0.0	0.0	0.0	0.0	0.0	0.0	0.0	0.0	0.0	0.0	0.0
Sps	54.7	55.0	54.6	61.8	60.9	59.7	59.7	60.3	60.1	60.1	60.0	59.7	60.5	59.6	60.4	59.0	60.0	59.0	59.6	59.4	58.9
Adr	2.1	2.3	2.4	2.0	2.0	2.0	2.0	2.2	2.1	2.2	2.0	2.2	2.3	1.9	2.0	2.0	2.2	2.2	2.1	2.1	3.4

Composition of epidote from the Preissac plutton

Sample	Two-mica monzogranite 902	Muscovite monzogranite 302	Schist 26	921	921
SiO2	39.23	38.88	38.06	38.76	39.19
TiO2	0.05	0.01	0.13	0.07	0.09
Al2O3	23.68	23.02	22.77	23.85	23.54
Fe2O3	12.78	13.34	13.16	11.52	11.69
MnO	0.61	0.45	0.61	0.31	0.32
CaO	22.52	22.53	22.37	22.15	22.37
OH	3.56	3.53	3.48	3.53	3.55
Si	3.297	3.303	3.277	3.214	3.233
Ti	0.003	0.001	0.008	0.004	0.006
Al	2.345	2.304	2.311	2.331	2.289
Fe3+	0.809	0.853	0.853	0.719	0.726
Mn	0.043	0.033	0.044	0.022	0.022
Ca	2.028	2.050	2.064	1.968	1.977

Composition of oxide minerals and titanite from the Preissac pluton

	Two-mica monzogranite										Muscovite monzogranite						
Sample	902	902	902	903	903	903	903	903	903	903	903	302	302	302	402	903	302
Fe2O3	0.62	1.12	0.38	0.00	0.16	3.56	3.27	0.54	3.10	3.77	0.00	20.63	16.21	1.20	16.98		
FeO	35.94	36.99	35.67	35.15	37.25	38.67	36.10	37.84	35.94	36.58	34.91	19.43	11.91	37.67	18.92	4.51	4.36
MnO	11.13	10.09	11.27	11.46	9.68	7.13	10.04	9.10	9.45	8.70	11.49	9.87	8.25	9.07	13.59	3.30	
SiO2	0.00	0.00	0.00			0.02							6.78			21.89	31.28
Al2O3	0.00	0.00	0.00			0.04							1.83			6.10	6.22
CaO	0.00	0.00	0.00										5.72			28.85	28.23
TiO2	52.51	52.51	52.36	53.59	52.36	50.96	51.44	52.38	50.66	50.54	52.65	49.19	48.53	52.20	49.56	33.01	28.87
Total	100.20	100.71	99.68	100.20	99.45	100.28	100.85	99.86	99.15	99.59	99.05	99.12	99.23	100.14	99.05	97.66	98.96
Fe3+	0.024	0.042	0.014	0.000	0.006	0.135	0.123	0.020	0.119	0.144	0.000	0.851	0.626	0.046	0.699		0.000
Fe2+	1.514	1.550	1.510	1.470	1.578	1.624	1.512	1.596	1.529	1.551	1.481	0.721	0.414	1.586	0.700	0.562	0.409
Mn	0.475	0.429	0.483	0.486	0.415	0.304	0.426	0.389	0.407	0.374	0.494	0.412	0.323	0.387	0.566	0.417	0.002
Si	0.000	0.000	0.000	0.000	0.000	0.001		0.000			0.000		0.313		0.004	3.262	3.902
Al	0.000	0.000	0.000	0.000	0.000	0.003		0.000			0.000	0.000	0.100		0.004	1.072	0.915
Ca	0.000	0.000	0.000	0.000	0.000	0.001		0.000			0.000	0.000	0.283		0.000	3.489	3.773
Ti	1.988	1.979	1.992	2.015	1.994	1.930	1.937	1.986	1.938	1.927	2.008	1.824	1.685	1.977	1.833	3.700	2.709

Composition of biotite from the Moly Hill pluton

Sample	29	31	31	21*	26	26	41**	41
SiO2	36.81	37.61	36.04	37.40	36.85	35.81	35.86	35.32
TiO2	2.71	3.04	2.68	2.03	2.20	3.18	2.86	1.95
Al2O3	16.57	17.01	16.23	18.75	17.94	16.88	16.85	17.40
FeO	23.72	22.45	24.40	23.84	23.15	25.17	23.00	25.22
MnO	0.60	0.37	0.52	1.12	0.94	0.97	2.26	1.90
MgO	6.02	5.69	6.28	3.34	4.13	3.97	4.78	5.06
Na2O	0.09	0.03	0.02	0.07	0.06	0.03	0.05	0.08
K2O	9.90	9.89	9.52	9.40	9.63	10.01	9.70	8.77
F	0.83	0.91	0.69	0.48	0.77	0.81	0.51	0.68
Total	97.25	97.00	96.38	96.43	95.67	96.83	95.87	96.38
F=O	0.35	0.38	0.29	0.20	0.32	0.34	0.21	0.29
Total	96.90	96.62	96.09	96.23	95.35	96.49	95.66	96.09
Si	5.674	5.755	5.618	5.755	5.739	5.609	5.621	5.539
Ti	0.314	0.350	0.315	0.235	0.258	0.374	0.338	0.230
iv Al	2.327	2.245	2.382	2.245	2.261	2.391	2.379	2.461
vi Al	0.684	0.822	0.600	1.154	1.032	0.726	0.735	0.756
Al(t)	3.010	3.067	2.982	3.400	3.293	3.117	3.114	3.216
Fe 2+	3.057	2.873	3.180	3.067	3.016	3.297	3.016	3.307
Mn	0.078	0.048	0.068	0.146	0.124	0.129	0.301	0.252
Mg	1.383	1.298	1.459	0.765	0.958	0.928	1.116	1.183
Na	0.027	0.008	0.007	0.021	0.017	0.009	0.016	0.025
K	1.947	1.931	1.892	1.846	1.914	2.000	1.939	1.755
F	0.404	0.438	0.340	0.236	0.381	0.400	0.255	0.337

Composition of muscovite from the Moly Hill pluton

	Biotite monzogranite										Two-mica monzogranite								
Sample	29		31	31	31	31	31	31	31	31	31	21	21	26	26	32	32	32	35
SiO2	46.27	46.67	47.09	46.71	47.17	46.72	47.04	46.13	47.15	46.96	46.42	46.09	46.01	47.16	45.78	46.58	46.46	47.14	46.75
TiO2	0.00	1.77	0.06	1.29	0.65	1.29	1.36	0.92	0.36	0.90	0.74	0.41	0.49	0.54	0.57	0.53	0.61	0.51	0.41
Al2O3	30.25	27.39	31.18	28.57	28.57	28.05	28.12	30.10	29.80	29.01	29.75	29.17	28.76	31.90	29.76	30.95	30.49	30.54	29.89
FeO	5.75	5.84	4.53	5.42	6.16	5.24	5.63	5.39	5.00	5.71	5.28	6.29	6.57	5.29	5.96	4.85	5.06	4.93	5.81
MnO	0.00	0.14	0.06	0.02	0.01	0.00	0.07	0.04	0.03	0.04	0.03	0.17	0.23	0.13	0.16	0.11	0.17	0.08	0.09
MgO	1.18	1.50	0.84	1.34	1.65	1.46	1.56	1.39	1.38	1.47	1.15	1.28	1.25	1.18	1.18	0.80	0.92	0.87	0.91
Na2O	0.30	0.23	0.37	0.20	0.18	0.16	0.19	0.23	0.26	0.27	0.26	0.46	0.32	0.17	0.29	0.22	0.34	0.35	0.31
K2O	11.37	11.49	11.36	11.23	11.43	11.50	11.32	11.16	11.13	11.19	11.14	11.16	11.09	9.18	11.39	11.54	11.44	11.44	11.27
F	0.60	0.71	0.51	0.32	0.41	0.45	0.28	0.35	0.34	0.34	0.21	1.59	0.29	0.49	0.55	0.21	0.17	0.04	0.76
Total	95.72	95.74	96.00	95.10	96.23	94.87	95.57	95.71	95.45	95.89	94.98	96.62	95.01	96.04	95.64	95.79	95.66	95.90	96.20
F=O	0.25	0.30	0.21	0.13	0.17	0.19	0.12	0.15	0.14	0.14	0.09	0.67	0.12	0.21	0.23	0.09	0.07	0.02	0.32
Total	95.47	95.44	95.79	94.97	96.06	94.68	95.45	95.56	95.31	95.75	94.89	95.95	94.89	95.83	95.41	95.70	95.59	95.88	95.88
Si	6.348	6.446	6.388	6.432	6.447	6.461	6.452	6.309	6.435	6.418	6.390	6.367	6.385	6.331	6.316	6.342	6.344	6.395	6.397
Ti	0.000	0.185	0.630	0.133	0.067	0.134	0.140	0.095	0.037	0.092	0.077	0.042	0.052	0.055	0.059	0.054	0.063	0.052	0.042
Iv Al	1.652	1.554	1.612	1.568	1.553	1.539	1.548	1.691	1.565	1.582	1.610	1.633	1.615	1.669	1.684	1.659	1.656	1.605	1.603
vi Al	1.588	2.908	3.373	3.068	2.509	3.032	2.998	3.161	3.229	3.092	3.188	3.116	3.088	3.380	3.156	3.308	3.251	3.278	3.217
AL(I)	3.240	4.462	4.985	4.636	4.062	4.571	4.546	4.852	4.794	4.674	4.798	4.750	4.703	5.049	4.840	4.966	4.907	4.883	4.820
Fe 2+	0.660	0.675	0.514	0.624	0.704	0.606	0.646	0.617	0.571	0.653	0.608	0.727	0.763	0.594	0.688	0.552	0.578	0.559	0.665
Mn	0.006	0.016	0.640	0.003	0.002	0.000	0.009	0.005	0.004	0.005	0.003	0.020	0.027	0.015	0.018	0.013	0.020	0.010	0.011
Mg	0.242	0.310	0.170	0.274	0.336	0.300	0.320	0.284	0.281	0.300	0.236	0.263	0.258	0.236	0.242	0.162	0.187	0.176	0.185
Na	0.080	0.062	0.098	0.053	0.049	0.043	0.052	0.062	0.070	0.071	0.068	0.124	0.085	0.044	0.077	0.059	0.089	0.092	0.082
K	1.990	2.025	1.966	1.972	1.993	2.029	1.980	1.946	1.938	1.951	1.956	1.966	1.963	1.572	2.004	2.005	1.993	1.980	1.968
F	0.259	0.310	0.218	0.141	0.179	0.198	0.123	0.151	0.147	0.147	0.090	0.695	0.129	0.209	0.240	0.092	0.074	0.018	0.330

Composition of muscovite from the Moly Hill pluton

	Two-mica monzogranite														Muscovite monzogranite				
Sample	36	36	38	38	38	38	38	38	40	40	40	41	41	41	3	3	3	4	4
SiO2	46.50	47.27	45.69	45.92	45.53	45.48	45.66	46.14	45.89	46.30	47.16	45.89	46.67	46.63	45.46	45.62	45.76	45.70	45.80
TiO2	0.40	0.60	0.45	0.52	0.50	0.46	0.56	0.00	0.51	0.44	0.00	0.71	0.23	0 30	0.28	0.30	0.35	0.26	0.31
Al2O3	29.61	27.32	31.46	30.79	30.80	31.05	30.96	36.31	30.04	28.39	35.19	29.75	29.18	29.34	31.61	32.30	31.44	32.38	32.25
FeO	5.44	7.09	5.25	5.05	5.22	5.03	5.63	1.21	4.84	4.77	0.42	5.15	6.11	5.75	4.56	4.18	4.51	4.61	4.60
MnO	0.13	0.15	0.06	0.15	0.09	0.09	0.03	0.08	0.22	0.21	0.03	0.16	0.25	0.22	0.07	0.04	0.07	0.09	0.10
MgO	0.92	1.29	0.79	0.95	0.89	0.84	0.66	0.02	0.97	1.12	0.09	1.12	1.36	1.29	0.90	0.73	0.88	0.71	0.73
Na2O	0.33	0.19	0.38	0.34	0.46	0.32	0.23	0.16	0.47	0.36	0.16	0.20	0.16	0.16	0.35	0.29	0.45	0.49	0.26
K2O	11.14	11.43	11.39	11.14	11.11	11.27	11.49	11.95	11.32	11.31	11.35	11.33	11.54	11.61	11.29	11.22	11.23	11.00	11.40
F	0.60	0.31	0.34	0.34	0.68	0.68	0.55	0.13	0.60	0.30	0.13	0.20	0.27	0.00	0.15	0.15	0.26	0.37	0.51
Total	95.07	95.65	95.83	95.20	95.28	95.22	95.77	96.00	94.86	93.20	94.53	94.51	95.77	95.30	94.67	94.83	94.95	95.61	95.96
F=O	0.25	0.13	0.14	0.14	0.29	0.29	0.23	0.05	0.25	0.13	0.05	0.08	0.11	0.00	0.06	0.06	0.11	0.16	0.21
Total	94.82	95.52	95.69	95.06	94.99	94.93	95.54	95.95	94.61	93.07	94.48	94.43	95.66	95.30	94.61	94.77	94.84	95.45	95.75
Si	6.417	6.532	6.246	6.304	6.277	6.267	6.272	6.138	6.348	6.495	6.307	6.351	6.411	6.409	6.261	6.239	6.276	6.222	6.233
Ti	0.042	0.062	0.047	0.054	0.051	0.047	0.057	0.000	0.053	0.046	0.000	0.074	0.023	0.031	0.028	0.031	0.037	0.027	0.031
Iv Al	1.583	2.468	1.754	1.696	1.723	1.733	1.728	1.863	1.652	1.505	1.694	1.649	1.590	1.591	1.739	1.761	1.724	1.778	1.767
vi Al	3.232	1.980	3.313	3.285	3.283	3.310	3.284	3.829	3.246	3.188	3.853	3.203	3.135	3.162	3.372	3.445	3.358	3.418	3.407
AL(t)	4.815	4.448	5.068	4.981	5.005	5.042	5.012	5.692	4.898	4.693	5.546	4.852	4.725	4.753	5.111	5.206	5.082	5.197	5.173
Fe 2+	0.628	0.820	0.600	0.580	0.602	0.580	0.647	0.135	0.560	0.560	0.047	0.596	0.702	0.661	0.523	0.478	0.518	0.525	0.524
Mn	0.015	0.018	0.009	0.017	0.011	0.010	0.004	0.009	0.026	0.025	0.003	0.019	0.029	0.026	0.009	0.004	0.009	0.011	0.012
Mg	0.190	0.267	0.161	0.194	0.182	0.172	0.134	0.004	0.200	0.233	0.018	0.230	0.278	0.263	0.183	0.150	0.180	0.143	0.149
Na	0.089	0.051	0.100	0.090	0.122	0.085	0.062	0.040	0.127	0.098	0.042	0.053	0.042	0.043	0.093	0.077	0.119	0.131	0.068
K	1.960	2.015	1.986	1.951	1.954	1.982	2.013	2.027	1.998	2.024	1.937	1.999	2.022	2.036	1.976	1.957	1.965	1.910	1.979
F	0.260	0.136	0.147	0.148	0.296	0.296	0.240	0.055	0.261	0.133	0.055	0.088	0.118	0.000	0.064	0.064	0.112	0.159	0.221

Composition of muscovite from the Moly Hill pluton

	Muscovite monzogranite															Aplite		
Sample	5	6	6	6	9	9	10	12+	13	13	17+	17	17	20++	20	24+*	30	30
SiO2	46.39	46.14	45.69	45.48	45.20	45.80	47.10	45.52	46.37	46.06	46.49	45.99	46.42	45.68	46.11	45.58	46.49	46.20
TiO2	0.38	0.40	0.38	0.37	0.31	0.33	0.34	0.68	0.76	0.51	0.43	0.69	0.04	0.41	0.41	0.36	0.32	0.36
Al2O3	30.63	31.33	31.76	31.41	32.45	31.67	31.09	30.53	30.74	30.90	30.83	29.31	25.12	31.25	30.59	31.07	30.87	30.96
FeO	5.35	4.95	5.02	5.01	5.06	5.25	5.40	4.98	5.88	5.10	5.27	5.58	8.01	4.66	4.88	4.80	5.53	5.38
MnO	0.08	0.01	0.13	0.06	0.05	0.06	0.07	0.06	0.09	0.03	0.06	0.14	0.18	0.15	0.07	0.05	0.00	0.10
MgO	0.81	0.94	0.92	0.82	0.61	0.72	0.66	1.02	0.83	0.69	0.71	0.83	2.75	0.67	0.79	0.71	0.49	0.54
Na2O	0.26	0.35	0.35	0.32	0.30	0.24	0.26	0.41	0.52	0.33	0.22	0.28	0.05	0.38	0.36		0.17	0.21
K2O	11.55	11.34	11.22	11.47	11.20	11.24	10.90	11.23	11.18	11.39	11.52	11.46	11.33	11.41	11.19	11.40	11.38	11.54
F	0.04	0.59	0.51	0.07	0.26	0.29	0.39	0.22			0.39	0.19	0.46			0.16	0.37	0.07
Total	95.49	96.05	95.98	95.01	95.44	95.60	96.21	94.65	96.37	95.01	95.92	94.47	94.36	94.61	94.40	94.13	95.62	95.36
F=O	0.02	0.25	0.21	0.03	0.11	0.12	0.16	0.09	0.00	0.00	0.16	0.08	0.19	0.00	0.00	0.07	0.16	0.03
Total	95.47	95.80	95.77	94.98	95.33	95.48	96.05	94.56	96.37	95.01	95.76	94.39	94.17	94.61	94.40	94.06	95.46	95.33
Si	6.344	6.304	6.232	6.247	6.182	6.257	6.378	6.282	6.292	6.315	6.344	6.386	6.534	6.284	6.351	6.291	6.359	6.327
Ti	0.039	0.041	0.039	0.039	0.032	0.034	0.035	0.071	0.078	0.052	0.045	0.072	0.057	0.043	0.042	0.037	0.033	0.037
Iv Al	1.656	1.696	1.768	1.753	1.818	1.743	1.622	1.718	1.708	1.685	1.656	1.615	1.466	1.716	1.649	1.708	1.641	1.673
vi Al	3.280	3.314	3.338	3.331	3.412	3.356	3.340	3.248	3.208	3.308	3.303	3.181	2.702	3.350	3.317	3.346	3.335	3.324
AL(t)	4.936	5.010	5.106	5.085	5.230	5.099	4.962	4.966	4.916	4.993	4.959	4.796	4.168	5.066	4.966	5.055	4.976	4.997
Fe 2+	0.611	0.565	0.573	0.575	0.579	0.600	0.612	0.575	0.668	0.585	0.601	0.648	0.943	0.537	0.563	0.554	0.633	0.616
Mn	0.009	0.001	0.015	0.007	0.005	0.008	0.008	0.008	0.011	0.004	0.007	0.016	0.021	0.018	0.009	0.006	0.002	0.011
Mg	0.166	0.191	0.187	0.169	0.125	0.147	0.134	0.211	0.167	0.141	0.144	0.173	0.577	0.137	0.161	0.145	0.099	0.111
Na	0.070	0.091	0.093	0.066	0.079	0.063	0.068	0.110	0.136	0.087	0.058	0.075	0.013	0.102	0.096	0.099	0.046	0.056
K	2.015	1.977	1.952	2.009	1.954	1.959	1.884	1.978	1.935	1.991	2.006	2.029	2.034	2.003	1.965	2.007	1.986	2.017
F	0.017	0.254	0.222	0.032	0.111	0.127	0.166	0.097			0.166	0.085	0.205			0.068	0.159	0.029

Composition of feldspar from the Moly Hill pluton

	Biotite monzogranite							Two-mica monzogranite											
Sample	29	29	29	29	31	31	31	21	21	24	24	26	26	32	32	35	35	35	36
SiO2	66.85	65.41	65.85	65.13	65.75	66.46	65.00	66.93	64.79	65.99	65.05	64.71	65.13	66.74	65.49	67.45	65.50	64.81	68.59
Al2O3	21.32	21.61	18.12	18.18	21.05	20.98	17.62	20.64	17.98	20.65	18.30	18.17	21.34	20.42	17.48	20.02	17.77	18.48	19.36
Na2O	10.38	9.86	0.43	0.39	10.08	9.95	0.36	10.71	0.35	10.59	1.24	0.58	10.38	10.28	0.35	10.78	0.51	0.36	11.54
K2O	0.14	0.15	16.98	17.12	0.12	0.13	17.11	0.09	16.74	0.15	15.86	16.48	0.13	0.13	16.94	0.12	16.61	16.96	0.13
CaO	2.25	3.15	0.00	0.00	2.94	3.15	0.00	1.63	0.01	1.90			2.58	0.01	0.00	1.51	0.00	0.02	0.40
Total	100.94	100.18	101.38	100.82	99.94	100.67	100.09	100.00	99.87	99.31	100.45	100.11	99.56	97.58	100.26	99.88	100.39	100.63	100.02
Si	2.182	2.156	2.258	29.995	2.894	2.902	3.012	2.932	3.006	2.918	2.993	2.998	2.879	2.928	3.016	2.957	3.019	2.988	2.995
Al	0.817	0.839	0.732	0.987	1.092	1.080	0.962	1.066	0.983	1.076	0.992	0.992	1.112	1.056	0.968	1.035	0.965	1.004	0.997
Na	0.657	0.630	0.029	0.035	0.860	0.842	0.033	0.910	0.031	0.908	0.111	0.052	0.890	0.874	0.031	0.916	0.046	0.033	0.977
K	0.006	0.006	0.743	10.059	0.007	0.750	1.012	0.005	0.991	0.009	0.931	0.974	0.008	0.007	0.995	0.007	0.976	0.997	0.008
Ca	0.079	0.111	0.000		0.139	0.147	0.000	0.077	0.000	0.090	.	0.010		0.117	0.000	0.071	0.000	0.001	0.019
Ab	88.6	84.3	3.7	3.4	85.6	84.5	3.1	91.8	3.0	90.2	10.6	5.1	87.3	87.6	3.0	92.2	4.5	3.2	97.4
Or	0.8	0.9	96.3	96.6	0.7	0.8	96.9	0.5	96.9	0.9	89.4	94.9	0.7	0.7	97.0	0.7	95.5	96.7	0.8
An	10.6	14.9	0.0	0.0	13.8	14.8	0.0	7.7	0.0	8.9	0.0	0.0	12.0	11.7	0.0	7.2	0.0	0.1	1.9

Composition of feldspar from the Moly Hill pluton

	Muscovite monzogranite																	
Sample	36	36	38	38	40	40	40	40	40	41	41	3	3	4	4	4	6	6	6
SiO2	66.51	64.55	66.10	64.52	65.94	68.82	66.12	64.36	64.58	65.96	65.10	64.6[illegible]	67.13	64.67	63.69	66.00	65.51	64.04	63.66
Al2O3	20.79	18.27	21.03	18.39	20.90	19.00	21.38	18.09	17.99	21.15	17.97	18.58	20.22	18.53	18.25	19.92	21.21	18.49	18.62
Na2O	10.35	0.96	10.53	0.42	10.47	11.72	10.35	0.33	0.37	10.42	0.53	0.48	11.44	0.38	0.65	11.70	10.98	0.57	0.39
K2O	0.12	16.30	0.14	16.86	0.06	0.06	0.12	17.03	17.11	0.08	16.67	16.64	0.13	16.83	16.40	0.03	0.09	16.55	16.71
CaO	1.87	0.00	1.93	0.00	2.39	0.38	2.76	0.01	0.01	2.30	0.02		0.85			0.37	1.72		
Total	99.64	100.08	99.73	100.19	99.76	99.98	100.73	99.82	100.06	99.91	100.29	100.32	99.77	100.41	98.99	100.02	99.51	99.65	99.38
Si	2.924	2.989	2.909	2.987	2.994	2.256	2.887	2.994	2.998	2.899	0.651	2.984	2.948	2.983	2.983	2.971	2.892	2.979	2.971
Al	1.077	0.997	1.091	1.004	1.085	0.734	1.100	0.992	0.984	1.096	0.180	1.011	1.047	1.011	1.008	1.026	1.104	1.014	1.024
Na	0.883	0.086	0.898	0.037	0.895	0.745	0.876	0.030	0.034	0.888	0.005	0.043	0.974	0.034	0.059	0.991	0.940	0.052	0.036
K	0.007	0.963	0.008	0.996	0.004	0.003	0.007	1.011	1.014	0.004	0.167	0.980	0.007	0.994	0.980	0.001	0.005	0.982	0.995
Ca	0.088	0.000	0.091	0.000	0.113	0.014	0.129	0.001	0.000	0.108	0.000		0.040			0.017	0.081		
Ab	90.3	8.2	90.1	3.6	88.5	98.0	86.6	2.9	3.2	88.7	4.6	4.2	95.4	3.3	5.7	98.2	91.6	5.0	3.5
Or	0.7	91.8	0.8	96.4	0.4	0.3	0.7	97.1	96.8	0.4	95.[illegible]	95.8	0.7	96.7	94.2	0.1	0.5	95.0	96.5
An	9.0	0.0	9.1	0.0	11.2	1.7	12.8	0.1	0.0	10.8	0.1	0.0	3.9	0.0	0.0	1.7	7.9	0.0	0.0

Composition of feldspar from the Moly Hill pluton

Sample	9	9	13	13	12	12	20	20	20	20
SiO2	64.16	65.55	64.08	66.97	63.45	66.05	64.84	64.88	66.39	66.67
Al2O3	18.54	21.18	18.33	20.24	18.56	20.89	18.23	18.25	20.16	20.43
Na2O	0.59	10.51	0.59	11.06	0.39	10.68	0.39	0.86	11.11	10.87
K2O	16.54	0.10	16.74	0.15	16.69	0.14	17.16	16.48	0.09	0.14
CaO		1.70	0.02	1.43		1.31		0.02	1.51	1.66
Total	99.89	99.04	99.83	99.85	99.09	99.15	100.65	100.49	99.26	99.80
Si	2.978	2.902	2.981	2.941	2.972	2.919	2.994	2.992	2.923	2.931
Al	1.014	1.105	1.005	1.048	1.025	1.088	0.992	0.992	1.070	1.058
Na	0.053	0.902	0.053	0.942	0.035	0.915	0.035	0.077	0.948	0.926
K	0.979	0.006	0.993	0.008	0.998	0.008	1.010	0.970	0.530	0.790
Ca		0.081	0.001	0.067		0.062			7.130	7.820
Ab	5.2	91.3	5.1	92.6	3.4	92.9	3.3	7.4	92.5	91.5
Or	94.9	0.6	94.9	0.8	96.6	0.8	96.7	92.6	0.5	0.8
An	0.0	8.2	0.1	6.6	0.0	6.3	0.0	0.0	7.0	7.7

Composition of garnet from the Moly Hill pluton

	Two-mica monzogranite								Muscovite monzogranite											
Sample	35	35	35	36	36	36	36	36	3	3	3	3	4	4	4	4	5	5	10	10
SiO2	36.17	36.37	36.50	36.78	36.84	36.83	37.02	36.96	36.31	36.83	36.36	36.60	36.33	36.83	0.36	37.18	36.22	36.48	36.50	36.68
TiO2	0.14	0.19	0.17	0.04	0.07	0.05	0.03	0.01	0.12	0.11	0.10	0.04	0.10	0.03	0.08	0.05	0.17	0.11	0.12	0.15
Al2O3	20.13	20.02	19.79	20.26	20.02	20.37	20.27	20.35	20.31	20.17	20.34	20.36	20.30	20.61	20.27	20.69	20.01	20.42	20.41	20.44
FeO	17.52	18.06	17.06	19.90	18.90	19.64	20.18	20.35	21.00	20.87	20.98	21.04	21.24	22.37	22.02	22.20	20.17	22.52	21.44	21.80
Fe2O3	0.68	0.94	1.06	0.52	0.87	0.45	0.54	0.57	0.38	0.82	0.41	0.56	0.46	0.34	0.55	0.34	0.69	0.38	0.29	0.38
MgO	0.28	0.30	0.27	0.33	0.34	0.32	0.33	0.33	0.59	0.64	0.56	0.61	0.48	0.55	0.53	0.55	0.48	0.47	0.49	0.45
MnO	23.99	23.62	24.34	20.19	20.99	20.64	19.55	19.65	20.02	20.00	20.28	20.34	20.02	19.43	19.35	19.49	20.64	19.14	19.85	19.76
CaO	1.11	1.19	1.10	1.62	1.74	1.72	1.53	1.68	1.16	1.14	1.08	0.96	1.22	0.83	1.15	0.87	1.16	1.01	1.05	1.09
Total	100.02	100.69	100.29	99.64	99.77	100.02	99.45	100.10	99.89	100.58	100.11	100.51	100.16	100.98	100.21	101.36	99.74	100.53	100.15	100.75
Si	5.977	5.981	6.020	6.054	6.064	6.041	6.090	6.055	5.978	6.014	5.976	5.988	5.972	5.997	5.962	6.020	5.981	5.976	5.991	5.990
Ti	0.017	0.024	0.021	0.005	0.009	0.006	0.004	0.001	0.015	0.013	0.013	0.005	0.013	0.004	0.010	0.006	0.021	0.014	0.015	0.018
IvAl	0.023	0.020							0.023		0.024	0.012	0.027	0.004	0.038		0.019	0.024	0.009	0.010
vlAl	3.898	3.860	3.847	3.930	3.884	3.938	3.930	3.929	3.918	3.881	3.915	3.926	3.907	3.951	3.891	3.948	3.876	3.919	3.940	3.924
Fe2+	2.422	2.483	2.354	2.740	2.603	2.694	2.776	2.788	2.891	2.850	2.883	2.879	2.920	3.046	3.029	3.006	2.786	3.085	2.944	2.977
Fe3+	0.058	0.116	0.132	0.065	0.107	0.056	0.066	0.070	0.048	0.101	0.051	0.070	0.057	0.041	0.068	0.041	0.086	0.047	0.036	0.047
Mg	0.069	0.074	0.066	0.081	0.083	0.078	0.081	0.081	0.145	0.155	0.137	0.150	0.117	0.133	0.131	0.133	0.118	0.115	0.120	0.109
Mn	3.358	3.290	3.401	2.815	2.927	2.668	2.724	2.727	2.791	2.767	2.823	2.819	2.788	2.679	2.695	2.674	2.916	2.656	2.761	2.734
Ca	0.197	0.210	0.194	0.286	0.307	0.302	0.270	0.330	0.204	0.199	0.191	0.169	0.215	0.146	0.203	0.151	0.205	0.178	0.184	0.191
Alm	40	41	39	46	44	45	47	47	48	48	48	48	48	51	50	50	46	51	49	50
Prp	1.1	1.2	1.1	1.4	1.4	1.3	1.4	1.4	2.4	2.6	2.3	2.5	2.0	2.2	2.2	2.2	2.0	1.9	2.0	1.8
Grs	0.7	0.0	0.0	3.1	2.3	3.5	2.8	3.8	1.8	0.5	1.6	1.0	1.8	1.3	1.4	1.4	0.7	1.5	1.8	1.6
Sps	56	54	57	48	49	48	47	46	46	46	47	47	46	45	45	45	49	44	46	46
Adr	2.5	3.5	3.2	1.8	2.9	1.6	1.8	1.8	1.4	2.7	1.5	1.8	1.6	1.1	1.8	1.1	2.5	1.4	1.1	1.5

Composition of garnet from the Moly Hill pluton

	Muscovite monzogranite																	Aplite		
Sample	10	12	12	17	17	17	17	19	19	19	19	20	20	20	22	22	22	30	30	30
SiO2	36.58	36.62	36.48	36.85	37.02	36.71	36.70	36.51	36.70	36.87	36.94	36.38	36.89	36.60	36.79	37.05	37.02	36.31	36.35	36.72
TiO2	0.06	0.07	0.10	0.01	0.06	0.09	0.11	0.07	0.13	0.01	0.04	0.09	0.13	0.09	0.04	0.11	0.01	0.06	0.07	0.04
Al2O3	20.32	19.94	19.94	20.29	20.21	20.18	20.43	20.01	19.61	20.27	20.02	20.50	20.24	20.20	20.33	20.07	20.38	20.31	20.21	20.64
FeO	22.34	19.11	14.53	21.15	20.54	19.82	20.14	20.47	20.63	21.91	21.59	21.55	21.01	22.27	21.91	19.37	21.86	21.08	21.33	21.58
Fe2O3	0.61	0.84	2.58	0.64	0.65	0.61	0.04	0.65	1.18	0.64	0.95	0.45	0.65	0.60	0.45	0.82	0.51	0.47	0.47	0.07
MgO	0.59	0.37	0.31	0.35	0.32	0.29	0.29	0.38	0.42	0.43	0.51	0.44	0.40	0.44	0.48	0.42	0.51	0.30	0.29	0.29
MnO	19.08	21.06	24.37	19.43	19.47	21.05	20.87	20.07	19.41	19.22	18.06	20.34	20.22	19.31	18.15	21.16	18.22	20.33	19.86	19.63
CaO	0.95	1.41	1.04	1.56	1.54	1.23	1.14	1.01	1.02	0.89	1.78	0.90	1.08	1.10	1.52	0.94	1.43	1.30	1.16	1.32
Total	100.53	99.42	99.35	100.28	99.81	99.98	99.72	99.17	99.10	100.24	99.89	100.65	100.62	100.81	99.67	99.94	99.94	100.16	99.74	100.29
Si	5.989	6.056	6.052	6.041	6.079	6.041	6.017	6.053	6.093	6.050	6.069	5.995	6.025	5.985	6.049	6.085	6.066	5.976	5.999	6.011
Ti	0.007	0.009	0.013	0.001	0.007	0.011	0.014	0.009	0.016	0.001	0.005	0.011	0.016	0.011	0.005	0.014	0.001	0.007	0.009	0.510
IvAl	0.011											0.005		0.015				0.025	0.001	
vlAl	3.909	3.887	3.899	3.920	3.912	3.914	3.996	3.910	3.837	3.920	3.877	3.928	3.920	3.877	3.940	3.885	3.936	3.914	3.930	3.982
Fe2+	3.058	2.644	2.249	2.899	2.822	2.728	2.794	2.839	2.665	3.006	2.967	2.934	2.869	3.045	3.013	2.661	2.995	2.901	2.944	2.955
Fe3+	0.075	0.105	0.089	0.079	0.081	0.075	0.005	0.081	0.147	0.079	0.118	0.056	0.080	0.098	0.055	0.101	0.063	0.059	0.059	0.009
Mg	0.144	0.091	0.077	0.086	0.078	0.071	0.072	0.094	0.104	0.105	0.125	0.107	0.098	0.108	0.118	0.103	0.125	0.073	0.071	0.072
Mn	2.646	2.950	3.425	2.698	2.709	2.934	2.934	2.819	2.730	2.672	2.514	2.805	2.797	2.674	2.528	2.944	2.529	2.834	2.776	2.722
Ca	0.166	0.250	0.185	0.274	0.271	0.217	0.203	0.179	0.181	0.157	0.313	0.158	0.189	0.193	0.268	0.165	0.251	0.230	0.206	0.231
Alm	51	45	38	49	48	46	47	48	49	51	50	49	48	51	51	45	51	48	49	49
Prp	2.4	1.5	1.3	1.4	1.3	1.2	1.2	1.6	1.8	1.8	2.1	1.8	1.6	1.8	1.9	1.8	2.1	1.2	1.2	1.2
Grs	0.7	1.4	0.6	2.6	2.4	1.5	2.9	0.7	0.0	0.6	2.2	1.0	0.7	0.5	3.0	0.0	2.6	1.8	3.4	3.9
Sps	44	50	58	45	16	49	49	48	46	45	42	47	47	45	43	50	43	47	46	46
Adr	2.0	2.9	2.6	2.0	2.3	2.2	0.5	2.3	3.1	2.0	3.1	1.6	2.3	2.6	1.5	2.8	1.6	2.0		

Composition of oxide minerals from the Moly Hill pluton

	Biotite monzogranite		Two-mica monzogranite							
Sample	31	31	31	26	40	40	40	40	40	40
Fe2O3	0.00	3.77	67.87	67.84	7.34	0.00	69.18	68.48	68.93	69.29
FeO	35.19	41.30	30.71	31.15	19.96	34.43	31.02	30.78	30.91	31.11
MnO	8.80	3.83	0.04		22.36	11.77	0.10	0.04	0.11	0.08
SiO2	0.71	0.04	0.10			0.23	0.05	0.07	0.03	0.04
Al2O3	0.47	0.02	0.05			0.09	0.04	0.03	0.03	0.04
CaO	0.13	0.40	0.02			0.21	0.00	0.00		0.00
TiO2	53.29	50.29	0.10	0.02	49.08	52.51	0.00	0.00		
Total	98.59	99.65	98.89	99.01	98.74	99.24	100.39	99.40	100.01	100.56
Fe3+	0.000	0.144	15.892	15.912	0.282	0.000	15.968	15.963	15.977	15.973
Fe2+	1.478	1.752	7.993	8.121	0.851	1.456	7.959	7.976	7.963	7.971
Mn	0.374	0.165	0.011		0.965	0.504	0.027	0.011	0.030	0.020
Si	0.036	0.002	0.033	0.000	0.000	0.012	0.016	0.023	0.009	0.012
Al	0.028	0.001	0.019	0.000	0.000	0.006	0.016	0.010	0.012	0.015
Ca	0.007	0.022	0.007	0.000	0.000	0.011	0.000	0.008		
Ti	2.013	1.919	0.024	0.005	1.881	1.997	0.000			

Composition of biotite from the Lamotte pluton

Biotite monzogranite

Sample	767	767	768	768	782	782	782	782	797	797	908	908	908	911	911	911	911	766	766
SiO2	37.11	35.65	35.99	34.76	36.02	35.82	37.17	36.83	36.59	35.72	37.80	38.84	37.77	38.32	38.83	38.42	36.95	36.80	38.29
Al2O3	18.37	17.90	18.67	17.83	17.29	17.48	18.04	18.27	20.95	20.31	20.09	20.03	20.02	20.90	21.02	19.98	21.12	19.20	18.63
TiO2	0.93	1.97	1.06	2.43	2.40	2.30	1.20	0.96	1.35	1.56	1.35	1.33	1.31	2.23	2.01	2.10	2.21	1.05	1.16
FeO	23.13	24.12	24.13	25.30	23.50	23.99	22.23	22.16	22.10	23.27	21.14	20.62	21.42	19.97	17.95	19.50	20.70	21.78	21.18
MgO	4.94	4.75	4.56	4.89	5.00	5.12	5.30	5.57	2.71	2.63	3.52	3.29	3.25	3.28	3.39	3.38	2.91	4.49	4.74
MnO	0.82	0.90	0.69	0.68	0.78	0.79	0.77	0.96	0.54	0.60	0.72	0.61	0.81	0.47	0.57	0.66	0.58	1.00	1.02
Na2O	0.06	0.02	0.07	0.02	0.02	0.03	0.04	0.02	0.05	0.06	0.06	0.01	0.03	0.04	0.04	0.03	0.03	0.02	0.04
K2O	9.29	9.99	9.83	9.30	10.10	9.61	9.70	9.42	9.12	8.91	9.92	9.81	9.79	9.80	10.11	10.09	9.78	9.63	9.13
F	0.71	0.80	0.59	0.72	0.83	0.85	1.01	1.31	0.91	0.86	0.80	0.93	0.72	1.20	1.21	1.32	1.08	0.77	0.90
total	95.36	96.10	95.59	95.93	95.94	95.99	95.46	95.50	94.32	93.92	95.40	95.47	95.12	96.21	95.13	95.48	95.36	94.74	95.09
F=O	0.30	0.34	0.25	0.30	0.35	0.36	0.43	0.55	0.38	0.36	0.34	0.39	0.30	0.51	0.51	0.56	0.45	0.32	0.38
Total	95.06	95.76	95.34	95.63	95.59	95.63	95.03	94.95	93.94	93.56	95.06	95.08	94.82	95.70	94.62	94.92	94.91	94.42	94.71
Si	5.770	5.595	5.636	5.481	5.642	5.608	5.779	5.743	5.705	5.640	5.812	5.932	5.826	5.730	5.894	5.882	5.684	5.740	5.900
ivAl	2.230	2.405	2.364	2.519	2.359	2.392	2.221	2.257	2.295	2.360	2.188	2.068	2.174	2.270	2.106	2.118	2.316	2.260	2.100
vlAl	1.137	0.906	1.081	0.795	0.833	0.833	1.085	1.099	1.555	1.420	1.453	1.537	1.465	1.414	1.655	1.486	1.513	1.269	1.284
Al(t)	3.367	3.312	3.446	3.314	3.192	3.225	3.306	3.357	3.850	3.780	3.641	3.605	3.639	3.684	3.761	3.604	3.829	3.529	3.384
Ti	0.109	0.233	0.125	0.277	0.283	0.271	0.140	0.113	0.158	0.185	0.157	0.153	0.152	0.251	0.230	0.242	0.256	0.123	0.134
Fe	3.008	3.166	3.160	3.336	3.078	3.141	2.904	2.890	2.882	3.073	2.719	3.633	2.763	2.497	2.278	2.496	2.665	2.842	2.729
Mg	1.145	1.111	1.064	1.149	1.166	1.195	1.227	1.295	0.630	0.619	0.806	0.749	0.748	0.731	0.767	0.772	0.668	1.044	1.090
Mn	0.108	0.120	0.092	0.091	0.104	0.105	0.102	0.126	0.071	0.080	0.094	0.078	0.106	0.060	0.074	0.086	0.076	0.133	0.133
Na	0.017	0.006	0.021	0.005	0.007	0.009	0.013	0.007	0.015	0.018	0.018	0.004	0.009	0.012	0.123	0.008	0.009	0.007	0.011
K	1.842	2.000	1.963	1.870	2.018	1.919	1.923	1.875	1.814	1.795	1.946	1.911	1.927	1.870	1.957	1.971	1.919	1.917	1.795
F	0.350	0.397	0.290	0.359	0.412	0.423	0.495	0.647	0.444	0.425	0.387	0.447	0.351	0.568	0.583	0.637	0.524	0.380	0.437

Composition of biotite from the Lamotte pluton

	Biotite monzogranite			Two-mica monzogranite		
Sample	766	791*	791	796	796	907
SiO2	36.41	35.22	38.07	36.67	36.18	37.15
Al2O3	17.84	20.24	20.93	21.00	21.00	22.23
TiO2	2.76	1.05	1.86	1.62	1.50	0.75
FeO	23.44	20.46	20.04	23.06	23.54	21.18
MgO	3.69	3.69	3.91	1.60	1.57	1.60
MnO	0.83	0.70	0.72	0.64	0.69	0.62
Na2O	0.04	0.06	0.00	0.02	0.02	0.00
K2O	10.07	9.90	9.98	9.14	9.00	9.43
F	1.00	0.77	0.89	0.77	0.65	1.41
total	96.08	95.09	96.40	94.52	94.15	94.37
F=O	0.42	0.32	0.37	0.32	0.27	0.59
Total	95.66	94.77	96.03	94.20	93.88	93.78
Si	5.689	5.864	5.701	5.723	5.681	5.780
ivAl	2.311	2.136	2.299	2.277	2.319	2.220
viAl	0.975	1.523	1.395	1.586	1.567	1.858
Al(t)	3.286	3.659	3.695	3.863	3.886	4.077
Ti	0.324	0.121	0.210	0.190	0.177	0.088
Fe	3.064	2.625	2.510	3.010	3.091	2.757
Mg	0.860	0.844	0.873	0.372	0.368	0.370
Mn	0.109	0.091	0.091	0.846	0.092	0.082
Na	0.013	0.016		0.006	0.006	0.000
K	2.007	1.937	1.907	1.820	1.803	1.872
F	0.493	0.376	0.422	0.377	0.326	0.691

Composition of muscovite from the Lamotte pluton

	Biotite monzogranite																Two-mica monzogranite			
Sample	766	766	766	766	767	767	767	768	768	768	782	797	797	797	908	908	911	791	791	791
SiO2	47.47	47.11	46.49	45.72	47.17	47.25	46.75	46.87	47.14	49.53	47.30	45.91	46.39	46.29	47.12	47.06	46.31	46.62	47.49	47.63
Al2O3	29.27	30.41	30.95	29.13	30.18	30.38	31.82	32.26	31.06	30.99	29.38	30.33	32.36	32.28	30.79	30.07	31.19	29.51	30.27	31.35
TiO2	0.22	0.20	0.04	0.70	0.13	0.12	0.05	0.12	0.06	0.53	0.23	0.36	0.25	0.17	0.12	0.09	0.34	0.21	0.12	0.12
FeO	5.89	4.87	4.57	6.02	5.15	5.25	4.57	4.00	3.96	4.50	5.07	5.60	4.77	4.47	4.80	5.40	4.22	4.97	4.65	4.10
MgO	1.99	1.36	1.19	1.64	1.18	1.17	0.81	0.86	1.09	1.42	1.62	1.35	1.05	1.00	1.48	1.70	1.46	1.97	1.67	1.41
MnO	0.26	0.14	0.09	0.18	0.08	0.08	0.06	0.12	0.05	0.08	0.11	0.07	0.10	0.05	0.17	0.09	0.12	0.10	0.13	0.10
Na2O	0.13	0.25	0.29	0.20	0.18	0.20	0.34	0.28	0.30	0.17	0.26	0.20	0.19	0.21	0.16	0.14	0.32	0.19	0.20	0.21
K2O	10.68	10.62	10.87	11.47	10.26	10.36	10.79	11.22	11.19	8.89	10.93	10.55	10.44	10.46	10.75	10.19	11.24	11.23	10.96	10.79
F	0.56	0.43	0.41	0.55	0.43					0.42	0.53				0.49	0.56	0.54	0.51	0.61	0.34
Total	96.47	95.39	94.90	95.61	94.76	94.81	95.19	95.73	94.85	96.53	95.43	94.37	95.55	94.93	95.88	95.30	95.74	95.31	96.10	96.05
F=O	0.24	0.18	0.17	0.23	0.18	0.00	0.00	0.00	0.00	0.18	0.22	0.00	0.00	0.00	0.21	0.24	0.23	0.21	0.26	0.14
Total	96.23	95.21	94.73	95.38	94.58	94.81	95.19	95.73	94.85	96.35	95.21	94.37	95.55	94.93	95.67	95.06	95.51	95.10	95.84	95.91
Si	6.443	6.416	6.366	6.319	6.457	6.440	6.343	6.321	6.414	6.547	6.468	6.326	6.267	6.284	6.389	6.423	6.305	6.400	6.435	6.406
IvAl	1.557	1.584	1.634	1.681	1.544	1.560	1.657	1.679	1.586	1.453	1.532	1.674	1.733	1.716	1.611	1.578	1.696	1.600	1.566	1.594
vIAl	3.126	3.298	3.361	3.065	3.324	3.320	3.432	3.449	3.394	3.375	3.205	3.251	3.420	3.449	3.310	3.260	3.309	3.174	3.269	3.376
Al(t)	4.683	4.882	4.995	4.746	4.868	4.880	5.089	5.128	4.980	4.828	4.736	4.925	5.152	5.165	4.920	4.838	5.004	4.774	4.834	4.970
Ti	0.023	0.021	0.004	0.073	0.013	0.012	0.005	0.013	0.006	0.053	0.024	0.037	0.025	0.017	0.012	0.009	0.035	0.022	0.012	0.012
Fe	0.669	0.555	0.523	0.696	0.589	0.599	0.519	0.451	0.450	0.497	0.580	0.645	0.539	0.508	0.545	0.616	0.481	0.570	0.527	0.461
Mg	0.403	0.276	0.243	0.339	0.240	0.238	0.163	0.173	0.221	0.279	0.330	0.277	0.212	0.202	0.299	0.316	0.296	0.403	0.338	0.282
Mn	0.030	0.016	0.011	0.022	0.009	0.009	0.007	0.014	0.006	0.009	0.012	0.008	0.011	0.006	0.020	0.010	0.014	0.012	0.015	0.011
Na	0.033	0.066	0.077	0.055	0.048	0.053	0.090	0.073	0.079	0.043	0.069	0.053	0.050	0.055	0.043	0.037	0.083	0.050	0.054	0.056
K	1.849	1.845	1.898	2.022	1.791	1.801	1.868	1.930	1.942	1.500	1.906	1.854	1.799	1.812	1.860	1.774	1.952	1.966	1.895	1.852
F	0.240	0.185	0.176	0.240	0.186	0.109	0.104			0.177	0.230				0.212	0.243	0.232	0.221	0.263	0.146

Composition of muscovite from the Lamotte pluton

	Two-mica monzogranite							Muscovite monzogranite		Aplite-pegmatite				
Sample	791	796	796	796	907	907	907	LM101	101	795	795	795	912	912
SiO2	46.53	46.33	45.21	46.43	45.93	46.16	46.71	46.78	46.73	46.74	46.04	46.30	46.79	46.70
Al2O3	29.45	32.74	32.26	33.13	31.48	28.95	31.05	33.14	33.23	35.24	34.41	34.61	31.96	31.37
TiO2	0.13	0.20	0.20	0.17	0.08	0.14	0.08	0.28	0.20	0.21	0.32	0.21	0.03	0.04
FeO	5.07	4.70	4.90	4.79	5.10	7.15	5.26	3.70	3.79	2.77	2.78	2.55	4.85	4.62
MgO	1.82	0.76	0.79	0.79	0.98	1.40	1.01	0.68	0.68	0.51	0.54	0.59	0.28	0.34
MnO	0.21	0.13	0.15	0.14	0.09	0.17	0.15	0.05	0.07	0.07	0.09	0.06	0.30	0.40
Na2O	0.15	0.25	0.27	0.24	0.21	0.12	0.20	0.30	0.32	0.31	0.26	0.33	0.12	0.20
K2O	11.50	10.29	10.50	10.29	10.86	10.31	10.71	11.12	11.01	9.88	10.47	10.42	10.28	10.78
F	0.77		0.50		0.54	0.77	0.71	0.36	0.27				0.77	0.71
Total	95.63	95.40	94.78	95.98	95.27	95.17	95.88	96.41	96.30	95.73	94.91	95.07	95.38	95.16
F=O	0.32	0.00	0.21	0.00	0.23	0.32	0.30	0.15	0.11	0.00	0.00	0.00	0.32	0.30
Total	95.31	95.40	94.57	95.98	95.04	94.85	95.58	96.26	96.19	95.73	94.91	95.07	95.06	94.86
Si	6.400	6.260	6.212	6.237	6.293	6.402	6.363	6.271	6.266	6.201	6.193	6.206	6.372	6.393
ivAl	1.600	1.740	1.788	1.763	1.707	1.598	1.637	1.729	1.734	1.799	1.807	1.794	1.628	1.607
vlAl	3.174	3.384	3.436	3.482	3.376	3.134	3.347	3.507	3.517	3.711	3.648	3.674	3.501	3.453
Al(t)	4.773	5.124	5.224	5.245	5.083	4.733	4.985	5.236	5.251	5.510	5.455	5.468	5.129	5.061
Ti	0.014	0.020	0.021	0.017	0.008	0.014	0.009	0.028	0.020	0.021	0.032	0.021	0.003	0.005
Fe	0.583	0.531	0.563	0.538	0.584	0.830	0.599	0.415	0.426	0.304	0.313	0.286	0.552	0.530
Mg	0.374	0.153	0.162	0.158	0.200	0.290	0.206	0.137	0.135	0.101	0.108	0.118	0.058	0.070
Mn	0.025	0.015	0.018	0.016	0.011	0.019	0.017	0.006	0.008	0.008	0.010	0.007	0.035	0.046
Na	0.040	0.066	0.072	0.063	0.056	0.033	0.053	0.078	0.082	0.080	0.068	0.086	0.032	0.052
K	2.018	1.774	1.841	1.763	1.898	1.824	1.861	1.902	1.884	1.672	1.797	1.782	1.786	1.882
F	0.333		0.216		0.235	0.340	0.306	0.152	0.115				0.333	0.305

Composition of feldspar from the Lamotte pluton

Biotite monzogranite

Sample	767	767	767	767	768	768	768	768	768	782	782	782	782	782	782	782	782	782	797
SiO2	66.24	67.43	67.00	65.99	66.69	66.66	65.21	65.35	64.81	65.31	65.02	65.91	65.02	68.08	65.34	65.85	64.87	65.03	67.11
Al2O3	21.58	20.92	21.58	18.39	21.63	21.15	17.96	17.45	17.18	22.29	22.12	22.21	21.97	20.28	22.14	21.94	18.21	17.99	21.66
CaO	1.64	1.35	1.58	0.00	1.67	1.35	0.02	0.00	0.00	3.68	3.51	3.24	3.01	0.47	2.31	2.37	0.01	0.00	1.61
Na2O	10.05	9.67	9.85	0.40	10.01	10.08	0.36	0.43	0.53	9.51	9.64	9.83	9.95	11.10	9.73	9.85	0.38	0.33	10.31
K2O	0.10	0.06	0.04	15.90	0.08	0.04	16.94	17.30	16.79	0.20	0.20	0.20	0.20	0.03	0.07	0.07	16.62	16.88	0.14
Total	99.51	99.43	100.05	100.68	100.08	99.28	100.49	100.53	99.31	100.99	100.49	101.39	100.15	99.96	99.59	100.08	100.09	100.23	100.83
Si	2.910	2.953	2.922	3.016	2.912	2.931	3.008	3.022	3.027	2.850	2.852	2.864	2.860	2.970	2.875	2.884	3.001	3.006	2.913
Al	1.117	1.080	1.109	0.991	1.113	1.096	0.976	0.951	0.946	1.146	1.144	1.133	1.139	1.043	1.148	1.133	0.992	0.980	1.108
Ca	0.073	0.063	0.074	0.000	0.078	0.064	0.001	0.000	0.000	0.172	0.165	0.151	0.142	0.022	0.109	0.111	0.001	0.000	0.075
Na	0.856	0.821	0.833	0.035	0.848	0.859	0.032	0.039	0.048	0.804	0.820	0.829	0.849	0.939	0.830	0.836	0.034	0.030	0.868
K	0.006	0.003	0.002	0.927	0.005	0.002	0.997	1.021	1.001	0.011	0.011	0.011	0.011	0.002	0.004	0.004	0.980	0.995	0.008
Ab	91.6	92.5	91.6	3.7	91.1	92.9	3.1	3.6	4.6	81.5	92.4	83.7	84.7	97.5	88.0	87.9	3.4	2.9	91.3
Or	0.6	0.4	0.2	96.3	0.5	0.2	96.8	96.4	95.4	1.1	1.1	1.1	1.1	0.2	0.4	0.4	96.6	97.1	0.8
An	7.8	7.1	8.1	0.0	8.4	6.9	0.1	0.0	0.0	17.4	16.5	15.2	14.2	2.3	11.6	11.7	0.1	0.0	7.9

Composition of feldspar from the Lamotte pluton

	Biotite monzogranite											Two-mica monzogranite							
Sample	797	797	797	797	797	908	908	908	911	911	911	766	766	766	766*	766	791	791	791
SiO2	66.75	67.07	64.92	64.20	65.07	66.99	67.05	64.34	65.35	65.37	64.61	66.10	65.97	66.41	65.42	65.33	67.09	67.36	66.96
Al2O3	20.58	20.45	17.97	18.60	18.19	21.00	20.78	18.45	21.71	17.79	17.15	22.11	22.24	22.18	18.50	18.44	20.86	20.40	21.38
Ca	1.53	1.60	0.00	0.00	0.07	1.49	1.37	0.01	2.77	0.03	0.00	2.33	2.07	1.96	0.00	0.00	1.53	1.27	1.80
Na2O	10.29	10.03	0.35	0.22	0.29	10.19	10.04	0.59	10.12	0.76	0.37	9.68	9.71	9.76	1.30	0.37	10.14	10.02	9.79
K2O	0.03	0.06	16.71	16.91	16.95	0.06	0.02	17.22	0.07	16.72	16.88	0.10	0.03	0.03	15.41	16.73	0.05	0.09	0.09
Total	99.18	99.21	99.95	99.93	100.57	99.73	99.26	100.61	100.02	100.67	99.01	100.32	100.02	100.34	100.63	100.87	99.67	99.14	100.02
Si	2.942	2.952	3.009	2.981	3.001	2.934	2.946	2.977	2.872	3.011	3.028	2.886	2.885	2.894	2.997	2.999	2.940	2.961	2.924
Al	1.069	1.061	0.982	1.018	0.989	1.084	1.076	1.006	1.124	0.966	0.947	1.138	1.146	1.139	0.999	0.998	1.077	1.057	1.100
Ca	0.072	0.076	0.000	0.000	0.004	0.070	0.065	0.001	0.130	0.001	0.000	0.109	0.097	0.092	0.000	0.000	0.072	0.060	0.084
Na	0.879	0.856	0.032	0.020	0.026	0.865	0.856	0.053	86.260	0.068	0.034	0.819	0.823	0.825	0.116	0.033	0.861	0.854	0.829
K	0.002	0.003	0.988	1.002	0.997	0.004	0.001	1.016	0.004	0.983	1.009	0.006	0.002	0.002	0.901	0.980	0.003	0.005	0.005
Ab	92.2	91.6	3.1	1.9	2.5	92.2	92.9	4.9	86.6	6.5	3.2	87.7	89.3	89.9	11.4	3.3	92.0	93.0	90.3
Or	0.2	0.4	96.2	98.1	97.1	0.4	0.1	95.0	0.4	93.4	96.8	0.6	0.2	0.2	88.6	96.8	0.3	0.5	0.5
An	7.6	8.1	0.0	0.0	0.3	7.4	7.0	0.1	13.1	0.1	0.0	11.7	10.5	10.0	0.0	0.0	7.7	9.5	9.2

Composition of feldspar from the Lamotte pluton

	Two-mica monzogranite							Aplite-pegmatite						
Sample	791	796	796	907	907	907	907	101	101	912	912	912	912	912
SiO2	65.16	66.72	65.00	66.93	68.12	64.05	64.90	66.12	65.41	68.43	68.19	69.28	65.08	65.08
Al2O3	17.82	20.65	18.14	20.97	20.17	18.42	18.53	21.60	18.10	19.75	19.60	19.62	18.15	18.03
Ca	0.00	1.76	0.00	0.97	0.37	0.01	0.00	10.30	0.29	0.17	0.18	0.14	0.00	0.01
Na2O	0.42	10.62	0.44	10.34	11.10	0.36	0.31	0.19	17.00	11.29	11.23	11.45	0.43	0.54
K2O	17.41	0.14	16.93	0.02	0.10	17.05	17.18	2.47	0.00	0.03	0.02	0.03	16.91	16.50
Total	100.81	99.89	100.51	99.23	99.86	99.89	100.92	100.70	100.80	99.67	99.22	100.52	100.57	100.16
Si	3.007	2.929	2.999	2.941	2.975	2.981	2.986	2.887	3.005	2.993	2.994	3.004	3.001	3.007
Al	0.969	1.068	0.986	1.086	1.038	1.010	1.005	1.112	0.982	1.018	1.014	1.003	0.986	0.982
Ca	0.000	0.083	0.000	0.046	0.017	0.001	0.000	0.870	0.026	0.008	0.008	0.006	0.000	0.001
Na	0.038	0.903	0.040	0.881	0.940	0.032	0.028	0.010	1.000	0.957	0.956	0.963	0.039	0.048
K	1.025	0.008	0.996	0.001	0.005	1.012	1.009	0.115	0.000	0.002	0.001	0.002	0.995	0.973
Ab	3.6	90.9	3.8	95.0	97.7	3.1	2.7	87.0	2.5	99.0	99.0	99.2	3.7	4.7
Or	96.4	0.8	96.2	0.1	0.6	96.9	97.3	1.0	97.5	0.2	0.1	0.2	96.3	95.2
An	0.0	8.3	0.0	4.9	1.8	0.1	0.0	12.0	0.0	0.8	0.9	0.0	0.0	0.1

Composition of biotite from Lacorne pluton

	Biotite monzogranite																			
Sample	613	613	616	616	616	620	620	621A	621A	621A	622	622	630	630	634	634	665	665	666	666
SiO2	37.76	38.07	37.77	38.54	39.10	37.82	37.69	38.14	37.55	36.61	37.68	38.25	38.48	37.87	39.39	38.43	36.08	36.53	37.33	36.98
Al2O3	21.43	20.48	20.49	20.34	20.47	19.89	19.76	19.54	19.46	18.86	18.76	18.83	19.93	20.31	21.07	19.85	18.84	18.30	17.86	17.89
TiO2	1.79	1.72	1.95	1.57	1.90	1.83	1.70	1.91	2.23	2.08	1.97	1.99	1.77	1.76	1.84	1.91	1.72	1.70	1.89	1.91
FeO	19.15	20.05	19.94	18.83	19.41	20.56	21.08	20.27	21.85	22.43	22.24	22.06	20.22	20.20	19.94	20.15	25.32	24.80	21.67	22.44
MnO	0.80	1.01	0.70	0.77	0.70	0.80	0.74	0.68	0.78	0.86	0.83	0.83	1.00	0.81	0.81	0.65	0.53	0.63	0.76	0.83
MgO	2.66	2.60	3.93	3.75	3.79	4.24	4.09	3.98	3.93	4.30	4.16	4.38	3.20	2.94	3.23	3.62	3.97	3.72	4.97	4.85
Na2O	0.01	0.00	0.02	0.01	0.04	0.03	0.04	0.04	0.02	0.07	0.03	0.02	0.07	0.04	0.02	0.02	0.01	0.02	0.06	0.02
K2O	10.06	9.90	9.94	9.98	9.90	9.97	9.90	10.06	10.15	9.60	9.91	9.77	10.04	9.93	9.81	9.67	9.50	9.87	9.70	9.76
F	1.02	1.39	0.83	1.06	1.20			0.78	0.86	1.26	1.06	1.10	1.05	0.90	0.93	0.98	0.53	0.55	0.75	0.92
	94.70	95.42	95.57	94.85	96.51	95.14	95.00	95.60	96.83	96.27	96.66	97.23	95.76	94.76	97.04	95.68	96.50	96.32	94.99	95.60
F=O	0.43	0.59	0.35	0.45	0.51			0.33	0.36	0.53	0.45	0.46	0.44	0.38	0.39	0.41	0.22	0.23	0.32	0.39
Total	94.27	94.83	95.22	94.40	96.00	95.14	95.00	95.27	96.47	95.74	96.21	96.77	95.32	94.38	96.65	95.27	96.28	96.09	94.67	95.21
Si	5.801	5.854	5.763	5.898	5.888	5.772	5.775	5.834	5.731	5.696	5.781	5.813	5.885	5.840	5.885	5.859	5.602	5.688	5.756	5.697
IvAl	2.199	2.146	2.237	2.102	2.112	2.228	2.225	2.166	2.269	2.305	2.219	2.187	2.115	2.160	2.115	2.141	2.398	2.312	2.245	2.303
VIAl	1.681	1.566	1.448	1.565	1.520	1.350	1.344	1.357	1.231	1.135	1.173	1.186	1.476	1.532	1.595	1.425	1.049	1.047	1.002	0.940
Al(t)	3.880	3.712	3.685	3.667	3.633	3.578	3.569	3.523	3.501	3.439	3.392	3.373	3.591	3.692	3.709	3.566	3.447	3.359	3.246	3.243
Ti	0.206	0.199	0.224	0.181	0.215	0.210	0.196	0.220	0.256	0.242	0.228	0.228	0.204	0.204	0.207	0.219	0.201	0.199	0.219	0.221
Fe	2.461	2.578	2.544	2.409	2.444	2.624	2.701	2.593	2.789	2.902	2.654	2.804	2.586	2.605	2.491	2.569	3.287	3.230	2.794	2.891
Mn	0.104	0.132	0.090	0.099	0.089	0.103	0.096	0.115	0.101	0.112	0.108	0.106	0.130	0.106	0.102	0.110	0.069	0.109	0.099	0.108
Mg	0.610	0.643	0.893	0.856	0.851	0.964	0.934	0.908	0.893	0.992	0.955	0.993	0.729	0.677	0.719	0.868	0.920	0.864	1.142	1.114
Na	0.003	0.000	0.006	0.002	0.010	0.009	0.012	0.012	0.006	0.020	0.009	0.007	0.021	0.013	0.006	0.005	0.002	0.005	0.018	0.006
K	1.976	1.942	1.935	1.948	1.903	1.941	1.935	1.962	1.977	1.695	1.939	1.894	1.959	1.953	1.870	1.881	1.882	1.960	1.906	1.918
F	0.010	0.678	0.399	0.512	0.571			0.379	0.416	0.619	0.517	0.527	0.506	0.441	0.440	0.471	0.262	0.273	0.366	0.448

Composition of biotite from Lacorne pluton

	Biotite monzogranite								Two-mica monzogranite						
Sample	666	666	666	673	673	673	673	673	652	672	672	672	707	707	692
SiO2	35.71	36.72	36.91	36.91	36.79	37.40	38.10	37.12	35.48	35.42	35.87	36.87	38.43	38.68	39.00
Al2O3	18.44	17.87	17.69	17.99	18.19	18.67	18.60	18.57	17.66	17.22	19.38	19.46	20.44	21.70	20.81
TiO2	1.98	2.13	2.23	2.45	2.43	2.17	2.06	2.09	1.82	2.12	1.93	2.00	2.06	1.91	1.40
FeO	23.08	23.15	22.08	23.24	22.39	21.65	21.12	22.19	25.88	26.41	25.07	23.81	20.22	19.35	19.90
MnO	0.68	0.74	0.73	1.09	0.96	0.73	0.80	0.94	0.79	0.76	0.69	0.60	0.73	0.69	0.63
MgO	5.05	4.86	5.04	4.07	4.28	3.99	4.92	4.02	3.35	3.15	2.89	2.91	2.44	2.40	2.99
Na2O	0.04	0.03	0.04	0.03	0.03	0.02	0.03	0.03	0.02	0.02	0.04	0.05	0.02	0.01	0.04
K2O	9.12	9.80	9.85	9.73	9.81	10.00	9.80	9.74	10.05	10.02	9.76	10.13	9.76	9.95	9.70
F	0.59	0.66	0.73	0.96	1.10	0.82	1.07	0.82	0.72	0.97	0.40	0.51	0.96	1.05	0.97
	94.69	96.16	95.50	96.47	95.98	95.45	96.50	95.52	95.95	96.09	96.03	96.34	95.06	95.74	95.44
F=O	0.25	0.36	0.31	0.40	0.46	0.35	0.45	0.35	0.30	0.41	0.17	0.21	0.40	0.44	0.41
Total	94.44	95.80	95.19	96.07	95.52	95.10	96.05	95.17	95.65	96.09	95.86	96.13	94.66	95.30	95.03
SI	5.601	5.699	5.729	5.718	5.715	5.786	5.814	5.768	5.622	5.657	5.596	5.696	5.889	5.855	5.926
IVAl	2.399	2.301	2.271	2.282	2.285	2.214	2.186	2.242	2.378	2.343	2.404	2.304	2.111	2.145	2.074
VIAl	1.009	0.968	1.000	1.003	1.046	1.191	1.159	1.153	0.958	0.878	1.158	1.239	1.582	1.727	1.653
Al(I)	3.408	3.268	3.271	3.285	3.331	3.405	3.345	3.395	3.336	3.221	3.562	3.543	3.693	3.872	3.727
TI	0.234	0.248	0.260	0.285	0.284	0.253	0.236	0.244	0.217	0.253	0.226	0.232	0.238	0.218	0.161
Fe	3.028	3.005	2.866	3.011	2.909	2.801	2.695	2.879	3.427	3.505	3.271	3.075	2.592	2.449	2.529
Mn	0.091	0.097	0.096	0.144	0.126	0.096	0.103	0.124	0.106	0.102	0.091	0.078	0.095	0.089	0.081
Mg	1.180	1.125	1.167	0.939	0.992	0.920	1.120	0.930	0.791	0.745	0.672	0.670	0.557	0.542	0.676
Na	0.012	0.010	0.012	0.009	0.009	0.006	0.008	0.010	0.006	0.006	0.012	0.014	0.007	0.003	0.013
K	1.824	1.940	1.950	1.922	1.943	1.974	1.908	1.927	2.017	2.018	1.943	1.996	1.909	1.922	1.881
F	0.292	0.422	0.358	0.471	0.542	0.404	0.515	0.403	0.361	0.487	0.195	0.251	0.464	0.504	0.466

Composition of muscovites from Lacorne pluton

Biotite monzogranite

Sample	613	614	614	616	616	616	617	620	620	620	621A	621A	630	630	634	634	634	665	666	666
SiO2	46.85	46.43	49.46	47.33	46.21	46.30	46.07	46.25	46.96	46.83	46.75	45.61	45.93	46.55	47.43	46.67	46.92	50.24	46.18	46.65
Al2O3	28.49	28.32	27.39	28.36	27.90	30.19	32.76	30.86	28.64	27.92	28.36	28.68	28.69	29.77	28.89	27.63	29.24	29.96	29.80	30.95
TiO2	0.40	0.11	0.43	0.41	0.34	0.13	0.13	0.07	0.44	0.32	0.42	0.54	0.40	0.44	0.44	0.41	0.28	0.19	0.36	0.02
FeO	7.77	6.22	6.84	6.77	6.32	5.39	4.17	4.78	5.19	5.40	5.99	5.61	5.82	5.54	5.99	5.80	5.84	5.45	5.12	4.32
MnO	0.36	0.25	0.29	0.16	0.26	0.15	0.10	0.08	0.13	0.15	0.16	0.17	0.14	0.09	0.25	0.23	0.22	0.13	0.08	0.06
MgO	1.09	1.68	2.18	1.89	1.73	1.33	0.49	1.00	1.74	1.84	1.80	1.59	1.58	1.64	1.99	2.04	1.73	1.54	1.34	0.98
Na2O	0.06	0.17	0.11	0.15	0.15	0.28	0.30	0.25	0.22	0.13	0.14	0.20	0.27	0.26	0.09	0.12	0.11	0.14	0.24	0.30
K2O	10.04	11.12	9.89	11.25	11.26	11.13	11.27	11.19	11.02	11.01	11.50	11.58	11.19	10.97	10.58	10.99	10.27	9.18	10.97	11.11
F	1.20	0.47	0.62	0.88	0.86	0.70	0.19	0.42	0.67	1.02	0.75	0.90	0.86	0.56	0.94	1.04	1.03	0.58	0.42	0.35
OH	4.39			4.39	4.29	4..36		4.41	4.38	4.34	4.30		4.30	4.38	4.48	4.30	4.36	4.54	4.35	4.37
	96.26	94.77	97.21	97.20	95.03	95.60	95.50	94.90	95.01	94.62	95.67	94.88	94.88	95.82	96.60	94.93	95.64	97.41	94.51	94.74
F=O	0.51	0.20	0.26	0.37	0.36	0.29	0.08	0.18	0.28	0.43	0.32	0.38	0.36	0.24	0.40	0.44	0.43	0.24	0.18	0.15
Total	95.75	94.57	96.95	96.83	94.67	95.31	95.42	94.72	94.73	94.19	95.55	94.50	94.52	95.58	96.20	94.49	95.21	97.17	94.33	94.59
Si	6.453	6.454	6.650	6.453	6.447	6.359	6.253	6.329	6.475	6.517	6.445	6.370	6.397	6.369	6.393	6.497	6.441	6.632	6.356	6.392
IvAl	1.547	1.546	1.350	1.547	1.553	1.641	1.747	1.671	1.525	1.483	1.555	1.630	1.603	1.632	1.607	1.503	1.559	1.369	1.644	1.608
vIAl	2.713	3.093	2.989	3.010	3.035	3.246	3.496	3.305	3.129	3.097	3.053	3.091	3.107	3.167	2.983	3.030	3.171	3.292	3.191	3.390
Al(t)	4.260	4.639	4.339	4.557	4.588	4.887	5.243	4.976	4.654	4.580	4.608	4.720	4.710	4.800	4.590	4.534	4.730	4.660	4.835	4.998
Ti	0.041	0.011	0.044	0.042	0.036	0.013	0.013	0.007	0.045	0.034	0.044	0.056	0.042	0.045	0.045	0.043	0.028	0.018	0.037	0.002
Fe	0.895	0.723	0.769	0.772	0.737	0.619	0.474	0.547	0.599	0.628	0.691	0.655	0.678	0.634	6.393	0.675	0.670	0.602	0.589	0.495
Mn	0.042	0.029	0.033	0.019	0.030	0.017	0.012	0.009	0.016	0.018	0.019	0.020	0.017	0.010	0.029	0.027	0.026	0.015	0.009	0.006
Mg	0.224	0.347	0.437	0.383	0.360	0.273	0.100	0.204	0.359	0.382	0.369	0.331	0.329	0.335	0.400	0.424	0.353	0.302	0.275	0.199
Na	0.016	0.045	0.028	0.040	0.041	0.075	0.080	0.065	0.060	0.035	0.036	0.053	0.074	0.069	0.024	0.031	0.030	0.036	0.064	0.078
K	1.764	1.972	1.696	1.956	2.004	1.951	1.951	1.953	1.939	1.954	2.022	2.063	1.989	1.915	1.819	1.952	1.799	1.545	1.926	1.942
F	0.523	0.207	0.262	0.381	0.380	0.304	0.083		0.290	0.451	0.327	0.398	0.380	0.243	0.401	0.457	0.445	0.244	0.183	0.151

Composition of muscovite from Lacorne pluton

	Biotite monzogranite				Two-mica monzogranite											Muscovite monzogranite				
Sample	666	672	673	673	652	652	652	692	692	692	707	707	707	742	742	603	633	637	637	648
SiO2	48.49	46.63	45.82	45.60	48.49	46.72	46.96	47.19	46.54	46.04	45.65	46.80	46.74	46.69	46.42	45.99	47.15	47.32	48.01	46.31
Al2O3	32.06	29.89	28.02	28.58	31.35	31.36	31.81	28.00	27.36	27.05	27.51	27.21	28.27	28.60	30.66	30.93	31.33	31.05	31.20	30.42
TiO2	0.01	0.13	0.48	0.61	0.27	0.21	0.28	0.10	0.44	0.47	0.52	0.34	0.38	0.24	0.13	0.49	0.50	0.31	0.31	0.32
FeO	4.38	5.18	6.25	6.25	4.66	4.74	4.95	6.71	6.73	7.04	7.00	6.80	6.71	6.28	4.81	5.41	6.14	5.07	4.65	5.84
MnO	0.06	0.09	0.21	0.20	0.09	0.09	0.06	0.30	0.25	0.28	0.25	0.26	0.24	0.18	0.09	0.25	0.22	0.16	0.14	0.15
MgO	1.06	1.17	1.73	1.66	1.06	0.98	1.01	1.55	1.78	1.73	1.66	1.74	1.59	1.29	0.89	1.00	0.74	0.60	0.72	0.76
Na2O	0.21	0.21	0.19	0.21	0.23	0.20	0.24	0.06	0.15	0.15	0.09	0.12	0.14	0.25	0.29	0.14	0.24	0.14	0.18	0.24
K2O	9.51	11.45	11.37	11.10	10.19	10.64	10.66	11.43	11.34	11.30	11.61	11.39	11.13	10.95	10.89	11.34	10.32	11.30	10.38	11.13
F	0.25	0.17	0.73	0.91	0.38	0.43	0.16	0.54	0.84	0.88	0.78	1.03	0.87			0.38	0.23	0.47	0.57	0.41
OH	4.50	4.36	4.28	4.30	4.50	4.40	4.45	4.35	4.30	4.27	4.27	4.31	4.34	4.35	4.37		4.46	4.43	4.45	4.37
	96.09	94.92	94.80	95.12	96.72	95.37	96.17	95.90	95.43	94.94	95.07	95.69	96.07	94.68	94.18	95.93	96.87	96.44	96.16	95.58
F=O	0.11	0.07	0.31	0.38	0.16	0.18	0.07	0.23	0.35	0.37	0.33	0.43	0.37	0.00	0.00	0.16	0.10	0.20	0.24	0.17
Total	95.98	94.85	94.49	94.74	96.56	95.19	96.10	95.67	95.08	94.57	94.74	95.26	95.70	94.68	94.18	95.77	96.77	96.24	95.92	95.41
Si	6.451	6.412	6.407	6.355	6.462	6.357	6.324	6.506	6.480	6.465	6.407	6.511	6.447	6.451	6.386	6.284	6.337	6.402	6.459	6.354
iv Al	1.549	1.588	1.593	1.645	1.538	1.643	1.676	1.494	1.520	1.535	1.593	1.489	1.553	1.549	1.614	1.716	1.663	1.598	1.541	1.646
vi Al	3.481	3.257	3.024	3.049	3.385	3.386	3.373	3.054	2.970	2.942	2.958	2.973	3.042	3.142	3.359	3.265	3.299	3.352	3.406	3.273
*Al	5.030	4.845	4.617	4.694	4.923	5.029	5.049	4.549	4.490	4.477	4.551	4.462	4.595	4.691	4.972	4.981	4.962	4.950	4.947	4.919
Ti	0.001	0.013	0.050	0.064	0.027	0.021	0.029	0.010	0.046	0.049	0.055	0.036	0.040	0.025	0.014	0.050	0.051	0.031	0.031	0.033
Fe	0.488	0.596	0.731	0.728	0.519	0.539	0.558	0.773	0.783	0.827	0.821	0.792	0.774	0.726	0.553	0.618	0.690	0.574	0.523	0.670
Mn	0.009	0.010	0.025	0.023	0.010	0.011	0.009	0.035	0.029	0.034	0.030	0.031	0.028	0.021	0.011	0.029	0.025	0.020	0.016	0.017
Mg	0.214	0.240	0.361	0.345	0.211	0.198	0.203	0.319	0.369	0.362	0.347	0.362	0.327	0.266	0.183	0.205	0.149	0.121	0.145	0.155
Na	0.054	0.056	0.052	0.057	0.060	0.054	0.062	0.022	0.041	0.041	0.025	0.033	0.036	0.067	0.077	0.037	0.062	0.036	0.048	0.063
K	1.613	2.009	2.029	1.974	1.732	1.846	1.835	2.010	2.015	2.024	2.078	2.022	1.959	1.930	1.911	1.977	1.769	1.949	1.782	1.948
F	0.105	0.076	0.325	0.402	0.160	0.187	0.069	0.233	0.369	0.390	0.347	0.453	0.380			0.164	0.096	0.200	0.243	0.178

Composition of muscovite from Lacorne pluton

	Muscovite monzogranite				Aplite			Aplite/pegmatite										
Sample	648	684	684	684	701	606	606	624B	624B	640	646A	646B	646C	709C	710 Lepidolite	710	710	1001
SiO2	46.01	47.46	46.33	46.43	45.95	47.57	46.76	45.95	45.76	45.39	46.12	47.19	46.53	45.87	51.99	53.34	47.35	45.55
Al2O3	31.43	30.28	32.63	32.47	30.61	34.89	33.63	30.16	31.35	28.62	32.10	31.67	30.80	34.43	31.52	25.92	37.28	32.12
TiO2	0.34	0.27	0.15	0.20	0.62	0.11	0.09	0.00	0.01	0.40	0.15	0.19	0.37	0.00	0.00	0.00	0.00	0.11
FeO	5.28	4.81	3.97	4.47	6.27	4.05	3.74	5.26	4.54	6.75	4.17	4.25	4.61	1.99	0.44	0.51	0.17	3.79
MnO	0.10	0.13	0.08	0.08	0.35	0.27	0.14	0.32	0.25	0.15	0.12	0.15	0.10	0.22	0.54	0.89	0.12	0.14
MgO	0.72	0.64	0.65	0.61	1.03	0.32	0.30	0.25	0.14	0.41	0.49	0.72	0.82	0.01	0.00	0.00	0.00	0.39
Na2O	0.37	0.22	0.41	0.25	0.13	0.24	0.17	0.16	0.13	0.18	0.33	0.26	0.28	0.34	0.21	0.14	0.14	0.44
K2O	11.34	10.66	10.88	11.09	10.76	9.14	8.91	11.15	11.29	11.18	11.34	10.96	11.25	11.42	6.75	8.87	9.76	10.88
F	0.34				0.58	0.87	0.51				0.48	0.60	0.55		3.42	5.75	0.29	
OH	4.39	4.43	4.44	4.43	4.39	4.55	4.43				4.39	4.43	4.38					
	95.93	94.87	95.10	95.60	96.30	97.46	94.25	93.25	93.47	93.28	95.30	95.99	95.31	94.28	96.87	95.42	95.11	93.42
F=O	0.14	0.00	0.00	0.00	0.24	0.37	0.21	0.00	0.00	0.00	0.20	0.25	0.23	0.00	1.44	2.42	0.12	0.00
Total	95.79	94.87	95.10	95.60	96.06	97.09	94.04	93.25	93.47	93.28	95.10	95.74	95.08	94.28	95.43	93.00	94.99	93.42
Si	6.276	6.469	6.281	6.282	6.277	6.260	6.324	6.417	6.351	6.401	6.299	6.383	6.371	6.225	6.876	7.356	6.227	6.290
iv Al	1.724	1.531	1.719	1.718	1.723	1.740	1.676	1.583	1.649	1.599	1.702	1.617	1.629	1.775	1.124	0.644	1.773	1.710
vi Al	3.328	3.335	3.495	3.460	3.204	3.673	3.685	3.381	3.479	3.190	3.464	3.430	3.341	3.733	3.790	3.569	4.006	3.518
•Al	5.052	4.865	5.215	5.178	4.927	5.412	5.361	4.964	5.128	4.789	5.166	5.048	4.970	5.508	4.914	4.213	5.779	5.228
Ti	0.035	0.003	0.015	0.020	0.064	0.011	0.009	0.000	0.001	0.042	0.016	0.019	0.038	0.000	0.000	0.000	0.000	0.012
Fe	0.602	0.548	0.450	0.506	0.717	0.446	0.423	0.614	0.527	0.796	0.476	0.481	0.527	0.225	0.049	0.059	0.019	0.438
Mn	0.012	0.015	0.604	0.009	0.041	0.030	0.016	0.038	0.030	0.018	0.014	0.017	0.012	0.026	0.061	0.104	0.014	0.017
Mg	0.146	0.171	0.131	0.123	0.210	0.063	0.061	0.051	0.030	0.086	0.100	0.145	0.168	0.002	0.000	0.000	0.000	0.080
Na	0.098	0.058	0.108	0.066	0.034	0.061	0.044	0.042	0.034	0.049	0.087	0.068	0.074	0.090	0.053	0.037	0.035	0.119
K	1.973	1.889	0.188	1.914	1.875	1.535	1.538	1.987	1.998	2.010	1.967	1.890	1.964	1.977	1.477	1.561	1.637	1.916
F	0.145				0.251	0.361	0.216				0.207	0.255	0.237		1.432	2.509	0.119	

Composition of feldspar from Lacorne pluton

Biotite monzogranite

Sample	613	613	613	614	614	616	616	617	617	620	620	620	620	621	621	621	621A	621A	621A	622
SiO2	66.81	66.98	64.78	65.07	64.65	66.06	65.01	66.87	64.52	66.69	66.99	66.70	64.94	65.74	65.17	64.99	65.84	66.10	64.73	66.20
Al2O3	21.32	21.25	18.20	21.43	17.96	21.11	17.82	19.94	18.57	19.63	20.93	21.43	17.85	21.43	17.62	18.00	21.50	20.13	18.30	21.68
Na2O	10.17	10.05	0.29	10.07	0.33	10.18	0.37	11.31	0.49	10.94	10.28	9.91	0.34	9.90	0.53	0.34	10.57	10.37	0.40	9.35
K2O	0.15	0.06	17.06	0.09	16.99	0.19	17.08	0.06	16.46	0.08	0.05	0.06	16.94	0.17	16.97	17.23	0.06	0.13	16.98	0.17
CaO	2.10	2.36	0.00	2.75	0.00	2.38	0.03	0.59	0.02	0.74	1.80	2.28	0.01	2.72	0.00	0.00	2.65	2.28	0.00	3.11
Total	100.55	100.72	100.33	99.41	99.93	99.92	100.31	100.77	100.06	100.08	100.05	100.38	100.08	99.96	100.29	100.56	100.62	99.01	100.41	100.51
Si	2.912	2.914	2.997	2.879	3.003	2.904	3.009	2.983	2.986	2.991	2.928	2.909	3.007	2.890	3.016	3.002	2.880	2.931	2.992	2.889
Al	1.096	1.090	0.993	1.118	0.983	1.094	0.972	1.018	1.013	1.007	1.078	1.101	0.974	1.110	0.961	0.980	1.109	1.052	0.997	1.116
Na	0.860	0.848	0.026	0.864	0.030	0.867	0.033	0.950	0.044	0.924	0.872	0.838	0.030	0.844	0.047	0.030	0.898	0.892	0.036	0.791
K	0.008	0.004	1.007	0.005	1.007	0.011	1.009	0.003	0.971	0.004	0.003	0.003	1.001	0.010	1.002	1.015	0.003	0.007	1.001	0.010
Ca	0.098	0.110		0.130		0.112	0.002	0.028	0.001	0.035	0.084	0.107	0.001	0.128	0.000	0.000	0.124	0.108	0.000	0.145
Ab	88.98	88.11	2.50	86.45	2.87	88.00	3.00	96.64	4.35	95.95	90.89	88.40	2.92	86.00	5.00	3.00	87.57	88.54	3.44	84.00
Or	0.86	0.46	97.50	0.50	97.11	1.00	97.00	0.35	95.54	0.44	0.32	0.36	97.02	1.00	95.00	97.00	0.31	0.72	96.54	1.00
An	10.15	11.43	0.00	13.05		11.00	0.00	2.81	0.11	3.61	8.79	11.24	0.06	13.00			12.13	10.74		15.00

Composition of feldspar from Lacorne pluton

	Biotite monzogranite																	Two-mica monzogranite		
Sample	622	630	630	634	634	634	665	665	666	666	673	673	673	673	742	742	742	652	652	652
SiO2	65.25	67.02	65.42	66.27	66.52	65.51	66.51	64.97	66.32	65.70	66.62	67.52	64.26	64.93	69.07	67.48	65.86	66.97	65.68	66.46
Al2O3	18.38	20.51	18.18	20.75	21.41	17.99	20.62	18.26	21.43	18.14	20.54	20.14	18.32	18.33	19.57	20.57	17.62	20.97	17.05	21.31
Na2O	0.41	10.02	0.59	9.26	9.15	0.42	9.87	0.31	9.50	0.35	10.50	11.03	0.28	0.42	10.66	10.30	0.39	10.83	0.36	10.30
K2O	16.87	0.18	16.66	0.26	0.25	16.57	0.23	17.05	0.21	16.60	0.08	0.05	17.30	16.89	0.15	0.06	16.45	0.09	16.78	0.12
CaO	0.00	2.22	0.00	2.96	2.87	0.00	2.06	0.00	2.51	0.00	1.83	0.50	0.00	0.02	0.71	1.60	0.00	2.09	0.01	2.50
Total	100.91	99.95	100.85	99.50	100.20	100.49	99.29	100.59	99.97	100.79	99.57	99.24	100.16	100.59	100.16	100.01	100.32	100.95	99.88	100.69
Si	2.997	2.938	3.004	2.920	2.907	3.014	2.932	2.997	2.906	3.012	2.932	2.969	2.984	2.994	3.002	2.948	3.032	2.919	3.044	2.998
Al	0.995	1.059	0.984	1.078	1.103	0.975	1.072	0.993	1.106	0.980	1.066	1.044	1.003	0.996	1.002	1.059	0.956	1.068	0.931	1.096
Na	0.037	0.852	0.052	0.791	0.775	0.037	0.843	0.028	0.807	0.031	0.896	0.940	0.025	0.037	0.899	0.873	0.034	0.916	0.032	0.872
K	0.989	0.010	0.976	0.015	0.014	0.972	0.013	1.004	0.012	0.971	0.005	0.003	1.025	0.994	0.009	0.003	0.966	0.005	0.992	0.007
Ca	0.000	0.105	0.000	0.140	0.135	0.000	0.098	0.000	0.118	0.000	0.086	0.024	0.000	0.001	0.033	0.075	0.000	0.097	0.001	0.117
Ab	3.56	88.16	5.09	83.70	84.00	4.00	88.43	2.68	88.16	3.09	90.80	97.26	2.39	3.60	95.56	91.75	3.44	89.94	3.16	87.57
Or	96.44	1.03	94.91	1.50	1.50	96.00	1.34	97.32	1.26	96.91	0.45	0.31	97.61	96.29	0.91	0.35	96.56	0.49	96.80	0.67
An		10.82		14.80	14.50		10.22	0.00	12.59		8.74	2.43		0.11	3.53	7.90		9.57	0.05	11.76

Composition of feldspar from Lacorne pluton

	Two-mica monzogranite					Muscovite monzogranite													
Sample	652	652	652	652	652	672	672	701	701	707	707	603	603	603	603	633	633	633	633	633
SiO2	66.67	67.56	68.48	66.25	65.84	65.59	65.42	67.23	64.73	66.07	64.74	66.67	60.92	65.30	65.30	67.40	65.59	67.14	64.77	64.56
Al2O3	20.39	20.38	19.96	17.59	17.76	21.19	16.76	20.91	18.04	20.84	18.30	20.86	20.42	18.04	18.23	20.52	18.17	20.14	18.14	17.80
Na2O	10.48	10.73	11.49	0.29	0.38	10.16	0.43	10.27	0.20	10.37	0.51	10.37	10.38	0.35	0.39	10.43	0.33	10.58	0.23	0.41
K2O	0.10	0.07	0.04	16.14	16.28	0.05	16.70	0.07	16.56	0.07	17.01	0.16	0.05	17.06	16.87	0.05	16.78	0.05	17.04	16.79
CaO	2.23	1.82	0.98	0.00	0.00	2.29	0.00	1.95	0.11	2.06	0.00	1.80	1.70	0.00	0.00	1.84	0.00	1.82	0.00	0.00
	100.07	100.56	100.95	100.27	100.26	99.28	99.31	100.43	99.64	99.41	100.56	100.06	99.47	100.75	100.79	100.24	100.87	99.73	100.18	99.56
Si	2.932	2.943	2.969	3.042	3.029	2.899	3.034	2.931	3.005	2.915	2.990	2.927	2.944	3.007	3.003	2.942	3.010	2.940	3.000	3.008
Al	1.054	1.046	1.020	0.952	0.963	1.104	0.016	1.074	0.987	1.083	0.996	1.077	1.059	0.979	0.988	1.056	0.983	1.053	0.990	0.977
Na	0.891	0.906	0.966	0.025	0.034	0.871	0.039	0.868	0.018	0.887	0.046	0.880	0.885	0.031	0.035	0.882	0.029	0.899	0.020	0.037
K	0.006	0.004	0.002	0.946	0.955	0.003	0.988	0.004	0.981	0.004	1.002	0.009	0.003	1.002	0.990	0.003	0.982	0.003	1.007	0.998
Ca	0.105	0.085	0.045		0.000	0.109		0.091	0.006	0.097	0.000	0.084	0.080			0.086	0.000	0.086	0.000	
Ab	98.01	91.09	95.28	2.62	3.43	88.65	3.77	90.12	1.81	89.79	4.34	90.41	91.43	3.02	3.39	90.83	2.87	91.02	1.98	3.60
Or	0.55	0.38	0.24	97.37	96.53	0.30	96.23	0.40	97.63	0.37	95.66	0.92	0.29	96.98	96.61	0.29	97.13	0.31	98.01	96.40
An	10.44	8.54	4.48			11.05	0.00	9.48	0.56	9.84		8.67	8.28	0.00	0.00	8.88	0.00	8.67	0.01	0.00

Composition of feldspar from Lacorne pluton

	Muscovite monzogranite										Aplite-pegmatite									
Sample	637	637	648	648	648	648	648	684	684	684	606	606	624B	640	640	646A	646A	646B	646B	646C
SiO2	66.24	64.66	66.64	65.02	67.06	68.06	65.29	69.29	66.94	65.49	69.42	65.34	68.52	67.72	65.17	69.03	68.73	68.48	68.52	67.49
Al2O3	20.65	18.25	20.96	18.01	20.57	20.31	18.17	19.70	20.63	18.21	19.34	18.01	18.70	19.58	17.93	19.46	19.19	19.72	19.51	20.78
Na2O	10.57	0.40	10.69	0.36	10.72	11.25	0.42	10.92	10.45	0.39	11.07	0.35	11.59	11.41	0.43	11.25	11.41	11.43	11.45	10.33
K2O	0.08	16.91	0.08	17.09	0.08	0.05	16.97	0.05	0.07	16.59	0.06	16.71	0.05	0.04	16.79	0.05	0.08	0.05	0.06	0.19
CaO	1.82	0.00	1.77	0.00	1.53	0.97	0.02	0.68	1.77	0.02	0.48	0.00	0.25	0.84	0.00	0.28	0.36	0.50	0.55	1.65
Total	99.36	100.22	100.34	100.48	99.96	100.64	100.87	100.64	100.06	100.70	100.37	100.41	99.11	99.59	100.32	100.07	99.77	100.18	100.09	100.44
Si	2.923	2.993	2.915	3.003	2.938	2.958	3.002	2.999	2.929	3.003	3.012	3.012	3.018	2.975	3.010	3.005	3.006	2.984	2.991	2.940
Al	1.074	0.996	1.081	0.981	1.062	1.040	0.984	1.005	1.074	0.984	0.989	0.978	0.971	1.014	97.630	0.998	0.989	1.013	1.004	1.067
Na	0.904	0.036	0.924	0.033	0.911	0.948	0.038	0.917	0.887	0.035	0.931	0.032	0.989	0.972	0.039	0.950	0.967	0.966	0.969	0.874
K	0.004	0.998	0.005	1.007	0.005	0.003	0.995	0.003	0.004	0.971	0.003	0.983	0.003	0.003	0.989	0.003	0.005	0.003	0.003	0.011
Ca	0.086	0.000	0.083	0.000	0.072	0.045	0.001	0.032	0.083	0.001	0.022	0.000	0.012	0.040		0.013	0.017	0.023	0.026	0.077
Ab	91.00	4.00	91.33	3.12	92.28	95.16	3.65	96.38	91.07	3.49	97.00	3.00	98.57	95.64	3.75	98.34	97.85	97.38	97.09	90.87
Or	0.50	96.00	0.45	96.88	0.46	0.29	96.26	0.29	0.41	96.43	0.50	97.00	0.27	0.25	96.25	0.30	0.46	0.28	0.34	1.12
An	8.50	0.00	8.21	0.00	7.25	4.53	0.09	3.33	8.52	0.06	2.50		1.16	3.92		1.36	1.68	2.34	2.56	8.01

Composition of feldspar from Lacorne pluton

	Aplite-pegmatite						Albitite									
Sample	646C	646C	646C	646C	709C	709C	1001	1001	721	722	722	723	724	724	772B	772B
SiO2	64.52	68.38	67.86	67.75	68.75	68.66	68.12	68.60	68.16	68.76	68.94	68.61	69.24	69.35	68.32	60.18
Al2O3	18.22	20.01	20.90	20.48	19.20	19.09	18.94	19.21	19.94	19.44	19.68	20.52	19.90	19.44	18.91	23.78
Na2O	0.67	10.81	10.32	10.32	11.59	11.58	11.71	11.62	11.33	11.61	11.49	11.34	11.31	11.24	11.40	7.95
K2O	16.85	0.10	0.09	0.10	0.06	0.05	0.13	0.08	0.05	0.00	0.00	0.06	0.00	0.00	0.04	0.04
CaO	0.00	0.76	1.70	1.67	0.38	0.36	0.29	0.45	0.45	0.14	0.26	0.25	0.23	0.30	0.42	6.14
Total	100.26	100.06	100.87	100.32	100.00	99.74	99.19	99.96	99.93	99.95	100.37	100.78	100.68	100.33	99.09	98.09
Si	2.989	2.981	2.941	2.952	3.003	3.006	3.002	2.999	2.978	3.000	2.990	2.968	2.996	3.010	3.008	2.723
Al	0.995	1.028	1.068	1.052	0.989	0.985	0.984	0.990	1.027	1.000	1.008	1.046	1.015	0.995	0.983	1.268
Na	0.060	0.914	0.867	0.872	0.982	0.983	1.001	0.985	0.960	0.982	0.968	0.951	94.910	94.630	0.974	0.697
K	0.996	0.005	0.005	0.006	0.005	0.003	0.007	0.004	0.003	0.000	0.000	0.003	0.000	0.000	0.002	0.002
Ca	0.000	0.036	0.079	0.078	0.018	0.017	0.014	0.021	0.021	0.006	0.123	0.012	0.011	0.014	0.020	0.298
Ab	5.68	95.71	91.19	91.28	97.77	98.04	97.96	97.51	98.00	99.00	99.00	98.00	99.00	98.00	97.79	69.91
Or	94.31	0.56	0.53	0.57	0.45	0.30	0.69	0.42	0.00		0.00	0.50	0.00	0.00	0.24	0.24
An		3.73	8.28	8.15	1.77	1.67	1.35	2.07	2.00	1.00	1.00	1.50	1.00		1.98	29.85

Composition of garnet from Lacorne pluton

	Biotite monzogranite																			
Sample	613	613	613	613	630	631	631	631	634	634	634	634	634	634	634	634	634	634	665	665
SiO2	36.76	36.85	36.83	36.68	36.57	36.59	36.52	36.77	36.39	36.56	36.72	36.66	36.84	36.88	36.31	36.18	36.61	36.83	36.47	36.36
Al2O3	19.97	20.06	20.06	20.09	19.78	20.15	19.49	20.41	20.27	20.16	20.42	20.11	19.97	20.24	20.04	19.97	19.96	20.14	20.24	19.87
TiO2	0.08	0.07	0.05	0.02	0.05	0.03	0.17	0.02	0.01	0.02	0.03	0.15	0 15	0.22	0.03	0.10	0.03	0.02	0.03	0.12
FeO	18.60	18.82	19.11	19.72	18.27	19.75	16.59	21.32	24.79	24.41	24.57	24.14	23.66	20.41	20.82	22.84	24.62	25.16	19.80	17.01
Fe2O3	0.97	0.85	0.98	0.73	1.06	0.71	1.31	0.52	0.24	0.39	0.19	0.58	0.67	0.24	0.50	0.54	0.69	0.56	0.57	0.88
MgO	0.50	0.48	0.49	0.37	0.44	0.42	0.49	0.40	0.36	0.40	0.37	0.39	0.36	0.39	0.37	0.37	0.35	0.35	0.47	0.44
MnO	21.62	21.20	21.51	20.70	21.25	20.62	23.49	19.27	16.22	16.31	16.67	17.35	17.15	20.90	20.44	18.35	16.35	15.72	21.77	24.33
CaO	1.56	1.57	1.53	1.34	1.85	1.73	1.17	1.83	0.70	0.61	0.65	0.57	0.57	0.35	0.42	0.50	0.58	0.69	0.88	0.80
Total	100.06	99.90	100.56	99.65	99.27	100.00	99.23	100.54	98.98	98.86	99.62	99.95	99.57	99.63	98.93	98.85	99.19	99.47	100.23	99.81
Si	6.045	6.057	6.033	6.052	6.057	6.021	6.066	6.013	6.030	6.048	6.045	6.031	6.072	6.066	6.030	6.013	6.061	6.066	6.002	6.016
Al	3.870	3.886	3.873	3.906	3.861	3.961	3.815	3.934	3.959	3.931	3.961	3.898	3.880	3.923	3.923	3.912	3.895	3.100	3.926	3.875
Ti	0.010	0.009	0.006	0.003	0.006	0.004	0.021	0.003	0.002	0.002	0.003	0.019	0.019	0.027	0.004	0.013	0.004	0.002	0.004	0.015
Fe2+	2.557	2.588	2.618	2.721	2.531	2.718	2.305	2.916	3.435	3.376	3.382	3.321	3.290	2.807	2.891	3.174	3.409	3.465	2.725	2.354
Fe3+	0.120	0.105	0.121	0.091	0.133	0.088	0.164	0.064	0.030	0.049	0.023	0.072	0.083	0.030	0.063	0.068	0.086	0.069	0.071	0.110
Mg	0.123	0.118	0.120	0.091	0.109	0.103	0.121	0.098	0.088	0.099	0.091	0.097	0.088	0.095	0.091	0.092	0.086	0.087	0.115	0.109
Mn	3.011	2.952	2.985	0.289	2.981	2.874	3.305	2.670	2.276	2.285	2.327	2.418	2.395	2.911	2.875	2.584	2.293	2.193	3.035	3.410
Ca	0.275	0.277	0.269	0.237	0.328	0.305	0.208	0.321	0.124	0.109	0.114	0.100	0.101	0.062	0.074	0.088	0.103	0.122	0.155	0.142
Alm	42.86	43.61	43.70	45.79	42.54	45.29	38.81	48.57	57.95	57.51	57.16	55.93	55.91	47.62	48.71	53.49	57.81	59.01	45.18	39.14
Prp	2.05	1.96	2.00	1.53	1.83	1.72	2.04	1.62	1.50	1.68	1.54	1.61	1.51	1.63	1.54	1.54	1.47	1.47	1.91	1.80
Grs	1.34	1.78	1.30	1.62	2.02	2.78		3.69	1.24	0.43	1.07	0.00	0.00	0.00	0.00	0.00	0.00	0.03	0.72	0.00
Sps	50.48	49.75	49.82	48.69	50.11	47.90	55.65	44.46	38.45	38.97	39.36	40.76	40.86	49.69	48.48	43.47	38.97	37.44	50.33	56.70
Adr	3.27	2.88	3.18	2.37	3.50	2.30	3.51	1.65	0.86	1.41	0.87	1.69	1.72	1.05	1.26	1.50	1.75	2.05	1.85	2.36

Composition of garnet from Lacorne pluton

	Biotite monzogranite				Two-mica monzogranite															
Sample	665	665	673	675	652	652	652	652	652	652	672	672	672	672	672	672	672	672	672	672
SiO2	36.41	36.63	36.57	36.59	36.78	36.77	36.78	36.54	36.91	36.72	36.87	36.41	36.69	36.54	36.83	36.64	36.49	36.19	36.28	36.44
Al2O3	19.82	20.43	20.06	19.93	19.66	19.92	19.84	20.34	19.77	19.87	19.80	20.09	20.04	20.21	20.23	20.63	20.34	19.98	19.64	19.63
TiO2	0.19	0.01	0.06	0.02	0.06	0.11	0.03	0.00	0.05	0.06	0.12	0.07	0.08	0.05	0.06	0.01	0.07	0.13	0.08	0.10
FeO	17.67	19.41	19.62	22.71	23.73	23.73	23.94	23.78	23.21	24.18	20.50	21.36	21.41	22.63	23.01	24.18	24.40	23.46	22.95	23.15
Fe2O3	0.97	0.40	0.72	0.88	1.21	0.80	0.98	0.40	1.08	1.07	1.05	0.50	0.60	0.51	0.55	0.00	0.29	0.49	1.01	1.06
MgO	0.45	0.49	0.68	0.80	0.48	0.50	0.53	0.44	0.55	0.48	0.51	0.57	0.52	0.53	0.50	0.52	0.51	0.47	0.51	0.42
MnO	23.98	22.03	20.77	16.94	16.68	16.90	16.61	17.75	17.00	17.24	19.87	19.17	18.70	18.21	17.78	17.01	16.94	17.39	17.69	17.48
CaO	0.85	0.94	0.99	1.28	0.62	0.52	0.51	0.69	0.58	0.57	0.78	0.79	0.82	0.79	0.79	0.59	0.65	0.72	0.65	0.68
Total	100.34	100.34	99.69	99.15	99.44	99.25	99.22	99.94	99.15	100.19	99.50	98.96	98.86	99.67	99.75	99.58	99.69	98.83	98.81	98.96
Si	6.002	6.006	6.032	6.056	6.093	6.087	6.094	6.021	6.113	6.052	6.091	6.043	6.082	6.030	6.061	6.031	6.020	6.028	6.055	6.071
Al	3.856	3.949	3.903	3.888	3.842	3.886	3.875	3.950	3.859	3.860	3.855	3.929	3.915	3.931	3.924	4.002	3.955	3.922	3.863	3.854
Ti	0.024	0.001	0.007	0.003	0.008	0.014	0.004	0.000	0.006	0.007	0.015	0.009	0.010	0.006	0.007	0.001	0.009	0.016	0.010	0.013
Fe2+	2.436	2.662	2.734	3.143	3.288	3.285	3.318	3.276	3.214	3.333	2.832	2.965	2.968	3.152	3.167	3.329	3.366	3.268	3.204	3.226
Fe3+	0.120	0.050	0.069	0.110	0.150	0.100	0.122	0.050	0.135	0.133	0.130	0.062	0.075	0.063	0.069	0.000	0.036	0.062	0.127	0.133
Mg	0.111	0.120	0.167	0.197	0.119	0.123	0.131	0.108	0.136	0.118	0.126	0.141	0.129	0.130	0.123	0.128	0.125	0.117	0.127	0.104
Mn	3.348	3.061	2.902	2.375	2.369	2.370	2.331	2.478	2.385	2.407	2.781	2.695	2.626	2.546	2.479	2.372	2.367	2.454	2.501	2.467
Ca	0.150	0.165	0.175	0.227	0.110	0.092	0.091	0.122	0.103	0.101	0.138	0.105	0.146	0.140	0.139	0.104	0.115	0.129	0.116	0.121
Alm	40.29	44.31	45.74	52.69	55.67	55.96	56.51	54.73	55.06	55.93	48.19	49.91	50.58	52.81	53.61	56.11	56.35	54.77	53.86	54.51
Prp	1.83	1.99	2.80	3.32	2.01	2.10	2.23	1.82	2.33	1.98	2.14	2.38	2.20	2.17	2.09	2.14	2.08	1.95	2.13	1.76
Grs	0.00	1.48	0.50	0.98	0.00	0.00	0.00	41.42	0.00	0.00	0.00	0.58	0.32	0.61	0.43	1.72	0.79	0.20	0.00	0.00
Sps	55.39	50.94	48.54	39.97	40.25	40.37	39.71	0.73	40.65	40.40	47.32	45.36	44.75	42.66	41.96	39.98	36.63	41.12	42.05	41.68
Adr	2.48	1.27	2.43	2.64	1.87	1.57	1.54	1.31	1.76	1.69	2.35	1.83	1.87	1.84	1.74	0.01	1.04	1.96	1.95	2.05

Composition of garnet from Lacorne pluton

	Two-mica monzogranite																		
Sample	672	707	707	707	707	707	707	707	707	707	742	742	742	742	742	692	692	692	692
SiO2	36.28	36.51	36.61	36.66	36.29	36.37	36.50	36.64	36.67	36.38	36.84	37.21	36.68	36.50	37.00	37.50	37.29	37.66	37.18
Al2O3	19.82	20.06	20.33	19.94	20.06	19.70	19.72	19.76	20.08	19.91	19.88	19.87	19.13	19.38	19.37	20.44	20.12	20.34	20.53
TiO2	0.03	0.04	0.03	0.06	0.06	0.14	0.09	0.11	0.04	0.08	0.05	0.03	0.01	0.10	0.02	0.02	0.07	0.06	0.04
FeO	23.97	17.60	18.17	19.11	19.73	16.52	16.37	16.68	17.60	19.45	24.18	24.38	24.57	25.06	23.84	20.67	18.54	20.63	21.39
Fe2O3	0.78	0.73	0.45	0.90	0.61	0.95	1.16	1.07	0.72	0.82	1.06	1.06	1.94	1.37	1.68	0.69	0.92	0.79	0.44
MgO	0.46	0.48	0.46	0.50	0.46	0.40	0.43	0.41	0.44	0.50	0.43	0.50	0.47	0.53	0.47	0.57	0.60	0.57	0.52
MnO	16.64	23.04	22.71	21.69	21.63	23.95	24.52	23.70	22.94	21.33	16.96	15.87	15.91	15.13	16.42	19.99	21.86	19.58	19.76
CaO	0.70	1.05	1.17	0.84	0.83	0.96	1.05	1.14	1.09	1.00	0.57	0.49	0.66	0.64	0.54	0.91	0.84	0.95	0.83
Total	98.68	99.71	99.93	99.70	99.69	98.99	99.84	99.51	99.58	99.47	99.97	99.43	99.37	98.71	99.34	100.79	100.24	100.58	100.69
Si	6.055	6.029	6.022	6.054	6.006	6.053	6.038	6.063	6.052	6.028	6.075	6.138	6.110	6.096	6.138	6.092	6.098	6.121	6.056
Al	3.898	3.904	3.941	3.881	3.916	3.864	3.844	3.854	3.906	3.888	3.864	3.863	3.755	3.815	3.787	3.914	3.878	3.896	3.941
Ti	0.004	0.005	0.004	0.006	0.006	0.018	0.011	0.014	0.005	0.010	0.006	0.004	0.001	0.013	0.003	0.002	0.009	0.007	0.005
Fe2+	3.346	2.458	2.499	2.639	2.731	2.299	2.264	2.308	2.430	2.696	3.336	3.363	3.423	3.500	3.308	2.809	2.535	2.804	2.914
Fe3+	0.098	0.091	0.005	0.111	0.076	0.119	0.144	0.133	0.098	0.102	0.130	0.134	0.243	0.173	0.210	0.084	0.114	0.097	0.054
Mg	0.114	0.118	0.113	0.123	0.114	0.099	0.106	0.101	0.108	0.124	0.106	0.123	0.117	0.132	0.116	0.138	0.146	0.138	0.126
Mn	2.352	3.229	3.164	3.034	3.032	3.376	3.436	3.322	3.207	2.994	2.369	2.217	2.245	2.141	2.308	2.751	3.028	2.696	2.727
Ca	0.125	0.186	0.206	0.149	0.147	0.171	0.186	0.202	0.193	0.178	0.101	0.089	0.118	0.115	0.096	0.158	0.147	0.165	0.145
Alm	56.34	41.07	41.78	44.39	45.33	38.66	37.78	38.90	40.92	45.00	56.43	58.06	57.99	59.46	56.76	47.96	43.29	48.32	49.30
Prp	1.93	1.97	1.89	2.07	1.88	1.67	1.77	1.70	1.82	2.06	1.79	2.12	1.98	2.24	1.99	2.36	2.50	2.38	2.14
Grs	0.00	0.70	1.97	0.00	0.36	0.00	0.00	0.00	0.87	0.16	0.00	0.00	0.00	0.00	0.00	0.49	0.00	0.17	0.96
Sps	39.62	53.85	52.89	51.04	50.34	56.79	57.34	55.99	54.01	49.98	40.06	38.30	38.03	36.36	39.59	46.98	51.70	46.45	46.12
Adr	2.11	2.40	1.48	2.50	2.08	2.88	3.11	3.41	2.38	2.80	1.70	1.50	2.00	1.95	1.65	2.21	2.51	2.69	1.49

Composition of garnet from Lacorne pluton

	Muscovite monzogranite							Aplite-pegmatite												
Sample	637	647	647	647	647	647	647	684	701	701	701	701	709C	709C	709C	709C	709C	709C	709C	709C
SiO2	36.56	36.65	36.63	36.62	36.36	36.43	36.66	36.60	36.29	36.31	36.17	36.29	36.64	36.76	36.97	37.07	36.90	36.81	36.54	36.79
Al2O3	19.57	19.96	20.11	19.96	20.03	19.66	19.62	20.21	19.35	19.53	19.64	20.06	19.96	20.19	20.05	20.07	20.29	20.13	20.12	20.30
TiO2	0.05	0.05	0.04	0.06	0.06	0.09	0.05	0.04	0.21	0.10	0.17	0.06	0.04	0.04	0.05	0.01	0.03	0.04	0.05	0.00
FeO	19.39	24.69	24.15	23.16	22.93	22.47	22.10	25.91	15.21	17.29	17.71	19.36	17.63	17.87	13.72	11.13	10.66	17.29	17.83	8.03
Fe2O3	1.27	0.88	0.79	0.90	0.67	0.79	1.23	0.59	1.30	1.24	0.92	0.59	0.73	0.62	0.54	0.52	0.29	0.57	0.45	0.27
MgO	0.24	0.53	0.54	0.56	0.57	0.52	0.52	0.40	0.47	0.38	0.41	0.30	0.16	0.17	0.10	0.04	0.04	0.19	0.13	0.02
MnO	20.24	16.58	17.68	18.37	18.59	18.57	18.53	15.82	25.16	23.77	23.11	22.09	23.53	23.75	27.02	29.67	30.55	23.77	23.69	32.67
CaO	1.75	0.46	0.48	0.53	0.46	0.48	0.51	0.62	0.75	0.73	0.73	0.92	0.69	0.69	0.61	0.54	0.64	0.73	0.53	0.81
Total	99.07	100.02	100.42	100.20	99.69	99.23	99.22	100.19	98.76	99.35	98.86	99.69	99.38	100.09	99.06	99.05	99.40	99.53	99.34	99.09
Si	6.079	6.045	6.023	6.033	6.017	6.049	6.089	6.026	6.064	6.044	6.037	6.009	6.059	6.036	6.101	6.120	6.083	6.063	6.047	6.071
Al	3.835	3.884	3.897	3.879	3.907	3.890	3.841	3.922	3.811	3.632	3.864	3.919	3.890	3.908	3.899	3.906	3.941	3.907	3.926	3.947
Ti	0.006	0.006	0.005	0.010	0.010	0.011	0.006	0.005	0.026	0.013	0.021	0.008	0.005	0.004	0.007	0.002	0.003	0.005	0.006	0.000
Fe2+	2.696	3.433	3.321	3.191	3.173	3.120	3.069	3.568	2.126	2.407	2.473	2.680	2.438	2.454	1.894	1.536	1.469	2.382	2.468	1.108
Fe3+	0.159	0.110	0.098	0.111	0.083	0.099	0.153	0.073	0.163	0.156	0.115	0.074	0.091	0.077	0.066	0.064	0.036	0.071	0.056	0.034
Mg	0.060	0.130	0.132	0.138	0.141	0.129	0.129	0.098	0.117	0.094	0.102	0.074	0.038	0.042	0.025	0.009	0.011	0.046	0.032	0.005
Mn	2.851	2.317	2.463	2.563	2.606	2.612	2.607	2.207	3.564	3.352	3.268	3.098	3.295	3.303	3.777	4.149	4.266	3.317	3.321	4.594
Ca	0.332	0.081	0.085	0.094	0.082	0.085	0.091	0.109	0.134	0.130	0.131	0.163	0.122	0.122	0.109	0.095	0.113	0.128	0.095	0.143
Alm	45.56	57.59	55.34	53.31	52.87	52.47	52.06	59.64	35.78	40.23	41.40	44.55	41.01	41.44	32.45	26.26	24.89	40.47	41.64	18.60
Prp	1.01	2.19	2.21	2.30	2.34	2.16	2.18	1.64	1.97	1.58	1.71	1.23	0.71	0.70	0.43	0.17	0.17	0.80	0.54	0.08
Grs	1.09	0.00	0.00	0.00	0.00	0.00	0.00	0.00	0.00	0.00	0.00	0.68	0.00	0.00	0.00	0.00	0.53	0.09	0.00	1.34
Sps	48.17	38.86	41.04	42.83	43.42	43.93	44.22	36.69	59.99	56.02	54.71	51.50	56.21	55.81	65.26	71.91	73.01	56.53	56.22	78.67
Adr	4.18	1.36	1.41	1.56	1.36	1.44	1.54	1.83	2.26	2.18	2.19	2.03	2.07	5.05	1.86	1.66	1.40	2.11	1.59	1.11

Composition of garnet from Lacorne pluton

	Aplite-pegmatite																		
Sample	709C	709C	709C	709C	795	795	606	606	617	624B	624B	624B	624B	640	640	640	646A	646A	757	757
SiO2	36.55	36.61	36.47	36.61	36.46	36.79	37.21	37.53	36.19	36.48	36.72	36.37	36.67	36.62	36.78	36.54	36.68	36.37	37.06	36.39
Al2O3	20.21	20.36	20.36	20.03	20.49	20.35	20.15	20.58	20.08	20.02	19.91	20.42	19.98	19.95	20.18	19.89	19.72	19.55	20.38	20.38
TiO2	0.05	0.07	0.05	0.04	0.08	0.11	0.06	0.02	0.08	0.03	0.03	0.04	0.05	0.03	0.05	0.07	0.05	0.09	0.07	0.01
FeO	15.72	17.73	16.65	10.77	25.32	24.71	16.46	13.79	22.36	17.81	17.40	19.24	18..68	18.37	18.24	18.23	18.28	19.56	5.39	9.78
Fe2O3	0.35	0.26	0.23	0.62	0.34	0.60	0.74	0.44	0.38	0.61	0.78	0.07	0.87	0.69	0.37	0.62	1.05	1.22	0.31	0.45
MgO	0.09	0.16	0.12	0.05	0.49	0.54	0.09	0.07	0.32	0.12	0.14	0.13	0.17	0.12	0.10	0.11	0.21	0.27	0.00	0.02
MnO	25.45	23.86	25.36	30.15	16.59	16.98	24.85	27.46	19.98	23.74	23.65	22.66	22.66	22.91	23.11	22.76	23.12	21.67	36.21	31.99
CaO	0.75	0.67	0.50	0.74	0.55	0.46	0.43	0.86	0.49	0.40	0.36	0.44	0.37	0.41	0.41	0.42	0.31	0.42	0.60	0.76
Total	99.17	99.72	99.74	99.21	100.32	100.54	99.99	100.75	99.88	99.21	98.99	99.37	80.97	99.10	99.24	98.64	99.42	99.15	100.02	99.78
Si	6.043	6.027	6.018	6.076	5.957	5.983	6.113	6.101	6.029	6.060	6.010	6.024	6.085	6.062	6.078	6.067	6.070	6.034	6.070	6.053
Al	3.937	3.950	3.959	3.897	3.946	3.901	3.901	3.943	0.394	3.920	3.899	3.988	3.886	3.891	3.929	3.893	3.846	3.822	3.934	3.931
Ti	0.006	0.008	0.007	0.005	0.010	0.014	0.007	0.002	0.010	0.004	0.004	0.005	0.006	0.004	0.006	0.009	0.006	0.011	0.009	0.001
Fe2+	2.173	2.441	2.298	1.486	3.459	3.361	2.261	1.875	3.115	2.474	2.418	2.665	2.606	2.543	2.521	2.532	2.530	2.713	0.738	1.339
Fe3+	0.043	0.032	0.028	0.077	0.042	0.074	0.091	0.054	0.047	0.077	0.098	0.009	0.108	0.086	0.046	0.077	0.131	0.152	0.038	0.056
Mg	0.022	0.039	0.029	0.012	0.118	0.132	0.022	0.017	0.080	0.030	0.034	0.032	0.042	0.029	0.026	0.027	0.051	0.065	0.000	0.004
Mn	3.563	3.327	3.544	4.216	2.296	2.339	3.458	3.782	2.679	3.341	3.329	3.179	3.168	3.212	3.234	3.201	3.241	3.044	5.024	4.434
Ca	0.133	0.119	0.088	0.131	0.097	0.080	0.076	0.150	0.088	0.070	0.064	0.077	0.065	0.073	0.072	0.075	0.055	0.075	0.105	0.133
Alm	36.85	41.18	38.53	25.31	58.01	56.97	38.67	32.20	52.26	41.82	41.36	44.75	44.31	43.38	42.95	43.34	43.01	46.05	12.38	22.96
Prp	0.38	0.66	0.50	0.21	2.00	2.21	0.38	0.29	1.33	0.50	0.59	0.54	0.71	0.51	0.42	0.47	0.88	1.13	0.04	0.08
Grs	0.93	0.93	0.56	0.00	0.58	0.00	0.00	1.11	0.02	0.00	0.00	0.96	0.00	0.00	0.00	0.00	0.00	0.00	0.25	1.44
Sps	60.52	56.17	59.49	72.23	38.39	39.47	59.45	64.94	44.94	56.47	56.95	53.40	53.67	54.88	55.38	54.91	55.17	51.55	85.78	74.71
Adr	1.33	1.06	0.92	2.24	1.03	1.35	1.30	1.46	1.45	1.20	1.10	0.35	1.11	1.24	1.24	1.28	0.94	1.26		

Composition of garnet from Lacorne pluton

	Aplite-pegmatite													
Sample	757	757	757	757	1007	772B	772B	772B	772B	1001	1001	1001	1001	1001
SiO2	37.05	37.13	37.09	36.39	36.53	37.64	37.50	37.71	37.62	36.63	36.48	36.16	36.30	36.83
Al2O3	20.17	20.36	20.16	20.43	20.07	20.66	20.67	20.36	20.99	19.89	19.83	20.03	19.88	20.10
TiO2	0.01	0.04	0.05	0.03	0.04	0.04	0.04	0.02	0.02	0.04	0.04	0.02	0.03	0.03
FeO	11.75	13.26	3.64	12.14	16.19	7.78	9.39	13.00	19.38	18.25	18.45	19.02	18.23	19.41
Fe2O3	0.57	0.71	0.44	0.06	0.60	0.13	0.32	0.69	0.05	0.80	0.89	0.52	0.88	0.58
MgO	0.02	0.00	0.02	0.02	0.10	0.14	0.32	0.56	1.16	0.11	0.13	0.12	0.11	0.16
MnO	29.65	29.12	37.32	29.30	23.58	31.96	30.59	26.01	19.82	23.29	23.22	22.71	23.91	22.10
CaO	0.53	0.75	0.56	0.42	0.38	1.87	1.95	1.97	1.86	0.38	0.38	0.47	0.34	0.37
Total	99.75	101.37	99.28	98.79	99.49	100.22	100.78	100.32	100.90	99.39	99.42	99.05	99.68	99.58
Si	6.069	6.034	6.110	6.067	6.055	6.117	6.063	6.111	6.049	6.062	6.046	6.015	6.012	6.074
Al	3.907	3.900	3.913	3.965	3.921	3.953	3.939	3.888	3.978	3.879	3.873	3.927	3.881	3.907
Ti	0.001	0.005	0.007	0.004	0.005	0.005	0.004	0.002	0.002	0.005	0.005	0.002	0.002	0.004
Fe2+	1.615	1.802	0.501	1.672	2.522	1.056	1.270	1.762	2.606	2.525	2.557	2.645	2.524	2.677
Fe3+	0.070	0.087	0.055	0.008	0.074	0.016	0.039	0.084	0.006	0.100	0.111	0.065	0.110	0.072
Mg	0.006	0.000	0.006	0.004	0.025	0.033	0.076	0.136	0.279	0.026	0.032	0.029	0.027	0.039
Mn	4.128	4.009	5.207	4.087	3.311	4.396	4.189	3.570	2.700	3.264	3.260	3.200	3.354	3.087
Ca	0.094	0.130	0.099	0.074	0.068	0.326	0.338	0.342	0.321	0.068	0.068	0.084	0.060	0.065
Alm	27.46	30.30	8.29	28.72	42.56	17.84	21.48	30.12	44.03	42.86	43.21	44.43	42.37	45.51
Prp	0.08	0.04	0.08	0.08	0.42	0.59	1.32	2.34	4.72	0.46	0.54	0.50	0.45	0.67
Grs	0.00	0.00	0.00	1.17	0.00	4.46	4.38	3.22	4.96	0.00	0.00	0.00	0.00	0.00
Sps	70.84	67.46	89.91	69.93	55.88	75.95	71.44	61.64	45.81	55.53	55.10	53.67	56.17	52.70
Adr					1.14	1.16	1.39	2.68	0.48	1.15	1.14	1.40	1.01	1.12

Composition of epidote from Lacorne pluton

	Biotite monzogranite																	Two-mica monzogranite	
Sample	603	603	613	613	613	614	614	616	620	621	622	622	622	634	665	666	673	707	707
SiO2	38.39	39.20	39.24	38.44	38.23	38.34	39.57	38.45	38.32	38.45	38.59	38.30	38.23	39.01	38.15	38.73	38.05	38.94	38.30
TiO2	0.00	0.00	0.30	1.16	0.20	0.17	0.00	0.27	0.30	0.00	0.10	0.28	0.15	0.00	0.06	0.06	0.09	0.02	0.19
Al2O3	22.80	24.83	22.35	22.31	21.91	22.10	23.79	21.54	21.83	22.15	21.13	21.45	21.95	23.06	23.33	20.94	21.69	22.93	22.58
Fe2O3	13.78	10.95	12.95	12.86	13.88	14.87	11.72	15.02	14.40	13.90	16.03	14.85	15.03	13.37	13.01	14.86	15.20	13.01	13.44
MnO	0.37	0.16	2.47	0.46	0.54	0.46	0.65	0.41	0.25	0.15	0.36	0.13	0.62	0.37	0.42	0.57	0.27	0.27	0.46
CaO	22.86	22.96	22.74	22.67	22.54	22.88	22.17	23.09	22.08	23.28	22.59	22.99	21.85	22.57	22.86	21.27	22.77	22.77	22.77
OH	3.51	3.58				3.50	3.56	3.50	3.46	3.49	3.49	3.48	3.47	3.54	3.51	3.43	3.47	3.52	3.50
Total	98.20	98.12	100.05	97.90	97.30	98.82	98.10	98.78	97.18	97.93	98.80	98.00	97.83	98.38	97.83	96.43	98.07	97.94	97.74
Si	3.170	3.196	3.198	3.177	3.190	3.160	3.237	3.179	3.197	3.187	3.189	3.182	3.178	3.202	3.155	3.256	3.163	3.209	3.176
Ti	0.000	0.000	0.018	0.072	0.013	0.011	0.000	0.017	0.019	0.000	0.006	0.018	0.009	0.000	0.004	0.004	0.006	0.001	0.012
Al	2.219	2.387	2.147	2.174	2.155	2.148	2.294	2.094	2.147	2.164	2.059	2.101	2.151	2.231	2.275	2.075	2.126	2.227	2.207
Fe3+	0.856	0.672	0.794	0.800	0.872	0.922	0.721	0.932	0.904	0.867	0.997	0.928	0.940	0.826	0.810	0.940	0.951	0.807	0.839
Mn	0.026	0.011	0.171	0.032	0.038	0.032	0.059	0.029	0.018	0.011	0.025	0.009	0.044	0.026	0.029	0.041	0.019	0.017	0.032
Ca	2.022	2.008	1.986	2.008	2.015	2.021	1.943	2.048	1.974	2.062	2.000	2.047	1.946	1.985	2.026	1.916	2.028	2.010	2.023

Composition of columbite-tantalite from the Preissac pluton

Rock	Muscovite-garnet monzogranite							
Sample	471	471	471	471	474	477	477	477
	1	2	3	4	1			
Nb2O5	72.5	72.2	71.6	73.0	71.6	72.3	72.4	72.2
MgO	0.06	0.04	0.05	0.05	0.02	0.07	0.07	0.06
CaO	0.02	0.00	0.01	0.01	0.01	0.19	0.07	0.40
TiO2	1.13	1.04	1.12	1.16	1.08	0.98	0.97	1.28
FeO	10.5	10.4	10.4	10.3	10.7	10.1	10.4	9.68
MnO	9.62	9.83	9.72	9.99	9.98	9.59	9.56	10.07
Ta2O5	5.24	5.10	5.37	5.04	5.34	5.09	5.10	5.19
Total	99.1	98.6	98.2	99.6	98.7	98.3	98.6	98.9
Nb	1.887	1.888	1.881	1.888	1.873	1.895	1.893	1.879
Mg	0.005	0.004	0.004	0.004	0.002	0.006	0.006	0.005
Ca	0.001	0.000	0.001	0.001	0.000	0.012	0.004	0.025
Ti	0.049	0.045	0.049	0.050	0.047	0.043	0.042	0.055
Fe	0.505	0.503	0.504	0.495	0.517	0.488	0.503	0.466
Mn	0.469	0.482	0.478	0.485	0.489	0.471	0.468	0.491
Ta	0.082	0.080	0.085	0.079	0.084	0.080	0.080	0.081
A site	0.98	0.99	0.99	0.98	1.01	0.98	0.98	0.99
B site	2.02	2.01	2.01	2.02	2.00	2.02	2.01	2.02
Ta/(Ta+Nb)	0.04	0.04	0.04	0.04	0.04	0.04	0.04	0.04
Mn/(Mn+Fe)	0.48	0.49	0.49	0.49	0.49	0.49	0.48	0.51
ΣCation	3.00	3.00	3.00	3.00	3.01	2.99	3.00	3.00

Composition of columbite-tantalite from the Moly Hill pluton

Rock	Aplite dike						
Sample	30	30	30	30	30	30	30
	1	1	1 Core 2				rim 2
Nb2O5	64.5	69.6	68.3	69.0	63.2	58.3	43.8
MgO	0.11	0.13	0.11	0.12	0.12	0.14	0.15
CaO	0.03	0.03	0.01	0.02	0.01	0.00	0.02
TiO2	1.11	1.07	1.02	1.16	1.53	1.70	1.38
FeO	13.5	13.7	13.9	13.8	13.6	13.3	12.1
MnO	5.92	6.21	6	5.89	5.78	5.48	5.09
Ta2O5	14.06	8.91	9.7	8.97	15.22	20.67	37.4
Total	99.2	99.7	99.1	99.0	99.5	99.7	100.0
Nb	1.738	1.828	1.813	1.824	1.705	1.606	1.295
Mg	0.010	0.011	0.010	0.010	0.011	0.013	0.014
Ca	0.002	0.002	0.000	0.001	0.001	0.000	0.002
Ti	0.050	0.047	0.045	0.051	0.069	0.078	0.068
Fe	0.673	0.666	0.682	0.677	0.678	0.679	0.664
Mn	0.299	0.305	0.298	0.292	0.292	0.283	0.282
Ta	0.228	0.141	0.155	0.143	0.247	0.342	0.666
A site	0.98	0.98	0.99	0.98	0.98	0.97	0.96
B site	2.02	2.02	2.01	2.02	2.02	2.03	2.03
Ta/(Ta+Nb)	0.12	0.07	0.08	0.07	0.13	0.18	0.34
Mn/(Mn+Fe)	0.31	0.31	0.30	0.30	0.30	0.29	0.30
ΣCation	3.00	3.00	3.00	3.00	3.00	3.00	2.99

Composition of columbite-tantalite from the Lamotte pluton

	764 1	764 2	764 3	764 4	795 1	795 2	795 3	795 4	795 5	795 6	795 7	912 1	912 2	912 3
Nb2O5	72.48	63.07	73.69	72.98	69.36	69.64	68.07	70.26	70.81	71.28	71.16	70.83	67.77	71.22
MgO	0.09	0.05	0.09	0.13	0.14	0.15	0.18	0.09	0.15	0.17	0.16	0.01	0.06	0.06
CaO	0	0.03	0.01	0.44	0.01	0	0.02	0.51	0.02	0	0.01	0	0.05	0.02
TiO2	0.58	0.85	0.44	0.8	0.73	0.66	0.75	0.64	0.79	0.45	0.41	0.35	0.4	0.6
FeO	13.15	10.96	14.28	13.13	14.75	15.26	15.86	11.95	13.6	15.42	15.33	13.18	12.79	13.28
MnO	6.73	8.27	5.72	6.16	5.32	4.96	4.19	8.02	6.04	4.22	4.27	6.46	6.42	7.68
Ta2O5	6.81	16.63	5.49	5.52	7.94	8.03	10.57	6.89	7.98	7.14	7.22	7.78	11.62	5.63
TOTAL	99.84	99.86	99.72	99.16	98.25	98.7	99.64	98.36	99.39	98.68	98.56	98.61	99.11	98.49
Nb	1.886	1.708	1.911	1.898	1.845	1.845	1.804	1.856	1.858	1.881	1.881	1.876	1.814	1.874
Mg	0.008	0.005	0.008	0.011	0.012	0.013	0.015	0.008	0.013	0.014	0.014	0.001	0.005	0.005
Ca	0.000	0.002	0.001	0.027	0.001	0.000	0.001	0.032	0.001	0.000	0.001	0.000	0.003	0.001
Ti	0.025	0.038	0.019	0.035	0.032	0.029	0.033	0.028	0.035	0.020	0.018	0.015	0.018	0.026
Fe	0.633	0.549	0.685	0.632	0.725	0.748	0.777	0.585	0.660	0.753	0.749	0.646	0.633	0.644
Mn	0.328	0.420	0.278	0.300	0.265	0.246	0.208	0.397	0.297	0.209	0.211	0.321	0.322	0.375
Ta	0.107	0.271	0.086	0.086	0.127	0.128	0.169	0.110	0.126	0.113	0.115	0.124	0.187	0.089
A site	0.99	1.01	0.99	1.00	1.04	1.04	1.04	1.05	1.01	1.00	0.99	0.97	0.96	1.02
B site	1.99	1.98	2.00	1.98	1.97	1.97	1.97	1.97	1.98	1.99	2.00	2.02	2.02	1.99
Ta'	0.05	0.14	0.04	0.04	0.06	0.06	0.09	0.06	0.06	0.06	0.06	0.06	0.09	0.05
Mn'	0.34	0.43	0.29	0.32	0.27	0.25	0.21	0.40	0.31	0.22	0.22	0.33	0.34	0.37
Σcat	2.99	2.99	2.99	2.99	3.01	3.01	3.01	3.02	2.99	2.99	2.99	2.98	2.98	3.01

Ta': Ta/(Ta+Nb), Mn': Mn/(Mn+Fe)

Composition of columbite-tantalite from the Lamotte pluton

	912 4	961 1	961 2	961 3	961 opaq	961 trans	961 5	961 7	TMC-2 opaque	TMC-2 opaque	TMC-2 opaque	TMC-2 opaque	TMC-2 opaque
Nb2O5	72.13	40.85	31.41	40.62	35.13	46.36	39.51	39.69	34.19	34.61	33.55	30.03	34.04
MgO	0.05	0.03	0.02	0.02	0.05	0	0.05	0.03	0.01	0.01	0.02	0	0.02
CaO	0.01	0.01	0.01	0.02	0	0.02	0.01	0.01	0.01	0.07	0.03	0.02	0.02
TiO2	0.31	0.3	0.71	1.06	0.41	0.65	0.5	0.46	0.13	0.16	0.16	0.18	0.18
FeO	13.53	10.47	9.68	8.84	10.62	6.35	11.13	11.01	6.24	6.17	6.53	5.72	5.66
MnO	6	6.45	6.33	8.53	6	11	5.92	6.44	10.12	10.06	9.83	9.88	10.71
Ta2O5	7.74	40.9	51.42	40.67	47.11	34.26	42.6	42.38	48.32	47.94	49.19	53.36	48.42
TOTAL	99.77	99.01	99.58	99.76	99.32	98.64	99.72	100.02	99.02	99.02	99.31	99.19	99.05
Nb	1.886	1.249	1.002	1.227	1.103	1.377	1.207	1.207	1.084	1.096	1.063	0.974	1.078
Mg	0.004	0.003	0.003	0.002	0.005	0.000	0.005	0.003	0.005	0.005	0.010	0.000	0.010
Ca	0.000	0.001	0.001	0.001	0.000	0.001	0.001	0.001	0.001	0.052	0.002	0.002	0.000
Ti	0.013	0.015	0.038	0.053	0.021	0.032	0.025	0.023	0.007	0.004	0.008	0.010	0.009
Fe	0.655	0.593	0.571	0.494	0.617	0.349	0.629	0.619	0.366	0.362	0.383	0.343	0.332
Mn	0.294	0.370	0.378	0.483	0.353	0.612	0.339	0.367	0.601	0.597	0.584	0.660	0.636
Ta	0.122	0.752	0.987	0.739	0.890	0.612	0.783	0.779	0.921	0.913	0.938	1.041	0.923
A site	0.95	0.97	0.95	0.98	0.98	0.96	0.97	0.99	0.97	1.02	0.98	1.00	0.98
B site	2.02	2.02	2.03	2.02	2.01	2.02	2.02	2.01	2.01	2.01	2.01	2.02	2.01
Ta'	0.06	0.38	0.50	0.38	0.45	0.31	0.39	0.39	0.46	0.45	0.47	0.52	0.46
Mn'	0.31	0.38	0.40	0.49	0.36	0.64	0.35	0.37	0.62	0.62	0.60	0.66	0.66
Σcat	2.97	2.98	2.98	3.00	2.99	2.98	2.99	3.00	2.98	3.03	2.99	3.03	2.99

Ta': Ta/(Ta+Nb), Mn': Mn/(Mn+Fe)

Composition of columbite-tantalite from the Lamotte pluton

	TMC-2 Trans	TMC-2 Trans	TMC-2 opaq	TMC-2 1	TMC-2 2	HP5-9 1	HP5-9 2	HP5-9 3	HP5-9 4	HP5-9 5	HP5-9 6	HP5-9 7	HP5-9 8	HP5-9 9
Nb2O5	52.73	51.18	47.11	67.35	67.29	15.27	10.76	8.33	17.3	27.88	10	9.07	23.72	20.38
MgO	0	0	0.03	0.03	0.02	0	0.01	0	0	0.05	0.01	0	0.02	0
CaO	0.02	0.02	0.03	0	0	0.01	0.01	0.02	0	0.02	0.01	0.01	0	0.01
TiO2	0.09	0.09	0.14	0.12	0.18	0.19	0.2	0.2	0.25	0.32	0.21	0.22	0.15	0.2
FeO	5.39	5.27	8.4	9.29	9.85	0.32	0.18	0.45	0.3	4.8	0.17	0.18	3.77	0.43
MnO	12.47	12.39	8.85	10.01	9.46	14.76	14.14	14.12	14.9	11.17	14.15	13.98	11.62	15.12
Ta2O5	29.01	30.69	34.57	12.39	12.25	70.39	74.9	77.4	67.89	56.55	74.54	75.75	61.42	64.55
TOTAL	99.71	99.64	99.13	99.19	99.05	100.9	100.2	100.5	100.6	100.8	99.09	99.21	100.7	100.7
Nb	1.513	1.481	1.393	1.805	1.806	0.530	0.386	0.303	0.594	0.900	0.364	0.332	0.786	0.688
Mg	0.000	0.000	0.015	0.013	0.009	0.001	0.002	0.000	0.000	0.005	0.001	0.000	0.002	0.000
Ca	0.001	0.001	0.009	0.001	0.000	0.001	0.001	0.002	0.000	0.002	0.001	0.001	0.000	0.001
Ti	0.004	0.004	0.006	0.005	0.008	0.011	0.012	0.012	0.014	0.017	0.013	0.014	0.008	0.011
Fe	0.286	0.282	0.460	0.461	0.489	0.020	0.012	0.030	0.019	0.287	0.011	0.013	0.231	0.027
Mn	0.670	0.672	0.490	0.503	0.476	0.959	0.951	0.961	0.959	0.676	0.966	0.959	0.722	0.956
Ta	0.501	0.534	0.615	0.200	0.198	1.469	1.618	1.691	1.403	1.098	1.633	1.668	1.225	1.310
A site	0.96	0.95	0.97	0.98	0.97	0.98	0.97	0.99	0.98	0.97	0.98	0.97	0.96	0.98
B site	2.02	2.02	2.01	2.01	2.01	2.01	2.02	2.01	2.01	2.02	2.01	2.01	2.02	2.01
Ta'	0.25	0.27	0.31	0.10	0.10	0.73	0.81	0.85	0.70	0.55	0.82	0.83	0.61	0.66
Mn'	0.70	0.70	0.52	0.52	0.49	0.98	0.99	0.97	0.98	0.70	0.99	0.99	0.76	0.97
Σcat	2.98	2.97	2.99	2.99	2.99	2.99	2.98	3.00	2.99	2.98	2.99	2.99	2.97	2.99

Ta': Ta/(Ta+Nb), Mn': Mn/(Mn+Fe)

Composition of columbite-tantalite from Lamotte

	HP5-9 10	HP5-9 11	HP5-9 12
Nb2O5	9.12	19.18	30.12
MgO	0	0.01	0
CaO	0.01	0	0
TiO2	0.23	0.25	0.11
FeO	0.25	0.28	0.25
MnO	13.68	15.06	16.01
Ta2O5	76.02	64.73	54.01
TOTAL	99.31	99.51	100.5
Nb	0.334	0.658	0.965
Mg	0.000	0.001	0.000
Ca	0.001	0.000	0.000
Ti	0.014	0.014	0.006
Fe	0.017	0.018	0.015
Mn	0.938	0.968	0.961
Ta	1.673	1.336	1.040
A site	0.96	0.99	0.98
B site	2.02	2.01	2.01
Ta'	0.83	0.67	0.52
Mn'	0.98	0.98	0.98
∑cat	2.98	2.99	2.99

Ta': Ta/(Ta+Nb), Mn': Mn/(Mn+Fe)

Composition of columbite-tantalite from the Lacorne pluton

	633 1	606 1	606 2	606 3	617 1C	617 1R	1001 1	1001 2	1001 rim 3	1001 4	1001 5	1001 6	1001 7
Nb2O5	70.85	69.12	70.44	69.22	70.96	71.47	70.5	64.15	37.82	40.52	38.41	71.33	70.56
MgO	0.05	0.08	0.05	0.07	0.12	0.13	0.06	0.07	0.05	0.07	0.06	0.07	0.05
CaO	0.02	0.01	0.01	0.01	0	0	0.03	0.01	0.01	0	0.01	0.03	0
TiO2	1.17	0.52	0.45	0.45	0.26	0.29	0.79	0.68	2.07	1.79	2.01	0.96	0.76
FeO	11.34	11.05	11.64	11.02	13.35	13.47	12.14	12.55	10.45	10.22	10.35	11.86	11.54
MnO	7.97	9.11	8.54	9.12	6.59	6.3	7.87	7.25	6.78	6.83	6.63	7.95	8.57
Ta2O5	7.62	9.23	9.12	8.84	7.97	7.45	8.94	14.52	41.79	40.06	41.65	6.88	8.78
TOTAL	99.02	99.12	100.3	98.73	99.25	99.11	100.3	99.23	98.97	99.49	99.12	99.08	100.3
Nb	1.860	1.833	1.845	1.841	1.870	1.881	1.831	1.729	1.140	1.202	1.155	1.860	1.834
Mg	0.004	0.007	0.004	0.006	0.010	0.011	0.006	0.007	0.005	0.007	0.006	0.006	0.004
Ca	0.001	0.001	0.001	0.001	0.000	0.000	0.002	0.001	0.000	0.000	0.001	0.002	0.000
Ti	0.051	0.023	0.020	0.020	0.011	0.013	0.034	0.030	0.104	0.088	0.100	0.042	0.033
Fe	0.550	0.542	0.564	0.542	0.651	0.656	0.583	0.626	0.583	0.561	0.576	0.572	0.555
Mn	0.392	0.453	0.419	0.455	0.325	0.311	0.383	0.366	0.383	0.380	0.373	0.389	0.417
Ta	0.120	0.147	0.144	0.141	0.126	0.118	0.140	0.235	0.758	0.715	0.754	0.108	0.137
A site	0.95	1.00	0.99	1.00	0.99	0.98	0.97	1.00	0.97	0.95	0.96	0.97	0.98
B site	2.03	2.00	2.01	2.00	2.01	2.01	2.00	1.99	2.00	2.01	2.01	2.01	2.00
Ta'	0.06	0.07	0.07	0.07	0.06	0.06	0.07	0.12	0.40	0.37	0.39	0.05	0.07
Mn'	0.42	0.46	0.43	0.46	0.33	0.32	0.40	0.37	0.40	0.40	0.39	0.40	0.43
ΣCat	2.98	3.01	3.00	3.01	2.99	2.99	2.98	2.99	2.97	2.95	2.96	2.98	2.98

Ta':Ta/(Ta+Nb); Mn': Mn/(Mn+Fe)

Composition of columbite-tantalite from the Lacorne pluton

	1001 8	1001 9	1001 10	1001 11	1001 12	1001 13	1001 14	1001A 1	1001A 2	1001A 3	1001A 4	1001A 5	1001A 6
Nb2O5	69.63	69.12	69.57	68.89	68.9	70.51	50.4	41.16	44.29	43.81	41.81	40.57	43.42
MgO	0.07	0.05	0.05	0.07	0.04	0.07	0.02	0.05	0.07	0.06	0.05	0.04	0.06
CaO	0.02	0.01	0.22	0.01	0.59	0.02	0.45	0.1	0	0.03	0.055	0	0.03
TiO2	0.67	0.6	0.84	0.73	0.5	0.66	2.16	1.21	1.6	0.82	1.095	1.2	1.23
FeO	12.78	11.89	11.94	12.34	11.93	12.86	8.93	10.24	10.72	10.82	9.65	11.03	11.25
MnO	7.5	8.36	7.83	7.63	0.732	7.35	8.53	6.59	6.61	6.56	7.56	6.3	6.29
Ta2O5	8.79	10	9.1	9.49	9.52	9.29	28.07	39.37	36.53	37.91	38.95	40.8	36.86
TOTAL	99.46	100	99.55	99.16	92.21	100.8	98.56	98.72	99.82	100	99.17	99.94	99.14
Nb	1.830	1.816	1.823	1.819	1.827	1.830	1.429	1.248	1.306	1.302	1.260	1.223	1.296
Mg	0.006	0.004	0.004	0.006	0.004	0.006	0.002	0.005	0.007	0.006	0.005	0.004	0.006
Ca	0.001	0.001	0.013	0.001	0.037	0.002	0.031	0.007	0.000	0.002	0.004	0.000	0.002
Ti	0.029	0.026	0.037	0.032	0.022	0.029	0.103	0.061	0.078	0.041	0.055	0.060	0.061
Fe	0.621	0.578	0.579	0.603	0.586	0.617	0.472	0.575	0.585	0.595	0.538	0.615	0.622
Mn	0.369	0.412	0.385	0.378	0.365	0.357	0.457	0.374	0.365	0.365	0.426	0.356	0.352
Ta	0.139	0.158	0.144	0.151	0.152	0.145	0.483	0.718	0.648	0.678	0.706	0.740	0.662
A site	1.00	0.99	0.98	0.99	0.99	0.98	0.96	0.96	0.96	0.97	0.97	0.97	0.98
B site	2.00	2.00	2.00	2.00	2.00	2.00	2.01	2.03	2.03	2.02	2.02	2.02	2.02
Ta'	0.07	0.08	0.07	0.08	0.08	0.07	0.25	0.37	0.33	0.34	0.36	0.38	0.34
Mn'	0.37	0.42	0.40	0.39	0.38	0.37	0.49	0.39	0.38	0.38	0.44	0.37	0.36
ΣCat	3.00	3.00	2.98	2.99	2.99	2.99	2.98	2.99	2.99	2.99	2.99	3.00	3.00

Ta':Ta/(Ta+Nb); Mn': Mn/(Mn+Fe)

Composition of columbite-tantalite from the Lacorne plu

	1001A 7 core	1001A 7 rim	1001A 8	1001B 1	1001B 2	1001B 3	1007.3 1	1007 2	1007 3	1007 4	1007 Core	1007 mid	1007 rim
Nb2O5	52.19	46.7	35.22	46.95	50.02	56.18	55.52	62.51	60.56	66.53	58.36	60.07	55.96
MgO	0.02	0.04	0	0.07	0.03	0.08	0.05	0.08	0.06	0.08	0.04	0.05	0.05
CaO	0.03	0.01	1.34	0.01	0.03	0.02	0.01	0.01	0	0	0.01	0.02	0.01
TiO2	0.46	0.68	3.3	1.73	0.49	1.08	1.07	0.82	0.4	0.41	0.843	0.89	0.906
FeO	9.26	9.42	6.76	10.55	9.04	11.09	12.08	12.28	11.88	12.81	12.03	12.27	12.11
MnO	8.89	8.27	0	7.08	8.61	7.25	6.74	6.99	7.13	6.59	7.02	6.85	6.556
Ta2O5	29.07	34.59	35.22	32.8	30.81	23.27	23.32	16.25	19.3	11.96	21.3	19.3	24.19
TOTAL	99.92	99.71	81.84	99.19	99.03	98.97	98.79	98.94	99.33	98.38	99.6	99.45	99.78
Nb	1.494	1.372	1.241	1.371	1.456	1.579	1.567	1.708	1.672	1.790	1.637	1.648	1.562
Mg	0.002	0.004	0.000	0.007	0.003	0.008	0.005	0.007	0.006	0.036	0.019	0.025	0.024
Ca	0.002	0.001	0.112	0.001	0.002	0.001	0.001	0.001	0.000	0.000	0.001	0.001	0.001
Ti	0.022	0.033	0.193	0.084	0.024	0.051	0.050	0.037	0.018	0.018	0.004	0.041	0.042
Fe	0.490	0.512	0.441	0.570	0.487	0.577	0.631	0.621	0.607	0.638	0.624	0.623	0.626
Mn	0.477	0.455	0.000	0.387	0.470	0.382	0.356	0.358	0.369	0.332	0.369	0.352	0.343
Ta	0.500	0.612	0.747	0.576	0.540	0.394	0.396	0.267	0.321	0.194	0.355	0.319	0.406
A site	0.97	0.97	0.55	0.96	0.96	0.97	0.99	0.99	0.98	1.01	1.01	1.00	0.99
B site	2.02	2.02	2.18	2.03	2.02	2.02	2.01	2.01	2.01	2.00	2.00	2.01	2.01
Ta'	0.25	0.31	0.38	0.30	0.27	0.20	0.20	0.14	0.16	0.10	0.18	0.16	0.21
Mn'	0.49	0.47	0.00	0.40	0.49	0.40	0.36	0.37	0.38	0.34	0.37	0.36	0.35
ΣCat	2.99	2.99	2.73	3.00	2.98	2.99	3.01	3.00	2.99	3.01	3.01	3.01	3.00

Ta':Ta/(Ta+Nb); Mn': Mn/(Mn+Fe)

Composition of columbite-tantalite from the Lacorne pluton

	mus-r			r UCT		ab			ab	ab	
	623.1 1C	623.1 2C	623.1 3	623.2 1	623.2 2	624.B 1	624.B 2	624.B 3	624.B 3	624.B 4C	624.B 4R
Nb2O5	63.21	67.54	63.35	59.8	55.99	70.52	68.68	64.26	69.21	70.07	63.62
MgO	0.04	0.05	0.04	0.05	0.09	0.03	0.04	0.04	0.03	0.06	0.04
CaO	0	0.02	0.03	0.01	0.02	0.02	0.01	0.01	0.02	0.02	0.01
TiO2	0.72	0.46	0.59	0.68	0.93	0.54	0.6	0.69	0.9	0.51	0.7
FeO	11.89	11.27	10.53	11.67	11.26	12.08	12.14	11.68	11.29	11.73	12.05
MnO	7.4	8.55	8.66	7.39	7.26	7.78	8.17	7.62	8.64	8.13	7.25
Ta2O5	16.02	12.01	16.87	20.14	23.24	8.88	8.82	15.04	8.63	9.12	15.42
TOTAL	99.28	99.9	100.07	99.74	98.79	99.85	98.46	99.34	98.72	99.64	99.09
Nb	1.720	1.797	1.715	1.648	1.578	1.851	1.831	1.740	1.835	1.846	1.730
Mg	0.004	0.005	0.004	0.005	0.008	0.003	0.004	0.004	0.003	0.005	0.004
Ca	0.000	0.001	0.002	0.001	0.001	0.001	0.001	0.001	0.001	0.001	0.001
Ti	0.033	0.020	0.027	0.031	0.044	0.024	0.027	0.031	0.040	0.022	0.032
Fe	0.598	0.555	0.527	0.595	0.587	0.587	0.598	0.585	0.554	0.572	0.606
Mn	0.377	0.426	0.439	0.382	0.384	0.383	0.408	0.386	0.430	0.401	0.369
Ta	0.262	0.192	0.275	0.334	0.394	0.140	0.141	0.245	0.138	0.145	0.252
A site	0.98	0.99	0.97	0.98	0.98	0.97	1.01	0.98	0.99	0.98	0.98
B site	2.01	2.01	2.02	2.01	2.02	2.02	2.00	2.02	2.01	2.01	2.01
Ta'	0.13	0.10	0.14	0.17	0.20	0.07	0.07	0.12	0.07	0.07	0.13
Mn'	0.39	0.43	0.45	0.39	0.40	0.39	0.41	0.40	0.44	0.41	0.38
∑Cat	2.99	3.00	2.99	3.00	3.00	2.99	3.01	2.99	3.00	2.99	2.99

Ta':Ta/(Ta+Nb); Mn': Mn/(Mn+Fe)

Composition of columbite-tantalite from the Lacorne pluton

	624.B 5	624.B 6	624.B 7	624.B 8	624.B 9	624.B 10	624.B 11	624.B 12	624.B 13C[ab]	624.B 13E	624.B 14	624.B 15C	624.B 15R?
Nb2O5	70.62	69.64	66.88	67.42	69.88	70.08	68.09	69.18	70.69	64.15	63.17	50	58.53
MgO	0.05	0.06	0.05	0.05	0.03	0.05	0.03	0.03	0.06	0.04	0.05	0.05	0.06
CaO	0	0	0.01	0.01	0	0.01	0.01	0.02	0.02	0.01	0	0	0.02
TiO2	0.48	0.45	0.54	0.63	0.53	0.54	0.55	0.74	0.66	0.48	0.67	0.72	0.59
FeO	11.87	11.82	11.81	12.35	12.26	12.11	12.08	9.98	12.18	11.68	12.25	11.28	11.4
MnO	7.87	7.93	7.7	8.38	7.66	7.69	8.46	9.84	8.23	7.58	7.31	6.8	7.34
Ta2O5	9.27	9.19	14.24	8.93	9.2	9.09	8.93	10.93	8.91	15.57	15.6	31.18	22.62
TOTAL	100.2	99.09	101.2	97.77	99.56	99.57	98.15	100.7	100.8	99.51	99.05	100	100.6
Nb	1.851	1.846	1.769	1.811	1.843	1.847	1.822	1.813	1.840	1.739	1.722	1.442	1.615
Mg	0.004	0.005	0.004	0.004	0.003	0.005	0.003	0.002	0.005	0.003	0.005	0.005	0.005
Ca	0.000	0.000	0.001	0.001	0.000	0.001	0.001	0.001	0.001	0.000	0.000	0.000	0.001
Ti	0.021	0.020	0.024	0.028	0.023	0.024	0.025	0.032	0.029	0.022	0.030	0.035	0.027
Fe	0.575	0.580	0.578	0.613	0.598	0.591	0.598	0.484	0.586	0.586	0.618	0.602	0.583
Mn	0.386	0.394	0.381	0.422	0.378	0.380	0.424	0.483	0.402	0.385	0.373	0.367	0.380
Ta	0.146	0.147	0.227	0.144	0.146	0.144	0.144	0.172	0.139	0.254	0.256	0.541	0.376
A site	0.97	0.98	0.96	1.04	0.98	0.98	1.03	0.97	0.99	0.97	1.00	0.97	0.97
B site	2.02	2.01	2.02	1.98	2.01	2.01	1.99	2.02	2.01	2.01	2.01	2.02	2.02
Ta'	0.07	0.07	0.11	0.07	0.07	0.07	0.07	0.09	0.07	0.13	0.13	0.27	0.19
Mn'	0.40	0.40	0.40	0.41	0.39	0.39	0.41	0.50	0.41	0.40	0.38	0.38	0.39
ΣCat	2.98	2.99	2.98	3.02	2.99	2.99	3.02	2.99	3.00	2.99	3.00	2.99	2.99

Ta':Ta/(Ta+Nb); Mn': Mn/(Mn+Fe)

Composition of columbite-tantalite from the Lacorne pluton

	U-CT	U-CT			r mus					
	624.B 16	624.B 17	624.B 18	640 1	640 2	646.1	703.B 1	708 1	708 2	708 3	708 4
Nb2O5	69.23	33.92	49.26	65.71	66.8	71.5	63.23	63.35	62.96	62.29	62.33
MgO	0.01	0	0	0.06	0.04	0.07	0.07	0.06	0.05	0.05	0.06
CaO	0.01	0	0.05	0.02	0.02	0	0.03	0.02	0	0.02	0.01
TiO2	0.68	0.8	1.25	0.44	0.45	0.74	1.2	0.9	0.87	0.8	0.75
FeO	10.92	8.39	6.2	10.95	11.51	11.72	12.12	11.11	11.01	10.45	10.54
MnO	8.83	3.97	2.19	8.26	7.83	8.08	8.71	8.13	8.24	8.84	8.58
Ta2O5	9.89	50.84	13.7	13.42	12.26	6.95	13.55	16.2	16.71	17.74	17.84
TOTAL	99.57	97.92	72.65	98.86	98.91	99.06	98.91	99.77	99.84	100.19	100.11
Nb	1.830	1.089	1.807	1.827	1.797	1.876	1.713	1.714	1.706	1.690	1.693
Mg	0.001	0.000	0.000	0.006	0.004	0.006	0.006	0.005	0.004	0.005	0.005
Ca	0.000	0.000	0.004	0.001	0.001	0.000	0.002	0.001	0.000	0.002	0.001
Ti	0.030	0.043	0.076	0.054	0.020	0.032	0.054	0.041	0.039	0.036	0.034
Fe	0.534	0.498	0.421	0.583	0.573	0.569	0.607	0.556	0.552	0.524	0.529
Mn	0.437	0.239	0.151	0.415	0.395	0.397	0.442	0.412	0.418	0.449	0.437
Ta	0.157	0.982	0.302	0.128	0.198	0.110	0.221	0.264	0.272	0.290	0.291
A site	0.97	0.74	0.58	1.01	0.97	0.97	1.06	0.97	0.97	0.98	0.97
B site	2.02	2.11	2.19	2.01	2.02	2.02	1.99	2.02	2.02	2.02	2.02
Ta'	0.08	0.47	0.14	0.07	0.10	0.06	0.11	0.13	0.14	0.15	0.15
Mn'	0.45	0.32	0.26	0.42	0.41	0.41	0.42	0.43	0.43	0.46	0.45
ΣCat	2.99	2.85	2.76	3.01	2.99	2.99	3.05	2.99	2.99	2.99	2.99

Ta':Ta/(Ta+Nb); Mn': Mn/(Mn+Fe)

Composition of columbite-tantalite from North Lacorne Spodumene pegmatite

	708 5	708 6	708 7	709.c 1	756.S 1	756.S 2	756.S 3	756.S 4	756.S 5	756.S 6	756.L 1	756.L 2
				wt halit								
Nb2O5	62.35	62.81	63.53	51.48	56.18	62.65	62.06	35.37	58.86	62.85	43.9	36.43
MgO	0.01	0.06	0.04	0.01	0.02	0.02	0.01	0.01	0.01	0	0	0
CaO	0.23	0.08	0.02	0.05	0	0.01	0.01	0.02	0.04	0.02	0.03	0.04
TiO2	0.79	0.89	0.79	0.66	1.05	0.45	0.73	0.55	0.62	0.7	0.59	0.44
FeO	6.34	10.2	10.92	4.93	3.72	4.96	5.23	5.71	4.07	5.31	0.83	0.31
MnO	12.45	8.89	8.13	12.98	14.76	14.57	13.84	10.71	14.59	14.16	16.63	16.57
Ta2O5	17.12	16.59	16.51	29.19	23.81	17.14	18.05	46.98	21.5	16.69	38.4	46.7
TOTAL	99.29	99.52	99.94	99.3	99.54	99.8	99.93	99.35	99.69	99.73	100.38	100.49
Nb	1.701	1.706	1.718	1.482	1.572	1.705	1.689	1.107	1.631	1.707	1.302	1.124
Mg	0.001	0.005	0.004	0.001	0.002	0.002	0.001	0.001	0.001	0.000	0.000	0.000
Ca	0.015	0.005	0.001	0.004	0.000	0.001	0.001	0.002	0.002	0.001	0.002	0.003
Ti	0.036	0.040	0.035	0.032	0.049	0.021	0.033	0.029	0.029	0.032	0.029	0.022
Fe	0.320	0.512	0.546	0.262	0.192	0.250	0.263	0.331	0.209	0.267	0.046	0.018
Mn	0.636	0.453	0.412	0.700	0.774	0.743	0.706	0.628	0.757	0.721	0.924	0.958
Ta	0.281	0.271	0.269	0.505	0.401	0.281	0.296	0.885	0.358	0.273	0.685	0.867
A site	0.97	0.98	0.96	0.97	0.97	1.00	0.97	0.96	0.97	0.99	0.97	0.98
B site	2.02	2.02	2.02	2.02	2.02	2.01	2.02	2.02	2.02	2.01	2.02	2.01
Ta'	0.14	0.14	0.14	0.25	0.20	0.14	0.15	0.44	0.18	0.14	0.34	0.44
Mn'	0.67	0.47	0.43	0.73	0.80	0.75	0.73	0.66	0.78	0.73	0.95	0.98
ΣCat	2.99	2.99	2.98	2.98	2.99	3.00	2.99	2.98	2.99	3.00	2.99	2.99

Ta':Ta/(Ta+Nb); Mn': Mn/(Mn+Fe)

Composition of columbite-tantalite from the Lacorne pluton

	756.L 3	757 1	757 2	757 3	757 4	757 5	757 6	757 7	757 8	736 1	736 2	736 3	736 4
Nb2O5	36.76	43.21	30.15	47.31	40.61	39.22	46	42.81	49.53	1.73	14.75	46.01	46.62
MgO	0	0	0.02	0	0	0	0	0	0.01	0	0	0.01	0
CaO	0.08	0.02	0.03	0.01	0.02	0.03	0.03	0.03	0.01	0.05	0	0.01	0.01
TiO2	0.36	0.28	0.58	0.39	0.44	0.53	0.46	0.24	0.38	0.63	0.53	0.36	0.5
FeO	0.32	3.57	5.92	4.95	5	4.92	6.18	3.28	5.37	2.87	2.9	4.19	2.2
MnO	16.29	13.73	9.94	12.43	11.71	11.86	10.99	13.75	11.9	10.65	11.95	13.17	15.63
Ta2O5	46.45	39.49	53.04	34.11	41.5	42.02	37.17	40.19	32.8	82.39	69.5	36.84	35.95
TOTAL	100.26	100.3	99.68	99.2	99.28	98.58	100.83	100.3	100	98.32	99.63	100.6	100.9
Nb	1.136	1.292	0.968	1.396	1.239	1.211	1.350	1.283	1.438	0.067	0.518	1.353	1.360
Mg	0.000	0.000	0.002	0.000	0.000	0.000	0.000	0.000	0.001	0.000	0.000	0.001	0.000
Ca	0.006	0.002	0.003	0.001	0.002	0.002	0.002	0.003	0.001	0.005	0.000	0.000	0.001
Ti	0.018	0.014	0.031	0.019	0.022	0.027	0.022	0.012	0.018	0.041	0.031	0.017	0.024
Fe	0.018	0.197	0.352	0.270	0.282	0.281	0.336	0.182	0.289	0.205	0.188	0.228	0.119
Mn	0.942	0.769	0.598	0.687	0.669	0.686	0.605	0.772	0.647	0.768	0.786	0.725	0.855
Ta	0.863	0.710	1.025	0.605	0.762	0.780	0.655	0.725	0.573	1.908	1.468	0.652	0.631
A site	0.97	0.97	0.95	0.96	0.95	0.97	0.94	0.96	0.94	0.98	0.97	0.95	0.97
B site	2.02	2.02	2.02	2.02	2.02	2.02	2.03	2.02	2.03	2.02	2.02	2.02	2.02
Ta'	0.43	0.35	0.51	0.30	0.38	0.39	0.33	0.36	0.28	0.97	0.74	0.33	0.32
Mn'	0.98	0.80	0.63	0.72	0.70	0.71	0.64	0.81	0.69	0.79	0.81	0.76	0.88
ΣCat	2.98	2.98	2.98	2.98	2.98	2.99	2.97	2.98	2.97	2.99	2.99	2.98	2.99

Ta':Ta/(Ta+Nb); Mn': Mn/(Mn+Fe)

Composition of columbite-tantalite from the Lacorne pluton

	736 5	736 6	736 7	736 8c	736 8r	736 9	736 10	736 11	721 1	721 2	721 3	721 4	721 5
Nb2O5	55.06	57.95	47.84	1.98	0.68	33.17	59.89	22.87	40.39	24.13	28.23	35.85	21.64
MgO	0	0.01	0	0.01	0	0.02	0.01	0.01	0.46	0.02	0.38	0.52	0.23
CaO	0.02	0.01	0.01	0.01	0.02	0.05	0.02	0.02	0.04	0.03	0.07	0.06	0.05
TiO2	0.57	0.57	0.41	0.38	0.31	0.35	0.92	0.45	0.35	0.46	1.34	0.41	0.73
FeO	1.71	4.01	4.02	1.65	1.51	3.28	4.04	3.57	8.94	2.43	8.53	9.15	6.77
MnO	16.68	14.83	13.87	11.79	12.04	12.42	14.57	11.89	7.13	12.94	6.52	6.78	7.88
Ta2O5	26.06	23.34	33.98	83.17	85.06	50.14	20.42	61.36	42.74	60.77	53.11	47.93	62.59
TOTAL	100.1	100.7	100.1	98.99	99.62	99.43	99.87	100.17	100.05	100.78	98.18	100.7	99.89
Nb	1.550	1.601	1.397	0.076	0.026	1.053	1.644	0.763	1.224	0.795	0.921	1.106	0.726
Mg	0.000	0.001	0.000	0.001	0.000	0.003	0.001	0.001	0.046	0.002	0.041	0.053	0.025
Ca	0.001	0.000	0.001	0.001	0.002	0.004	0.001	0.002	0.003	0.003	0.005	0.005	0.004
Ti	0.027	0.026	0.020	0.024	0.020	0.019	0.042	0.025	0.018	0.025	0.072	0.021	0.041
Fe	0.089	0.205	0.217	0.117	0.107	0.193	0.205	0.220	0.501	0.148	0.513	0.522	0.420
Mn	0.879	0.768	0.759	0.847	0.867	0.739	0.749	0.743	0.405	0.799	0.397	0.392	0.495
Ta	0.441	0.388	0.597	1.918	1.968	0.957	0.337	1.231	0.779	1.204	1.039	0.889	1.263
A site	0.97	0.97	0.98	0.97	0.98	0.94	0.96	0.97	0.95	0.95	0.96	0.97	0.94
B site	2.02	2.02	2.01	2.02	2.01	2.03	2.02	2.02	2.02	2.02	2.03	2.02	2.03
Ta'	0.22	0.20	0.30	0.96	0.99	0.48	0.17	0.62	0.39	0.60	0.53	0.45	0.63
Mn'	0.91	0.79	0.78	0.88	0.89	0.79	0.78	0.77	0.45	0.84	0.44	0.43	0.54
ΣCat	2.99	2.99	2.99	2.98	2.99	2.97	2.98	2.98	2.98	2.98	2.99	2.99	2.97

Ta':Ta/(Ta+Nb); Mn': Mn/(Mn+Fe)

Composition of columbite-tantalite from the Lacorne pluton

	721 7	721 8	721 2	721 6	QL-32	812 1	812 2	812 3c	812 mid	812 rim	812 4	812 5
Nb2O5	35.22	34.04	16.21	35.02	70.37	53.03	61.77	62.16	57.71	57.07	54.18	53.51
MgO	0.37	0.12	0.07	0.02	0.08	0.07	0.09	0.09	0.08	0.07	0.09	0.09
CaO	0.06	2.07	13.48	11.5	0.24	0.1	0.3	0.19	0.41	0.43	0.28	0.06
TiO2	0.2	0.49	1.5	0.5ó	0.37	2.05	1.3	1.07	1.46	1.72	1.94	2.13
FeO	8.52	6.05	6.8	1.45	12.4	2.47	2.29	2.44	2.24	2.3	2.75	2.65
MnO	7.15	8.28	3.68	3.44	6.35	14.82	15.34	16.29	15.77	15.34	14.56	14.87
Ta2O5	48.89	49.7	54.75	48.2	8.25	25.65	18.51	18.13	21	22.23	25.03	25.45
TOTAL	100.41	100.75	96.49	100.19	98.06	98.19	99.6	100.37	98.67	99.16	98.83	98.76
Nb	1.096	1.055	0.464	1.053	1.847	1.510	1.680	1.680	1.606	1.585	1.527	1.512
Mg	0.038	0.013	0.007	0.003	0.007	0.007	0.008	0.008	0.008	0.007	0.008	0.008
Ca	0.004	0.152	0.911	0.819	0.015	0.007	0.019	0.012	0.027	0.029	0.018	0.004
Ti	0.010	0.025	0.071	0.028	0.016	0.097	0.059	0.048	0.068	0.079	0.091	0.100
Fe	0.490	0.346	0.323	0.073	0.611	0.130	0.115	0.122	0.115	0.118	0.144	0.138
Mn	0.417	0.481	0.196	0.194	0.317	0.791	0.782	0.825	0.822	0.798	0.769	0.787
Ta	0.915	0.926	0.939	0.871	0.132	0.439	0.303	0.295	0.352	0.371	0.424	0.433
A site	0.95	0.99	1.44	1.09	0.95	0.93	0.92	0.97	0.97	0.95	0.94	0.94
B site	2.02	2.01	1.47	1.95	2.00	2.05	2.04	2.02	2.02	2.04	2.04	2.04
Ta'	0.46	0.47	0.67	0.45	0.07	0.23	0.15	0.15	0.18	0.19	0.22	0.22
Mn'	0.46	0.58	0.38	0.73	0.34	0.86	0.87	0.87	0.88	0.87	0.84	0.85
∑Cat	2.97	3.00	2.91	3.04	2.95	2.98	2.97	2.99	3.00	2.99	2.98	2.98

Ta':Ta/(Ta+Nb); Mn': Mn/(Mn+Fe)

INDICATORS OF COMPOSITION AND DEGREE OF Al-Si ORDER IN PERTHITE OF REPRESENTATIVE SAMPLES OF THE PREISSAC-LACORNE PEGMATITE FIELD

	Grp	$\underline{N}_{Or}$	$\underline{t}_1O$	Δ	An	$\underline{N}_{Or}$	$\underline{t}_1O$	Δ131
623	B	99.0	1.00	0.94	0	0.2	1.01	1.10
623.p	B	99.7	1.01	0.98	0	0.9	0.99	1.14
753	B+S	100.5	1.01	1.00	0	0.7	0.99	1.13
756.S	B+S	99.8	1.00	0.97	0	0.5	0.98	1.13
908	B+S	97.0	1.00	0.96	0	0	1.01	1.11
912	B+S	99.4	1.01	0.97	0	1.3	0.98	1.14
736	S	101.8	1.00	0.93	0	0	1.01	1.11
812	S	101.4	1.01	0.99	1	1.1	0.97	1.19

Composition $\underline{N}_{Or}$ is expressed in mol % Or, and was calculated using the equations of Kroll & Ribbe (1983) relating unit-cell volume to $\underline{N}_{Or}$ for feldspar compositions that are structurally ordered (i.e., that belong to the low microcline - low albite series). The degree of Al-Si order, expressed by $\underline{t}_1O$, was computed using the equations of Blasi (1977). The error in $\underline{N}_{Or}$ and $\underline{t}_1O$ is believed to be ±0.015 in most cases. The obliquity Δ of a microcline is equal to $12.5(\underline{d}_{131} - \underline{d}_{1\bar{3}1})$; it should have a value of 1.00 for fully ordered microcline. The Δ131 indicator of a plagioclase is the calculated angular separation of the 131 and 131 diffraction maxima, in °2θ ($Cu\underline{K}\alpha_1$ radiation); it should be close to 1.10° in end-member ordered albite. The An content is estimated visually from coordinates in the $\beta^* - \gamma^*$ diagram of Smith (1974, Fig. 7-44). Grp: B: beryl-bearing pegmatite, B+S: (beryl + spodumene)-bearing pegmatite, S: spodumene-bearing pegmatite.

Appendix 3

Whole-rock geochemistry

Geochemistry of the Preissac monzogranite

	Biotite	Two-mica monzogranite						
Sample	402	11	12	29	902	903	LC-5*	LC-5*
SiO2	72.38	75.06	74.5	75.1	74.72	74.76	74.8	74.4
TiO2	0.16	0.08	0.12	0.11	0.11	0.11	0.09	0.11
Al2O3	15.41	14.44	14.72	14.4	14.08	14.04	14.3	14.6
Fe2O3	1.75	0.69	0.92	0.91	1.06	1.1	0.67	0.67
FeO								
MnO	0.06	0	0	0.03	0.04	0.03	0.05	0.04
MgO	0.03	0.2	0.22	0.06	0.23	0.25	0.17	0.2
CaO	0.5	0.71	0.87	0.71	0.8	0.85	0.6	0.6
Na2O	4.21	3.91	3.95	3.8	3.97	4	4.82	4.65
K2O	5.63	4.37	4.43	3.9	4.24	4.15	4.13	4.17
P2O5	0.03	0.01	0.06	0.02	0.02	0.03	0.03	0.04
L.O.I	0.49	0.56	0.46	0.67	0.7	0.6	0.47	0.7
		11	12					
Ga				26			24	28
Li	91			131			63	81
Be				7			4	4
Ba	6.76			486	521	483	286	320
Rb	450	397	331	360	392	324	375	377
Sr	10.5	79	116	110	112	111	72	85
Zr	33	60	86	92	63	62	52	67
Nb	28	24	22	21	17	16	23	31
Y	24	14	10	25	13	12	7	6
Ta	4.82	6		6.6				
Hf	2.76	3		2.8				
Th	10.37	11.6		14				
La	5.22	18.4		24				
Ce	15.74	31		41				
Pr	1.514							
Nd	6.23	10.6		16				
Sm	2.47	2.6		2				
Eu	0.092	0.1		0.3				
Gd	3.05							
Tb	0.49	0.4		0.3				
Dy	3.14							
Ho	0.6	0.9		0.9				
Er	1.51							
Tm	0.23			0.8				
Yb	1.55	1.3		0.8				
Lu	0.2	0.2		0.1				

*from Feng (1992)

Geochemistry of the Preissac monzogranite

	Muscovite monzogranite											
Sample	303	304	318	319	406	424	320	428	434	435A	439	443
SiO2							75.71	75.32	76	76.31	75.08	74.65
TiO2							0.04	0.03	0.03	0.02	0.05	0.04
Al2O3							14.34	14.64	14.45	14.59	14.87	14.32
Fe2O3							0.53	0.32	0.45	0.25	0.51	0.26
FeO												
MnO							0.13	0	0	0	0	0
MgO							0.01	0.13	0	0.05	0.17	0.13
CaO							0.22	0.43	0.57	0.38	0.52	0.59
Na2O							4.38	4.29	4.25	4.73	4.25	4.26
K2O							3.95	3.83	3.92	3.67	4.1	4.29
P2O5							0.02	0.04	0.04	0.04	0.04	0.03
L.O.I							0.6	0.68	0.92	0.08	0.6	0.88
Ga												
Li							28.45					
Be							3					
Ba							13.82					
Rb	518	567	458	528	476	515	470	441	489	596	478	399
Sr	6	7	9	8	8	11	10.2	6	11	8	10	21
Zr	68	84	45	53	49	47	38	46	54	140	41	27
Nb	26	69	56	25	45	32	34	32	42	42	16	8
Y	16	6	29	40	38	35	15	21	36	16	36	18
Ta							7.675					
Hf							2.204					
Th							6.95					
La							3.18					
Ce							10.31					
Pr							0.98					
Nd							3.6					
Sm							1.54					
Eu							0.044					
Gd							2.065					
Tb							0.398					
Dy							2.409					
Ho							0.414					
Er							1.149					
Tm							0.17					
Yb							0.91					
Lu							0.108					

Geochemistry of the Preissac monzogranite

Muscovite monzogranite					MGG*		
Sample	445	14	15	16	471	477	17
SiO2	76.1	75.45	75.34	74.89	75.75	75.76	76.91
TiO2	0.03	0.03	0.05	0.04	0.02	0.02	0.02
Al2O3	14.39	13.87	14.45	14.01	14.49	14.51	13.61
Fe2O3	0.37	0.29	0.35	0.32	0.43	0.42	0.47
FeO							
MnO					0	0	0
MgO	0.13	0.06	0.08	0.09	0.07	0.04	0.07
CaO	0.49	0.47	0.65	0.61	0.31	0.31	0.24
Na2O	4.46	4.11	3.89	3.98	4.76	4.88	4.42
K2O	3.55	4.11	4.64	4.44	3.62	3.67	3.6
P2O5	0.04	0.04	0.04	0.03	0.04	0.03	0.04
L.O.I	0.77	0.4	0.4	0.33	0.4	0.44	0.32
Ga							
Li					44.31		
Be					2.25		
Ba					4.62		
Rb	488				472		481
Sr	9				6.62		9
Zr	42				18.41		14
Nb	40				58.22		88
Y	31				24.2		24
Ta					7.22		12
Hf					2.97		2.2
Th					1.36		1
La					0.638		1.2
Ce					1.67		0.9
Pr					0.23		
Nd					0.902		0.4
Sm					0.877		0.8
Eu					0.016		
Gd					2.077		
Tb					0.615		0.4
Dy					4.222		
Ho					0.702		0.7
Er					1.869		
Tm					0.354		
Yb					2.7		2.1
Lu					0.362		0.3

* Muscovite-garnet monzogranite

Geochemistry of the Moly Hill monzogranite

	Biotite	Two-mica			Muscovite monzogranite						
Sample	29	26	35	40	13	14	15	16	17	20	71
SiO2	73.81	74.3		73.1	76.3	75.5	75.3	74.9	76.1	75.2	74.1
TiO2	0.16	0.13		0.02	0.03	0.03	0.05	0.04	0.03	0.03	0.02
Al2O3	14.61	14.8		14.4	15.1	13.9	14.5	14	14.6	14.4	14.7
Fe2O3	1.33	1.1		2.18	0.35	0.29	0.35	0.32	0.39	0.43	0.74
MnO	0	0.06		0.04	0	0	0	0	0	0	0.02
MgO	0.31	0.18		0.1	0.01	0.06	0.08	0.09	0.05	0.02	0.06
CaO	1.26	1.29		0.88	0.52	0.47	0.65	0.61	0.7	0.63	0.67
Na2O	3.73	4.31		4.42	4.47	4.11	3.89	3.98	4.29	4.16	4.53
K2O	4.37	4.14		4.77	4.26	4.11	4.64	4.44	3.98	3.83	4.45
P2O5	0.07	0.05		0.01	0.03	0.03	0.04	0.03	0.04	0.04	0.01
L.O.I	0.4	0.34		0.2	0.44				0.44	0.56	0.5
Li	134	118									
Be	2.6	3.6	4								
Ba	788	610	60	39							9.5
Rb	350	348	360	337	474				469	449	469
Sr	165	121	18	31	18				22	19	17
Y	8.68	7.6	14	10	46				36	36	14
Zr	142	61		46	33				35	33	57
Nb	22.81	22.5		23	22				18	19	31
Ta	3.96	4.85	3.9	2.63							5.6
Hf	4.5	2.72	3	1.21							1.43
Th	19.5	12	10	19.6							11.7
La	50.32	14.5	4.1	4.3							7.46
Ce	91.5	26.6	13	8.85							15.6
Pr	9.72	2.92		1.05							1.92
Nd	31.73	10.2	5	3.98							7.44
Sm	4.57	2.31	1.4	1.27							2.38
Eu	0.67	0.39	0.2	0.22							0.14
Gd	3.1	2.19		1.4							2.61
Tb	0.34	0.29		0.22							0.4
Dy	1.84	1.5		1.55							2.53
Ho	0.31	0.25		0.28							0.43
Er	0.74	0.74		0.8							1.18
Tm	0.12	0.11		0.13							0.17
Yb	0.64	0.74		0.78							1
Lu	0.1	0.11	0.41	0.11							0.14

Geochemistry of the Lamotte monzogranite

	Biotite monzogranite							
Sample	19	151	204	806	797	768	8204	898
SiO2	74.3	75	73.7	73.4	74.9	75		
Al2O3	14.3	14.3	14.1	14.2	14.53	13.6		
TiO2	0.14	0.07	0.08	0.04	0.06	0.09		
Fe2O3	0.93	0.66	0.98	0.91	0.13	0.8		
MnO	0.03	0.04	0.04	0.03	0.1	0.04		
MgO	0.06	0.05	0.12	0.05	0.01	0.14		
CaO	1.13	1.04	0.96	0.81	0.88	0.68		
Na2O	3.81	3.77	3.67	4	3.96	3.72		
K2O	4.24	4.3	4.33	4.27	4.62	4.41		
P2O5	0.05	0.01	0.05	0.01	0.02	0.03		
LOI	0.52	0.24		0.34	0.23	0.41		
Ga	27	21	18	22		17		
Li	129	180	354	265		175		
Be	5	2	4	4		3		
Ba	630	647	399	302	414	621		
Rb	290	250	260	320	311	270		
Sr	150	140	100	77	94	100		
Zr	120	75	95	67	73	100		
Nb	19	16	11	19	16	12		
Y	18	20	16	22	13	14		
Ta	7.7	4.6	2.8	9.4				
Hf	3.5	2.3	3.4	2.5				
Th	16	9.8	22	15		20		
U	5.8	2.8	3	4.9				
La	27	13		13			24	20.4
Ce	52	24		28			50	33.3
Pr								
Nd	18	8.3		11			21	11.5
Sm	2.1	1.4		1.4			2.6	2.9
Eu	0.4	0.3		0.3			0.5	0.3
Gd								
Tb	0.3	0.2		0.3			0.6	0.4
Dy								
Ho	0.7	0.7		0.5			0.6	0.8
Er								
Tm	0.9	0.6		1				0.1
Yb	0.5	0.7		1			1	1.1
Lu	0.1	0.1		0.9			0.2	0.2

Geochemistry of the Lamotte monzogranite

	Two-mica monzogranite										
Sample	895	896	908	8910	796	799	801	41	57	894	892
SiO2	74.81	75.21	75	75.32							
Al2O3	14.56	13.93	14.1	14.88							
TiO2	0.03	0.02	0.08	0.03							
Fe2O3	0.63	0.3	1.11	0.69							
MnO	0	0	0.05	0							
MgO	0.08	0.03	0.17	0.15							
CaO	0.78	0.71	0.93	0.69							
Na2O	4.22	4	3.86	4							
K2O	4.41	4.24	4.51	4.56							
P2O5	0.05	0.05	0.01	0.05							
LOI	0.28	0.28	0.71	0.44							
Ga			23				25	25			
Li			420				189	410			
Be			3		5		7	8			
Ba			99		170	216	102	138			
Rb	361	347	340	383	410	335	330	430			
Sr	54	54	39	55	31	43	48	45			
Zr	36	36	95	37		51	41	74			
Nb	17	14	17	18		19	18	22			
Y	19	14	22	23	7	10	36	23			
Ta	4.8			5.6	5		8.7				
Hf	2.2			1.7	3		1.4				
Th	14		19	13	22		13				
U	4.6		10	5.6	12		8				
La	11.8			10.3	12		8.4		14.3	15	10.4
Ce	20.4			17.9	29		19		24.5	25.6	17.2
Pr											
Nd	7.8			7.2	10		9.1		8.1	9.5	7
Sm	2.6			2.5	3		1.7		2.3	2.6	2.3
Eu	0.4			0.2	0.4		0.2		0.2	0.2	0.2
Gd											
Tb	0.4			0.5			0.5		0.3	0.3	0.5
Dy											
Ho	1			1.2			0.8		0.6	0.5	1
Er											
Tm	0.1			0.1			0.1				0.2
Yb	2			2.3	4.7		2.6		0.9	1.2	2.1
Lu	0.3			0.3	0.63		0.3		0.1	0.2	0.3

Geochemistry of the Lamotte monzogranite

Muscovite monzogranite			Spodumene pegmatite		
Sample	16	17	SC-2	TMC-7	881
SiO2	75.9	76.2	74	74.8	
Al2O3	14.6	14.6	15.7	16.31	
TiO2	0.03	0.02	0.01	0.01	
Fe2O3	0.56	0.64	0.85	1.09	
MnO	0.07	0.24	0.17	0.14	
MgO	0.13	0.05	0.09	0.39	
CaO	0.38	0.27	0.1	0.43	
Na2O	4.55	4.83	2.94	4.87	
K2O	3.61	3.16	2.37	1.66	
P2O5	0.03	0.01	0.01	0.01	
LOI	0.41	0.5	0.29	0.3	
Ga	34		46		
Li	46	110	10060	3410	
Be	3	6			
Ba	17	8	16	5	
Rb	450	460	1300	9.8	
Sr	12	9	22	22	
Zr	28	9	19	33	
Nb	36	48	52	68	
Y	45	40	19	10	
Ta	13	11	87		
Hf	1.8	2.5	4		
Th	7.5	1.6	2.4		
U	10	4.6	1.7		
La	5.1		0.8		0.8
Ce	16		2		1.5
Pr					
Nd	8		6.2		0.8
Sm	2.6		0.5		0.8
Eu	0.1		0.1		0.1
Gd					
Tb	0.9		0.2		0.1
Dy					
Ho	1.5		0.5		0.2
Er					
Tm	1.3				
Yb	2.2		0.2		
Lu	0.3		0.1		0.1

Geochemistry of the Lacorne monzogranite

	Biotite monzogranite										
Sample	614	616	621	634	635	673	15B-5	3060*	3061*	3062*	30**
SiO2	75.44	75.18	75.75	74.71	74.86		72.9	73.7	73.6	74.6	73.9
TiO2	0.08	0.07	0.09	0.1	0.07		0.06	0.1	0.1	0.1	0.09
Al2O3	14.11	13.92	14.44	14.28	14.04		14.1	13.5	13.9	14	14.6
Fe2O3	0.97	1.12	1.13	1.18	1.28		2.84	1.45	1.17	1.16	0.88
MnO	0.04	0.04	0.05	0.04	0.05		0.04	0.04	0.04	0.02	0.05
MgO	0.09	0.17	0.21	0.15	0.22		0.05	0.22	0.2	0.17	0.21
CaO	0.86	0.96	1.03	0.99	0.87		0.96	0.83	0.78	0.94	0.94
Na2O	3.99	3.87	4.12	3.75	3.83		3.55	3.96	4.06	4.46	4.49
K2O	4.47	4.32	4.12	4.53	4.32		4.31	5.32	5.36	4.88	4.6
P2O5	0.02	0.01	0.04	0.03	0.01		0.04	0.05	0.03	0.03	0.04
L.O.I	0.38	0.3	0.38	0.44	0.5		0.34	0.46	0.33	0.34	0.31
Ga							21				16
Li				495			295	100	200	100	189
Be				4.75		3	5	4	4	6	4
Ba	361	526	704.5	457.5	418	470	652	520	460	660	822
Rb	345	433	456.5	423	452	360	420	330	370	350	360
Sr	96	112	143.5	112.5	96		150	120	100	150	144
Zr	64	55	96	84.79	60		82	95	87	73	96
Nb	18	12	17.36	17.1	15		25	18	13	9	15
Y	26	13	9.925	8.185	14	12	22	25	29	27	3
Ta			3.31	3.47		3.4	11.4	7	3	5	2.4
Hf			3.78	3.33		4	2.2	3	4	3	3.5
Th			25.75	30.97		26	15.5	21	15	18	24
U			2.64	4.34		3.4	2.3	4	2	3	4
La			28.78	20.81		37	23.4				27
Ce	39	53	52.71	40.18	69	73	32.3				52
Pr			5.23	4							
Nd			15.89	13.22		23	9				18
Sm			2.6	2.38		3.8	2.2				3.4
Eu			0.45	0.38		0.5	0.3				0.49
Gd			2.32	2.11							
Tb			0.28	0.26		0.2-0.3	0.2				0.4
Dy			1.54	1.47							
Ho			0.27	0.27			0.4				
Er			0.71	0.67							
Tm			0.12	0.103							
Yb			0.76	0.72		2.3	0.8				1.1
Lu			0.13	0.115		0.33	0.1				0.17

* from Feng 1992; ** from Danis 1985

Geochemistry of the Lacorne monzogranite

	Two-mica monzogranite							
Sample	652	672	692	742	1655	3036	701	707
SiO2	76.2	75.2	74.86	75.2	76.1	74.2	75.68	75.87
TiO2	0.03	0.06	0.03	0.03	0.1	0.1	0.06	0.06
Al2O3	13.7	13.8	14	14.1	13.2	13.6	14.08	14.03
Fe2O3	0.57	0.64	1.78	0.65	0.72	0.8	0.73	0.69
MnO	0.05	0.04		0.03	0.02	0.07	0.05	0.06
MgO	0.05	0.07	0.33	0.08	0.1	0.1	0.05	0.05
CaO	0.59	0.63	0.85	0.72	0.54	0.72	0.61	0.71
Na2O	3.88	4.15	4.06	4.49	4.35	4.46	4.06	3.94
K2O	4.56	3.98	4.39	3.86	4.45	4.76	3.66	4.61
P2O5	0.01	0.01	0.01	0.01	0.03	0.02	0.02	0.02
L.O.I	0.67	0.5	0.6	0.41	0.48	0.35	0.6	0.34
Ga	23	24		22				
Li	86	64	255	110	94	290		
Be	4	6		5	7	7		
Ba	78	280	114	226	110	100	150	173
Rb	430	640	630	620	540	440	1304	523
Sr	40	62	58	75	51	59	63	67
Zr	64	93	54	85	45	51	47	50
Nb	25	26	28.5	15	12	18	26	31
Y	29	27	21	20	40	39	17	22
Ta	6	6	6		4			
Hf	1.5		2		2			
Th	18	23	24	25	14			
U	4.5	8	6	5	4			
La	11.6		13.95					
Ce	25.35		29.35					
Pr	3		3.3					
Nd	11.4		11.75					
Sm	3.26		3.2					
Eu	0.25		0.23					
Gd	3.35		3.2					
Tb	0.57		0.53					
Dy	4		3.7					
Ho	0.73		0.73					
Er	2.13		2.2					
Tm	0.35		0.35					
Yb	2.53		2.34					
Lu	0.35		0.36					

Geochemistry of the Lacorne monzogranite

	Muscovite monzogranite				
Sample	648	684	603	637	EC-60
SiO2	76.8	76.3	75.28	74.99	75.2
TiO2	0.03	0.02	0.04	0.04	0.1
Al2O3	14.1	13.9	14.51	14.63	14.9
Fe2O3	0.35	0.44	0.48	0.6	0.72
MnO	0.06	0.07	0	0.02	0.15
MgO	0.1	0.05	0.01	0.05	0.06
CaO	0.61	0.49	0.64	0.61	0.41
Na2O	4.05	4.36	4.39	4.04	5.25
K2O	4.17	4.35	4.01	4.26	4.2
P2O5	0.01	0.01	0.04	0.04	0.02
L.O.I	0.53	0.58	0.38	0.56	0.43
Ga	25	28	26		
Li	270	60	190	208	140
Be	6	7	7	9	8
Ba	68	71	24	23	37
Rb	450	525	438	970	700
Sr	35	38	16.5	22.5	16
Zr	65	55	38.5	39	43
Nb	23	26	42.5	43	60
Y	32	29	23	21.4	55
Ta	4	5	10	9	1
Hf	1.95				4
Th	18	13	11	11	5
U	5.2	4	14	19	1
La	9.35			5.54	
Ce	19.2			11.76	
Pr	2.4			1.34	
Nd	8.93			4.73	
Sm	2.62			1.63	
Eu	0.19			0.139	
Gd	2.9			1.93	
Tb	0.51			0.346	
Dy	3.7			2.4	
Ho	0.7			0.455	
Er	2.1			1.36	
Tm	0.34			0.201	
Yb	2.42			1.323	
Lu	0.35			0.157	

Geochemistry of the Lacorne monzogranite

	Aplite	Beryl pegmatite					Spd*
Sample	606	646A	751	646P	667	624	736
SiO2	73.37	73.8	76.6	76	77		73.65
TiO2	0.02	0.01	0.02	0.02	0.01		0.01
Al2O3	15.95	15	14.51	14.4	14.5		16.02
Fe2O3	0.56	0.63	0.39	0.55	0.47		0.16
MnO	0.03	0.7	0.45	0.04	0.02		0.13
MgO	0.01		0.01		0.09		0.01
CaO	0.22	0.21	0.15	0.39	0.45		0.06
Na2O	4.29	5.88	4.92	4.21	5.51		4.31
K2O	5.43	2.66	2.94	4.54	2.33		4
P2O5	0.12	0.02	0.01	0.02			0.04
L.O.I	0.54	0.5	0.44	0.64	0.6		0.31
Ga		44	52	34	43		
Li	225	142	294	226	365		
Be	6						
Ba	6.59	24	7	31	27		3.2
Rb	2122	530	0.16%	600	700		4875
Sr	6.82	14	30	23	57		53
Zr	5.8	99	25	27	23		7
Nb	177	97	88	83	100		50
Y	2.13	26	14	18	8		0.6
Ta	25	23	190 ?	8	19		67
Hf	0.878						2
Th	3.47	16	8	10	4		2
U	10.69	28	8	19	17		
La	0.96					5.72	0.2
Ce	3.22					18.04	0.52
Pr	0.512					2.71	0.06
Nd	2					10.45	0.24
Sm	1.81					8.68	0.34
Eu	0.052					0.03	0.014
Gd	1.43					5.63	0.33
Tb	0.165					0.63	0.06
Dy	0.467					1.62	0.18
Ho	0.049					0.13	0.017
Er	0.101					0.18	0.02
Tm	0.008					0.02	0.006
Yb	0.055					0.12	0.06
Lu	0.018					0.02	0.01

*spodumene pegmatite

Geochemistry of the albitite dikes associated with the Lacorne pluton

Sample	721	722	723	724	733	772
SiO2	67.98	67.99	67.8	67.95	68.31	72.2
TiO2	0.01	0.02	0.01	0.02	0.01	0.01
Al2O3	20.15	20.12	20.07	19.98	20.42	17.05
Fe2O3	0.14	0.11	0.1	0.11	0.13	0.27
MnO	0.02	0.2	0.08	0.04	0.03	0.13
MgO	0.01	0.01	0.01	0.01	0.01	0.01
CaO	0.4	0.13	0.3	0.11	0.44	0.97
Na2O	10.67	10.84	10.76	10.91	10.64	8.48
K2O	0.07	0.3	0.05	0.02	0.04	0.2
P2O5	0.06	0.05	0.02	0.05	0.03	0.01
L.O.I	0.26	0.26	0.24	0.36	0.19	0.6
Ga	61	58	54	61		
Li	7	4.77	6	7		
Be	45	22.13	16	14		
Ba	42.5	64.16	37.5	74	56	57
Rb	1.15	1.66	2.4	3	2.8	47
Sr	77.5	472	72.5	545.5	81	59
Zr	24	77.4	37.5	31.5	12	52
Nb	46.5	70	36	20	34	67
Y	0.85	3.67	2		1.8	4.7
Ta	180	136	270	110		
Hf						
Th	4	5.12				
U	5	12.235	6	6		
La		1.86				
Ce		3.35				
Pr		0.37				
Nd		1.63				
Sm		1.18				
Eu		0.058				
Gd		1.024				
Tb		0.193				
Dy		0.683				
Ho		0.061				
Er		0.113				
Tm		0.018				
Yb		0.164				
Lu		0.032				

Appendix 4

Chemistry of decrepitated fluid inclusions

Beryl in beryl pegmatite						Quartz in beryl pegmatite					Qtz in spodumene pegmatite				
Mound	Na	K	Ca	Fe	Cl	Mound	Na	Ca	S	Cl	Mound	Na	Ca	S	Cl
1	56.44	0.00	00.00	00.00	37.98	1	46.79	0.00	0.00	48.63	1	37.30	13.62	0.00	49.09
2	47.34	0.00	14.46	00.00	31.39	3	50.92	0.00	0.00	49.08	2	43.55	00.00	0.00	53.30
3	39.30	1.01	08.95	10.22	40.52	4	43.40	0.00	9.96	36.65	3	38.36	06.67	0.00	47.88
4	50.74	0.00	00.00	00.00	37.47	5	50.87	0.00	5.14	44.00	4	31.34	12.21	4.21	52.26
5	57.45	0.00	00.00	09.89	29.82	7	47.27	0.00	4.57	41.60	5	35.45	18.35	0.00	44.19
6	66.86	0.00	00.00	00.00	23.05	8	46.80	0.00	7.07	32.55	6	45.02	00.00	0.00	51.14
7	48.31	0.00	04.06	11.28	36.36	9	44.69	0.00	8.99	44.92	7	41.52	03.71	0.00	52.42
8	37.27	0.00	16.18	03.14	39.88	10	48.78	0.00	3.38	44.46	8	40.73	17.55	0.00	39.68
9	42.18	0.00	15.24	14.20	25.56	11	48.96	0.00	7.59	39.23	9	43.29	03.06	0.00	48.73
10	41.79	0.00	08.95	15.23	32.39	12	47.84	0.00	0.00	46.34	10	26.58	16.04	3.16	54.22
11	53.36	0.00	00.00	00.00	38.75	13	46.71	0.00	0.00	50.02	11	40.71	05.81	2.00	50.36
12	47.00	0.00	11.79	00.00	35.91	14	49.22	6.78	0.00	39.78	12	36.82	08.15	1.10	52.85
13	54.26	0.00	11.10	00.00	27.13	15	46.43	0.00	0.00	51.26	13	35.28	08.50	2.38	52.86
14	44.58	1.30	00.00	14.60	36.92	16	45.27	0.00	8.54	39.79	14	33.99	11.99	1.77	51.22
15	52.55	0.00	00.00	00.00	44.34	17	45.74	0.00	0.00	40.89	15	24.15	21.66	2.19	50.20
16	62.65	0.00	00.00	08.61	24.93	18	37.18	9.38	0.00	53.44	16	38.31	07.94	2.35	51.01
17	51.52	0.00	00.00	10.56	31.93	19	36.74	7.65	0.00	55.60	17	39.81	10.15	1.21	48.60
18	54.91	0.00	00.00	24.60	20.49	20	37.78	6.15	0.00	54.04	18	35.31	12.13	1.48	47.88
19	50.23	0.00	01.30	06.72	38.61	21	47.44	0.00	0.00	46.40	19	35.04	14.27	0.00	47.89
20	43.71	0.00	04.02	18.19	31.67	22	48.08	0.00	2.01	48.02	21	28.70	16.48	5.69	48.06
1A	52.83	0.00	00.00	00.00	46.00	23	43.05	5.62	0.57	50.14	22	25.73	17.73	2.39	53.18
2A	49.06	0.32	00.00	00.00	46.41	24	45.60	0.00	0.00	51.27	23	28.17	17.13	3.64	49.97
3A	49.20	0.34	00.00	00.00	48.91						24	32.48	09.37	0.00	56.51
4A	52.90	0.00	00.00	00.00	42.51						25	43.88	03.41	5.25	46.37
											26	16.72	26.16	2.51	54.62
											27	29.17	16.68	0.00	51.92

Values are in wt%.

Spodumene in spodumene pegmatite							Beryl in spodumene-beryl pegmatite							Qtz in spd-beryl peg		
Mound	Na	K	Ca	Mn	S	Cl	Mound	Na	K	Ca	Fe	S	Cl	Mound	Na	Cl
1	46.0	9.78	0.00	0.00	3.13	32.4	1	56.49	0.00	0.00	0.00	0.00	37.35	1	47.11	47.46
2	36.2	0.00	13.38	5.58	0.00	44.8	2	51.31	7.47	0.00	5.98	2.85	29.69	2	50.31	49.36
3	47.6	0.00	5.80	1.67	0.00	36.8	3	39.39	12.75	12.05	6.38	3.83	20.33	4	50.36	47.62
4	36.2	0.00	8.22	8.21	0.00	42.9	4	59.30	0.34	1.51	0.75	1.43	32.30	5	49.37	46.89
5	35.2	0.00	12.39	5.42	0.00	45.5	5	52.95	4.92	1.28	0.00	0.38	35.21	6	43.91	53.88
6	23.6	4.88	6.82	0.00	4.13	51.1	6	53.17	0.00	0.00	0.00	2.16	42.07	7	49.20	47.13
7	36.5	0.00	12.99	1.22	0.41	45.4	7	37.10	7.41	23.02	0.00	0.00	27.86	8	49.11	48.78
8	23.0	0.00	14.06	0.00	0.00	63.0	8	51.33	0.00	5.23	0.00	0.00	40.55	9	49.64	49.78
9	41.8	0.00	1.96	2.12	0.00	45.2	9	43.32	0.00	4.07	13.25	0.67	35.30	10	47.01	46.23
10	43.9	0.00	0.00	0.00	2.00	50.8	10	52.92	0.00	2.29	0.00	0.00	38.80	11	48.75	48.05
11	41.1	0.00	16.11	0.00	0.00	42.8	11	46.97	0.00	0.00	0.00	0.00	34.86	13	47.97	52.03
12	36.9	0.00	14.02	2.91	0.00	43.1	12	51.93	2.27	0.00	0.00	0.00	43.61	14	47.01	47.76
13	28.1	0.00	12.15	0.00	1.41	55.1	13	52.90	0.00	0.00	0.00	1.20	43.01	15	43.96	56.04
14	36.2	0.00	16.04	0.00	0.00	40.6	14	50.74	0.83	0.00	0.00	0.00	42.90	16	45.98	54.02
15	61.4	0.51	8.53	0.65	0.00	26.5	15	51.70	0.00	0.00	0.00	0.00	39.96	17	52.93	47.07
16	44.9	0.00	12.09	1.80	0.00	39.4								18	54.01	45.99
17	45.9	0.00	6.09	1.80	0.00	41.8								19	53.49	43.64
18	43.1	0.00	11.83	0.00	0.00	41.6								20	51.18	48.82
19	29.2	0.00	8.96	0.00	0.00	55.2								21	46.02	48.57
20	31.1	2.76	5.02	0.00	0.00	47.1								22	45.13	52.45
21	25.2	9.49	2.81	4.45	0.00	47.6								23	52.49	38.68
22	37.5	13.21	2.27	0.00	0.00	43.2								24	46.94	53.06
23	38.2	25.61	1.47	0.00	0.00	30.4								25	45.92	40.99
24	22.4	0.00	4.74	0.00	0.00	67.3								26	49.52	47.98
25	59.6	0.00	15.49	0.00	0.00	23.7								27	47.11	42.88